LIÈGE université
Gembloux
Agro-Bio Tech

Stomatal and non-stomatal responses of typical temperate C3 crops to soil water stress

Quentin BEAUCLAIRE

COMMUNAUTÉ FRANÇAISE DE BELGIQUE
UNIVERSITÉ DE LIÈGE - GEMBLOUX AGRO-BIO TECH

Stomatal and non-stomatal responses of typical temperate C3 crops to soil water stress

Quentin BEAUCLAIRE

Dissertation originale présentée en vue de l'obtention du grade de docteur en sciences agronomiques et ingénierie biologique

Promoteur:

Pr. Bernard LONGDOZ (Université de Liège, Belgique)

Membres du Jury:

Pr. Bernard HEINESCH (Université de Liège, Belgique),
Pr. François JONARD (Université de Liège, Belgique),
Pr. Patrick DU JARDIN (Université de Liège, Belgique),
Dr. Valérie LE DANTEC (Université de Toulouse Paul Sabatier, France),
Dr. Olivier ROUPSARD (Centre de coopération internationale en recherche agronomique pour le développement, France).

Année civile 2024

Citation: : BEAUCLAIRE Quentin, 2024. Stomatal and non-stomatal responses of typical temperate C3 crops to soil water stress. Thèse de doctorat, Gembloux Agro-Bio Tech – Université de Liège, Gembloux, 267 p.

Photo credits: Quentin BEAUCLAIRE unless otherwise stated.

Abstract

Photosynthesis plays a key role in the carbon cycle, being the primary mechanism through which carbon dioxide (CO_2) is converted into organic compounds by plants, algae, and certain bacteria. On average, terrestrial ecosystems uptake around one-third of anthropogenic CO_2 emissions and participate to the mitigation of climate change. Temperature, solar irradiance or soil water availability are important factors mediating the strength of terrestrial ecosystems. Therefore, drought poses a major threat on the atmospheric CO_2 balance due to its profound implications for plant survival, ecosystem dynamics and agricultural productivity.

Water stress induces a cascade of physiological responses in plant functioning. During hot and dry weather, plants often close their stomata to save water and prevent dehydration at the expanse of a decrease in CO_2 supply to the chloroplasts, which results in a decrease in both carbon assimilation and transpiration. In addition, photosynthesis and stomatal closure can be impacted by non-stomatal factors, which complexifies the mechanisms regulating plant responses to water stress. Models of photosynthesis and stomatal conductance still lack from a detailed characterization of the intertwined physiological processes under soil water-limiting conditions. Understanding, disentangling and quantifying the importance of photosynthesis limiting factors is crucial for selecting drought-tolerant varieties and for improving model predictions.

The gold standard method for estimating photosynthesis is the measurement of the CO_2 net assimilation rate by gas exchange techniques. While providing key information on the factors influencing the temporal variability of photosynthesis, gas exchanges alone do not allow to fully characterize the limitations on carbon assimilation under water stress. Additional measurements of chlorophyll fluorescence by active methods are needed to improve the knowledge about these constraints and to quantify the importance of each limiting factors. In particular, the response of mesophyll conductance to water stress remains a pivotal uncertainty in models of photosynthesis.

The interpretation of actively-induced chlorophyll fluorescence measurements is however limited to the leaf scale and does not allow to elucidate the impact of water stress on large patches of vegetation. The recent emergence of passive techniques has allowed the monitoring of fluorescence emission induced by solar irradiance (SIF) at different temporal scales and spatial resolutions. These measurements provide a promising indicator of vegetation physiological processes which can be used to calibrate empirical models to estimate carbon assimilation at local and large scales. However, such relationships typically fail in reproducing photosynthesis temporal evolution at short timescales or during climate extremes such as droughts or heatwaves. More mechanistic approaches are needed to fully exploit the physiological message carried by SIF measurements.

In this thesis, we first aimed to unravel the origins of photosynthesis limitations under water stress. The first chapters are dedicated to providing a calibration of the

response of stomatal and non-stomatal factors to the decrease in soil water availability. This method, first applied on forest ecosystems (chapter 3) and potato (chapter 4) with eddy covariance (EC) data, emphasizes the key role played by non-stomatal factors in regulating canopy-scale photosynthesis for these two very different plant functional types. By performing measurements of leaf-level chlorophyll fluorescence by active methods, and by using a new partitioning method, we also showed (chapter 5) that mesophyll conductance is a pivotal trait which regulates both carbon assimilation and stomatal conductance of potato. These chapters provide functions of soil water availability for stomatal and non-stomatal factors which can be used to reduce uncertainties in climate models. Finally, we evaluated the capability of a new mechanistic approach to model CO_2 assimilation and transpiration of a winter wheat crop from proximal sensing of SIF (chapter 6). A very strong correlation between model estimates and EC measurements was found across a wide range of environmental conditions including edaphic drought. A sensitivity analysis revealed that the fraction of open photosystem II centers is a key parameter affecting model robustness. This last chapter paves the way towards an improvement of the understanding of the interactions between the water and carbon cycles by using the physiological information carried by SIF.

Résumé

La photosynthèse joue un rôle essentiel dans le cycle du carbone, en tant que mécanisme principal par lequel le dioxyde de carbone (CO_2) est converti en composés organiques par les plantes, les algues et certaines bactéries. En moyenne, les écosystèmes terrestres absorbent environ un tiers des émissions anthropiques de CO_2, contribuant ainsi à la lutte contre le changement climatique. La température, l'irradiance solaire ou la disponibilité en eau du sol sont des facteurs importants qui influencent la force des puits de carbone terrestre. Par conséquent, la sécheresse constitue une menace majeure pour le cycle du carbone, en raison de ses implications profondes pour la survie des plantes, la dynamique des écosystèmes et la productivité agricole.

Le stress hydrique induit une cascade de réponses physiologiques et biochimiques chez les plantes. Par temps chaud et sec, les plantes ont tendance à fermer leurs stomates pour économiser de l'eau et éviter la déshydratation, au détriment d'une diminution de l'approvisionnement en CO_2 vers les chloroplastes, entrainant ainsi une réduction à la fois de l'assimilation du carbone et de la transpiration. De plus, la photosynthèse et la fermeture stomatique peuvent être affectées par des facteurs non-stomatiques comme les capacités photosynthétiques ou la conductance mésophylienne, ce qui complexifie les mécanismes régulant les réponses des plantes au stress hydrique. Les modèles de photosynthèse et de conductance stomatique manquent encore d'une caractérisation détaillée des processus physiologiques interconnectés dans des conditions de sécheresse édaphique. Comprendre, quantifier et clarifier l'importance des facteurs limitants la photosynthèse est crucial pour sélectionner des variétés tolérantes à la sécheresse et améliorer les prédictions des modèles climatiques.

La méthode de référence pour estimer la photosynthèse est la mesure du taux d'assimilation nette en CO_2 par des techniques d'échange gazeux. Bien que fournissant des informations clés sur les facteurs influencant la variabilité temporelle de la photosynthèse, les échanges gazeux seuls ne permettent pas une caractérisation complète de la limitation de la photosynthèse en cas de stress hydrique. Des mesures supplémentaires de fluorescence chlorophylienne par des méthodes actives sont nécéssaires afin de quantifier l'importance de chaque facteur limitant. En particulier, la réponse de la conductance mésophylienne au stress hydrique reste une importante source d'incertitude dans les modèles de photosynthèse.

L'interprétation des mesures de fluorescence chlorophylienne par des méthodes actives est néanmoins limitée à l'échelle de la feuille et ne permet pas de charactériser l'impact du stress hydrique sur des grandes étendues de végétation. L'émergence récente des méthodes passives pour mesurer la fluorescence chlorophylienne a permis de suivre l'émission de fluorescence naturellement induite par le soleil (SIF) à différentes échelles spatiales et temporelles. Ces mesures constituent un indicateur prometteur des processus physiologiques de la végétation et peuvent être utilisées pour calibrer des modèles empiriques qui fournissent une estimation directe de l'assimilation en

CO_2 à des échelles locales et plus larges. Cependant, de tels modèles ne permettent généralement pas de reproduire l'évolution temporelle de la photosynthèse à court terme ou pendant des extrêmes climatiques tels que des sécheresses ou des vagues de chaleur. Des approches plus mécanistes sont nécessaires pour exploiter pleinement le message physiologique transmis par la SIF.

Dans cette thèse, nous avons d'abord cherché à identifier les origines des limitations de la photosynthèse pendant des épisodes de sécheresse édaphique. Les premiers chapitres sont consacrés à la caractérisation complète de la réponse des facteurs stomatiques et non-stomatiques à la diminution de la disponibilité en eau du sol. Cette méthode, d'abord appliquée aux écosystèmes forestiers (chapitre 3) et aux pommes de terre (chapitre 4) avec des données d'eddy covariance (EC), a mis en évidence le rôle clé des facteurs non-stomatiques dans la régulation de la photosynthèse à l'échelle de la canopée pour ces deux différents types d'écosystèmes. En effectuant des mesures de fluorescence chlorophylienne actives et en utilisant une nouvelle méthode de partitionnement, nous avons également montré que la conductance mésophyllienne était un facteur essentiel qui régulait à la fois l'assimilation du carbone et la conductance stomatique de la pomme de terre (chapitre 5). Ces chapitres fournissent des fonctions de disponibilité en eau dans le sol pour l'influence des facteurs stomatiques et non-stomatiques sur la photosynthèse et la transpiration, qui peuvent être utilisés pour réduire les incertitudes dans les modèles climatiques. Dans le dernier chapitre, nous avons testé une nouvelle approche mécaniste visant à modéliser les échanges de carbone et d'eau d'une culture de blé d'hiver à partir de mesures de SIF à l'échelle de l'écosystème. Une corrélation très forte entre les estimations du modèle et les mesures d'EC a été trouvée, y compris pendant les périodes de sécheresse édaphique. Une analyse de sensibilité a révélé que la fraction de centres ouverts du photosystème II était un paramètre clé impactant les performances du modèle. Ce dernier chapitre ouvre la voie à une amélioration de notre compréhension des interactions entre les cycles de l'eau et du carbone en utilisant les informations physiologiques contenues dans la SIF.

Remerciements

Cette thèse de doctorat a été réalisée au sein de l'axe Biosystems Dynamics and Exchanges (BIODYNE) de Gembloux Agro-Bio Tech. Ce travail est le fruit d'un long parcours collaboratif qui n'aurait pu être accompli sans l'aide de nombreuses personnes que j'aimerais remercier ici.

Tout d'abord, je tiens à citer mon promoteur, Bernard Longdoz. Bernard a été mon professeur pendant mes années de master, notamment pour les cours d'échanges écosystèmes-atmosphère et de modélisation. Mon intérêt pour l'étude des écosystèmes est grandement lié à son implication dans l'enseignement de ces cours. Bernard a toujours gardé sa porte ouverte quand j'en avais besoin. Sa bienveillance, ses conseils, ainsi que son investissement personnel dans la relecture des nombreuses versions des manuscrits ont participé à la réussite de cette thèse. Je tiens également à associer à ces remerciements Bernard Heinesch et Louis Gourlez de la Motte, avec qui les discussions furent toujours instructives et les conseils précieux. Merci également aux membres de mon comité de thèse pour leurs conseils et leur accompagnement tout au long de ce doctorat. Enfin, merci à François Jonard et Simon De Cannière avec qui nous avons collaboré pendant ces trois dernières années, et qui ont permis que cette thèse s'oriente vers la télédétection au travers de la fluorescence chlorophylienne.

Une thèse ne peut être réussie sans un soutien continu et sans failles de l'équipe travaillant sur les sites de mesures, aussi bien pour le traitement des données que pour l'installation et la maintenance des capteurs. Je voudrais notamment mentionner Alain Debacq et Jérôme Pierreux pour l'installation de l'expérience sous serre, Henri Chopin et Gaëtan Bogaerts pour l'installation du spectromètre à Lonzée, et enfin Ayche Orgun et Ariane Faurès pour la mise à disposition des données d'eddy covariance. Un grand merci également à Katia Berghmans pour toute la gestion administrative. Je souhaite également remercier Florian Vanden Brande et Natacha Pezzetti que j'ai eu le plaisir d'encadrer pendant leur TFE.

Indissociable de la recherche dans un mandat d'assistant-doctorant, l'enseignement a également représenté une part importante de ces six années passées à Gembloux. À ce titre, j'aimerais remercier mes nombreux collègues avec qui j'ai travaillé pour les cours de mathématiques et physique. Merci à Esther Bustillo, François Boland, Florian Vanden Brande, Jonathan Bitton, Sophie Maloteau, Laura Delhez et Clément Dumont pour votre bonne humeur. Merci à mes collègues voisins de l'étage de statistiques : Lionel Luxen, Dominique Marchal, Yves Brostaux, Hélène Soyeurt et Mireille De Graeuwe d'Aoust pour ne citer qu'eux. Merci enfin à Catherine Charles et à nouveau Bernard Longdoz pour l'organisation des cours de mathématiques et de physique. Et surtout, je tiens à mentionner les nombreux étudiants et étudiantes qui se sont succédés depuis le début de ma thèse, et à qui j'ai eu le plaisir de transmettre mes connaissances pour la réalisation des travaux pratiques de mathématiques et de physique. Ce fut une expérience très enrichissante, et je vous remercie pour votre bienveillance.

Enfin, un immense merci à ma famille qui m'a continuellement soutenu depuis mon arrivée en Belgique il y a maintenant 11 ans pour commencer mes études de bio-ingénieur. Sans vous, je n'aurais certainement pas obtenu mon diplôme d'ingénieur et de docteur. Je pense également à Ania, qui partage ma vie depuis plus de 7 ans maintenant et qui m'a accompagné dans cette longue aventure. Merci de m'avoir soutenu dans toutes les situations.

Contents

List of Figures

List of Tables

Acronyms

ABA ABscissic Acid. 41, 43, 178

ADP Adenosine Di-Phosphate. 7

AGB AboveGround Biomass. 203

AIC Akaike Information Criterion. 116, 143, 145, 147, 154, 169

APAR Absorbed Photosynthetically Active Radiation. 159, 160, 162

ASCAT Advanced SCATterometer. 202

ASWC Available Soil Water Content. 43

ATP Adenosine Tri-Phosphate. 7–9, 136, 137, 160

BPGA 1,3-Biphosphoglycerate. 8, 9

CABLE Community Atmosphere Biosphere Land Exchange. 46, 178

CBB Calvin-Benson-Bassham. 5, 8, 9, 13, 16, 29, 30, 34, 44

ChlF Chlorophyll Fluorescence. i, 12, 13, 16–18, 24–26, 32, 33, 35–37, 51, 52, 177, 178, 180, 181, 188

CLM5 Community Land Model v5. 35, 192

cytb6f Cytochrome b6f. 7

DHAP Dihydroxyacetone Phosphate. 8

DT DayTime. 22, 23, 181–183, 196

EC Eddy Covariance. vi, 18–23, 27, 29, 35, 42, 51, 57–59, 70–72, 77, 178, 181, 183, 184, 189, 191, 196, 205

ECOSTRESS ECOsystem Spaceborne Thermal Radiometer Experiment on Space Station. 201

EnMAP Environmental Mapping and Analysis Program. 202

ENVISAT ENVIronmental SATellite. 27

FD FerreDoxine. 7

FLD Fraunhofer Line Depth. 26, 27, 180

FLEX FLuorescence EXplorer. 27, 29, 138, 199

FLORIS FLuORescence Imaging Spectrometer. 27, 29

FloX Fluorescence boX. 29, 138, 140, 146

FNR Ferredoxin-NADP+ reductase. 7

FTSW Fraction of Transpirable Soil Water. 43

FvCB Farquhar-von Caemmerer-Berry. iv, 29–32, 35–37, 45–47, 52, 58, 78, 110–112, 126, 137, 138, 177, 179, 193, 202

FWHM Full Width of the absorption band at Half of the Maximum depth. 25

G3P Glyceraldehyde 3-phosphate. 8, 9

GAI Green Area Index. 81

GAPDH 3-phosphate dehydrogenase. 8

GOME-2 Global Ozone Monitoring Experiment-2. 27

GOSAT Greenhouse gases Observing SATellite. 27

GPP Gross Primary Production. ii, v–vii, x, xii, 21–24, 27, 29, 30, 35–37, 51, 52, 57–65, 67, 69–73, 77–81, 85, 86, 91, 93, 95, 96, 99, 135–141, 143, 156, 159, 162–165, 171, 178–183, 187, 189, 195–199, 201, 202

HyPlant High-performance airborne imaging spectrometer for vegetation monitoring. 27

ICOS Integrated Carbon Observation System. 59, 77, 80, 109, 135, 139, 149, 181, 189, 205

IPCC Intergovernmental Panel on Climate Change. 35

IRGA Infrared Gas Analyser. 14, 21

JULES Joint UK Land Environment Simulator. 45, 178, 191

LAI Leaf Area Index. 58, 60, 70, 81, 197, 198

LE Latent heat. 20, 139, 140, 144, 145

LHCs Light Harvesting Centers. 5, 6, 11

LIFT Light-Induced Fluorescence Transients. 17, 18

LRC Light-Response Curve. 9, 12

LSMs Land Surface Models. 30, 32, 34, 43, 45, 46, 51, 77, 79, 111, 116, 123, 136, 138, 177, 178, 187, 189, 192, 195, 196

LST Land Surface Temperature. 200, 201

LUE Light-Use Efficiency. xi, 29, 35, 36, 137, 145, 150, 154, 159, 160, 163, 168, 201

LWP Leaf Water Potential. ii, 40–42, 192, 202, 204

MERIS Medium Resolution Imaging Spectrometer. 27

MLR Mechanistic Light Response. v–vii, xi–xiii, 36, 37, 52, 135, 137–139, 141, 143, 145, 147, 148, 156–165, 169, 171, 172, 180–182, 195–200, 202, 204, 205

MODIS Moderate Resolution Imaging Spectroradiometer. 202

MTG-S Meteosat Third Generation-Sounder. 199

NADP+ oxidized form of Nicotinamide Adenine Dinucleotide Phosphate. 7, 44

NADPH reduced form of Nicotinamide Adenine Dinucleotide Phosphate. 7–9, 136, 137, 160

NDVI Normalized Difference Vegetation Index. 142, 149, 150, 198

NEE Net Ecosystem Exchange. vi, 21–23, 81, 136, 139, 164, 181–183, 196

NIR Near-Infrared. 5, 11, 12, 24, 140–142, 146

NPQ Non-Photochemical Quenching. 12, 13, 36, 137, 147, 148, 158, 165, 201

NSOL Non-Stomatal Origin Limitation of photosynthesis. iii, vi, x, 44–46, 51, 52, 57–59, 63, 64, 67, 69–73, 77, 79, 80, 83, 86, 87, 91, 95–99, 111, 115, 117, 125, 178–180, 183, 186, 187, 189–191, 194, 196

NT NightTime. 22, 181–183, 196

OCO-2 Orbiting Carbon Observatory-2. 138, 199

OCO-3 Orbiting Carbon Observatory-3. 199

OEC Oxygen-Evolving Complex. 7

PAM Pulse Amplitude Modulation. 16, 17, 37

PAR Photosynthetically Active Radiation. 5, 16, 22, 29, 32, 33, 35, 113, 114, 136, 137, 140, 141, 146, 149, 151, 154, 155, 158–160, 162–165, 171, 197, 198, 201

PASWC Plant Available Soil Water Content. 43

PC Platocyanine. 7

PFT Plant Functional Type. 42, 46, 51, 79, 110–112, 123, 137, 158, 163, 181, 184, 187, 189, 190, 194, 195, 197, 199, 205

PG 2-phosphoglycolate. 9

PGA 3-Phosphoglycerate. 8, 9

PGK Phosphoglycerate kinase. 8

PheoD1 Pheophytin D1. 7

Pi Inorganic phosphate. 7

PM Penman-Monteith. 20, 144

PPFD Photosynthetic Photon Flux Density. 9, 14, 15, 22, 23, 113–115, 180

PQ Photochemical Quenching. 36, 136, 147, 160

PQH2 Plastoquinol. 7

PQi Plastoquinone. 7

PR Photorespiration. 9, 13

PRI Photochemical Reflectance Index. 201, 202

PSI Photosystem I. 6, 7, 12, 16, 30, 32, 37, 141, 146, 148, 158

PSII Photosystem II. v, 6, 7, 12, 16, 17, 30, 32, 36, 37, 131, 137, 141–143, 146, 148, 155, 159, 160, 165, 169–172, 174, 180

R_{ECO} Ecosystem Respiration. vi, 21–23, 181, 183, 196

RBD Root Biomass Density. xi, 45, 46, 166, 184, 185, 192

RCs Reaction Centers. 5, 6, 9, 12, 16

REW Relative Extractable Water. iv, vi, x–xii, 42, 43, 45, 46, 59–68, 70–73, 77, 79, 80, 82, 83, 86–88, 90–99, 109, 111, 112, 115, 117–119, 121–125, 129, 130, 145, 147–149, 152, 154–160, 163–166, 168, 173, 177–181, 183–187, 189–191, 196

ROS Reactive Organic Species. 12, 43, 44

RS Remote Sensing. vi, vii, 23, 27, 42, 177, 197–200, 202–204

Ru5P Ribulose 5-P. 9

Rubisco Ribulose 1,5-biphosphate carboxylase. 8

RuBP Ribulose-1,5-biphosphate. 8, 9, 31

RWU Root Water Uptake. 184, 192

SCOPE Soil Canopy Observation, Photochemistry and Energy fluxes. 137, 142

SFM Spectral Fitting Methods. 26, 140, 141, 180

SIF Sun-Induced chlorophyll Fluorescence. v, vi, xi, xii, 24–27, 29, 35–37, 52, 135–143, 145–149, 154, 158–160, 162–165, 171, 180, 181, 183, 188, 195–199, 201, 202, 204, 205

SMAP Soil Moisture Active Passive. 202, 203

SMOS Soil Moisture and Ocean Salinity. 202–204

SOL Stomatal Origin Limitation of photosynthesis. iii, vi, x, 44–46, 51, 52, 57–59, 62–64, 67, 69–71, 78–80, 83, 86, 87, 91, 96, 111, 115–118, 178, 180, 183, 187, 189, 190, 194

SPAC Soil-Plant-Atmosphere Continuum. ii, xii, 39–41, 187, 192, 195, 204

SPEI Standardized Precipitation Evaporation Index. 38

SVD Singular Vector Decomposition. 142

SWA Soil Water Availability. 43

SWC Soil Water Content. ii, 38, 39, 42, 43, 45, 60, 64, 67, 70, 79, 111–113, 130, 140, 145, 166, 177, 183–185, 189–191, 194, 195

SWP Soil Water Potential. vi, xii, 40–43, 183, 186, 187, 193–195

SWRC Soil Water Retention Curves. xii, 42, 43, 130, 183, 186, 194

TAW Total Available Water. 189, 190

TEMPO Tropospheric Emission Monitoring of POllution. 199

TIR Thermal InfraRed. 200

TPI Triose phosphate isomerase. 8

TPU Triose Phosphate Utilization. 30, 31

Tr Transpiration. 20, 37, 52, 135, 138, 139, 145, 156, 163, 165, 179, 180, 192

TROPOMI TROPOspheric Monitoring Instrument. 27, 138, 198

USO Unified Stomatal Optimality. iv–vi, xi, 34, 35, 44–47, 52, 58, 59, 61, 62, 71–73, 78, 111, 112, 115, 117, 118, 123, 126, 128, 135, 138, 139, 144, 145, 148, 156–159, 161–165, 167, 169, 171, 177, 179–182, 195, 196, 204, 205

UV Ultraviolet. 5, 11

VG van Genuchten. 42, 113, 186, 193

VOD Vegetation Optical Depth. 203–205

VPD Vapor Pressure Deficit. x, 3, 9, 14, 22, 29, 33, 39, 40, 58, 78, 110–113, 117, 118, 121–123, 126, 128–130, 138, 144, 179, 182, 195, 198

VRWC Vegetation Relative Water Content. 203

VWC Vegetation Water Content. 202–204

VWRC Vegetation Water Retention Curves. 204

WUE Water-Use Efficiency. 34, 35, 58, 62, 70–72, 115, 124, 125, 179

1

Introduction

1. Climate change

Since the middle of the 18th century, the concentration of carbon dioxide (CO_2) in the Earth's atmosphere has increased by about 52% up to a level that has never been reached since the mid-Pliocene, 3 million years ago (Keeling & Tans, 2023; Intergovernmental Panel On Climate Change, 2023). Anthropogenic fossil fuel emissions are responsible for the increase in CO_2 concentration, where coal burning still represented the largest contribution in annual carbon emissions in 2021 (Friedlingstein *et al.*, 2022). CO_2 emissions will cause irreversible changes in the climate, shifting conditions on Earth outside of the 'safe operating space' for humanity for at least the next millennia (Solomon *et al.*, 2009; Richardson *et al.*, 2023).

Once released in the atmosphere, CO_2 acts as a greenhouse: it absorbs and radiates heat in all directions, creating an insulating shell in the Earth's atmosphere. The fraction of solar energy radiated by the Earth's surface as heat towards the atmosphere is trapped and contributes to the 'greenhouse effect'. Climate model scenarios predict that the global surface temperature will increase within a range of 1.0°C to 5.7°C by the end of the 21st century compared to the 1850-1900 reference period (Masson-Delmotte *et al.*, 2021). A simulated change at 2°C global warming will cause an increase in 5°C to 7°C above the Arctic while Europe will warm up by 2°C to 3°C (Masson-Delmotte *et al.*, 2021).

The increase in the global surface temperature causes perturbations on the water cycle. One dominating thermodynamic constraint is the Clausius-Clapeyron (CC) equation, which predicts an increase in the water-holding capacity of the atmosphere (i.e., the saturated vapor pressure) of approximately 7% per degree Celsius of warming. In other words, the moisture content in the air must increase by 7% per degree Celsius to keep a constant relative humidity. Land surfaces warm up faster than oceans, mostly because of the predominance of sensible heat and longwave upward fluxes in the energy budget (Sutton *et al.*, 2007). As a result, the increase in saturated vapor pressure is higher over lands compared to oceans. However, the actual vapor pressure does not follow the CC rate and increases more slowly because of water atmospheric circulation and interactions between land surfaces and the atmosphere (Ficklin & Novick, 2017; Novick *et al.*, 2024). In particular, climate change is intensifying the strength of land-atmosphere feedbacks which limit evapotranspiration through, for instance, a lack of soil water, or by interacting with ecosystem carbon cycling (Ficklin & Novick, 2017). The difference between the saturation vapor pressure and the actual vapor pressure (i.e., the Vapor Pressure Deficit (VPD)) is a measurement of the evaporating force of the atmosphere, and acts as a major driver of the water cycle and plant-water relations (Grossiord *et al.*, 2020). Overall, a global increase in VPD has been observed in the past years and will continue to increase in a near future (Intergovernmental Panel On Climate Change, 2023).

The intensification of the hydrological cycle with climate change leads to very contrasting patterns of precipitation regimes. Although the increase in global mean precipitation is following the CC equation rate, major geographical heterogeneities in precipitation regime and distribution are observed because of the complex effects of climate change on the water cycle (Byrne & O'Gorman, 2015; Allan *et al.*, 2020). In particular, the occurrence of floods and extreme precipitation events is modulated by the availability of the water resource at the regional scale, also impacted by the seasonality of water availability (Tabari, 2020). Therefore, some regions are already facing an intensification of atmospheric water transport and precipitation frequency, while others are experiencing an increase in precipitation shortage episodes (Intergovernmental Panel On Climate Change, 2023). In Europe, major disruptions of seasonal precipitation regimes are expected with less precipitation on average but more frequent extreme events (Huo *et al.*, 2021). As a result, model simulations converge towards an increase in temperature and soil moisture anomalies in spring and summer across Europe, regardless of global warming scenarios (Spinoni *et al.*, 2018).

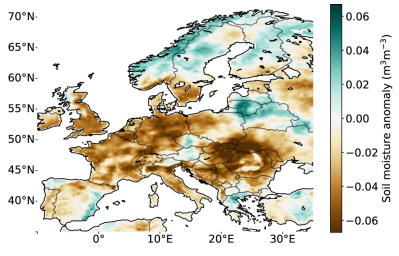

Figure 1.1: Soil moisture anomalies during the 2022 summer drought relative to the 1980–2022 reference period (not including 2022) in Europe. Soil moisture is taken from ERA5-Land (Muñoz-Sabater *et al.*, 2021). Adapted from Van Der Woude *et al.* (2023).

The increasing number of soil moisture and temperature anomalies over the past two decades in the Northern Hemisphere have shown that climate change is not only a model prediction, but is also becoming the new normal. These recent climate extremes include the 2003, 2018 and 2022 droughts (Ciais *et al.* (2005); Aalbers *et al.* (2023); Van Der Woude *et al.* (2023), Fig. 1.1), the 2010 heatwave in Russia, the 2020 warm anomaly over Siberia, or the combined droughts and heatwaves in Central Europe in summers 2015, 2018 and 2019 (Rousi *et al.*, 2022). Every year is a potential candidate for breaking previous-standing records (Fischer *et al.*, 2021). Summer droughts are also caused by a combination of lack of rainfall in winter and increasing evapotranspiration in early spring due to vegetation onset and seasonally increasing temperatures (Ionita *et al.*, 2020). Not only having considerable societal and economic impacts (Ionita & Nagavciuc, 2021; Yin *et al.*, 2023), water stress poses a major threat on terrestrial ecosystems. For instance, the 2003 drought caused a reduction in vegetation growth by ∼30% (Ciais *et al.*, 2005), while a reduction of net carbon uptake (∼60 TgC) by terrestrial ecosystems during the 2022 drought in Europe was observed (Van Der Woude *et al.*, 2023). Over the last five decades in Europe, crop losses have tripled (Beillouin *et al.*, 2020; Brás *et al.*, 2021). The combination of soil water stress and heatwave is the worst abiotic stress factor for global development (Yin *et al.*, 2023).

The net amount of CO_2 remaining in the atmosphere depends on the balance between CO_2 sources and natural sinks (i.e., land and ocean sinks). Each year, the land biosphere removes from the atmosphere around one third of the total carbon emitted by human activities (Friedlingstein *et al.*, 2022). The carbon uptake rate of land biosphere strongly depends on the ability of terrestrial ecosystems to keep removing carbon in the context of global climate change. Understanding the processes at the basis of CO_2 uptake by vegetation is pivotal for predicting ecosystem capacities to mitigate climate change in a near future (Rogger *et al.*, 2024).

2. Photosynthesis

The strength of the CO_2 land sink is regulated by the capacity of plants to convert atmospheric CO_2 into carbohydrates by photosynthesis as follows:

$$6CO_2 + 12H_2O + light \rightarrow C_6H_{12}O_6 + 6O_2 + 6H_2O \tag{1.1}$$

where the dioxygen (O_2) molecule released to the atmosphere originates from the oxidation of water (H_2O) and not from CO_2 (Blankenship, 2002). Not only photosynthesis uptake CO_2 from the atmosphere, but it also contributes to maintain O_2 concentration at a suitable level for sustaining life on Earth.

Photosynthesis is divided into four phases: (i) light is absorbed and transformed into chemical energy, (ii) electrons are transferred to reaction centers, (iii) solar irradiance energy is stabilized by the production of high energy molecules, and (iv) carbon is fixed, and final products are exported. In C3 plants (i.e., plants which produce a 3-carbon molecule from CO_2 fixation, see section 2.2), the first three phases are commonly referred to as the light reactions while the last phase is known as the Calvin-Benson-Bassham (CBB) cycle or dark reactions.

2.1. Absorption of light and electron transport

Light is absorbed by a complex structure combining proteins and pigments located in the thylakoids membrane within the chloroplasts, also known as Light Harvesting Centers (LHCs). Such structures regroup chlorophylls, carotenes and xanthophylls pigments. For example, one LHCs II monomer binds six chlorophylls *b*, eight chlorophylls *a* and four carotene molecules (Liguori *et al.*, 2015). LHCs are responsible for photon absorption and collection, acting like antennas within specific spectral regions. In particular, plant pigments can absorb solar irradiance between 400 nm and 700 nm (know as Photosynthetically Active Radiation (PAR)), with different peaks of absorbance. Chlorophyll pigments contain two major absorption bands in the Ultraviolet (UV) and Near-Infrared (NIR) regions, while carotenoids absorb most of the light in the near-UV (Fig. 1.2). LHCs concentrate sunlight energy towards Reaction Centers (RCs) where a cascade of redox reactions is initiated.

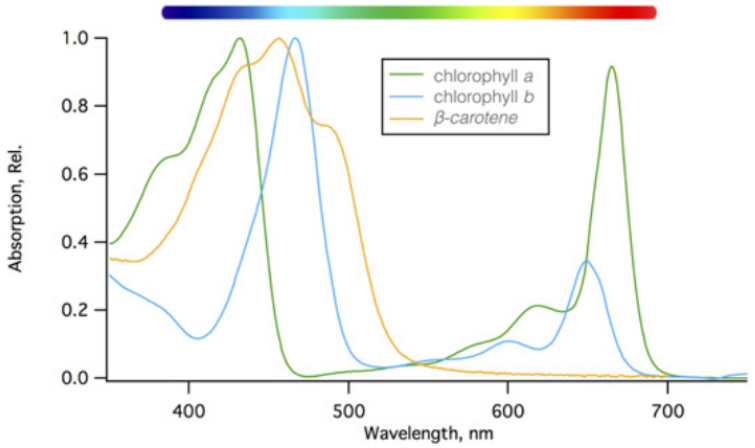

Figure 1.2: Absorption spectra of chlorophylls (chlorophyll a and chlorophyll b) and carotenoid (β carotene) pigments in plants (Johnson, 2016)

The light absorbed by LHCs excites pigments from ground to high electronic states. Before initiating photochemistry, this energy must be transferred to one of the RCs. This transfer of energy can be explained by the Förster theory (Förster, 1948), which is a very fast process (within femtoseconds) characterizing the nonradiative resonance transfer of energy between two chromophores (i.e., light-sensitive molecules). The Förster theory is based on several assumptions, including a weak coupling between two chromophores (distance superior to 10 nm) and an absence of quantum superpositions of excited electronic states. If these assumptions are met, the excitation can theoretically hop in a 'random walk' between two delocalized excitation states. As pigments are densely packed in LHCs, the hypothesises of the Förster theory are often challenged. Alternative mechanisms involving quantum coherence and excitons have been developed to describe the energy transfer dynamics in the antennas (Fassioli *et al.*, 2014; Ullah & Dral, 2022).

Photochemistry is initiated when the excitation energy is trapped by RCs, which are pigment-protein complexes, composed of chlorophylls, electron cofactors and hydrophobic peptides (Blankenship, 2002). RCs can lose or acquire an electron and therefore be oxidized or reduced. Once one of the RCs is promoted to a higher energy state by the electronic energy transferred by LHCs, it loses one electron to a primary acceptor, forming altogether an ion-pair state. This primary charge separation allows to transform electronic energy from solar irradiance into chemical energy. LHCs and RCs are regrouped within structural units known as Photosystem I (PSI) and Photosystem II (PSII), which differ by the main absorption bands of their primary acceptors, either at 680 nm (P680) or at 700 nm (P700).

PSII is the first complex in the light-dependant reactions of photosynthesis. Once excited, P680 is brought to an excited state ($P680^*$) and transfers one electron to the primary acceptor, a nearby Pheophytin D1 (PheoD1) molecule. P680 becomes photo-oxidized ($P680^*\bullet$) and the electron hole must be replenished by the oxidation of water. This chemical reaction, which consists in breaking two H_2O molecule into one O_2 while releasing four electrons and protons, is hard to initiate due to the high redox potential of H_2O (+820 mV). $P680^*\bullet$ is the strongest biological oxidizing agent and has a higher redox potential than H_2O (+1200 mV), which is sufficient to oxidize water (Johnson, 2016). However, more electrons are released from water oxidation than what is needed for reducing $P680^*\bullet$. Therefore, these highly reactive particles are stored in the Oxygen-Evolving Complex (OEC), a cluster of manganese, calcium and oxygen which has two main functions: binding water molecules and storing electrons from water oxidation. As the OEC can store up to four electrons, two water molecules are oxidized after four turnovers of primary charge separation. The OEC is connected to the reaction center by the active tyrosine and transfers, one at the time, the electrons needed to reduce $P680^*\bullet$. The OEC enzyme acts as a catalyst for water oxidation and is a key component of the light reactions of photosynthesis (Lubitz *et al.*, 2019). The electron carried by PheoD1 is then transferred to Plastoquinone (PQi), and ultimately reduced in Plastoquinol (PQH2) after the addition of two protons from the cytoplasm. As water oxidation releases four protons into the lumen while two protons are taken for forming PQH2, an electrochemical potential between the two sides of the thylakoid membrane is created, which contributes to the production of Adenosine Tri-Phosphate (ATP). PSII is also known as water-plastoquinone oxidoreductase for its ability to use light energy to oxidize water and to metabolically bound hydrogen.

Similarly, PSI utilizes light energy to bring the reaction center P700 to an excited state of energy ($P700^*$). One electron is lost by $P700^*$ (becoming $P700^*\bullet$) and is carried along a chain of electron carriers until ultimately being transferred to the final acceptor FerreDoxine (FD) (Grotjohann & Fromme, 2013). FD is one of the three substrates of Ferredoxin-NADP+ reductase (FNR) enzyme which catalyzes the production in the cytoplasm of the reduced form of Nicotinamide Adenine Dinucleotide Phosphate (NADPH) from the oxidized form of Nicotinamide Adenine Dinucleotide Phosphate (NADP+) by consuming one proton. The reduction of $P700^*\bullet$ is achieved by Platocyanine (PC) which transfers electrons from the Cytochrome b6f (cytb6f) to PSI. Not only providing a bridge for electrons between PSII and PSI, cytb6f and the Q-cycle oxidizes PQH2 and reduces PC (Malone *et al.*, 2021). The oxidation of PQH2 results in the release of protons in the lumen, thus increasing the H^+ concentration and supplying the proton gradient across the thylakoid membrane. The ATP synthase enzyme uses the energy provided by the electrochemical proton gradient to make ATP from Adenosine Di-Phosphate (ADP) and Inorganic phosphate (Pi). PSI, PSII and cytb6f are connected in series and allow the circulation of electrons in the thylakoid membrane from water oxidation to the production of NADPH by FNR. The final prod-

ucts of the light reactions and the electron transport chain are ATP and NADPH which provide chemical energy for CO_2 fixation by the CBB cycle (Fig. 1.3).

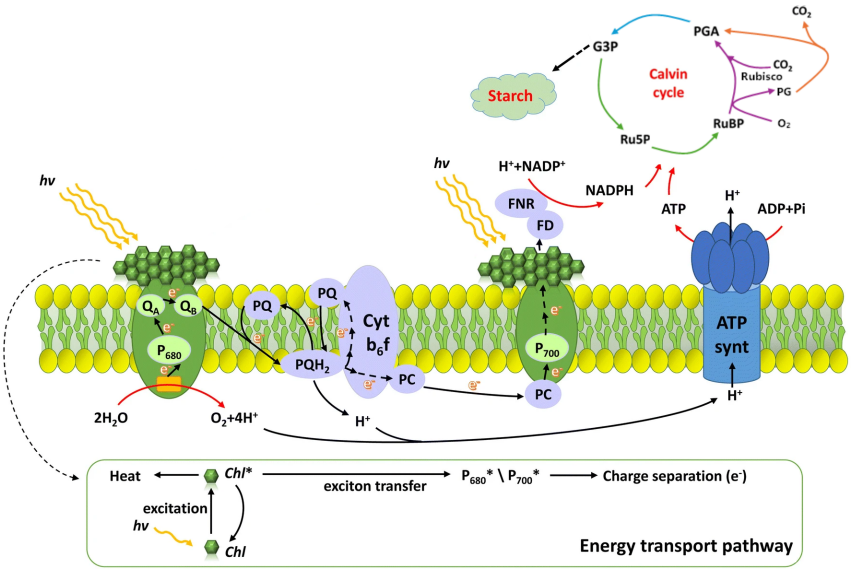

Figure 1.3: Schematic representation of the light and dark reactions of photosynthesis. The definition of acronyms can be found in the text. $h\nu$ is sunlight energy. In the CBB cycle, the purple, blue and green arrows represent respectively the fixation, reduction and regeneration steps. The orange arrow represents the photorespiratory cycle. The fatty acid synthesis is not represented. Adapted from Yang *et al.* (2020b) and Raines (2022).

2.2. CO_2 fixation

The CBB cycle (named after the American chemists Melvin Calvin, Andy Benson and James Bassham) is one of the most important biochemical cycles on Earth which fixes CO_2 into carbohydrates. It is a complex series of chemical reactions taking place in the chloroplast and divided into three phases: carboxylation, reduction, and regeneration (Blankenship, 2002). The carboxylation phase consists in the fixation of CO_2 into Ribulose-1,5-biphosphate (RuBP) which is catalyzed by Ribulose 1,5-biphosphate carboxylase (Rubisco). The fixation of CO_2 into RuBP gives two molecules of 3-Phosphoglycerate (PGA), which is an unstable carbon intermediate and is further phosphorylated by ATP into 1,3-Biphosphoglycerate (BPGA). NADPH is then needed for the reduction of BPGA into Glyceraldehyde 3-phosphate (G3P). The reduction of PGA in G3P consumes two molecules of ATP and NADPH and is catalyzed by Phosphoglycerate kinase (PGK) and 3-phosphate dehydrogenase (GAPDH). Triose phosphate isomerase (TPI) catalyzes the production of Dihydroxyacetone Phosphate (DHAP) from BPGA. BPGA and DHAP (also known as triose phosphates) are the starting point of the regeneration of RuBP. The triose phosphate pool is needed for

the regeneration of RuBP by the Ribulose 5-P (Ru5P) enzyme (Raines, 2022). These reactions consume one ATP for each CO_2 fixed. Since one G3P molecule has three carbon atoms, three CO_2 molecules must undergo the fixation and reduction steps to synthesize one GAP. In total, three ATP and two NADPH are needed for each CO_2 molecule fixed. Following the cycle stoichiometry, three CO_2 gives six BPGA and G3P. Among the six trioses phosphates produced by the fixation of three CO_2, five are used for RuBP regeneration and one is exported as carbohydrates.

Rubisco can also react with O_2 by photorespiration. This process releases one molecule of 2-phosphoglycolate (PG), which is a potential inhibitor of several enzymes involved in the CBB cycle and must be metabolized. The Photorespiration (PR) cycle converts PG into PGA which is fed back into the CBB cycle at the beginning of the reduction phase. The PR cycle also releases CO_2 by the conversion of glycine into serine in the mitochondria and produces hydrogen peroxide in the peroxisome (Busch, 2020; Shi & Bloom, 2021). The CO_2 concentration at which the rate of photorespiration equals the rate of photosynthesis is known as the CO_2 compensation point. Photorespiration (also known as 'respiration in the light') affects the net balance of CO_2 assimilated by plants. An overview of the light reactions and the CBB cycle is given below (Fig. 1.3).

Photosynthesis is strongly limited by the supply of CO_2 to chloroplast and the light intensity which fuels ATP and NADPH to the CBB cycle by the light reactions. The tight link between dark and light reactions leads to a nonlinear relationship between net CO_2 assimilation and solar irradiance, as illustrated by Light-Response Curve (LRC)s describing how net photosynthesis reacts to changes in light intensity (measured by the Photosynthetic Photon Flux Density (PPFD)). These curves show a strong increase in photosynthesis at low PPFD, before a gradual decrease of the slope and a saturation from a specific PPFD threshold where all RCs are closed and all primary acceptors oxidized. Very similar trends are observed when characterizing the response of photosynthesis to the increase in CO_2 supply. These two curves provide key information on the maximum capacities of plants for absorbing light and assimilating CO_2 (Kubiske & Pregitzer, 1996; Zi-Piao, 2010). Combining these measurements with models of photosynthesis provide key information on the response of plants to a changing climate (see section 4, (Sharkey *et al.*, 2007)).

2.3. Diffusion of gases from the leaf surface to chloroplasts

CO_2 diffusion to chloroplasts is a key factor limiting photosynthesis. Stomata are pores on the epidermis of leaf cells, which are bounded by guard cells and provide a direct pathway for CO_2 diffusion (Fig. 1.4). Many factors control stomatal opening, such as light intensity, VPD or molecular signaling (Buckley & Mott, 2013). For instance, stomata open as light intensity increases due to photoreceptors of blue light located on the guard cells (Shimazaki *et al.*, 2007). Under high VPD, water is being

evaporated from guard cells which causes membrane depolarization and stomatal closure (i.e., hydropassive mechanism). Stomata may also close in response to molecular signaling under drought by sensing of soil water status (i.e., hydroactive mechanism (Cowan, 1978)). Whether one contribution is predominent over the other is however often difficult to assess (Franks, 2013). Due to the difference in CO_2 and H_2O concentration between the inside of the leaf and the outer surrounding atmosphere, the opening of stomata leads to a diffusion of CO_2 to the mesophyll and an unavoidable loss of water by transpiration.

Stomatal response is coordinated to use the direct benefit of stomatal opening (i.e., fueling photosynthesis by facilitating CO_2 diffusion) while avoiding the corresponding penalty (i.e., losing water and increasing the risk of cavitation, Fig. 1.4, (Cowan & Farquhar, 1977)). This hypothesis has led to numerous optimization models which aimed at predicting stomatal conductance over a wide range of environmental conditions (Wang *et al.*, 2020b).

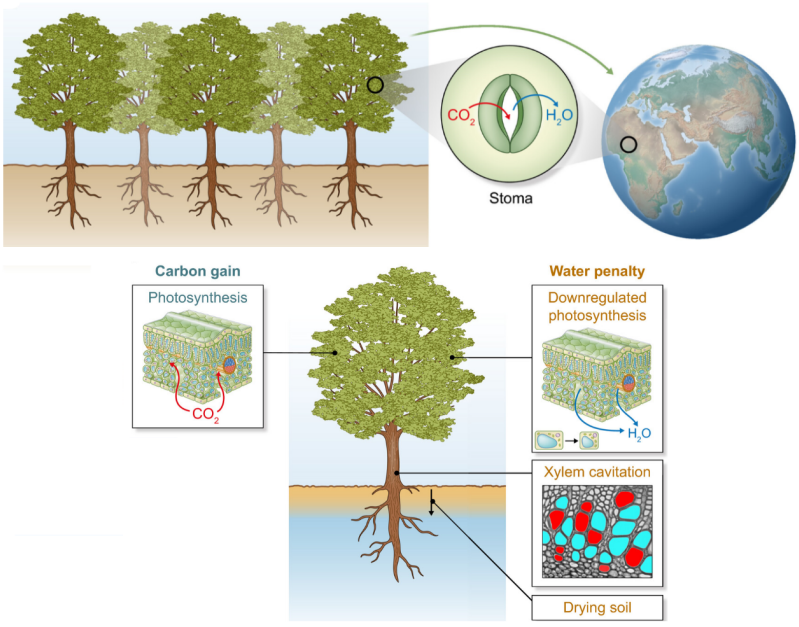

Figure 1.4: Stomata are tiny pores on leaf epidermis allowing CO_2 diffusion to chloroplasts where carbon fixation occurs. This carbon gain through photosynthesis comes at the expanse of a loss of water by transpiration, which increases the risk of cavitation under dry soil conditions. Adapted from Wang *et al.* (2020b).

The diffusion of CO_2 in the plant cells is also mediated by the size of mesophyll airspaces which forms a continuum for CO_2 diffusion to chloroplasts. A series of aqueous (i.e., diffusion through cell walls, lipid membranes, liquid cytoplasm and stroma)

and gaseous (i.e., diffusion through leaf mesophyll airspaces) barriers affect photosynthesis by limiting CO_2 diffusion. These diffusive limitations on photosynthesis are represented as two distinct conductances (i.e., the stomatal and mesophyll conductance) which determine the CO_2 flux through the cell by the Fick's diffusive law. Mesophyll conductance varies accordingly to anatomic traits (e.g., cell wall thickness or chloroplast surface area exposed to intercellular airspaces per unit of leaf area) or biochemical components (e.g., aquaporins or changes in carbonic anhydrase activity) (Flexas *et al.*, 2018a; Baillie & Fleming, 2020). It is a key ecophysiological parameter which allows to identify the diffusive constraints on photosynthesis others than stomatal closure and also characterizes the ability of CO_2 to diffuse through airspaces to the fixation sites in the chlorplasts (Fig. 1.5). Stomatal and mesophyll conductance are pivotal plant traits which limit the CO_2 diffusion to chloroplasts. Identifying the response of these diffusive conductances to environmental drivers is crucial for predicting the effects of climate change on plant gas exchanges.

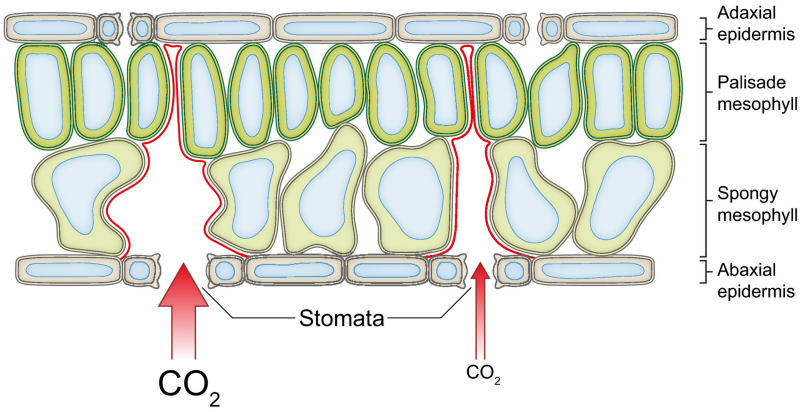

Figure 1.5: Leaf structure can increase CO_2 diffusion to chloroplasts through airspaces by rearranging mesophyll architecture. The red area represents the CO_2 diffusive continuum including substomatal cavities and mesophyll airspaces. Adapted from Baillie & Fleming (2020).

2.4. Fluorescence

As detailed in section 2.1, chlorophyll pigments have two absorption peaks in the NIR and UV regions, resulting in the absorption of blue photons ($\sim$ 400-500 nm) and red photons ($\sim$ 600-700 nm) by LHCs. Photon absorption by chlorophyll triggers the electron transfer from a ground state orbital (S_0) to a higher excited state orbital (S_1 or S_2) (Gouterman, 1961). Hopping from S_0 to S_1 requires less energy than hopping from S_0 to S_2. Therefore, the absorption of a blue photon brings an electron from S_0 to S_2 and a red photon from S_0 to S_1. The electron transferred in S_2 is highly unstable, and rapidly decays by molecular vibration (internal conservation) to S_1 (Fig. 1.6).

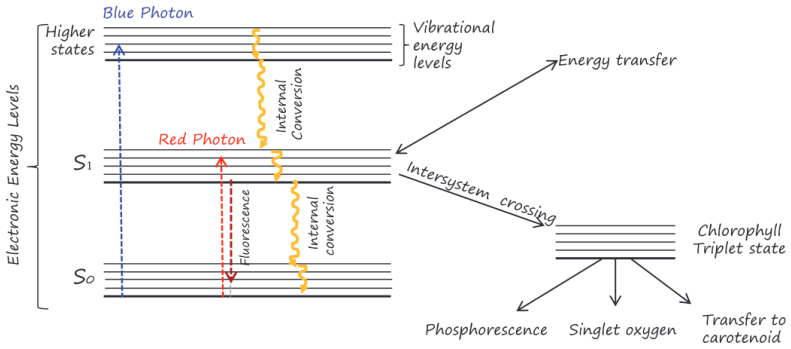

Figure 1.6: Idealized Jablonski diagram of the fates of electrons on chlorophyll excitation states (S_0, S_1). Higher states correspond to S_2. Adapted from Porcar-Castell *et al.* (2014)

The electron on S_1 has three possible fates: either returning to S_0, being lost as heat by molecular vibration, or being transferred to other chlorophyll pigments of the light harvesting complex through resonant energy or exciton transfer. This transfer (know as intersystem crossing) can lead to the formation of chlorophyll triplets, which can relax by transferring the energy to carotenoids, by phosphorescence or by reacting with oxygen producing reactive singlet oxygen (Clegg, 2004). These Reactive Organic Species (ROS) are highly reactive and can lead to damages in the cell by absorbing electrons from stable molecules or by disrupting cell functioning (Tripathy & Oelmüller, 2012). Returning to S_0 from S_1 can be done by molecular vibration or by emitting a photon at a longer wavelength than the absorbed photon. This process, known as Chlorophyll Fluorescence (ChlF), characterizes the emission of a photon resulting from an electron hopping from S_1 to S_0 (Fig. 1.6). The emission spectra of ChlF has two peaks, one at $\sim$ 685 nm in the red, and one at $\sim$ 740 nm in the NIR. While PSII contributes to these two peaks, PSI only emits at 740 nm (Fig. 1.7).

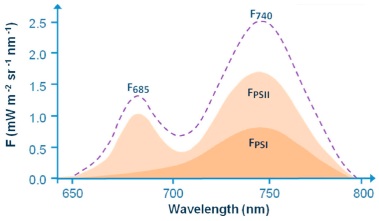

Figure 1.7: Chlorophyll fluorescence emission spectrum under steady state conditions. Two peaks can be observed at 685 nm (F_{685}) and 740 nm (F_{740}) resulting from the contribution of PSI (F_{PSI}) and PSII (F_{PSII}) emission spectra (Mohammed *et al.*, 2019)

Once on the saturation plateau of the LRC (i.e., RCs fully closed) or under stressed conditions (i.e., high temperature or low soil moisture), plants can no longer use all the incoming energy carried by solar irradiance for fixing CO_2. This excessive energy must be dissipated by alternative processes which are pivotal for avoiding stress on plants. Balancing the utilization and absorption of light energy to minimize the potential photo-oxidative damage is therefore crucial. Non-Photochemical Quenching

(NPQ) regroups the different mechanisms utilized by plants to dissipate the excess of energy mainly through heat, including internal conservation and intersystem crossing (Demmig-Adams *et al.*, 2014). Photosynthesis, fluorescence and heat dissipation are in competition for the incoming light energy. As a result, ChlF measurements can provide key information on carbon assimilation and on the the physiological barriers on CO_2 diffusion (Porcar-Castell *et al.*, 2021). An overview of the light and dark reactions of photosynthesis including ChlF and NPQ is given below (Fig. 1.8).

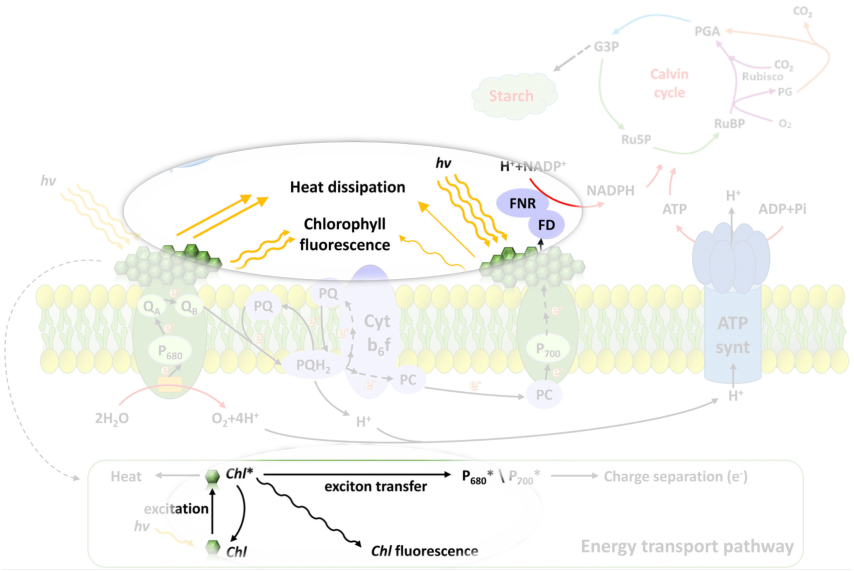

Figure 1.8: Heat dissipation and chlorophyll fluorescence in the light reactions of photosynthesis. The definition of acronyms can be found in the text. $h\nu$ is sunlight energy. In the CBB cycle, the purple, blue and green arrows represent respectively the fixation, reduction and regeneration steps. The orange arrow represents the PR cycle. The fatty acid synthesis is not represented. Adapted from Yang *et al.* (2020b) and Raines (2022).

3. Estimating photosynthesis and fluorescence at different spatial scales

Measuring photosynthesis is crucial for understanding how plants respond to changing environmental conditions. Moreover, ChlF provides additional information that can help in identifying the constraints of drought on the carbon cycle. The following section details the methods for measuring photosynthesis and fluorescence at the leaf level and at the ecosystem level.

3.1. Leaf-level measurements

3.1.1. Gas exchanges

Gas exchange systems measure the gas concentration (either CO_2 or H_2O) with an Infrared Gas Analyser (IRGA) and the flow rate at which the air interacts with leaf tissues. The technique used in IRGAs exploits the absorption proprieties of CO_2 and H_2O in the infrared wavelengths. In particular, IRGAs use an infrared source and detector to measure the difference of infrared radiation which depends on the concentration of the tracer. Most of commercially available gas exchange systems are designed to measure the response of carbon assimilation and transpiration to a wide variety of environmental conditions which can be set by the user (e.g., H_2O, CO_2 concentrations or light intensity). Gas exchange measurements are conducted by enclosing a part of a leaf (or the entirety) within a cuvette. Although many cuvette types exist to cover the wide variety of leaves anatomy, the characteristics of the cuvette must maintain uniform climate conditions across the leaf. For instance, cuvettes are constructed from a metal with high thermal conductivity and painted to reflect most of the solar radiation (Bernacchi *et al.*, 2012). The following paragraph details the functioning of the LI-COR LI-6400 device (LI-COR Inc., Lincoln, NE, USA), which has been and continues to be, used in numerous studies conducted in photosynthesis research (Savvides & Fotopoulos, 2018). This device is available at the Biosystem Dynamics and Exchanges (BIODYNE) research department of Gembloux Agro-Bio Tech. It was used in this thesis in chapter 5 and 6.

In an open system such as the LI-6400, the air flows into the console, and passes through a CO_2 scrubber and a desiccant, allowing to set specific concentrations in H_2O and CO_2 in the air surrounding the leaf sample by adjusting bypass valves. When the system is equipped with a CO_2 mixer, the CO_2 concentration in the air flow can be increased up to more than 2000 ppm to build CO_2 response curves. The flow rate is measured and adjusted by a flow meter and a pump before circulating through the cuvette in the sensor head. Two IRGAs are used to measure independently the gas concentration within the cuvette (i.e., the 'sample') and in a parallel branch of the circuit that does not interact with the cuvette (i.e., the 'reference'). In addition, the incident PPFD is measured by a quantum sensor on the sensor head. The PPFD inside the chamber can be set to ambient level or to a specific value by a parameterization of the LED light source to build light-response curves. Finally, leaf temperature is measured by a thermocouple in contact with the leaf sample while air temperature is measured by a thermistor located beneath the IRGA circulation fan. Many air humidity variables are also computed from the H_2O concentration and temperature measurement such as relative humidity, VPD or dewpoint temperature.

Open IRGA systems use measurements of sample and reference H_2O and CO_2 concentrations, as well as the flow rate to calculate the transpiration and the net carbon assimilation rate (A_n). This latter corresponds to photosynthesis (A) minus leaf respi-

ration (R_d):

$$A_n = A - R_d \tag{1.2}$$

R_d can be estimated by measuring the net CO_2 flux on a dark-adapted sample ($A = 0$ in Eq. 1.2), by being set as a fraction of photosynthetic capacities (see 4), or by being neglected when $A >> R_d$ under high irradiance. In addition, the degree of stomatal opening can be estimated by the calculation of the stomatal conductance from transpiration measurements and molar concentration of water vapor within the leaf by Fick's law of diffusion (Farquhar & Sharkey, 1982). Such system provides a complete characterization of leaf gas exchanges in a wide variety of environmental conditions through, for instance, light and CO_2 response curves. In these cases, the net assimilation rate is measured in response of changes in PPFD and reference CO_2 concentration. Instantaneous measurements are also very useful to measure plant responses to changes in ambient climate conditions over time, or to compare values between species.

Gas exchange measurements rely on steady state conditions at the leaf surface. Equilibrium must be reached before each measurement, which means that the variation through time of sample H_2O and CO_2 concentration must be minimum. The LI-6400 software provides stability variables to help in logging the measurements at the right time, such as the variation coefficient or the rate of change over time. Waiting for stability can take up to 1 hour, which makes leaf level measurements time-consuming and limits the maximum number of measurements per day. Problems can also be encountered, such as cuvette leakages, lateral fluxes through leaves or calibration issues (Bernacchi *et al.*, 2012), which may alter the interpretation of measurements. Despite these issues, gas exchange measurements have become the standard benchmark for measuring photosynthesis and transpiration at the leaf level when compared to other techniques (Siebers *et al.*, 2021).

Upscaling leaf-level measurements over space and time is challenging when using gas exchange systems. Not only time and labor-consuming, it also requires a representative sampling throughout the canopy and the study site for integrating the complexity of the ecosystem structure. The fraction of sunlit and shaded leaves, the leaf angle orientation to the sun, or the micro-climate gradients within the canopy are issues that are difficult to assess when upscaling local measurements over space. It is practically impossible to make enough measurements without sampling artefacts (Baldocchi, 2014). Another type of gas exchange measurement device is canopy chambers, which are whole plant enclosure systems allowing to measure plant-scale processes. Such systems are typically used to study the impact of increasing CO_2 concentration on vegetation processes, the exchanges processes of reactive trace gases, or continuous measurements of photosynthesis and transpiration (Perez-Priego, 2021). Although very suitable for measuring net fluxes of uniform and short vegetation, this technique suffers from several issues (Baldocchi, 2014; Perez-Priego, 2021). For instance, cham-

bers affect plant's microclimate by damping turbulent mixing or increasing humidity and heat. Moreover, many chambers are needed to sample the canopy (i.e., between 10 and 20). Such density is rarely seen in the literature (Baldocchi, 2014).

3.1.2. Measurements of chlorophyll fluorescence with active techniques

ChlF has been used for many years to monitor the photosynthetic activity of plants. ChlF intensity measurements can be used to infer many physiological parameters such as the proportion of open PSII RCs, the PSII maximum efficiency, or the PSII operating efficiency (Baker, 2008). In particular, this last characterizes the efficiency at which light absorbed by PSII is used for primary acceptor reduction, and is directly related to the electron transport rate and to carbon assimilation. These parameters are calculated from ChlF intensities in different light conditions. ChlF measurements consists in measuring the peak of ChlF induced by a pulse from a light source at a specific wavelength (usually at $\sim$ 650 nm to drive electron hopping from S_0 to S_1, Fig. 1.6). Such measurements are 'active' because the ChlF peak results from the application of a saturating pulse on the leaf. One of the challenges for measuring ChlF intensities is the identification of the ChlF peak among the natural sunlight reflected by the plant and the incident sunlight in the red and infrared bands. While not being necessary for the determination of photosynthetic parameters relying on dark-adapted sample measurements such as the PSII maximum efficiency, this is essential for deriving key parameters of the electron transport chain and the CBB cycle.

The key feature of active ChlF measurement devices is the selective capacity of the detection system to separate the ChlF signal from the ambient and reflected light within the chamber. Pulse Amplitude Modulation (PAM) fluorometers use lock-in amplifiers to measure the ChlF changes induced by the measuring light (i.e., the light signal which drives the ChlF peak) while ignoring the ChlF changes induced by the actinic light (i.e., the light signal which drives photo-chemistry - a full review of PAM fluorometry is given in Schreiber (2004) and in Cornic & Massacci (2004)). A typical ChlF quenching analysis from PAM fluorometry is described in Fig. 1.9. The analysis begins with a dark-adapted leaf, which has primary acceptors fully oxidized and RCs open. The measuring light is turned on, and the leaf is exposed to a very low PAR, resulting in a minimum level of ChlF (F_0) while primary acceptors remain fully oxidized. A saturating pulse is then applied (several thousand μmolm^{-2}s^{-1} in less than 1 s) to drive the closure of RCs and allow the measurement of the maximum ChlF intensity in the dark (F_m). The actinic light (the light driving the partial reduction of primary acceptors in PSII) is then set to a specific value, and the ChlF emission of a light-adapted sample (F_s or F) is measured. A saturating pulse is once again applied to fully reduce PSII primary acceptors and gives the maximum ChlF intensity in the light ($F_m^{'}$). Finally, the actinic light is turned off, and a weak far-red pulse of light is applied simultaneously to excite PSI RCs and to remove electrons on the primary acceptors, giving the minimum ChlF intensity in the dark ($F_0^{'}$) of a light-adapted sample.

Assuming a 'lake' model describing the structure of RC and antennas, the maximum quantum yield (i.e., the ratio of photons used for a process to the photons absorbed by the leaf) of PSII in the dark ($\phi_{PSII,max}$) or the quantum yield of PSII in the light (ϕ_{PSII}) and the fraction of open PSII centers (q_L) are directly calculated from ChlF intensities as (Baker, 2008):

$$\phi_{PSII} = \frac{F_m^{'} - F_0^{'}}{F_m^{'}} \tag{1.3}$$

$$\phi_{PSII,max} = \frac{F_m - F_0}{F_m} \tag{1.4}$$

$$q_L = \frac{F_m^{'} - F_s}{F_m^{'} - F_0^{'}} \frac{F_0^{'}}{F_s} \tag{1.5}$$

ChlF quenching analysis is a key tool for estimating the photosynthetic capacities of leaves. Actively-induced ChlF measurements can be coupled with gas exchange measurements, giving a complete set of parameters for characterizing photosynthetic capacities of a plant and limiting factors of photosynthesis. For example, the mesophyll conductance to CO_2 diffusion can be determined from ϕ_{PSII} and gas exchange measurements of the substomatal CO_2 concentration (detailed in section 4). These measurements can be performed using a LI-6400 device with a LI-6400-40 leaf chamber fluorometer which has similar technical properties as PAM fluorometers. The fluorescence chamber is available at the BIODYNE research department.

ChlF measurements with active techniques can only be performed at the leaf scale, so the same spatial extrapolation issues as gas exchange measurements are encountered (Amoros-Lopez *et al.*, 2008). Moreover, the physiological interpretation of ChlF measurements resulting from the application of saturating pulses with an intensity much greater than what plants experience in natural conditions may be challenged. The recent development of the Light-Induced Fluorescence Transients (LIFT) device aimed at overcoming these spatial upscaling issues (Raesch *et al.*, 2014; Kolber *et al.*, 2005; Pieruschka *et al.*, 2014). The first versions of LIFT devices used a laser beam to project the excited signal from a distance up to 50 m away onto a target area of about 100 cm² (Raesch *et al.*, 2014; Moya *et al.*, 2019). Because of the raising concerns for eye safety involving the use of lasers in terrestrial environments, Osmond *et al.* (2017) developed an eye-safe LIFT prototype using light emitting diodes rather than laser, which is suited for measuring photosynthesis parameters at a distance inferior to 2 m (Osmond *et al.*, 2017; Keller *et al.*, 2019). However, several aspects of the LIFT technique complicate the interpretation of ChlF measurements and the comparison with PAM fluorometry such as the influence of complex dense canopies or changes in leaf angle due to wind which impacts scattering and absorption proprieties of the target

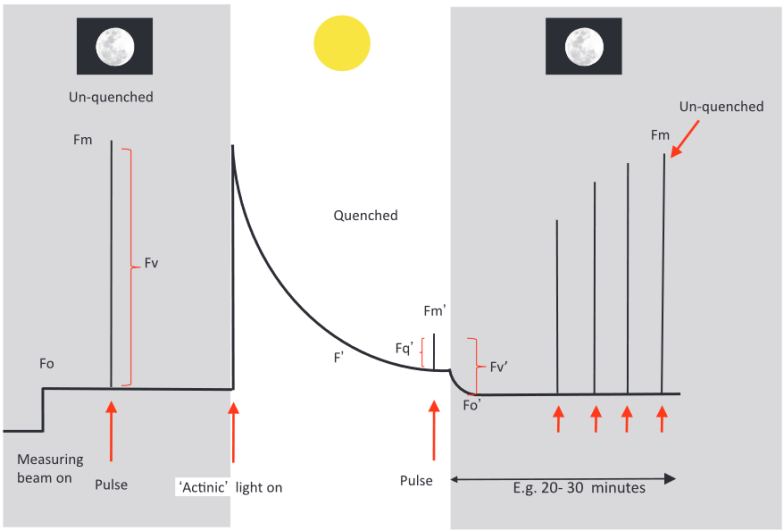

Figure 1.9: Example of ChlF quenching analysis using PAM fluorometry (Murchie & Lawson, 2013).

areas (Pieruschka *et al.*, 2014). Although promising for measuring photosynthetic parameters at larger scales, data analysis and processing with the LIFT technique needs further development (Pérez-Bueno *et al.*, 2019).

3.2. Ecosystem-level measurements

3.2.1. Eddy covariance

Undoubtedly, measuring gas exchanges at the interface between ecosystems and the atmosphere would significantly increase understanding of the functioning of ecosystems and the interactions with environmental drivers. The theoretical framework for measuring gas exchanges at the ecosystem surface was proposed by Montgomery (1948), Obukhov (1951) and Swinbank (1951). Sensors providing continuous measurements of flux densities at a high frequency were developed few decades later in the 90's. Since then, the Eddy Covariance (EC) technique has become widely used in climatology and ecophysiology, as it integrates the complexity of plants and canopies into a single high frequency measurement of gas exchanges.

3.2.1.1 Physical principle and main equations

The net flux exchanged at the ecosystem-atmosphere interface is calculated from the covariance between turbulent fluctuations of vertical wind and the dry mole fraction of the gas of interest (Foken *et al.*, 2012):

$$F_{EC} = \overline{\rho_d \, w \, s} \tag{1.6}$$

with F_{EC} the EC flux, ρ_d the dry molar air density, w the vertical wind speed and s the dry mole fraction of the gas of interest. Eq. 1.6 can be decomposed into the sum of the time-mean part and the fluctuation part (i.e., the Reynolds decomposition):

$$F_{EC} = \overline{(\overline{\rho_d} + \rho_d')(\overline{w} + w')(\overline{s} + s')} \tag{1.7}$$

with $'$ denoting the fluctuation term and $\overline{w}$, $\overline{\rho_d}$, $\overline{s}$ the time-mean terms. Eq. 1.7 is further simplified into:

$$F_{EC} = \overline{\rho_d} \, \overline{w} \, \overline{s} + \overline{\rho_d} \, \overline{w's'} + \overline{s} \, \overline{\rho_d' w'} + \overline{\rho_d' w'} \, \overline{s'} \tag{1.8}$$

As the air density fluctuations are assumed to be negligible (which is the case over flat and vast spaces) as well as the mean vertical flow (for homogeneous horizontal terrains), Eq. 1.8 can be written as:

$$F_{EC} \simeq \overline{\rho_d} \, \overline{w' \, s'} \tag{1.9}$$

Eq. 1.9 is valid only if most of the vertical transfer is assumed to be driven by eddies. Integrating the one-point equation conservation of dry mole fractions in the control volume (i.e., a parcel of air above the surface and below the height of measurements h_m) gives the total ecosystem flux (F_{ECO}) (Foken *et al.*, 2012):

$$F_{ECO} = F_{EC} + \int_0^{h_m} \overline{\rho_d} \frac{\overline{\delta s}}{\overline{\delta t}} dz = F_{EC} + F_S \tag{1.10}$$

Eq. 1.10 shows that the total flux exchanged between the ecosystem surface and the atmosphere is the sum of the EC flux (F_{EC}) and the storage flux (F_S) which is calculated from the integration of temporal changes over a time interval of the dry mole fraction with height ($\int_0^{h_m} \overline{\rho_d} \frac{\overline{\delta s}}{\overline{\delta t}} dz$). Storage calculations are important when turbulence is not the main governing transport, in case of low wind, stable stratification or decoupling between the surface and the atmosphere. Nighttime is often a critical period as most of these conditions are observed. Above homogeneous terrains, for small canopies and when turbulence is present, the storage flux may be neglected. Eq. 1.10 can be therefore simplified as (Foken *et al.*, 2012):

$$F_{ECO} = F_{EC} \simeq \overline{\rho_d} \overline{w's'} \tag{1.11}$$

which is the equation for EC fluxes calculation (Burba, 2021). Eq. 1.11 is valid for any gas and corresponds to the product of the mean air density and the mean covari-

ance between instantaneous deviations in vertical wind speed and dry mole fraction. Sensible heat (H) and Latent heat (LE) fluxes are calculated in a similar fashion:

$$H = \overline{\rho}\, c_p\, \overline{wT'_a} \tag{1.12}$$

$$LE = \lambda \frac{M_w/M_a}{P} \overline{\rho_d}\, \overline{we'_a} \tag{1.13}$$

where ρ is wet molar air density, c_p is heat capacity, T_a is air temperature, M_w/M_a is the ratio of molar masses of water and air, P is air pressure and e_a is air vapor pressure. The latent heat flux characterizes a flux of water changing from liquid to gaseous phase.

LE flux measurements can be used to derive canopy-scale stomatal conductance. In particular, LE is related to the water vapor pressure gradient between the ecosystem surface and the atmosphere, and the conductances opposing to the water vapor transfer to the atmosphere:

$$LE = \frac{\rho_a\, c_p\, (e^*(T_s) - e_a)}{\gamma} \frac{G_{aw}\, G_{sw}}{G_{aw} + G_{sw}} \tag{1.14}$$

with $e^*(T_s)$ the saturated air vapor pressure calculated at surface temperature (T_s), ρ_a the air density, c_p the heat capacity of dry air, γ the psychrometric constant, G_{aw} the aerodynamic resistance and G_{sw} the canopy-scale stomatal conductance to water vapor. When T_s is not measured, Eq. 1.14 can be written as:

$$LE = \frac{\Delta\, (R_n - G) + \rho_a\, c_p (e^*(T_a) - e_a)\, G_{aw}}{\Delta + \gamma(1 + \frac{G_{sw}}{G_{aw}})} \tag{1.15}$$

with G_{sw} the canopy-scale stomatal conductance to water vapor transfer, R_n the net radiation, G the ground heat flux and T_a the air temperature. Eq. 1.15 is also known as the Penman-Monteith (PM) equation (Monteith, 1965) and is widely used for (i) estimating the latent heat flux at the ecosystem scale from meteorological measurements (Maes *et al.*, 2019), and (ii) estimating canopy conductance to water vapor from LE measurements, under the assumption that evaporation is negligible compared to Transpiration (Tr) (i.e., LE∼Tr (Knauer *et al.*, 2018a)). Partitioning LE into evaporation and Tr is a currently active research topic (Nelson *et al.*, 2020). One of the most straightforward approaches for estimating Tr from LE measurements is to filter EC data for selecting active vegetation periods when the canopy surface is dry. Canopy dryness can be evaluated by calculating an index from a water balance model (Nelson *et al.*, 2018) or by excluding a certain number of days after a precipitation event (at least 2 days (Knauer *et al.*, 2018b)).

3.2.1.2 Eddy covariance setup

EC systems are composed of two key components which measure the wind speed in three dimensions, and the concentration of the gas of interest. The IRGA and the high-frequency three-dimensional (3D) sonic anemometer are both placed on a tower or on a mast. The wind speed is determined by knowing the forward and return transit time of ultrasonic pulses sent between two 3D sonic anemometers transductors. The air temperature can also be deduced from the speed of sound, calculated by the average of the inverse of the return and forward transit times. 3D sonic anemometers used in EC are made of three pairs of transductors, which are orientated to minimize wind perturbation and to reduce the impact of rain. A conversion to orthogonal 3D is needed to determine the wind speed in three dimensions (Aubinet, 2023).

Figure 1.10: Example of an eddy covariance system configuration with a three-directional sonic anemometer (Gill HS-50) and a closed-path infra-red gas analyzer (LICOR 7200). Photo taken in BE-Lon.

Gas concentrations are measured by the far-red absorption spectrometry. Most recent IRGAs used in EC have an enclosed path (Rebmann *et al.*, 2018), which allows to measure gas concentration during precipitation and icing, and do not require a filter for eliminating sunlight interference (Burba *et al.*, 2010). Enclosed analyzers use short intake tubes to pump the air to the measurement chamber, which minimizes frequency losses and sorption-desorption of water molecules (Burba *et al.*, 2010). Both IRGA and 3D sonic anemometer must be separated from the smallest distance possible to minimize frequency losses (Aubinet, 2023). A typical setup is shown in Fig. 1.10. More details about data post-processing steps are given in Aubinet *et al.* (2012) and Aubinet (2023).

3.2.1.3 Partitioning of the net CO_2 flux

The EC technique measures the Net Ecosystem Exchange (NEE) at the ecosytem-atmosphere interface, which is composed of Gross Primary Production (GPP) (i.e., the total amount of carbon fixed by all plants) and Ecosystem Respiration (R_{ECO}) (i.e., autotrophic and heterotrophic respiration):

$$F_{ECO} = NEE = R_{ECO} - GPP \tag{1.16}$$

GPP (or R_{ECO}) corresponds to a downward (or inward) carbon flux and is counted negative (or positive) by convention. When $|GPP| > |R_{ECO}|$, the ecosystem fixes more carbon through photosynthesis than it emits through respiration. A carbon sink is

therefore characterized by NEE<0 and a carbon source by NEE>0. Eq. 1.16 is the equivalent form of Eq. 1.2 written for a net CO_2 flux measured at the ecosystem scale.

An important step for interpreting EC measurements in physiological and modeling studies is the separation of NEE into GPP and R_{ECO}. This is carried out by partitioning methods, which are commonly classified into two categories. Either R_{ECO} is determined from nighttime CO_2 fluxes measurements (i.e., $GPP = 0$ in Eq. 1.16) and extrapolated with temperature (i.e., the NightTime (NT) partitioning method (Reichstein *et al.*, 2005)), or R_{ECO} is determined from daytime CO_2 fluxes measurements using the intercept of light response curves of NEE (Falge *et al.*, 2001). One important bias of the NT method is that it relies on data which can be significantly affected by low turbulence or advection, resulting in a limited dataset for extrapolating R_{ECO} with temperature. Lasslop *et al.* (2010) combined the two approaches by proposing a modified partitioning method using both the temperature-dependance of R_{ECO} and the light response curve of NEE. In this method, nighttime CO_2 measurements are first extrapolated with air temperature using an Arrhenius-type model:

$$R_{ECO} = R_b \exp\left[E_0\left(\frac{1}{T_{ref}-T_0}-\frac{1}{T_a-T_0}\right)\right] \tag{1.17}$$

where R_b is the base respiration at the reference temperature T_{ref} (set to 15 °C), E_0 is the temperature sensitivity, T_0 is set to -46.02 °C and T_a is air temperature (which can be replaced by soil temperature - the choice of driving temperature for R_{ECO} is discussed in Lasslop *et al.* (2012)). The rectangular hyperbolic light response curve (Falge *et al.*, 2001) is then modified to account for the temperature effect on R_{ECO} to model NEE using daytime data:

$$NEE = \frac{\alpha_{NEE}\,\beta_{NEE}\,R_g}{\alpha\,R_g + \beta_{NEE}} - R_b \exp\left[E_0\left(\frac{1}{T_{ref}-T_0}-\frac{1}{T_a-T_0}\right)\right] \tag{1.18}$$

where R_g is global radiation (can be replaced by PPFD, Gilmanov *et al.* (2013)), α_{NEE} is the canopy light utilization efficiency (representing the initial slope of the light response curve) and β_{NEE} the maximum NEE at light saturation. Modeling solely NEE from PAR and temperature without accounting for stomatal closure effects on GPP can also generate uncertainties in the results. Lasslop *et al.* (2010) modified β_{NEE} to account for the effect of stomatal closure on GPP through VPD as:

$$\beta_{NEE} = \begin{cases} \beta_{NEE,0} \exp^{-k(VPD-VPD_0)} & VPD > VPD_0 \\ \beta_{NEE,0} & VPD < VPD_0 \end{cases} \tag{1.19}$$

with VPD_0 set to 10 hPa and $\beta_{NEE,0}$ a fitted parameter. Lasslop *et al.* (2010) partitioning method is referred to as the DayTime (DT) partitioning method. The

multi-step process of model parameterization of the DT method is described in Lasslop *et al.* (2010) and in Wutzler *et al.* (2018).

3.2.1.4 Footprints and upscaling

EC fluxes originate from a target area (i.e., a footprint), which should be representative of the ecosystem of interest. An analysis of the turbulent field around the measurements point is required for identifying the contribution of all sources and sinks to EC fluxes. Footprint models use wind direction, height of the measurement point, surface roughness and stability conditions to provide a mapping of contributing areas around the EC tower (Schmid, 2002). Assessing the contribution of the target area to the global EC footprint is crucial prior to fluxes analysis (Burba, 2021).

The unique features of the EC technique (i.e., a non-destructive, automatic and high frequency method for measuring gas exchanges and energy fluxes greenhouse gases and energy fluxes at the ecosystem-atmosphere interface) have made it popular for understanding the impacts of climate on ecosystems (Baldocchi, 2014). EC measurements have been conducted on 2155 locations, and more than 900 sites are currently part of the FLUXNET network, covering all ecosystem types (Baldocchi *et al.*, 2001; Chu *et al.*, 2017; Burba, 2019). EC measurements have been regrouped within global datasets such as the 2007 LaThuile dataset with 965 site-years of data and the FLUXNET2015 dataset with 1532 site-years of data. These datasets provide high quality data using a common data processing pipeline (i.e., the ONEFLUX pipeline) for all stations and site-years (Pastorello *et al.*, 2020). Notably, this standardized data treatment provides gap-filling of missing data and partitioning of NEE between GPP and R_{ECO}. The joint measurements of EC fluxes along with meteorological variables (e.g., air vapor pressure, air temperature or PPFD), vegetation variables (e.g., leaf area index, crop yield or canopy cover), and edaphic variables (e.g., soil moisture or soil temperature) have made possible to study the response of ecosystems to climate drivers (see Baldocchi (2020) for several references).

Notwithstanding the undeniable contribution of EC to understanding of ecophysiological processes in ecosystems, EC stations only provide a partial spatial coverage of fluxes measurements. EC fluxes can only be interpreted within the footprint of the station, and providing fluxes "everywhere and all the time" (Chu *et al.*, 2021) is actually not really feasible, especially near the tropics where climate conditions and ecosystem structure complexifies the installation of EC stations. Despite the growing number of EC under the tropics (e.g., Sibret *et al.* (2022)), these regions still remain poorly monitored, even though they are the most important carbon sinks (Chu *et al.*, 2017). Alternatively, Remote Sensing (RS) of vegetation greenness provide a proxy of vegetation health which can be used to build machine learning algorithm to understand the response of fluxes to climate drivers at large scales (Jung *et al.*, 2020). Although GPP and vegetation greenness are undeniably linked, this relationship is typically weakened

under water or heat stress and it does not allow to detect early stress on vegetation (Zhao *et al.*, 2024; Maleki *et al.*, 2022). In particular, changes in biochemistry and photosynthetic activity cannot be related to greenness-based vegetation indexes. ChlF has the potential to capture the early response of ecosystems to climate extremes by being directly emitted from the core of photosynthesis reaction. One technical limitation remains : ChlF retrieved by active methods cannot be related to GPP because of the spatial and temporal mismatch of measurements. This has been overcome by the recent emergence of ChlF measurements with passive methods, which provide automatic ChlF measurements at a high frequency at larger spatial scale.

3.2.2. Measurements of chlorophyll fluorescence with passive techniques

Light is affected by absorption and scattering proprieties of molecules. In particular, solar irradiance is attenuated at specific wavelengths either by the Sun's atmosphere (i.e., known as Fraunhofer lines) or by the Earth's atmosphere (i.e., known as telluric absorption bands). More than 25 000 Fraunhofer lines have been identified such as the hydrogen Hα line (656 nm) or the potassium KD1 line (770 nm). Another example is O_2 which has several absorption lines regrouped as bands (i.e., O_2-A band 759-770 nm and O_2-B band 687-692 nm). When induced by natural sunlight, ChlF is known as Sun-Induced chlorophyll Fluorescence (SIF), at the opposite of ChlF measured by active methods which is based on the excitation of ChlF pigments by an artificial light. As mentioned before (see section 2.4), SIF has two peaks in the red ($\sim$685-690 nm) and in the NIR ($\sim$730-740 nm) region (Mohammed *et al.*, 2019). The peak in the red is very close to the O_2-B telluric absorption band, while the one in the NIR is slightly offset (Fig. 1.11).

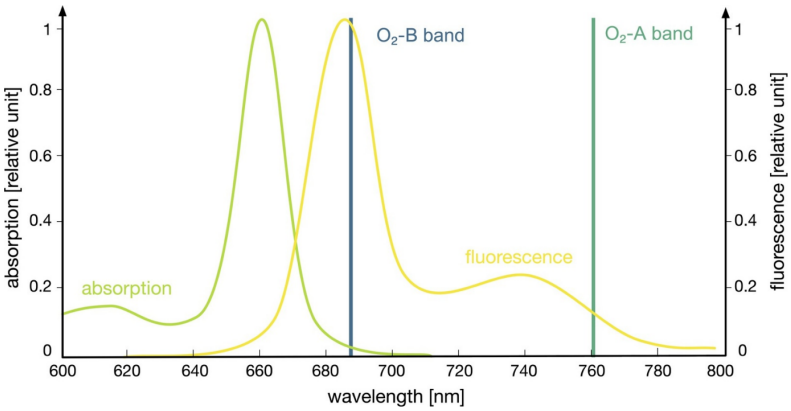

Figure 1.11: Absorption spectra, fluorescence emission spectra (yellow) and oxygen absorption bands of chlorophyll (light green). Only the near-infrared and red domains are shown (Jonard *et al.*, 2020)

The shape of telluric bands and absorption lines is strongly influenced by the spectral resolution of the spectrometer. One important parameter for assessing the precision of spectral measurements is the Full Width of the absorption band at Half of the Maximum depth (FWHM); the depth being the difference between maximum and minimum reflectance within the band (Kruse & Lefkoff, 1999). Since the FWHM of spectral features is measured by fitting a Gaussin curve on the dark well, the precision of FWHM measurements is directly dependent on the spectral resolution of the spectrometer (i.e., the ability to detect observable wavelength intervals). For example, the O_2-B band has a FWHM of 1.54 nm at 1 nm spectral resolution and a 0.03 FWHM at 0.005 nm spectral resolution (Meroni *et al.*, 2009). In other words, information on O_2-A and O_2-B bands is typically lost when spectral resolution increases (Fig. 1.12). One should note that the term FWHM can be used for both characterizing a spectral feature and the precision of a spectrometer. This is because the spectral resolution of a spectrometer is currently determined by measuring the FWHM of a reference light source.

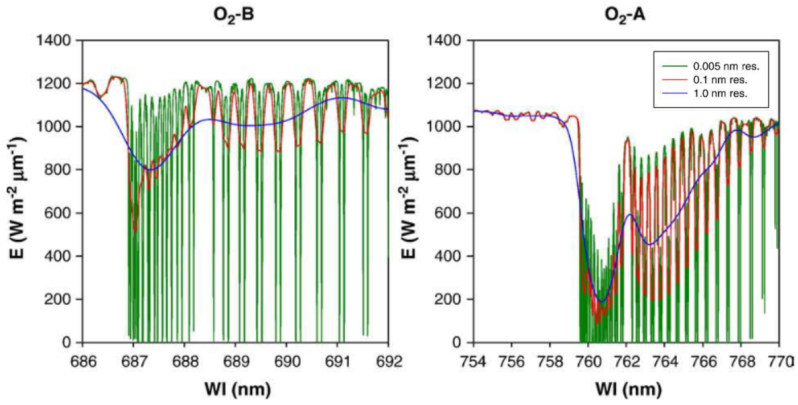

Figure 1.12: Incident irradiance (E) at ground levels and the two O_2 absorption bands at three different spectral resolutions (0.005, 0.1 and 2 nm). Adapted from Meroni *et al.* (2009).

Passive measurements of SIF use the similarity between dark lines and ChlF peaks to separate the SIF signal from the ambient light. More precisely, SIF contributes to fill-in the dark lines by adding a signal to the reflected radiance (the signal is directly proportional to the SIF emission spectrum). The upwelling radiance from vegetation ($L(\lambda)$ - in blue on Fig. 1.13-B) is therefore composed of a reflected component ($R(\lambda)$ - in green on Fig. 1.13-B) and an emitted component ($F(\lambda)$ - in red on Fig. 1.13-B), which is related to SIF. Therefore, following Lambert's law, one can write:

$$L(\lambda) = R(\lambda) + F(\lambda) = \frac{r(\lambda)\, E(\lambda)}{\pi} + F(\lambda) \tag{1.20}$$

with $E(\lambda)$ the incident solar irradiance on the target (in blue on Fig. 1.13-A) and

$r(\lambda)$ the reflectance. The utilization the SIF contribution to the reflected radiance is at the basis of the Fraunhofer Line Depth (FLD) – based methods (Plascyk & Gabriel, 1975). The FLD method uses radiance and irradiance measurements outside ($L(\lambda_{out})$, $E(\lambda_{out})$) and inside ($L(\lambda_{in})$, $E(\lambda_{in})$) the well. Assuming that $F(\lambda)$ and $r(\lambda)$ remain constant, the FLD method consists in solving Eq. 1.20 outside and inside the well, which gives (Meroni *et al.*, 2009):

$$F = \frac{E(\lambda_{out})\, L(\lambda_{in}) - E(\lambda_{in})\, L(\lambda_{out})}{E(\lambda_{out}) - E(\lambda_{in})} \tag{1.21}$$

The main underlying hypothesis of the FLD method is that ChlF and reflectance do not vary on both sides of a dark line. This hypothesis is actually often challenged, which has led to the development of alternative FLD-based methods which use correction factors or spectral curve fitting to account for variability in ChlF and reflectance (Meroni *et al.*, 2009). Finally the Spectral Fitting Methods (SFM) uses spectral curve fitting on all available hyperspectral bands to determine variations in both reflectance and ChlF (Cogliati *et al.*, 2015). Additional information on SIF retrieval methods can be found in Meroni *et al.* (2009), Cendrero-Mateo *et al.* (2019) and Chang *et al.* (2020).

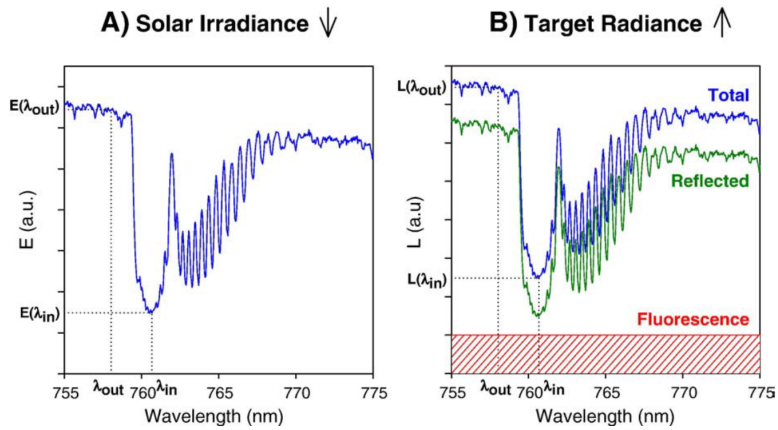

Figure 1.13: Solar irradiance measurements showing the O_2-A absorption band with a FWHM of 0.13 nm (A). Radiance measurements over vegetation (B) where the total signal (blue) is the sum of the reflected signal (green) and the fluorescence emission (red). λ_{out} and λ_{in} are the wavelengths nearby and inside the well (Meroni *et al.*, 2009).

3.3. Measuring SIF at large scales

SIF can be retrieved from spacebore, airborne or field spectrometers with a high spectral resolution (Jonard *et al.*, 2020). First SIF observations were retrieved from satellite measurements which had a general purpose of studying the Earth's atmo-

sphere. More than 15 years ago, the data acquired by the Medium Resolution Imaging Spectrometer (MERIS) on board of the ENVIronmental SATellite (ENVISAT) was used by Guanter *et al.* (2007) to retrieve SIF in the O_2-A band using the FLD method. Four years later, Joiner *et al.* (2011) used Greenhouse gases Observing SATellite (GOSAT) spectral measurements within the potassium Fraunhofer line KD1 to retrieve SIF (Fig. 1.14). The first comparison between SIF from GOSAT and GPP from EC towers on the ground was achieved the same year (Frankenberg *et al.*, 2011). A strong correlation between SIF and GPP was found, suggesting that SIF could be used to estimate GPP. As the technical characteristics of the following satellites improved (such as the Global Ozone Monitoring Experiment-2 (GOME-2) and the TROPOspheric Monitoring Instrument (TROPOMI)), spatial resolution increased and global SIF maps became more precise (Fig. 1.14 to 1.16). Current TROPOMI SIF product has a pixel resolution of 19 km² at nadir (i.e., the direction pointing directly below a particular location, orthogonal to a horizontal flat surface) (Guanter *et al.*, 2021).

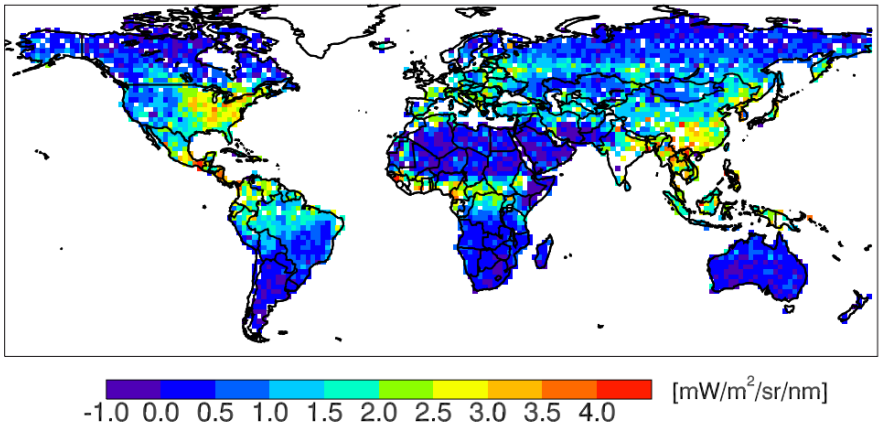

Figure 1.14: Global map of SIF monthly averages for July 2009 using GOSAT measurements. Data gridded in 2° grid boxes. Adapted from Joiner *et al.* (2011).

The first SIF-dedicated satellite will be launched by the FLuorescence EXplorer (FLEX) mission. FLEX will provide global maps of SIF emission of vegetation as primary measurement (Drusch *et al.*, 2017). The main instrument embedded on the FLEX space segment is the FLuORescence Imaging Spectrometer (FLORIS) payload, a high precision spectrometer with a spectral resolution of 0.1 nm in the O_2 telluric bands and a pixel size of 300x300 m every 10 to 25 days, which is very similar to most of EC tower footprints. FLEX will orbit in tandem with Sentinel-3, providing joint measurements of SIF and Sentinel-3 data products to unravel complex ecosystem processes.

The development of FLEX has led to many ground campaigns for direct validation of future RS SIF products with the development of the High-performance airborne

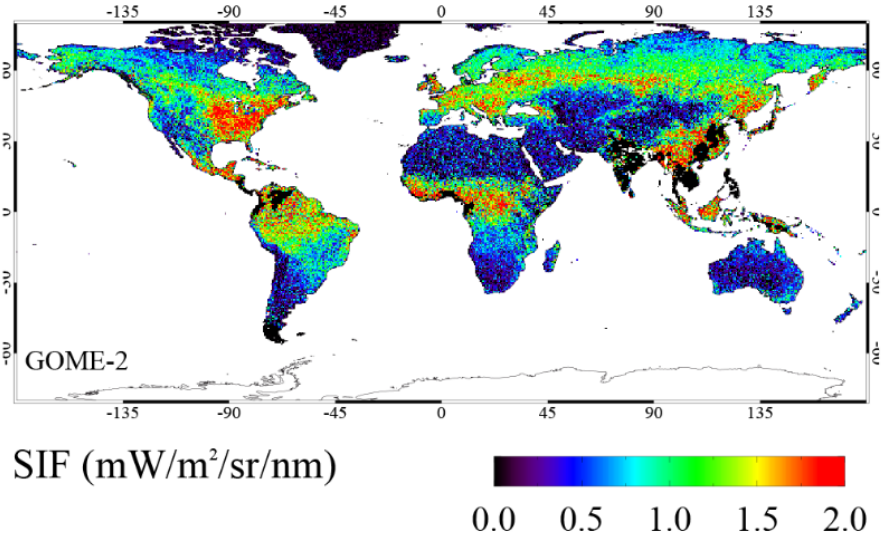

Figure 1.15: Global map of SIF monthly averages for July 2013 using GOME-2 measurements. Data gridded in 0.5° grid boxes. Adapted from Guanter *et al.* (2015).

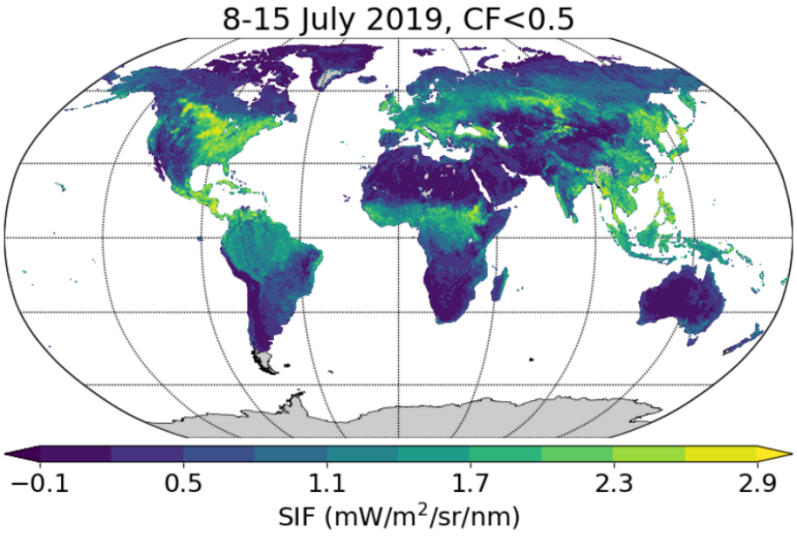

Figure 1.16: Global map of SIF averages between 8 and 15 July 2019 from TROPOMI measurements. Data gridded in 0.2° grid boxes. CF means cloud fraction. Adapted from Guanter *et al.* (2021).

imaging spectrometer for vegetation monitoring (HyPlant) airborne high-resolution spectrometer (Rascher *et al.*, 2015) or the field-based high-resolution Fluorescence boX (FloX) spectrometer (Buman *et al.*, 2022), which have similar technical features as FLORIS. While awaiting the launch of FLEX (expected for 2025), more than 40 FloX systems have been installed on EC sites, covering a wide variety of ecosystems (Buman *et al.*, 2022). Joint SIF and EC measurements have helped in understanding the relationship between SIF and GPP at the ecosystem scale (e.g., Helm *et al.* (2020); Magney *et al.* (2020); Marrs *et al.* (2020); Martini *et al.* (2022)), opening the way for building models estimating GPP from SIF (more details in section 4).

4. Photosynthesis modeling

Gas exchange measurements provide an important source of data describing the dynamics of net assimilation in a broad range of environmental conditions. For instance, gas exchange devices allow to change light intensity and CO_2 concentrations to build light-response or CO_2-response curves under varying abiotic factors (e.g., temperature, soil moisture or relative humidity). While the response of CO_2 exchange is quite predictable (e.g., a saturation under high irradiance and CO_2 concentration, or a decrease under increasing VPD and lack of soil water), and the underlying mechanisms were well understood even before the 1980s, a global scheme for representing these processes and their interactions with the environment was lacking. With the feeling of "one doesn't really understand something until one can describe it mathematically" (Farquhar *et al.*, 2001), Farquhar, Berry and von Caemmerer brought biochemistry and gas exchanges together into the Farquhar-von Caemmerer-Berry (FvCB) model (Farquhar *et al.*, 1980). The FvCB model is a biochemical model for C3 photosynthesis which is based on a mechanistic representation of the processes associated to carbon assimilation by the CBB cycle. It has been used for more than four decades to interpret gas exchange measurements and predict the impacts of environmental drivers on photosynthesis.

Biochemical processes in the FvCB model are dependant on the instantaneous supply of CO_2 and the effect of temperature on photosynthetic capacities, which leads to a nonlinear relationship between light and net assimilation (Farquhar *et al.*, 1980). When integrated over large spatial and time scales, ecosystem productivity is linearly proportional to the fraction of absorbed PAR by vegetation (Medlyn, 1998; Monteith *et al.*, 1997). These empirical relationships, also knows as Light-Use Efficiency (LUE) models, can be generalized to various environmental conditions by adding a multiplier factor which accounts for the effects of environmental variables (other than PAR) on GPP (Pei *et al.*, 2022). While this straightforward approach can be used to model GPP at large scales, it does not allow an identification of the physiological factors limiting photosynthesis. In this perspective, the FvCB model provides a mechanistic framework for assessing the impacts of water stress on ecosystem productivity. Yet,

the response of model parameters on soil water availability remains a key uncertainty when modeling photosynthesis under water stress (Rogers *et al.*, 2017).

4.1. The Farquhar-von Caemmerer-Berry (FvCB) model

The mathematical representation of photosynthetic physiological processes in the FvCB model is at the basis of the modeling of GPP in many Land Surface Models (LSMs) (Rogers *et al.*, 2017). Net CO_2 assimilation rate (A_n) is calculated as the minimum of three different processes: either by Rubisco activity (A_c), electron transport (A_j), or Triose Phosphate Utilization (TPU) (A_p) (see section 2.2 for the role of triose phosphate in the CBB cycle). The equations for these limiting rates are:

$$A_c = \frac{C_c - \Gamma^*}{C_c + K_m} V_{cmax} \tag{1.22}$$

$$A_j = \frac{C_c - \Gamma^*}{4C_c + 8\Gamma^*} J \tag{1.23}$$

$$A_p = 3T_p \tag{1.24}$$

with C_c the CO_2 concentration in the chloroplast, Γ^* the CO_2 compensation point, K_m the Michaelis-Menten constant for Rubisco kinetics, T_p the rate of inorganic phosphate supply to the chloroplast, V_{cmax} the maximum carboxylation rate of Rubisco and J the potential electron transport rate. A_n is estimated as the minimum of the potential rates of these three processes minus the respiration in the light R_d:

$$A_n = min(A_c, A_j, A_p) - R_d = A - R_d \tag{1.25}$$

While the modeling of the CBB cycle in the FvCB model is strictly mechanistic (i.e., based on Rubisco kinetics), the representation of light reactions is empirical. Indeed, the FvCB model calculates a potential electron transport rate between PSII and PSI instead of an actual rate. J is calculated using a rectangular hyperbola function of irradiance:

$$J = \frac{I_2 + J_{max} - \sqrt{(I_2 + J_{max}) - 4\theta_J \, I_2 \, J_{max}}}{2\theta_J} \tag{1.26}$$

with I_2 the actual light absorbed by PSII calculated from incident irradiance and leaf absorptance, J_{max} the maximum electron transport rate and θ_J a curvature factor. One should note that C_c in Eq. 1.22 and Eq. 1.23 is the CO_2 concentration in the chloroplast, which is different from the CO_2 concentration in substomatal cavities. CO_2 pathways in the cell can be described using the Fick's law of diffusion (i.e., the electricity analogy of resistances - Farquhar & Sharkey (1982)), with stomata and mesophyll being the two limiting factors to CO_2 diffusion from the surrounding atmosphere to chloroplasts connected in series:

$$C_c = C_i - \frac{A_n}{g_m} = C_s - \frac{A_n}{g_s} - \frac{A_n}{g_m} \tag{1.27}$$

where C_i is the CO_2 concentration in the substomatal cavities, C_s is the CO_2 concentration at the leaf surface, g_m is the mesophyll conductance and g_s is the stomatal conductance to CO_2 transfer. Note that $g_s = g_{sw}/1.6$ with 1.6 being the ratio of H_2O to CO_2 diffusivity. Most of the time, g_m is considered as infinite and Eq. 1.22 and Eq. 1.23 are used with C_i instead of C_c, and apparent V_{cmax} ($V_{cmax,app}$ instead of V_{cmax}). While kinetics constants of Rubisco (Γ^*, K_m) are regulated by leaf temperature in the same way for all C3 plants (Bernacchi *et al.*, 2001), J_{max} and V_{cmax} follow a species-specific relationship to temperature and are impacted by soil water status. The effect of these variables is commonly implemented using respectively a peak-Arrhenius model and an empirical factor considering the change in soil water availability (see section 5.2) (Medlyn *et al.*, 2002; Rogers *et al.*, 2017). These relationships must be calibrated on field data.

4.1.1. Determination of FvCB model parameters from CO_2 and light-response curves

CO_2-response curves are built by collecting net assimilation measurements under varying CO_2 concentration with a LI-6400 equipped with a CO_2 mixer. These curves typically show three phases illustrating the limiting rates of photosynthesis (Fig. 1.17). When CO_2 concentration is low, the slope of the curve (dA_n/dC_i) is high as CO_2 is rapidly fixed by Rubisco which induces a sharp increase in A_n. As Rubisco progressively becomes saturated in CO_2, dA_n/dC_i approaches zero and photosynthesis shifts from Rubisco-limiting to RuBP-limiting stage (Fig. 1.17). A second transition point may be observed when shifting to TPU-limiting stage with dA_n/dC_i slightly negative. This third limiting stage is not usually detected and therefore often neglected. FvCB model parameters (i.e., V_{cmax}, g_m, T_p, J and R_d) can be determined by fitting the FvCB model on gas exchange measurements with, for instance, the R package 'Plantecophys' (Duursma, 2015; R Core Team, 2020). However, estimating model parameters from fitting methods may be challenging (Long, 2003; Sharkey, 2016). The fitting procedure requires to find the minimum of two non-linear equations (either Eq. 1.23, or 1.22 and 1.27) while adjusting five parameters (or four if A_p is neglected).

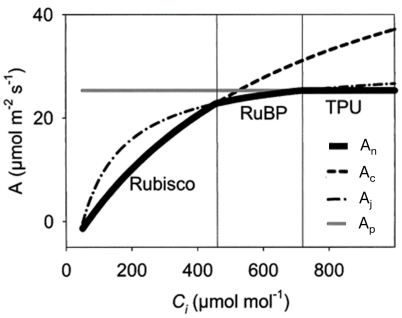

Figure 1.17: Idealized A_n vs C_i response curve simulated using the following FvCB model parameters: $V_{cmax} = 70$ μmol m^{-2} s^{-1}, $J = 130$ μmol m^{-2} s^{-1}, $T_p = 9.1$ μmol m^{-2} s^{-1} and $R_d = 2$ μmol m^{-2} s^{-1} (Long, 2003).

Several issues have been identified (Sharkey, 2016) such as strong variability of parameters according to the statistical fitting method (Miao *et al.*, 2009), or divergence of algorithms when data is collected on plants under water or heat stress as the saturation of A_n is not even reached (De Kauwe *et al.*, 2015b). The use of alternative methods for estimating parameters independently of gas exchanges is advised to reduce these uncertainties.

4.1.2. Determination of FvCB model parameters from a single measurement of gas exchanges

An alternative method for estimating V_{cmax} consists in measuring A_n and C_c under ambient CO_2 concentration and saturated irradiance ($R_d << A$, $A = A_c$, $A_n = A_c = A_{sat}$) by inverting Eq. 1.22, which gives:

$$V_{cmax} = A_{sat} \frac{C_c + K_m}{C_c - \Gamma^*} \tag{1.28}$$

In Eq. 1.28, g_m is considered as finite. The same equation can be applied considering a infinite mesophyll conductance (i.e., $C_c = C_i$). In these conditions, the apparent V_{cmax} parameter ($V_{cmax,app}$) can be calculated by Eq. 1.28. In a global analysis using CO_2-response curves from 594 species across various ecosystems, De Kauwe *et al.* (2015b) showed that $V_{cmax,app}$ estimated from these single measurements correlated well with $V_{cmax,app}$ estimated from A_n/C_i response curves (De Kauwe *et al.*, 2015b). These results support the use of one-point measurements of A_{sat} and C_i to estimate $V_{cmax,app}$ instead of $A_n - C_i$ response curves. Because of the challenges faced when estimating g_m and C_c, $V_{cmax,app}$ is generally reported in ecophysiological studies and used in LSMs (De Kauwe *et al.*, 2015b).

4.1.3. Estimation of the CO_2 concentration in the chloroplasts from gas exchange and ChlF measurements

Estimating C_c requires first the determination of the actual electron transport rate (J_F) which can be estimated from ChlF measurements of the quantum yield of PSII in the light (ϕ_{PSII}) as Genty *et al.* (1989) :

$$J_F = \alpha \, \beta_{PSII} \, \phi_{PSII} \, PPFD \tag{1.29}$$

with α the leaf absorptance and β_{PSII} the distribution of electrons between PSII and PSI. α and β_{PSII} should be ideally measured under non-photorespiratory conditions, or can also be set respectively to 0.83 and 0.5 (Genty *et al.*, 1989; Von Caemmerer, 2013). α and β_{PSII} measurement procedure is detailed in chapter 5. Eq. 1.29 hypothesizes that a certain fraction of PAR can be directly used to induce electron transport between PSII and PSI. J_F can be used in the FvCB model as an actual electron transport rate under two conditions (Pons *et al.*, 2009): if alternative electron sinks are negligible, and if the leaf cross-section sampled for ChlF measurements can be con-

sidered as similar to the one for gas exchange measurements. This can be challenged as ChlF measurements use a red light to induce electron hopping between S_0 and S_1 orbitals, which has different penetration properties within the leaves compared to sunlight. This will be further discussed in chapter 5. Eq. 1.23 can be solved for C_c using J_F, which gives:

$$C_c = \frac{\Gamma^*(J_F + 8(A_n + R_d))}{(J_F - 4(A_n + R_d)} \tag{1.30}$$

and g_m can be determined by the Fick's law using measured C_i and C_c from Eq. 1.30:

$$g_m = \frac{A_n}{C_i - C_c} \tag{1.31}$$

4.2. Stomatal conductance modeling

Stomatal apertures are the gates of photosynthesis (Gago *et al.*, 2020). As detailed in section 2.3, stomatal opening is sensitive to multiple environmental factors. Early approaches for modeling stomatal conductance used empirical multiplicative functions integrating the effects of PAR, temperature, VPD and C_s on g_s (Jarvis *et al.*, 1976). With experimental growing evidences that stomatal conductance is strongly correlated with net carbon assimilation (Wong *et al.*, 1979), Ball *et al.* (1987) and Leuning (1995) integrated the dependence of g_s on A_n as (Eq. 1.32 and Eq. 1.33):

$$g_s = g_0 + g_1 RH \frac{A_n}{C_s} \tag{1.32}$$

$$g_s = g_0 + g_1 \frac{A_n}{(1 + \frac{VPD}{VPD_0}(C_s - \Gamma^*))} \tag{1.33}$$

where VPD_0 is a constant. Note that g_0 represents the minimum leaf conductance. It corresponds either to a stomatal conductance to water vapor during nighttime when photosynthesis does not occur, or to a cuticle conductance facilitating water vapor diffusion which is typically non-negligible under water stress (Boyer, 2015a). g_0 is usually set to a constant value (Duursma *et al.*, 2019). In Eq. 1.32 and Eq. 1.33, the effect of temperature on g_s and A_n is implemented through RH or VPD (see Damour *et al.* (2010) for a review of empirical models of stomatal conductance).

An alternative to empirical approaches is to model g_s using the optimality framework of Cowan & Farquhar (1977). This approach assumes that stomata should be opened such as carbon assimilation is maximized while water losses are minimized, resulting in maximizing the following integral over a constant time interval (from t to t', Fig. 1.18):

$$\int_{t}^{t'} (A_n(t) - \lambda_{opt} T_r(t)) dt \tag{1.34}$$

where λ_{opt} is the marginal carbon cost of water use. Medlyn *et al.* (2011a) used the optimality theory to derive a formulation (i.e., the Unified Stomatal Optimality (USO) model) that is closely analogous to the empirical models of Ball *et al.* (1987) and Leuning (1995):

$$g_s = g_0 + \left(1 + \frac{g_1}{\sqrt{VPD}}\right) \frac{A_n}{C_s} \tag{1.35}$$

In the past 10 years, numerous stomatal conductance models have been developed based on the optimality theory (Mrad *et al.*, 2019). These models mainly differ from the formulation of the cost of stomatal opening, either attributed to maintaining a constant CO_2 concentration in the leaves (Prentice *et al.*, 2014), an impairment of the water flow through xylem cavitation and soil drying (Sperry *et al.*, 2016, 2017), or an impairment of photosynthetic apparatus through biochemical effects on the CBB cycle (Dewar *et al.*, 2018). The implementation of more mechanistic approaches for modeling g_s in LSMs is currently explored. While it is recognized that the representation of physiological processes is improved by such models, the calibration remains challenging because as it comes with a very high computational cost. So far, it does not seem that any stomatal conductance model rules all the others (Sabot *et al.*, 2022) and he USO model has become a reference for representing stomatal behavior in LSMs.

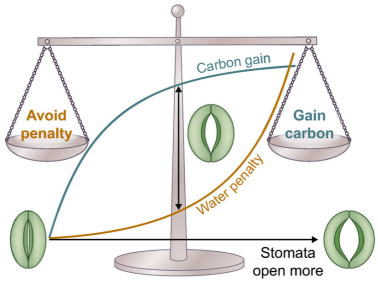

Figure 1.18: Stomatal optimization models hypothesize that the actual stomatal opening is what maximizes the difference between carbon gain and water penalty. Adapted from Wang *et al.* (2020b)

A key parameter of the USO model (Eq. 1.35) is the slope parameter g_1, which is inversely related to the Water-Use Efficiency (WUE) (i.e., the ratio of carbon gained to water use (Medlyn *et al.*, 2011a; Lin *et al.*, 2015a)). The concept of WUE is often used to characterize the productivity of ecosystems in relation to their water use and for understanding the response of photosynthesis to changes in water availability (Hatfield & Dold, 2019). The advantage of the USO model is that g_1 can be linked to plant physiology through WUE. A decrease in g_1 (i.e., increase in WUE) is expected when the optimality theory is verified (i.e., decreasing g_s while maximizing A_n (Mäkelä, 1996)). On the other hand, if A_n is limited by biochemical factors such as V_{cmax} or g_m in addition of the effect of decreasing CO_2 supply by stomatal closure, g_1 is expected to

increase (i.e., decrease of WUE and of the ratio A_n/g_s). Although the response of g_1 to decreasing soil water availability is still highly uncertain (Zhou *et al.*, 2013), the USO model is currently implemented in climate models such as the Australian Community Climate Earth Systems Simulator ACCESS1.3b (Kala *et al.*, 2015a) or the Community Land Model v5 (CLM5) which is the main resource for Intergovernmental Panel on Climate Change (IPCC) assessment reports (Lawrence *et al.*, 2019).

4.3. Scaling from leaves to ecosystems with 'big leaf' models

The FvCB and USO models describe gas exchanges and their interdependencies with biotic and abiotic factors at the leaf level. One important question is how these models can be used to interpret and model fluxes at the canopy level. The issue of spatial extrapolation of gas exchange measurements from leaves to canopy has been investigated in the late 70's by Sinclair *et al.* (1976) who compared a complex micro-meteorological model to simpler models which assumed either that environmental conditions are constant within the canopy, or that the canopy can be simplified as a single leaf (i.e., a 'big leaf'). 'big leaf' models differs from multi-layer canopy models which resolve vertical micro-climate profiles within the canopy. Those are especially relevant for dense forest canopies where within-canopy gradient of environmental conditions can be observed (Bonan *et al.*, 2021; Luo *et al.*, 2018). However, single-layer canopy models are preferred to multi-layer canopy models due to the simplicity of the approach which avoids a heavy computational cost while estimating GPP with a good accuracy (Bonan *et al.*, 2021; Lawrence *et al.*, 2019).

4.4. Photosynthesis modeling from passive measurements of chlorophyll fluorescence

Using SIF to estimate GPP has several advantages. First, measurements of ChlF with passive techniques can be collected at various spatial scales and do not require the installation of a complex structure on the ground such as an EC flux tower. Second, satellite measurements of SIF have the potential to unravel the spatial and temporal dynamics of vegetation growth at regional and global scales, thus providing a key tool to upscale GPP measurements (Pei *et al.*, 2022).

4.4.1. The Light-Use Efficiency approach

Similarly to GPP with the LUE model, a straightforward approach for estimating ground-based GPP from proximal sensing of SIF consists in assuming a proportionality to the absorbed PAR ($APAR$) and ChlF quantum yield (ϕ_F) (Joiner *et al.*, 2011):

$$SIF = APAR\,\phi_F\,f_{esc} \tag{1.36}$$

where τ_{atm} is the atmosphere transmittance which characterizes the scattering effect of the atmosphere (Köhler *et al.*, 2015) and f_{esc} is the probability that SIF photons

escape the canopy and reach the sensor (similar to Eq. 6.1). Combining the LUE approaches for SIF and GPP gives:

$$GPP = \frac{\phi_{PSII}}{\phi_F \, f_{esc}} \, SIF \tag{1.37}$$

Note that τ_{atm} can be neglected when SIF is measured at the ecosystem scale. Eq. 1.37 translates the close coupling between SIF and GPP. The LUE approach provides a rationale for establishing empirical relationship between SIF and GPP at large spatial and temporal scales by using machine learning techniques (Guanter *et al.*, 2014; Pickering *et al.*, 2022; Bai *et al.*, 2022; Pei *et al.*, 2022).

4.4.2. The Mechanistic Light-Response model

Empirical relationships do not always capture the variability of SIF and GPP. For instance, it has been shown that SIF may remain constant while GPP decreased during stomatal closure in several temperate tree species (Marrs *et al.*, 2020). A breakdown of the SIF-GPP relationship was also observed for forests during a heatwave (Martini *et al.*, 2022) or during fall transition (Kim *et al.*, 2021), which can be generalized at the canopy scale for several biomes (Liu *et al.*, 2022b). These evidences highlight a strong control of physiological and structural factors on the SIF-GPP relationship that are not capture by empirical relationships. Recently, Gu *et al.* (2019) combined the FvCB model and the first-order rate constants for the de-excitation of chlorophyll to link GPP to SIF using key physiological factors (i.e., the Mechanistic Light Response (MLR) model). The starting point of MLR model equations is the combination of Eq. 1.29 and Eq. 1.36, which gives:

$$J_{SIF} = \frac{\phi_{PSII}}{\phi_F} \frac{SIF}{f_{esc}} \tag{1.38}$$

with J_{SIF} the electron transport rate estimated from SIF. ϕ_{PSII} and ϕ_F can be expressed as a function of the first-order rate constants for the de-excitation of chlorophyll pigments after being excited by sunlight:

$$\phi_{PSII} = \frac{k_p}{k_D + k_F + k_{NPQ} + k_p} \tag{1.39}$$

$$\phi_F = \frac{k_F}{k_D + k_F + k_{NPQ} + k_P} \tag{1.40}$$

where k_D, k_F, k_{NPQ} and k_P are respectively the first-order rate constants for the de-excitation of chlorophyll pigments by constitutive thermal dissipation, ChlF emission, NPQ and Photochemical Quenching (PQ). The ratio ϕ_{PSII}/ϕ_F can be linked to the fraction of open PSII centers (q_L) and the maximum photochemical quantum yield

($\phi_{PSII,max}$), which can be measured by ChlF measurements with active techniques (Eq. 1.5 and Eq. 1.4):

$$\frac{\phi_{PSII}}{\phi_F} = q_L \frac{\phi_{PSII,max}(1+k_{DF})}{1-\phi_{PSII,max}} \tag{1.41}$$

with $k_{DF} = k_D/k_F$. Combining Eq. 1.41 with Eq. 1.38 gives:

$$J_{SIF} = q_L \frac{\phi_{PSII,max}(1+k_{DF})}{1-\phi_{PSII,max}} \frac{SIF}{f_{esc}} \tag{1.42}$$

Combining Eq. 1.42 with the FvCB model (Eq. 1.23) gives:

$$GPP = q_L \frac{\phi_{PSII,max}(1+k_{DF})}{1-\phi_{PSII,max}} \frac{SIF}{f_{esc}} \frac{C_c - \Gamma^*}{4C_c + 8\Gamma^*} \tag{1.43}$$

The main advantage of representing J_{SIF} as a function of SIF is to provide an instantaneous linkage between the light and dark reactions of photosynthesis. By calculating the actual linear electron transport rate between PSII and PSI, the MLR model integrates the complexity of the energy partitioning processes through q_L and SIF. Therefore, if SIF is observed, " (...) the complexity of modeling photosynthesis is greatly reduced because it integrates over this complexity" (Gu *et al.*, 2019).

In the MLR model, $\phi_{PSII,max}$ and q_L must be determined from leaf-level actively-induced ChlF measurements. The LeafWeb database (Han *et al.*, 2022a) regroups measurements of leaf gas exchanges and PAM fluorometry of light, CO_2, O_2, and temperature responses from several C3 and C4 species. Researchers can upload their measurements in the database, which contributes to the effort initiated by Gu *et al.* (2019) and Han *et al.* (2022a) to provide model parameters for different species. $\phi_{PSII,max}$ and q_L can also be found in the literature as numerous studies have already independently measured these parameters (e.g., Cendrero-Mateo *et al.* (2015); Zivcak *et al.* (2014)). Existing studies have tested the MLR model at the leaf scale under controlled conditions (Shi *et al.*, 2022), or at the ecosystem scale for an irrigated winter wheat crop (Liu *et al.*, 2022c). Large uncertainties remain on the capability of the MLR model for estimating GPP under water stress. In addition, coupling the MLR model to a model of stomatal conductance could allow the estimation of GPP and Tr from a single SIF measurements. These research questions should be addressed before considering an application of the model at larger scales with remote sensing data.

5. Drought impacts on photosynthesis

Unraveling the impacts of drought on carbon and water fluxes is pivotal for understanding ecosystem functioning and improving model predictions in the context of climate change. Photosynthesis model parameters must account for environmental effects on physiological processes to predict the future strength of carbon land sinks (Fisher *et al.*, 2014; Friedlingstein *et al.*, 2022).

5.1. What is drought ?

The World Meteorological Organization (1992) defines drought as a "period of abnormally dry weather sufficiently prolonged for the lack of precipitation to cause a serious hydrological imbalance". The diversity of temporal distribution, spatial scale and disciplines affected by drought explains that "...we cannot reasonably expect the existence of any workable generalized objective definition of drought." (Lloyd-Hughes, 2014). As a consequence, different drought definitions coexist. Among them, physical-based droughts are commonly classified into three categories (Belal *et al.*, 2014): meteorological drought (lack of precipitation compared to a reference period), agricultural drought (crop failure caused by a decrease in soil moisture), and hydrological drought (limiting period when surface water resources are no longer available for water management systems). These definitions must be associated to the calculation of parameters which characterizes the status of the physical variable of interest. Such parameters, also known as drought indexes, can be a single variable (e.g, precipitation) or a combination of different variables (e.g, the Standardized Precipitation Evaporation Index (SPEI) which uses both precipitation and potential evapotranspiration). A flurry of drought indexes has been defined over the past decades, which constantly evolves with the availability of new data or techniques to monitor the impact of climate change on vegetation (Gebrechorkos *et al.*, 2023).

A more relevant definition of drought when considering vegetation is ecological drought, which is defined as an "episodic deficit in water availability that drives ecosystems beyond thresholds of vulnerability, impacts ecosystem services, and triggers feedbacks in natural and/or human systems" (Crausbay *et al.*, 2017). This definition puts plant hydraulics and physiological processes at the core of the analysis of water stress effects on ecosystems. Assessing ecological droughts requires the joint analysis of the relationship between a plant functional trait and a physical variable characterizing the water status in the soil (e.g., the relationship between stomatal conductance, photosynthesis at light saturation, or the hydraulic conductivity with Soil Water Content (SWC) (Anderegg *et al.*, 2019; Maynard *et al.*, 2022; Quetin *et al.*, 2023)). For instance, the drought resistance of an ecosystem can be quantified by analyzing the differences in plant functional traits under similar edaphic conditions. A key aspect for characterizing ecological droughts is the separation of the effect of soil water status among all the other meteorological conditions which impact plant processes. This

requires a detailed knowledge of the effects of temperature or atmospheric dryness on photosynthesis-related variables such as stomata or Rubisco (see section 4).

5.2. Drought limitations on the water flow in plants

5.2.1. The transpiration stream from soil to atmosphere

Lack of soil water poses major perturbations on water, carbon and energy fluxes in the plant. The Soil-Plant-Atmosphere Continuum (SPAC) refers to a physically integrated and dynamic system which describes the water pathway from soil via plants to atmosphere. Water flows within a SPAC component (X) following Darcy's law (Darcy, 1856) which establishes a direct proportionality between a gradient of water potentials and the hydraulic conductance following:

$$q = K_X(\psi_X)(\psi_{X_{i-1}} - \psi_X) \tag{1.44}$$

with $\psi_{X_{i-1}} - \psi_X$ the difference in water potential between two consecutive SPAC components (with water flowing from more positive to more negative values), q the water flux and $K_X(\psi_X)$ the hydraulic conductance in the X SPAC component which is expressed as a function of ψ_X. For example, the flow equation in the leaf is represented by:

$$q = K_{leaf}(\psi_{leaf})(\psi_{xylem} - \psi_{leaf}) \tag{1.45}$$

Assuming a single component in the SPAC, a constant hydraulic conductance in the plant, no water storage and no cavitation, Eq. 1.44 gives:

$$q = K_{plant}(\psi_{soil} - \psi_{atm}) \tag{1.46}$$

This very simple representation of water flow in plants has served as a base for the development of more complex approaches where hydraulic conductances and potentials are broken down into different components as a function of plant tissues and organ proprieties (Carminati & Javaux, 2020). It is clearly evidenced in Eq. 1.46 that transpiration occurs only if the water potential of the atmosphere is lower than the water potential of the soil (counted negative). These water potentials are mediated respectively by the VPD in the atmosphere and the SWC in the soil, both related to the moisture of the media. This gradient of potentials between the soil and the atmopshere allows water to be transported by the cohesion-tension mechanism through the SPAC from roots to leaves (Wolfe *et al.*, 2023). Realistic representations of the SPAC includes many different structures, connected through a dense network of conductances and capacitances following the electric analogy (Hunt *et al.*, 1991). Recent models represent the SPAC as a complex network composed of numerous components including dozens of conductances and capacitances (Cochard *et al.*, 2020). Representing plant hydraulics

yields to complex models that will be described elsewhere in this manuscript (section 3.4). Among the different components of the SPAC, the Soil Water Potential (SWP) and Leaf Water Potential (LWP) are key regulators of the plant water status and its response to edaphic drought (De Swaef *et al.*, 2022; Carminati & Javaux, 2020).

5.2.2. Impact of drought on water potentials in the SPAC

When stomata open to sustain CO_2 diffusion to chloroplasts for photosynthesis, it inevitably leads to a loss of water through transpiration. Under high VPD, the water in the leaves is evaporated, the suction forces between water molecules and leaf cells increase, and so does the LWP towards negative values. Water flows from roots to leaves by either osmotic absorption (when the atmospheric demand is low) or passive absorption (when the atmospheric demand is high) through the SPAC. The tension in the xylem vessels can be modulated by aquaporins which facilitates water transport from the roots to the plant vascular system (Chavarria & dos Santos, 2012). The transpiration flux is maintained as long as roots keep supplying water from the soil to meet the evaporative demand of the atmosphere.

In any aqueous SPAC component, the water potential $\psi_{X,aq}$ can be decomposed as the sum of three components: the matric potential $\psi_{X,mat}$ (due to water-matrix interactions), the gravitational potential $\psi_{X,gra}$ (due to the gravitational force field) and the osmotic potential $\psi_{X,osm}$ (due to electrolytes in the water) (Or *et al.*, 2005):

$$\psi_{X,aq} = \psi_{X,gra} + \psi_{X,osm} + \psi_{X,mat} \tag{1.47}$$

In saturated soils (i.e., all soil pores are filled with water), the gravitational potential is dominant and the matric potential is negligible. In unsaturated soils, when gravitational water has drained out, soil pores exert a force on water molecule high enough to hold water against gravity. The SWP is therefore strongly constrained by the matric potential, which is determined by the surface tension (T_{cap}), the radius of the curvature of the air-water interface (r_{cap}), the soil-water contact angle (α_{cap}) and a adsorptive component directly related to the Van der Waals interaction forces, hydrogen bonding, and electrostatic forces between water molecules and soil pores ($A_{dv}(z)$ at a depth z), following (Tuller *et al.*, 1999):

$$\psi_{soil,mat} = -\frac{2T_{cap}\cos(\alpha_{cap})}{r_{cap}} + A_{dv}(z) = \underbrace{-\frac{2T_{cap}\cos(\alpha_{cap})}{r_{cap}}}_{\text{Capillary water}} + \underbrace{\frac{A_H}{6\pi z^3}}_{\text{Adsorptive water}} \tag{1.48}$$

where A_H is the Hamaker constant between soil pores and water molecules, which varies with the mineral type of the soil particle (Tuller *et al.*, 1999). In unsaturated soils, both capillary and adsorptive water co-exist above a typical value of -10^4 kPa. Under soil drying, capillary water is the being extracted by the plants or being evaporated at the soil surface. Soil water enters into the adsorptive film water regime, which

is the transition zone between capillary and adsorptive soil water. Capillary water disappears from -10^5 kPa for most soils (Luo *et al.*, 2022). It is assumed that water uptake can no longer occur from a matric potential of $\sim$ -1.5 x 10^3 kPa, known as the permanent wilting point located near the adsorbed film region (Richards & Weaver, 1943). From this point onwards, it is hypothesized that soil water cannot be extracted by the roots due to the increasing predominance of adsorptive forces over capillary forces. In the definition of the wilting point itself lies a strong assumption regarding the root water uptake capacities of plants. Is it impeded from the wilting point or from higher soil potential values? The capacity SPAC components to sustain the water flow is characterized by vulnerability curves, which are pivotal for predicting the distribution of water potential in the plant (see chapter 7, section 2.2.1). Water transport in the plant may cease when SWP is significantly higher than the wilting point. This is one of the main uncertainties when modeling the response of ecosystem to water stress (Rogers *et al.* (2017), see section 5.4).

Critical water potentials trigger hormonal and molecular responses at the whole plant level to avoid desiccation (Aroca *et al.*, 2012). For instance, closure of aquaporins, changes in morphological features (e.g., root depth, root length, or root angles) or tissue dehydration (Aroca *et al.*, 2012; Kou *et al.*, 2022; Jalakas *et al.*, 2021) disrupts the transpiration flow along the SPAC. In particular, aquaporins can facilitate the transport of solutes across the cell membrane and act as a regulator of root water uptake (Aroca *et al.*, 2012; Gambetta *et al.*, 2017; Javot & Maurel, 2002). ABscissic Acid (ABA) is also known to be a major hormone regulating the architecture of the root system and the overall plant response to drought (Harris, 2015; Sun *et al.*, 2018). Early sensing of root-induced ABA by leaves allows a quick reaction of plant to the increasing suction forces in the soil by closing stomata to prevent water losses even when LWP remained constant (Davies *et al.*, 2005). Moreover, ABA is known to affect aquaporins gene expression which results in a regulation of root hydraulic conductivity (Kapilan *et al.*, 2018). While it is well established that critical levels of turgor pressure in stomata guard cells triggers the synthesis of ABA (McAdam & Brodribb, 2016), the mechanisms inducing ABA production in roots during water are still poorly understood (Thompson *et al.*, 2007). The increase in ABA biosynthesis by the roots and the facilitation of ABA transport through xylem vessels to stomata is a key adaptive feature for regulating growth and gas exchanges (Davies *et al.*, 2005; Kou *et al.*, 2022; Liu *et al.*, 2022a). As a result, LWP is tightly linked to soil water status and is one of the most important ecophysiological variable for monitoring plant water stress (Ratzmann *et al.*, 2019). Consequently, stomatal dynamics operate on a thin safety margin by dynamically regulating the water flow to protect the vascular system from hydraulic failure while still facilitating CO_2 diffusion to chloroplasts for photosynthesis (Martínez-Vilalta & Garcia-Forner, 2017).

5.2.3. SWC as a proxy of LWP

While being directly related to the forces holding water to plant cells or soil pores, measuring water potentials presents some key limitations. First, LWP is typically measured by labor-consuming and destructive sampling techniques, which complicates the monitoring of plant water status at sub-daily and seasonal temporal scales, or across an entire ecosystem (García-Tejera *et al.*, 2021). Second, in-situ automatic measurements of SWP by tensiometers only provide limited data for studying the response of plants to water stress by (i) not covering the entire range of possible SWP values (Fig. 1.19) with an upper limit of SWP typically below 100 kPa due to cavitation (Menne *et al.*, 2022; Dasgupta *et al.*, 2015; Durner & Or, 2006), (ii) showing low sensitivity to drying-rewetting repeated cycles (noz Carpena *et al.*, 2005), (iii) showing lags in SWP readings when equilibrium is particularly slow to reach and (iv) being sensitive to cavitation of water bubbles at very high pressure in water-filled tensiometers (Bittelli, 2010). The recent development of microtensiometers might represent an interesting technical solution for continuous measurements of LWP (Pagay, 2022; Christenson *et al.*, 2024).

Field automatic SWC sensors are very common and do not suffer from the same shortcomings. SWC is routinely measured on EC sites and provides an estimation of the water content in the soil as a percentage of the control volume of the soil sampled by the sensor. Global in situ soil moisture measurements are also regrouped within unique datasets spanning across many Plant Functional Type (PFT) and climate zones (Dorigo *et al.*, 2011). In addition, SWC in the topsoil can be retrieved at large scales from RS of microwaves from satellites (Njoku & Entekhabi (1996); Zhang *et al.* (2019a), also detailed in chapter 7, section 3.9). The bridge between soil moisture and water potentials is provided by Soil Water Retention Curves (SWRC)s, which describe the relationship between SWC and SWP (Fig. 1.19). These curves are built from (i) joint measurements of SWP and SWC, and (ii) models for describing their relationship such as the van Genuchten (VG) (van Genuchten, 1980) and the Brooks-Corey (Brooks & Corey, 1966) models (Tuller & Or, 2005). SWRCs can also be built by using neural network predictions if the soil type is known (Pham *et al.*, 2019; Novick *et al.*, 2022). These curves are a major soil hydraulic propriety and can be used to illustrate the limiting soil water ranges for plant uptake (Fig. 1.19, (Pan *et al.*, 2019)).

For instance, SWRCs can be used to retrieve the lower and upper limits of accessible water for plant uptake (i.e., the SWC at a SWP of $\sim$-1500 kPa and $\sim$33 kPa or $\sim$10 kPa respectively) respectively known as the wilting point and the field capacity. The difference between the field capacity and the wilting point provides an estimation of the available water for plant uptake in the root zone. The ratio of the actual extractable water (i.e., the difference between the actual soil water content and the wilting point) to the available water (i.e., the difference between the field capacity and the wilting point) is known as Relative Extractable Water (REW) (Eq. 1.49), which is often used

for characterizing the soil water status (Granier *et al.*, 1999a, 2007a), or for defining thresholds from which water should be added to crops to avoid yield losses (Juenger & Verslues, 2022). Note that other names can be found in the literature such as Fraction of Transpirable Soil Water (FTSW), Plant Available Soil Water Content (PASWC), Available Soil Water Content (ASWC) or Soil Water Availability (SWA). The wide availability of SWC data, and the numerous evidences of a strong control of soil moisture on photosynthesis (e.g., Lv *et al.* (2023); Keenan *et al.* (2010b); Trugman *et al.* (2018)) have supported the use of SWC as a key variable controlling water and carbon exchanges. As a result, this variable is used in many LSMs to reproduce drought effects on photosynthesis with the empirical approach, which consists in downregulating model parameters from a threshold of REW. This is detailed in section 5.4 and further discussed in chapter 7, section 5.4.

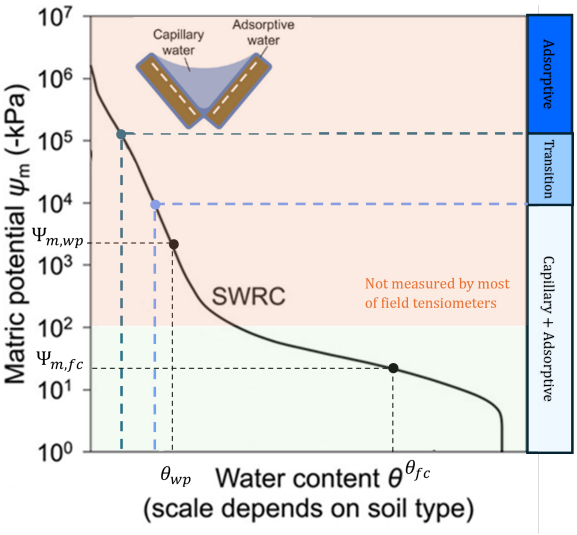

Figure 1.19: Conceptual illustrations of soil water retention regimes at different ranges of matric potential. Most of field tensiometers do not capture the full range of the SWRC. The field capacity and wilting points are set to the SWC at a SWP of -33 kPa and - 1500 kPa. Adapted from Luo *et al.* (2022).

5.3. How drought affects photosynthesis ?

Soil drying triggers complex mechanisms in the plant to avoid hydraulic failure and cavitation. One of these mechanisms is stomatal closure, which can be induced by either passive (i.e., a decrease in leaf water potential and a loss in turgor pressure induced by hydraulic signaling) or active factors (i.e., a sensing of molecules such as ABA, Ca^{2+}, or ROS) (Merilo *et al.*, 2018; Jalakas *et al.*, 2021; Nardini & Salleo, 2000). The closure of stomata limits the diffusion of CO_2 to chloroplasts, which in turn induces a decrease in photosynthesis. As being one of the three pathways for dissipating the

energy carried by sun irradiance, the limitation on photosynthesis triggers a cascade of effects which affects whole plant metabolism. One of the consequences of stomatal closure is the reduction of NADP+ regeneration in the CBB cycle, thus limiting light reactions and electron transport. The limitation of photosynthesis by constraining CO_2 supply also leads to an accumulation of ROS and photoinhibition damages (Cruz De Carvalho, 2008). Severe water shortage episodes also directly impacts the CBB cycle by regulating Rubisco synthesis through the production of tight-binding inhibitors (Parry, 2002). In addition, a decrease in mesophyll conductance can also be observed under water stress, which increase the constraint on CO_2 supply to chloroplasts (Flexas *et al.*, 2012). Additional information regarding drought effects on the photosynthetic apparatus will be described in the next chapters.

The origins of photosynthesis limitations have been historically defined along the stomatal versus non-stomatal categorization, first described by Jones (1985) and later mathematically formulated by Grassi & Magnani (2005). The Jones' definition is based on the assumption that photosynthesis limitations either originate from a closure of stomata through a decrease in stomatal conductance (g_s), and by non-stomatal factors through a decrease in the apparent maximum carboxylation rate of Rubisco ($V_{cmax,app}$). These origins are refereed in this thesis to as respectively Stomatal Origin Limitation of photosynthesis (SOL) and Non-Stomatal Origin Limitation of photosynthesis (NSOL). This framework has been widely used to determine the importance of each physiological factor in the reduction of carbon assimilation under water stress (e.g., Grassi & Magnani (2005); Grassi *et al.* (2009); Zait & Schwartz (2018)). One main drawback of this approach is the strong correlation between stomatal conductance and photosynthesis (Wong *et al.*, 1979). In particular, in most of stomatal conductance models such as the USO model, both variables are linked to coordinate the opening of stomata with the supply of CO_2 to the fixation sites in the chloroplasts (Lemonnier & Lawson, 2023). As a result, a decrease in g_s can also originate from a decrease in A_n, V_{cmax} or g_m, potentially leading to an underestimation of the contribution of NSOL in limiting photosynthesis (also corresponding to an overestimation of SOL). An alternative approach consists in using the USO model to quantitatively decompose the effects of stomatal closure drivers (i.e., VPD, A_n, g_1 or C_s, Eq. 1.35), and to redefine the stomatal control on photosynthesis. Instead of using a decrease in g_s as an evidence of SOL, Zhou *et al.* (2013) suggested to associate the stomatal effect on A_n to a change in the stomatal sensitivity to photosynthesis g_1, which varies according to the water cost of carbon gain (Medlyn *et al.*, 2011a). When photosynthesis limitations originate from NSOL, A_n is affected by additional internal factors (g_m, or V_{cmax}) which decouple the relationship between A_n and g_s, and is evidenced by an increase in g_1. On the other hand, SOL on photosynthesis is associated to an increase in the ratio A_n/g_s (i.e., maximizing carbon gains while minimizing water losses, decrease in g_1) or a constant A_n/g_s (i.e., no maximization of carbon gains : both A_n and g_s decrease with the same magnitude, g_1 constant). With this framework, variation of

g_1 can be used to clearly identify the role played by non-stomatal factors and avoids any underestimation of NSOL in limiting photosynthesis (Zhou *et al.*, 2013).

While the response of SOL and NSOL to water stress provides an indication of the dominant mechanism constraining photosynthesis, it does not allow to quantify the importance of these processes. To that end, partial derivative calculus can be used to link the total derivative of photosynthesis to the total derivative of the explanatory variables according to a selected model. With this approach, the relative variation of A_n compared to a reference value can be decomposed as a sum of the relative variations of the explanatory variables. The reference value can be typically associated to the soil water availability conditions that are not limiting for physiological processes. This framework can be adapted to any model for quantifying the role of model parameters in limiting photosynthesis under water stress if (i) the effects of other environmental factors are considered (e.g., by normalizing to 25°C and by collecting measurements at light saturation), (ii) the explanatory variables are measured and (iii) their relationship to soil water availability are characterized. It is therefore possible to combine the FvCB and USO models in the limitation analysis to quantitatively assess the importance of the constrains of VPD, g_1, C_s, g_m and V_{cmax} on A_n and g_s. See chapter 5 for more details.

5.4. How to implement drought effects on photosynthesis in modeling

Investigating the response of physiological processes to the decrease in soil water availability is pivotal for understanding drought effects on ecosystems. This can be used for studying ecosystem resilience to drought or for improving the representation of water stress impact on physiological processes in LSMs. Most LSMs use an empirical factor (i.e., the β factor) which acts as a modifier on model parameters to reproduce the effects of soil moisture on photosynthesis (Rogers *et al.*, 2017). β is directly linked to REW by (Egea *et al.*, 2011; Harper *et al.*, 2021):

$$\beta = \begin{cases} 1 & \theta \geq \theta_{sup} \\ \left(\dfrac{\theta - \theta_{wp}}{\theta_{fc} - \theta_{wp}} \right)^p = REW^p & \theta_{inf} < \theta < \theta_{sup} \\ 0 & \theta \leq \theta_{inf} \end{cases} \tag{1.49}$$

with p allowing to implement a nonlinear dependence of model parameters on REW, θ_{fc} the field capacity, θ_{wp} the wilting point and θ the actual SWC of the soil layer. Eq. 1.49 can be applied to the different soil layers in the root zone. A weighting parameter is used to consider the proportion of Root Biomass Density (RBD) or rooting depth within each soil layer. For instance, in the Joint UK Land Environment Simulator (JULES) model, this weighting factor is expressed as a function of the root fraction (Harper *et al.*, 2021):

$$\beta = \sum_{k=1}^{n_{soil}} e^{z_k/d_r}\ \beta_k \tag{1.50}$$

where k is the soil layer index, n_{soil} is the total number of soil layers, z is the depth of the k soil layer, β_k is β within each soil layer k, and d_r a PFT-specific parameter which consider the root mass distribution in the soil (i.e., the smaller the d_r, the more important root biomass in the shallow soil layers). Other approaches consist in weighting β by a factor proportional to the RBD as implemented in several LSMs such as in Community Atmosphere Biosphere Land Exchange (CABLE) or in ORCHIDEE (Haverd *et al.*, 2016; Best *et al.*, 2011; Haverd *et al.*, 2016).

In addition to the root distribution profile, other important aspects of β calculation should be highlighted. First, it is unclear which parameter should be affected by β to reproduce realistic responses of photosynthesis and transpiration to water stress (Trugman *et al.*, 2018; Rogers *et al.*, 2017). Second, in Eq. 1.49, β affects SOL or NSOL when REW drops below θ_{fc}. However, it has been shown that plants can maintain high photosynthetic capacities and sustain transpiration even when $\theta \leq \theta_{fc}$ (e.g., Granier *et al.* (2007a)). As a result, the shape and thresholds of β are PFTs-specific and induce major divergences in the response of net photosynthesis to water stress (e.g., Fig. 1.20). Calibrating β on field data is therefore needed (Rogers *et al.*, 2017; Vidale *et al.*, 2021). An overview of the interdependences between stomatal conductance, photosynthesis at light saturation and abiotic drivers as formulated in the FvCB and USO models is shown in Fig. 1.21.

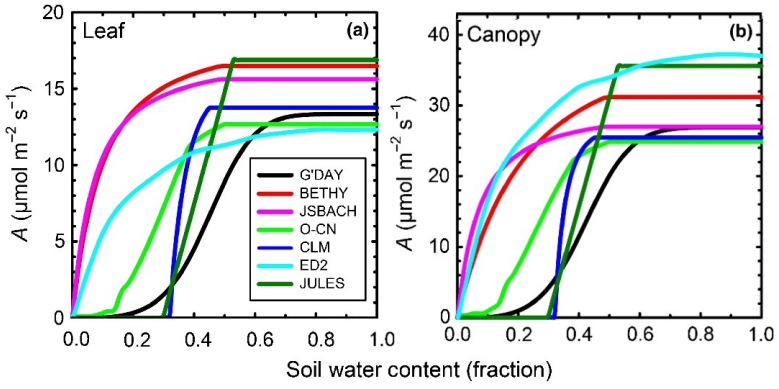

Figure 1.20: Examples of photosynthesis response to REW in several LSMs (Rogers *et al.*, 2017).

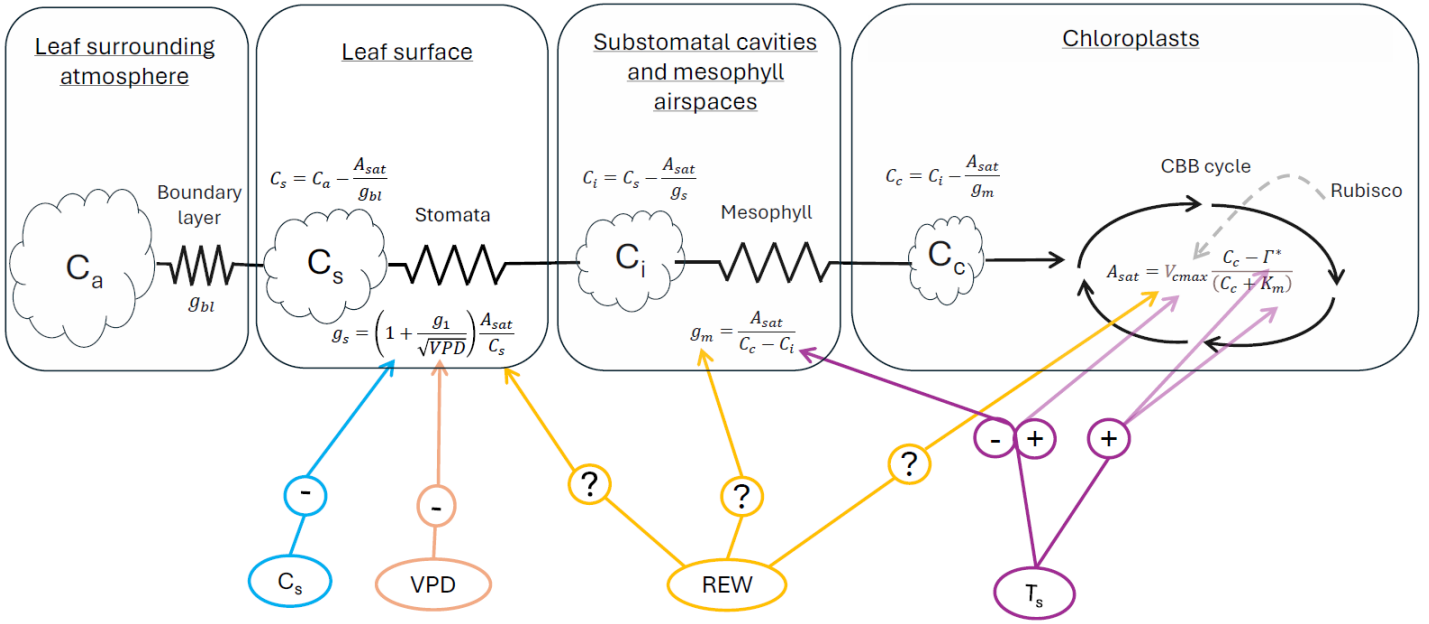

Figure 1.21: Diagram of the effects of abiotic factors on stomatal conductance and photosynthesis at light saturation. The control exerted by one variable over another (either a positive (+) or negative (–) relationship) is determined from calculating the partial derivatives using the FvCB and USO models. The equations for g_s, g_m, A_{sat}, C_i and C_c can be found in section 4. g_{bl} is boundary layer conductance. The double sign for the surface temperature T_s refers to the Arrhenius-peak model: either a positive relationship below the optimum (25°C), or negative above the optimum.

2

Objectives and structure of the thesis

1. Objectives of the thesis

Characterizing the response of photosynthesis model parameters under water stress is crucial for identifying the factors limiting GPP in the context of climate change. Modeling these constraints requires the calibration of β, an empirical factor responsible for implementing drought effects on photosynthesis in LSMs. In this thesis, we specifically focused on crops, which are key components of terrestrial ecosystems by participating to the regulation of the carbon and water cycles, and by providing pivotal ecosystem services such as food production for humanity and livestock. Large uncertainties still remain for identifying the physiological constraints on photosynthesis and transpiration of croplands under soil water stress (Yuan *et al.*, 2015; Xia *et al.*, 2021; Jiang *et al.*, 2023). The BIODYNE research department has a long-term expertise in analyzing gas exchanges of crops by managing the EC site of Lonzée (site code BE-Lon) for more than 20 years. This 4-year rotation cropland is typical of central Belgium and is equipped with a collection of instruments for monitoring fluxes and their environmental drivers at the ecosystem-atmosphere interface (Delandmeter *et al.*, 2023; MOUREAUX *et al.*, 2008; Lognoul *et al.*, 2019; Moureaux *et al.*, 2012; Buysse *et al.*, 2017; Moureaux *et al.*, 2006; Bachy *et al.*, 2013; Suleau *et al.*, 2011; Kutsch *et al.*, 2010).

This thesis started in 2018, which was a year of severe drought in western Europe. This year, potato (*Solanum tuberosum*) was cultivated at BE-Lon, as part of the 4-year rotation with winter wheat (*Triticum aestivum*) and sugar beet (*Beta vulgaris*). At the same time, Louis Gourlez de la Motte (former BIODYNE researcher) started his post-doc on the effects of drought on forest ecosystems. The objectives of his work were very similar to those of this thesis: understanding the constraints of drought on forests by calibrating β on SOL and NSOL and by using EC data during the 2018 drought. It was a natural step for us to work together. This study, to which I participated as co-author for helping in designing the method (chapter 3), laid the foundations of the following chapters dedicated to potato (chapter 4 and chapter 5).

While providing large datasets of gas exchanges which can be used to calibrate the response of photosynthetic processes to water stress, the EC technique does not allow to fully unravel the physiological mechanisms involved in fluxes limitations. In particular, the response of $V_{cmax,app}$ (i.e., considered as NSOL) can be driven by either the mesophyll conductance g_m or the true carboxylation rate V_{cmax}. Therefore, EC data only provides a limited understanding of the mechanisms regulating photosynthesis under water stress. Further information on photosynthesis constraints are provided by leaf-level measurements of ChlF, which allow to determine the mesophyll conductance, a critical ecophysiological parameter causing major restrictions in CO_2 diffusion to chloroplasts. While numerous studies have already highlighted that mesophyll conductance may decrease under water stress, strong uncertainties remain on the response of g_m to soil water availability, which is likely regulated by PFT and

specie-specific adaptive characteristics to drought. To reduce these uncertainties, we characterized the response of g_m and V_{cmax} to water stress by performing joint gas exchange and actively-induced chlorophyll fluorescence measurements at the leaf level during a drought experiment conducted on potato. In the perspective of improving crops yield, quantitatively assessing the most important constraints on photosynthesis under water stress is crucial. To that end, partitioning analysis can be used to decompose the relative variation of net photosynthesis into the sum of relative variations of SOL and NSOL (Grassi & Magnani, 2005). We aimed to modify this partitioning scheme by coupling the FvCB and USO models. The main advantage of this approach is to link the variability of A to g_m, VPD and g_1, which therefore allows to identify the feedback effect of non-stomatal factors on stomatal closure. Such method would help in unravelling the role played by the mesophyll conductance in constraining stomatal conductance and photosynthesis responses to soil water availability.

Leaf-level ChlF measurements are however limited for estimating g_m of large patches of vegetation and do not allow to track sub-daily variations of NSOL by being time and labor-consuming. The recent emergence of SIF has allowed the collection of automatic measurements of ChlF at the ecosystem scale. SIF provides a proxy of vegetation physiological processes, which allows a direct estimation of photosynthesis using a small set of mechanistic equations if few key physiological parameters are known. The last objective of this thesis consisted in testing the capability of the MLR-USO model for estimating GPP and Tr under natural conditions, including soil water availability-limiting conditions. This approach will help in investigating the response of physiological processes to drought and improving the understanding of carbon and water fluxes temporal variability in the context of climate change. The first SIF measurements campaign started in 2022 at BE-Lon, which was the year of winter wheat cultivation. As a result, this thesis exclusively focused on winter wheat in chapter 6. Their importance for the agricultural production system in Belgium and Western Europe is outlined in chapter 4, chapter 5 and chapter 6.

The objectives of this thesis can be summarized as (Fig. 2.1):

Objective 1: Calibrating the response of stomatal and non-stomatal limitations on photosynthesis to soil water availability (chapters 3, 4 and 5).

Objective 2: Using a new partitioning approach to quantify the contributions of stomatal and non-stomatal limitations to the decrease in photosynthesis under water stress (chapter 5).

Objective 3: Testing a novel mechanistic approach to model photosynthesis and transpiration from sun-induced chlorophyll fluorescence at the ecosystem scale (chapter 6).

2. List of publications

- Gourlez de la Motte L., **Beauclaire, Q**., Heinesch, B., Cuntz, M., Foltýnová, L., Šigut, L., Kowalska, N., Manca, G., Goded Ballarin, I., Vincke, C., Roland, M., Ibrom, A., Lousteau, D., Siebicke, L., Neiryink J., and Longdoz B., 2020. Non-stomatal processes reduce gross primary productivity in temperate forest ecosystems during severe edaphic drought. Philosophical Transactions of the Royal Society B-Biological Sciences.
https://doi.org/10.1098/rstb.2019.0527

- **Beauclaire, Q**., Heinesch, B., Longdoz, B., 2023. Non-stomatal processes are responsible for the decrease in gross primary production of a potato crop during edaphic drought. Agricultural and Forest Meteorology.
https://doi.org/10.1016/j.agrformet.2023.109782

- **Beauclaire, Q**., Vanden Brande F., Longdoz B. New method to partition the origins of photosynthesis limitations of potato under soil water availability-limiting conditions (*in prep*)

- **Beauclaire, Q**., De Cannière, S., Jonard, F., Delhez, L., Pezzetti, N., Longdoz, B., 2023. Modeling gross primary production and transpiration from sun-induced chlorophyll fluorescence using a mechanistic light-response approach. Remote Sensing of Environment.
https://doi.org/10.1016/j.rse.2024.114150

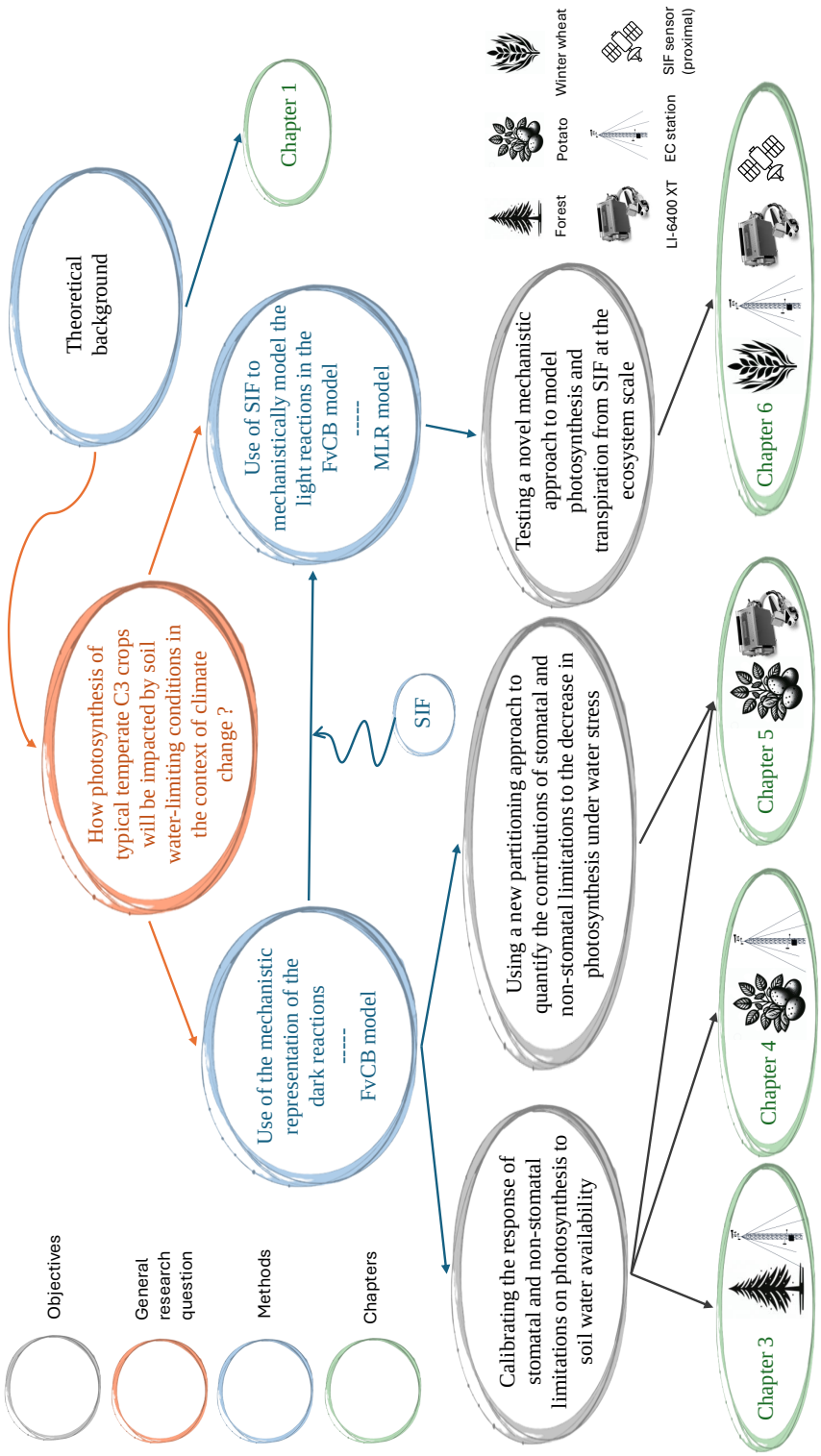

Figure 2.1: Flowchart of the thesis

3

Non-stomatal processes reduce gross primary productivity in temperate forest ecosystems during severe edaphic drought

This paper has been published as:

Gourlez de la Motte L., Beauclaire, Q., Heinesch, B., Cuntz, M., Foltýnová, L., Šigut, L., Kowalska, N., Manca, G., Goded Ballarin, I., Vincke, C., Roland, M., Ibrom, A., Lousteau, D., Siebicke, L., Neiryink J., and Longdoz B., 2020. Non-stomatal processes reduce gross primary productivity in temperate forest ecosystems during severe edaphic drought. Philosophical Transactions of the Royal Society B-Biological Sciences.
https://doi.org/10.1098/rstb.2019.0527

Abstract

Severe drought events are known to cause important reductions of GPP in forest ecosystems. However, it is still unclear whether this reduction originates from SOL and/or NSOL. In this study, we investigated the impact of edaphic drought in 2018 on GPP and its origin (SOL, NSOL) using a dataset of 10 European forest ecosystem flux towers. In all stations where GPP reductions were observed during the drought, these were largely explained by declines in the maximum apparent canopy scale carboxylation rate $V_{cmax,app}$ (NSOL) when the soil relative extractable water content dropped below around 0.4. Concurrently, we found that the stomatal slope parameter (G_1 , related to SOL) of the Medlyn et al. unified optimization model linking vegetation conductance and GPP remained relatively constant. These results strengthen the increasing evidence that NSOL should be included in stomatal conductance/photosynthesis models to faithfully simulate both GPP and water fluxes in forest ecosystems during severe drought.

This article is part of the special issue 'Impacts of the 2018 severe drought and heatwave in Europe: from site to continental scale'.

1. Introduction

With global climate change, droughts are likely to be more intense (Trenberth *et al.*, 2014; Vogel *et al.*, 2019). In 2018, a severe drought event occurred in Northern and central Europe causing forest fires and crop yield losses (Toreti *et al.*, 2019). Europe experienced a major reduction of GPP and transpiration (E) similarly to previous extreme events such as the 2003 Europe drought-heatwave (Ciais *et al.*, 2005) mostly because of soil water limitation (Granier *et al.*, 2007a; REICHSTEIN *et al.*, 2007). Continuous measurements of ecosystem CO_2 and water fluxes captured throughout Europe at EC flux tower stations thus provide a great large-scale 'natural experiment' to study the impact of drought on GPP and E (Sippel *et al.*, 2018).

There is increasing evidence that GPP reductions due to droughts could originate from both changes in stomatal behaviour (SOL) and non-stomatal traits (NSOL) (MIGLIAVACCA *et al.*, 2011; Egea *et al.*, 2011; Zhou *et al.*, 2013; Xu & Baldocchi, 2003; reichstein *et al.*, 2002). Proposed NSOL mechanisms are reduced Rubisco activity

(carboxylation rate) and/or electron transport activity (Reichstein, 2003), reduced active Leaf Area Index (LAI) (Reichstein *et al.*, 2003), reduced mesophyll conductance (including the intercellular airspace, cell walls, plasma membranes, cytoplasm and the chloroplast envelopes (Knauer *et al.*, 2019a), g_m) (Keenan *et al.*, 2010a) or a combination of those (Egea *et al.*, 2011; Zhou *et al.*, 2019b). The cause of GPP reduction is still subject to debate (Rogers *et al.*, 2017; Chaves *et al.*, 2009) and the modelling of SOL and NSOL and their (de)coupling is still poorly constrained by data. As a result, there is a strong need to examine whether different mechanisms are relevant and if models could be improved by developing more evidence-based functions for the impact of drought stress (Drake *et al.*, 2017; Medlyn *et al.*, 2016).

In leaf/canopy photosynthesis models, gross primary assimilation (A) is very often modelled using the FvCB photosynthesis model for C3 species (Zhou *et al.*, 2013; Xu & Baldocchi, 2003; Reichstein, 2003). In this model, Rubisco-limited photosynthesis (usually close to light saturation) is a function of the maximum carboxylation rate (V_{cmax}) and the internal CO_2 leaf concentration (C_i) which implicitly considers that C_i is equal to the CO_2 concentration in the chloroplasts (C_c). As C_i cannot be measured directly, it is usually approximated by employing Fick's diffusion law through the stomata using a stomatal conductance (g_s). This representation requires the determination of stomatal conductance by modelling. In this study, following (Zhou *et al.*, 2013), we use the concept of apparent V_{cmax} ($V_{cmax,app}$) recognizing that variations in $V_{cmax,app}$ can result either from changes in the actual maximum rate of carboxylation or from changes in g_m which are not explicitly represented in this diffusion model. Consequently, when drought occurs, it impacts directly stomatal behaviour (closure) and then photosynthesis by limiting the diffusion of CO_2 into the leaf which results in reduced C_i (SOL) or/and it impacts non-stomatal mechanisms (NSOL) which result in decreases of $V_{cmax,app}$ (Zhou *et al.*, 2013; Drake *et al.*, 2017).

A long standing stomatal conductance model from Cowan & Farquhar (1977) states that stomata should act to maximize carbon gains while minimizing water losses (transpiration, E), that is to maximize the integrated sum of A–E where λ (mol C mol^1 H2O) is the carbon cost of water gain $\rho A/\rho E$ or marginal water-use efficiency (Manzoni *et al.*, 2011) (note that we inverted the original expression). Medlyn *et al.* (2011a) proposed a reconciliation of the optimal stomatal behaviour theory (Cowan & Farquhar, 1977) with empirical stomatal models linking g_s and A. Their work resulted in a USO model with a form similar to former empirical expressions (see equation (2.3)) where the slope between g_s and $A * f(g_1)$ is a key parameter (called the stomatal slope parameter). g_1 is directly interpretable as inversely related to λ and to intrinsic WUE (A/g_s) normalized by VPD and CO_2 air concentration (C_a) (Knauer *et al.*, 2018b).

The USO model has been used both at the leaf level using leaf gas exchange data (Lin *et al.*, 2015b) and at the ecosystem level using EC flux observations (Medlyn *et al.*, 2017a) during non-water limited periods. During water limited periods, various

responses of g_1 (leaf level, SOL) to soil moisture were found (Zhou *et al.*, 2013) for a large range of species while a more consistent pattern of decreasing $V_{cmax,app}$ was found. In a recent work, a good correlation between leaf scale and ecosystem scale g_1 (or G_1) response to soil moisture was found in a woodland dominated by Acacia trees thereby demonstrating the ability of both leaf and ecosystem scale approaches to quantify drought effect (Tarin *et al.*, 2020b).

In this study, we used the USO model combined with the Farquhar C3 model (considering that $C_i = C_c$) to study the origin of edaphic drought impacts on GPP (SOL and/or NSOL) in forest ecosystems using EC flux measurements by replacing leaf-level variables by their ecosystems analogues using a big leaf framework (Knauer *et al.*, 2018b,a). The surface conductance (G_s analogous to g_s) was estimated by inverting the Penman–Monteith equation (Monteith, 1965). We then inferred the bulk stomatal slope parameter (G_1 analogous to g_1) and the maximum apparent carboxylation rate of the ecosystem ($V_{cmax,app}$) (Kosugi *et al.*, 2013) at a daily time step for each ecosystem. The study was restricted to the growing period excluding any autumn senescence or spring leaf emergence influence on the variation of $V_{cmax,app}$.

In addition, drought intensity was quantified using the REW as proposed by Granier *et al.* (1999a), which is a normalized index of soil water deficit varying from 0 to 1 that allows for edaphic status inter-site comparisons. This index was used in previous studies (Granier *et al.*, 1999a, 2007a) and, based on their results, we hypothesize that both E and GPP reductions will occur when REW falls below ~ 0.4.

The objective of this work is to examine the response of G_1, as a measure for SOL, and $V_{cmax,app}$, as a measure for NSOL, to soil water deficit using EC data collected in forests during the 2018 European drought. More specifically, we intend to answer the following questions: (1) how was REW impacted by the drought in forest sites in 2018? (2) Can we confirm the REW threshold of ~ 0.4 for GPP reductions found in previous studies (Granier *et al.*, 1999a, 2007a)? (3) To what degree did SOL and NSOL impact GPP during the drought? (4) What were G_1 and $V_{cmax,app}$ responses to REW function shapes and how did these responses vary across sites?

2. Material and methods

2.1. Site and data description

Data have been processed by the Ecosystem Thematic Centre of the Integrated Carbon Observation System (ICOS) and form the 2018 drought ICOS/Fluxnet dataset (Drought 2018 Team & ICOS Ecosystem Thematic Centre, 2019), which is a compilation of EC fluxes, meteorological and edaphic data during the 2018 European drought at half-hourly resolution. Only sites with a sufficiently resolved vertical profile of soil water content sensors were selected. The main site characteristics are summarized in table 3.1. Flux data followed the standard FLUXNET processing (Aubinet *et al.*,

1999), including friction velocity (u*) filtering (Papale *et al.*, 2006) and GPP determination by night-time flux partitioning (Reichstein *et al.*, 2005). Only data marked with highest quality flags were used for this study. Latent heat fluxes were not corrected for energy balance closure.

Table 3.1: Main characteristics of the flux tower sites included in this study. The LAI corresponds to the maximum LAI typically observed at the sites. Please refer to the online version of the article for references.

site ID	country	latitude	longitude	dominating species	LAI m^2 m^{-2}	soil texture	rooting depth m	ref
BE-Bra	Belgium	51.308	4.52	*Pinus syvlestris*	3	sand	1	[36]
BE-Vie	Belgium	50.305	5.998	*Fagus sylvatica/Pseudotsuga menziesii*	5	silty clay loam	1.4	[37]
CZ-Lnz	Czechia	48.682	16.946	*Quercus robur/Fraxinus angustifolia/Carpinus betulus/Tilia cordata*	6.5	sandy loam	1.2	[38]
CZ-Raj	Czechia	49.444	16.697	*Picea abies*	5	sandy loam	0.7	[39]
CZ-Stn	Czechia	49.036	17.97	*Fagus sylvatica*	5.5	sandy loam	0.7	[40]
DE-Hai	Germany	51.0792	10.453	*Fagus sylvatica*	6	clay loam	0.7	[41,42]
DK-Sor	Denmark	55.486	11.645	*Fagus sylvatica*	5	sandy clay loam	1	[43]
FR-Bil	France	44.494	−0.956	*Pinus pinaster*	2.5	sand	1.1	[44]
FR-Hes	France	48.674	7.065	*Fagus sylvatica*	6.5	silty clay loam	1.6	[45]
IT-Sr2	Italy	43.732	10.291	*Pinus pinea*	2.5	sand	1.2	

2.2. Quantification of drought

The intensity of edaphic drought was quantified by computing the REW content (Granier *et al.*, 2007a) at each time step and for the entire root depth using:

$$REW = \frac{\sum_i \left(SWC_i - SWC_{WP,i}\right) / \left(SWC_{FC,i} - SWC_{WP,i}\right)}{h_{max}} \tag{3.1}$$

where i is the index of each soil layer over the rooting depth, SWC_i is the actual SWC, SWC_{WP} is the SWC at the wilting point, SWC_{FC} is the SWC at field capacity, Δh is the thickness of each layer and h_{max} is the maximum rooting depth. Each soil horizon was divided into soil layers corresponding to the number of sensors installed in the horizon. The layer boundaries were the horizon limits or the midway point between two sensors. Soils related data are summarized in the supplements (electronic supplementary material, table S1). For each layer, SWC_{WP} and SWC_{FC} were estimated using soil retention curves based on either measurements (by research teams) or modelling (based on soil textures) and checked for consistency with SWC 48 h after a rain event for SWC_{FC} and with minimum SWC values observed at the site for SWC_{WP} to avoid negative REW values. When not available, the maximum depth was defined as the bedrock depth (Granier *et al.*, 2007a). When data were available

(BE-Vie and BE-Bra), REW was corrected for the coarse fraction by applying a correction factor for each layer. According to Granier *et al.* (2007a, 1999a) it is expected that both GPP and G_s start to decrease when REW drops below 0.4. The evolution of REW at each site in 2018 is presented in the electronic supplementary material, figure S1.

2.3. Canopy surface variables

Detailed computation procedures for canopy surface variables are fully described in Knauer *et al.* (2018a). First the aerodynamic conductance to water transfer (G_{aw}) was computed as a combination of an aerodynamic conductance to momentum (first term) and a boundary layer conductance (second term) as follows:

$$G_{aw} = \left(\frac{u_*^2}{u(z)} + \left(6.2 u_*^{-0.667}\right)^{-1} \right)^{-1} \tag{3.2}$$

where $u*$ is the friction velocity (m s^{-1}), and $u(z)$ the wind speed at measurement height (z). Canopy surface conductance for water (G_s, (m s^{-1}) was computed by inverting the Penman–Monteith equation (Monteith, 1965):

$$G_s = \frac{G_{aw}\gamma LE}{\Delta(R_n - G - S) + \rho_a c_p G_{ah} VPD_s - (\Delta + \gamma)LE} \tag{3.3}$$

where LE is the latent heat flux (W m^{-2}), γ is the psychrometric constant (Pa K^{-1}), s is the slope of the saturation vapour pressure curve at air temperature (Pa K^{-1}), R_n is the net radiation (W m^{-2}), G is the ground heat flux (W m^{-2}), S is the sum of all storage terms (W m^{-2}), C_p is the heat capacity of dry air (1005 J kg^{-1} K^{-1}) and VPD_a is the VPD of ambient air (Pa). G was considered negligible when not available while S was not available and was set to 0 at all sites. The CO_2 concentration at the canopy surface (C_s), needed in the USO and diffusion equations, was computed as:

$$C_s = C_a + \frac{NEE}{G_{aw}/1.32} \tag{3.4}$$

where C_a (μmol CO_2 mol^{-1}) is the CO_2 air concentration at the measurement height, NEE (μmol CO_2 m^{-2}) is the net CO_2 ecosystem exchange and the factor 1.32 is the ratio of diffusivities of CO_2 and water vapour in the boundary layer. The VPD at the canopy surface (VPD_s, Pa) was also computed (see Knauer *et al.* (2018a) for more details). G_s is a good predictor of bulk stomatal conductance only when evaporation is small compared to transpiration; data collected during a period of 48 h following a rain event were discarded. Secondly, the analysis was restricted to the growing season, avoiding senescence and leaf emergence periods. We defined this period as the days when the daily GPP (averaged over all the available years) smoothed with a 15 days

moving average window was higher than 70% of the 95th percentile of the daily GPP distribution. G_s data were also filtered excluding half hour with $LE < 0$ or $R_n < 0$. Negative G_s values were filtered and G_s outliers were also discarded by removing data when G_s were higher than the 98th percentile of the G_s distribution.

2.4. Stomatal origin limitation

Similarly to previous work (Zhou *et al.*, 2013; Héroult *et al.*, 2013), reductions of GPP originating from SOL were assessed by analysing dependence on REW of the G_1 parameter used in the USO model developed by Medlyn *et al.* (2011a) but adapted to the ecosystem scale using bulk ecosystem parameters (Knauer *et al.*, 2018a):

$$G_s = G_0 + 1.6 \left(1 + \frac{G_1}{\sqrt{VPD_s}}\right) \frac{GPP_{high}}{C_s} \tag{3.5}$$

where, GPP_{high} is the GPP at high radiation (R_g > 500 W m^{-2}) and replaces net assimilation in the original leaf scale expression of the model, G_s replaces stomatal conductance and leaf surface variables were replaced by their corresponding canopy surface values (Wang *et al.*, 2009) (C_s the air CO_2, VPD_s). In this expression, the nocturnal stomatal conductance G_0 was set to 0 as its magnitude can be considered negligible when compared to the other terms at saturating daylight conditions [27]. G_1, the slope parameter, is a physiologically meaningful parameter as it was shown to be inversely related to λ (Medlyn *et al.*, 2011a) and to iWUE (Knauer *et al.*, 2018a).

G_1 was obtained by inverting equation (3.5) using half-hourly measurements. Because leaf respiration was neglected in equation (3.5), the equation was inverted only for high radiation data so that GPP_{high} should be much higher than leaf respiration. Negative G_1 values were filtered and outliers were also discarded by removing data when absolute G_1 was two times higher than the average absolute deviation from the median. Finally, daily G_1 averages were then computed for days with at least five valid half-hourly values.

The response of G_1 to REW was fitted with a segmented linear response curve (two segments) in order to test the presence of an REW threshold (break point) above which G_1 is constant (no effect range) and under which stomatal regulation occurs (G_1 decreases or increases) (Oosterbaan *et al.*, 1990). After a first fit, outliers were removed by exclusion of the G_1 value having absolute residuals more than 2.2 times the standard deviation of the residuals distribution. A second fit was then done. Parameters obtained from a second fit were G_1^*, i.e. the average G_1 value within the 'no effect range', the break point REW value ($REW_{B,G1}$) and the slope/intercept of the G_1 decrease/increase. The presence of the break point was further tested by comparing the residuals of the model to those of a simple linear regression model using an F-test.

2.5. Non-stomatal origin limitation

Reductions of GPP originating from NSOL were studied by assessing the effect of water stress on apparent bulk V_{cmax} hereafter called $V_{cmax,app}$. It was obtained by inverting the expression of Rubisco-limited photosynthesis during high radiation conditions (Farquhar *et al.*, 1980):

$$V_{cmax,app} = \frac{GPP_{high}\,(C_i + K_m)}{(C_i - \Gamma^*)} \tag{3.6}$$

where $V_{cmax,app}$ is expressed per m^2 of soil and not of leaf as usual. K_m is the effective Michaelis Menten coefficient kinetics and Γ^* is the CO_2 compensation point, which were both computed using temperature responses following (Bernacchi *et al.*, 2001), GPP_{high} is the GPP at R_g > 500 W m^{-2} while C_i was computed using Fick's diffusion law (Farquhar & Sharkey, 1982):

$$C_i = C_s - \frac{GPP_{high}}{G_s/1.6} \tag{3.7}$$

Note than in equations (3.3)-(3.7), leaf respiration was neglected which should have a small effect on the results as, at high radiation, leaf respiration should be much smaller than GPP . Half-hourly values of $V_{cmax,app}$ were then normalized for temperature to 25°C using an Arrhenius equation (Knauer *et al.*, 2018a) fitted for each decile of REW as $V_{cmax,app}$ response to temperature was found to decrease under drought conditions. Finally, $V_{cmax,app}$ was averaged on a daily basis and days with less than 5 half-hourly values were discarded. Considering the way we estimated $V_{cmax,app}$, a decrease in $V_{cmax,app}$ indicates NSOL of GPP including either changes in mesophyll conductance or in actual V_{cmax} or other processes limiting GPP (apart from stomatal closure). The response of $V_{cmax,app}$ to REW was assessed using the same segmented linear regression model as explained in the previous section. $V^*_{cmax,app}$ and $REW_{B,Vcmax}$ were defined as the average of $V_{cmax,app}$ values (normalized at 25°C) within the no effect range and the break point REW value, respectively.

2.6. Degree of stomatal and non stomatal origin limitation

To illustrate the degree of SOL and NSOL due to edaphic drought, following Zhou *et al.* (2013), a sensitivity analysis was performed to explore the impact of drought-induced changes in G_1 and $V_{cmax,app}$ on GPP . The impact of NSOL was assessed by comparing measured GPP to a theoretical non-affected value corresponding to a 'modelled' GPP computed using inverted equation (3.5) with $V^*_{cmax,app}$ instead of $V_{cmax,app}$ and a C_i obtained from equation (3.6) using observed G_s values (equation (3.3)) and measured GPP values. Similarly, the impact of SOL was assessed by comparing measured GPP to 'modelled' unaffected GPP computed using constant G^*_1 values and ob-

served $V_{cmax,app}$ values. The degree of limitation (DoL) was computed as the ratio of modelled 'unaffected' GPP against measured GPP and represents the factor by which GPP was divided because of SOL or NSOL.

3. Results

3.1. G_s and GPP_{high}

GPP_{high} and G_s (for R_g > 500) normalized by their respective maximum values in relation with REW are presented in figure 1. At all sites, we can observe that both GPP_{high} and G_s behave similarly. High values of both GPP_{high} and G_s were observed for high REW while both variables decreased simultaneously with REW. There was an exception at BE-Vie where such a pattern was not observed although both variables still behaved similarly. The lowest GPP_{high} and G_s values were observed at sites such as CZ-Raj, FR-Bil and DE-Hai where very low REW values (lower than 0.15) were reached. At IT-Sr2, Gs and GPP_{high} were still quite high (around half of maximum values) even for very low REW values most probably because, in this sandy soil, rooting depth was probably deeper than the deepest available SWC sensor (1.2 m, see electronic supplementary material, table S1) which caused an underestimation of REW.

3.2. Response of G_1 to edaphic drought

G_1 was found to be constant at all sites apart from DE-Hai even for sites where REW values lower than 0.4 were observed (figure 2). In BE-Bra G1 seems to be enhanced at low REW but the segmented model did not perform significantly better than the linear one. In DE-Hai, G1 was found to increase when REW dropped below a very low value of 0.2, which is quite close to the wilting point. Such low REW were also observed during the growing season at CZ-Raj and IT-Sr2 but no similar behaviour was observed. The lowest G_1^* (1.5 $kPa^{0.5}$ at CZ-Raj) was three times lower than the highest value (4.5 $kPa^{0.5}$ at FR-Bil, table 2).

3.3. Response of $V_{cmax,app}$ to edaphic drought

The effect of NSOL caused by drought was studied by analysing the dependence of the temperature normalized $V_{cmax,app}$ values on REW (figure 3). At all sites that experienced low REW conditions (below $\sim$ 0.4) apart from BE-Vie and IT-Sr2, constant $V_{cmax,app}$ were observed for large REW values followed by a decrease when REW declined below an $REW_{B,Vcmax}$ threshold. The $REW_{B,Vcmax}$ were not significantly different (according to the confidence intervals) than the value of 0.4 which was found in previous studies, with an exception at DK-Sor where $REW_{B,Vcmax}$ was higher ($REW_{B,Vcmax}$ = 0.8 $\pm$ 0.09, table 2). The high $REW_{B,Vcmax}$ observed at DK-Sor

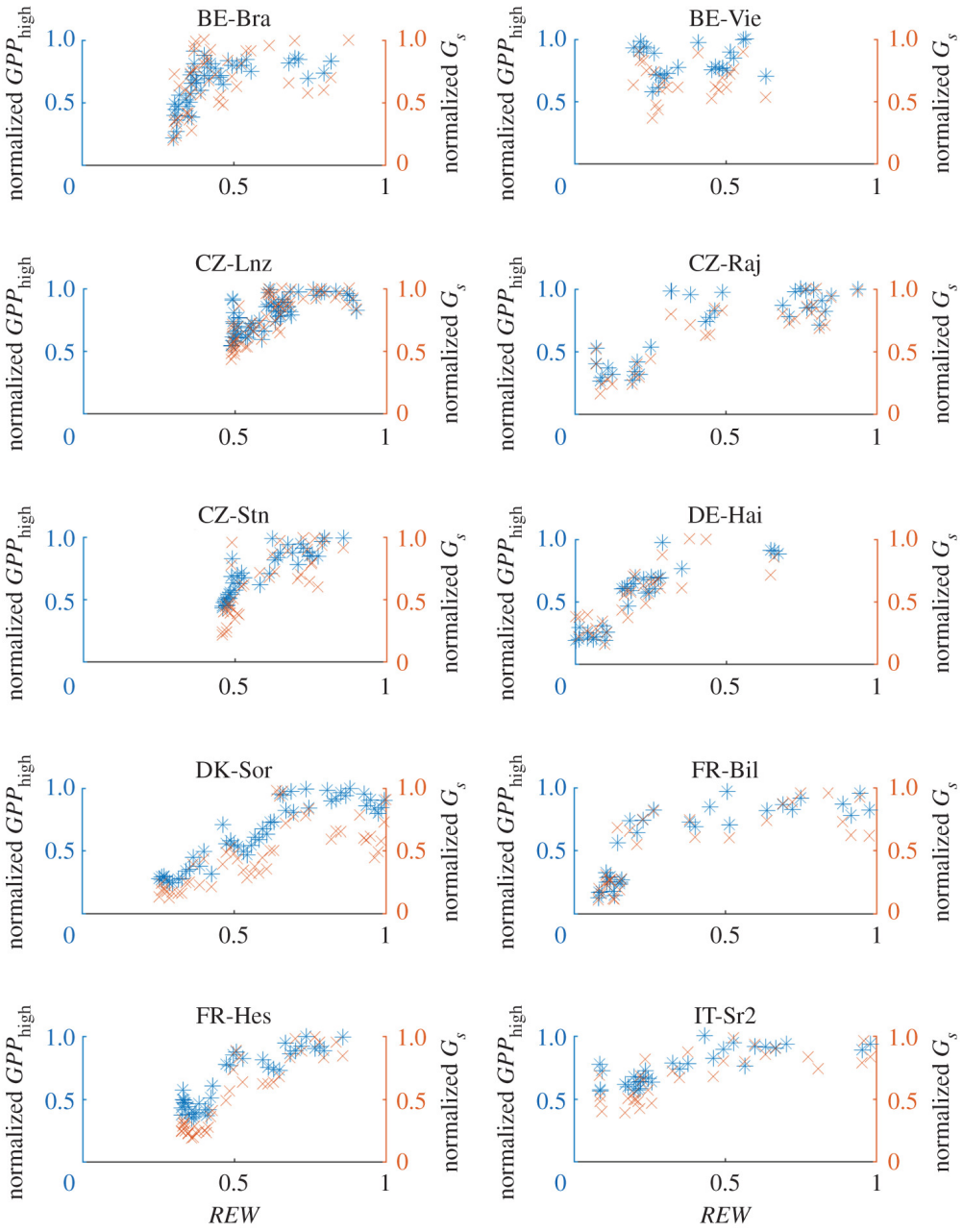

Figure 3.1: Dependence of GPP_{high} (blue, left axis) and G_s at high radiation (R_g > 500, red, right axis) normalized by their maximum value on REW for each site.

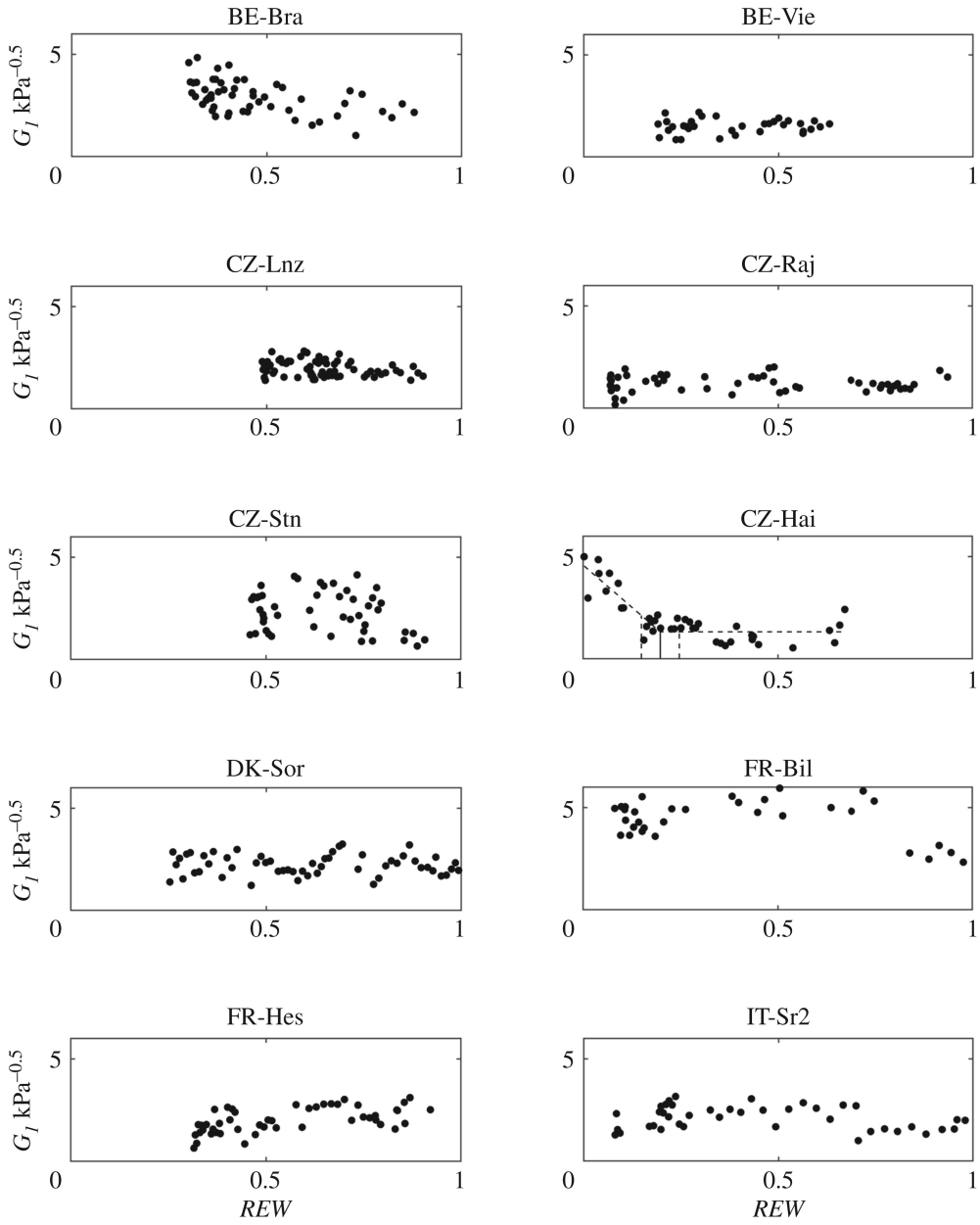

Figure 3.2: Dependence of G_1 on REW for each site. $REW_{B,G1}$ are marked by a vertical solid line with 95% confidence intervals (dashed vertical lines). Regression lines are only shown when F-test p-values (comparison with linear regression) were smaller than 0.05.

Table 3.2: Maximum extractable water (EW), minimum observed REW in 2018 during the growing season, $REW_{B,Vcmaxapp}$ and $REW_{B,G1}$ (REW break points for VCMAX,APP and G1, respectively) given with 95% confidence intervals. $V^*_{cmax,app}$ and G^*_1 ($V_{cmax,app}$ and G_1 values in unstressed conditions) given with 95% confidence intervals. P-values are given for the F-test comparing the segmented mode (three parameters) to the linear model (two parameters).

	EW	min *REW*	$V_{CMAX,APP}$*	$REW_{b,VCMAX}$	*p*-value	G_1*	$REW_{b,G1}$	*p*-value
site ID	mm	—	µmol m^{-2} s^{-1}	—	—	$kPa^{-0.5}$	—	—
BE-Bra	133	0.30	58 ± 3	0.57 ± 0.19	<0.05	2.9 ± 0.2	—	0.28
BE-Vie	215	0.19	81 ± 5	—	1	1.5 ± 0.1	—	1
CZ-Lnz	241	0.49	116 ± 10	—	1	2.0 ± 0.2	—	1
CZ-Raj	92	0.07	80 ± 7	0.36 ± 0.11	<0.001	1.2 ± 0.8	—	1
CZ-Stn	236	0.46	120 ± 7	—	1	2.3 ± 0.3	—	1
DE-Hai	143	0.00	86 ± 17	0.36 ± 0.07	<0.001	1.3 ± 0.2	0.2 ± 0.05	<0.001
DK-Sor	176	0.25	104 ± 3	0.80 ± 0.09	<0.001	2.2 ± 0.2	—	1
FR-Bil	159	0.08	76 ± 7	0.45 ± 0.15	<0.05	4.5 ± 0.4	—	1
FR-Hes	338	0.33	121 ± 13	0.44 ± 0.08	<0.05	2.0 ± 0.5	—	1
IT-Sr2	108	0.08	89 ± 6	—	1	2.1 ± 0.2	—	1

might result from an overestimation of REW as the shallowest available SWC probe was at 15 cm depth (see electronic supplementary material, table S1) and was not able to catch the beginning of the progressive drying of the upper layers that contain a large amount of roots. The most impacted site was DE-Hai where REW almost reached the wilting point (REW $\sim$ 0) with very low $V_{cmax,app}$ values ($\sim$15 μ mol m^{-2} s^{-1}) probably because of shallow soil and rooting depth (0.6 m).

3.4. Degree of stomatal and non-stomatal limitation

DoL reached values of 5 for NSOL at DE-Hai while it remained close to 1 for SOL at all sites (figure 4). This analysis therefore confirms that, at all sites, NSOL was the dominant mechanism. As a result, reducing $V_{cmax,app}$ while maintaining G_1 constant could capture the variations of both GPP_{high} and G_s with drought (identical conclusions are obtained if we focus the analysis on G_s instead of GPP , data not shown). It is also worthwhile noticing that the increasing G_1 observed at DE-Hai (and at BE-Bra to a lesser extent) did not lead to important changes in GPP .

4. Discussion

4.1. Methodological limitations

Although the responses of $V_{cmax,app}$ and G_1 to REW were relatively consistent, some sites showed unexpected behaviours. For example, $REW_{B,Vcmaxapp}$ at DK-Sor

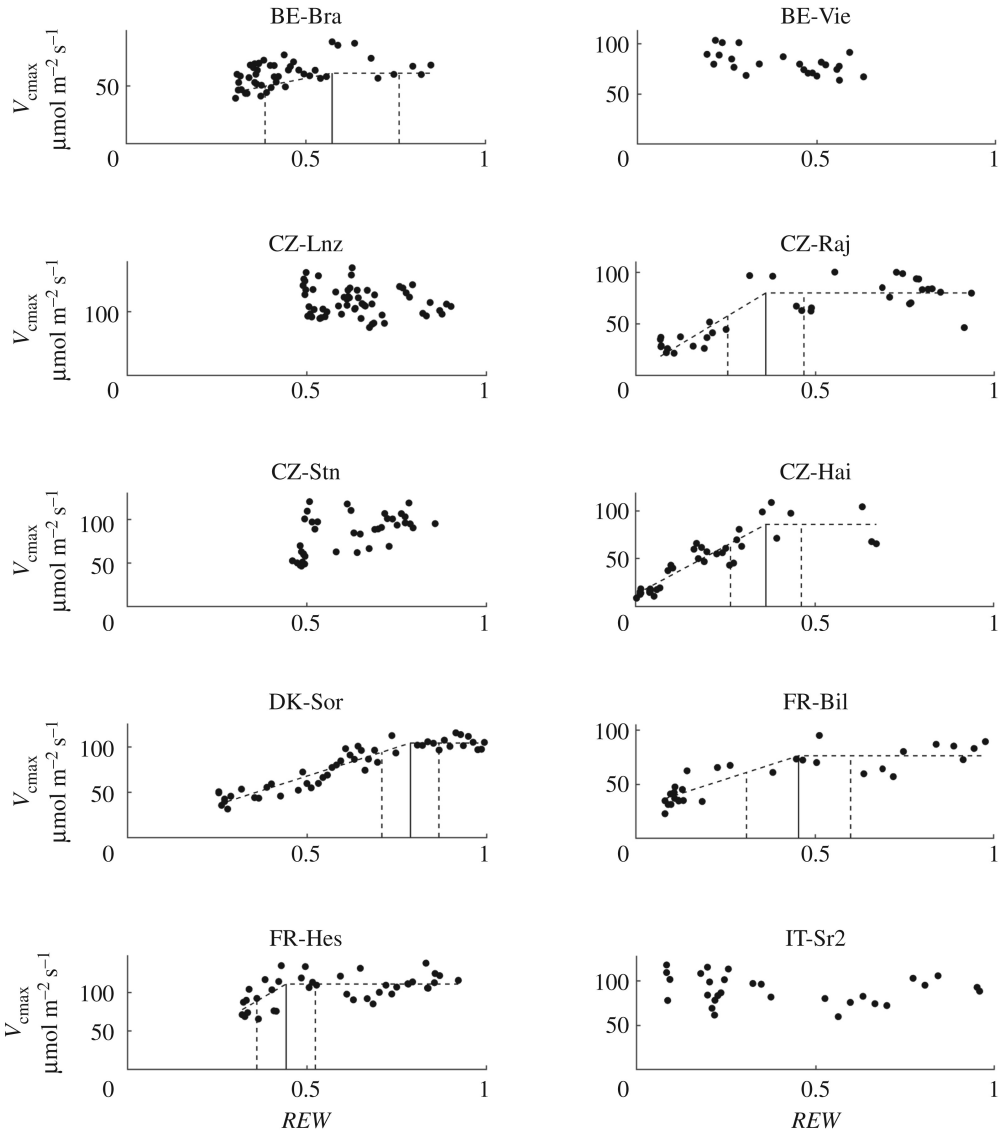

Figure 3.3: Dependence of $V_{cmax,app}$ normalized at 25°C on REW for each site. $REW_{B,Vcmax}$ are marked by a vertical solid line with 95% confidence intervals (dashed vertical lines). Regression lines are only shown when F-test p-values (comparison with linear regression) were smaller than 0.05.

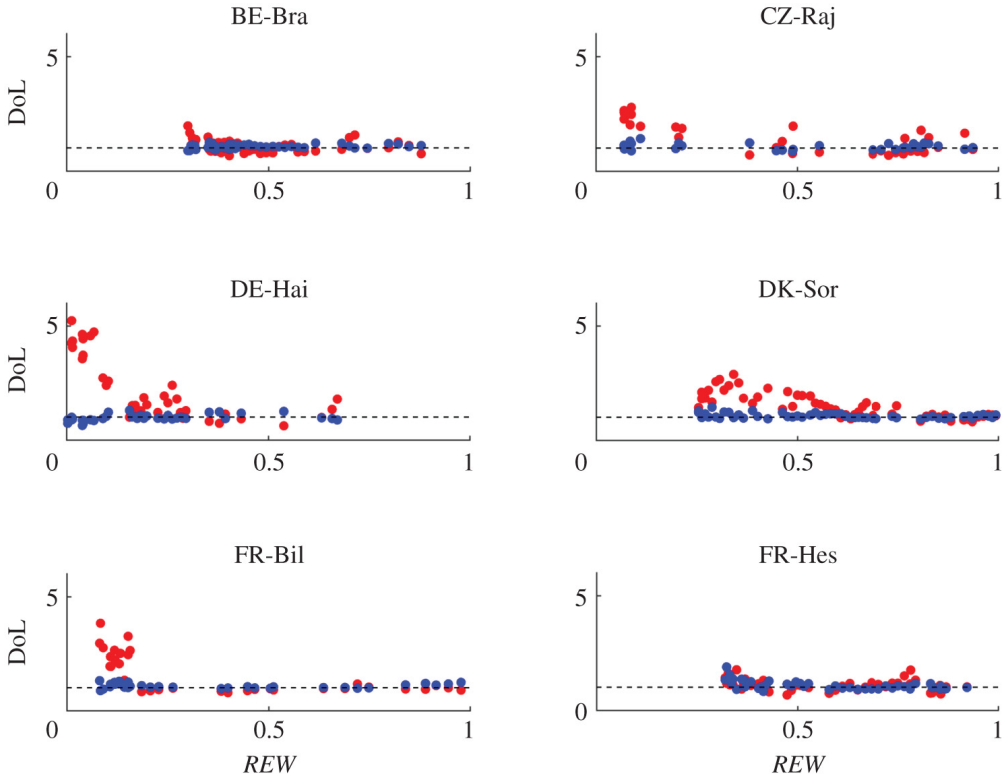

Figure 3.4: Degree of limitation (DoL) by both SOL and NSOL. The degree of limitation was computed as the ratio of modelled GPP on measured GPP at high radiation. Modelled GPP was computed by using either fixed $V^*_{cmax,app}$ (red points, NSOL) and varying G_1 or fixed G^*_1 and observed $V_{cmax,app}$ (blue points, SOL).

was much higher than expected (0.85) because some SWC sensors experienced failures during the drought. At IT-Sr2, no limitation of GPP was found although very low REW values were estimated, probably because the SWC sensor profile was not deep enough to capture the whole rooting depth. Multiple and deeper sensor profiles (with matching wilting points and field capacities) would certainly help to reduce these uncertainties. Complementary measurements such as predawn leaf water potential and soil matric potential (Rogers *et al.*, 2017; Anderegg *et al.*, 2017), when REW approaches values close to 0.4 at the site, would also be useful.

The big leaf approach used in this study also has several limitations (Knauer *et al.*, 2018a) which could be critical when comparing leaf scale-derived parameters to big leaf canopy scale estimates (Knauer *et al.*, 2018a,b; Medlyn *et al.*, 2017b) or when attributing a behaviour to a specific species. First, the approach is only able to derive bulk parameters and is unable to distinguish the vertical and horizontal distribution of the properties. Horizontal heterogeneity is especially crucial at mixed forest sites where different species could show different responses to drought (and different root depth and therefore REW) which would blur their respective responses in the measured signal. This is especially critical at BE-Vie where the two most frequent wind directions (southwest and northeast) correspond to different stands (coniferous and beech stands) with possibly different root depth, REW and weather conditions (Aubinet *et al.*, 2018). Separating the data between each sector did not however improve the relation because of the lack of data (data no shown).

At sites with dense canopy and high LAI, vertical gradients of the parameters (G_s, G_1 and $V_{cmax,app}$) could result from vertical gradients within plants of the same species or from physiological differences across species (Knauer *et al.*, 2018a). Sun leaves, developed under high irradiance, usually exhibit higher iWUE (lower G_1) than those developed under shady conditions (Sellin *et al.*, 2010), primarily because of higher photosynthetic capacities. However, more critical for this study, little is known about to what degree these vertical gradients (within and across species) could affect the response of G_1 and $V_{cmax,app}$ to drought. To our knowledge, in most Earth system models, the same reduction functions of photosynthesis during edaphic drought (either NSOL or SOL) are used for sun and shade leaves (Rogers *et al.*, 2017). More complex multiple layers and/or sun-shade models as well as additional data gathered at multiple canopy layers would be needed to assess this question more closely.

Moreover, soil and vegetation components cannot be distinguished so that critical variables such as G_s (and variables depending on it, such as G_1 and C_i) will inevitably contain some signal from the soil. This signal can be reduced by filtering the data after rain events (Knauer *et al.*, 2018a) and should be small for dense canopies with LAI higher than 2–3 (Kelliher *et al.*, 1995) (which is the case in all sites) and even smaller when the upper soil layer dries.

Finally, systematic errors (energy balance non-closure Wilson *et al.* (2002)) in EC

fluxes are also major sources of uncertainties that affect G_1 and $V_{cmax,app}$ magnitudes. However, it was found that, at multiple flux tower sites, the surface energy balance was not modified during the 2018 drought (Graf *et al.*, 2020). This source of error is therefore unlikely to affect G_1 and $V_{cmax,app}$ responses to REW.

Nevertheless, despite all the limitations of the big leaf approach detailed above, this framework was very suitable for this multi-site study as it relied on very few ancillary data (Knauer *et al.*, 2018a). If the comparison of G_1 and $V_{cmax,app}$ (which inherently has a different meaning than leaf-level $V_{cmax,app}$) is not straightforward, analysing the dynamics of these parameters inferred from in situ EC data during drought provides very useful information about how forest ecosystems reacted to these events.

4.2. Implications of non-stomatal origin limitation for the modelling of gross primary productivity and transpiration

In this study, similarly to Granier *et al.* (2007a), we found that GPP and G_s reductions can be expected when REW drops below ∼0.4. To account for these reductions, using empirical reduction factors (ranging from 1 to 0) when soil water content falls below a given threshold is a widely used approach (Rogers *et al.*, 2017). However, it is questionable whether the reduction factors should be applied to SOL and/or to NSOL. This was previously investigated in Mediterranean ecosystems (reichstein *et al.*, 2002; Reichstein *et al.*, 2003; Keenan *et al.*, 2009) and it was found that, calibrating the model on either GPP or transpiration (E) (not both) by considering only SOL during edaphic drought conditions systematically led to overestimates of WUE which did not allow the correct simulation of both fluxes. Surprisingly, it was found that applying NSOL only was sufficient to correctly simulate both GPP and E.

In this study, we found that reducing $V_{cmax,app}$ when REW dropped below ∼0.4 and using a constant G_1 parameter (from the USO model (Medlyn *et al.*, 2011a)) allowed the capture of both GPP and G_s reductions at European forest sites. Similar conclusions were also found by Chen *et al.* (2019a) in four different ecosystems (temperate grassland, tropical savannah, boreal and one temperate forest). More specifically, relatively consistent behaviour was observed at the three beech (Fagus sylvatica) forest sites (FR-Hes, DK-Sor and DE-Hai) where NSOL were the main source of photosynthesis reductions with relatively constant G_1. Similarly, in a study carried out on adult beech using leaf-level measurements, the Ball–Berry slope was found to be almost insensitive to soil water potential (Op de Beeck *et al.*, 2010). Our results are in agreement with Granier *et al.* (2007a) who observed constant WUE even for very low REW during the 2003 drought and with Hentschel *et al.* (2016) who also found unchanged annual WUE derived from tree ring carbon isotopic composition.

Studies were also performed at the leaf scale to study the impact of drought on NSOL and SOL. In their meta-analysis, Zhou *et al.* (2013) found highly variable responses of g_1 (leaf level) for woody species ranging from rather constant to severely decreasing

g_1 with drought. Decreasing $V_{cmax,app}$ (NSOL) were however found for all species. It was also highlighted that NSOL was the main factor limiting photosynthesis under severe stress in 10 Mediterranean herbs and shrubs species (Galmés *et al.*, 2007; Egea *et al.*, 2011) and, more importantly for this study, for four tree species (Drake *et al.*, 2017). Unfortunately, a direct comparison with our results cannot be carried out as the studied species were different. Such direct comparisons have been carried out in a woodland dominated by Acacia trees by Tarin *et al.* (2020a) who found a close agreement between G1 and g1 estimated from ecosystem (EC big leaf) and leaf-level approaches, respectively.

According to Keenan *et al.* (2010b), NSOL could be caused by the variations of a finite mesophyll conductance with soil water availability (Flexas *et al.*, 2004) which, if not taken into account, leads to wrong estimates of actual V_{cmax} (Flexas *et al.*, 2012) (which was implicitly taken into account by using $V_{cmax,app}$). In addition, the hypothesis that, under severe droughts, GPP can be directly impacted by biochemical limitations which cause the reduction of actual V_{cmax} should not be discarded (Lawlor & Tezara, 2009). Separating NSOL between these two mechanisms (mesophyll conductance and actual V_{cmax}) was not done in this study. Currently, without additional leaf-level data to better understand the mechanisms underlying mesophyll conductance changes during droughts, we use an apparent $V_{cmax,app}$ (Rogers *et al.*, 2017; Drake *et al.*, 2017; Keenan *et al.*, 2010a).

4.3. Optimal stomatal behaviour during drought and intrinsic water-use efficiency

We did not find a general pattern of systematically decreasing G1 during drought or, in other words, an increasing iWUE for stomatal closure (increasing λ) across ecosystems as theoretically predicted (Manzoni *et al.*, 2011; Mäkelä, 1996). To the contrary, we found constant G_1 (and therefore λ) values at most sites, and even increasing values at DE-Hai (and BE-Bra to a lesser extent). This result (a constant G_1) is rather surprising as it would suggest that changes in stomatal conductance responses were not needed to model G_s under long-term water stress events (Keenan *et al.*, 2009) and that λ does not increase with drought. We argue that this is caused by the fact that NSOL were not considered by Manzoni *et al.* (2011) and Mäkelä (1996) in their analyses as stomatal closure (reduced G_s) is known to regulate leaf water flows in response to soil water availability (Buckley, 2019); without such mechanisms, leaves would be quickly dehydrated. However, one should consider that stomatal closure in response to drought does not necessarily lead to a decrease in G_1 as, in USO , any reduction of $V_{cmax,app}$ lead to a reduction in stomatal conductance (Zhou *et al.*, 2013). At very low REW values, previous studies showed that C_i could even increase because of NSOL (Flexas, 2002), which would explain the increase of G_1 we observed at DE-Hai.

Another more complex approach to stomatal conductance modelling is to model

stomatal conductance in the function of leaf water potential which is expected to regulate G_s (TUZET *et al.*, 2003). This approach requires a complete model of water flow from the soil through the plant to the atmosphere (Tuzet *et al.*, 2017). This kind of model was tested by reducing the stomatal slope of the Ball–Berry–Leuning model (Leuning, 1995) with leaf water potential, but the model did not account for NSOL (Anderegg *et al.*, 2017). Recently, Dewar *et al.* (2018) proposed a new optimization model in which stomatal behaviour maximizes photosynthesis and where the costs of stomatal closure arise from NSOL (mesophyll conductance and/or carboxylation rate) and/or loss of hydraulic conductance (Sperry *et al.*, 2016). This results in a parameter, equivalent to G_1, which is expressed as a function of measurable variables such as hydraulic conductivity, leaf water potential and V_{cmax}. This model has been successfully tested on saplings for different plant functional types (Gimeno *et al.*, 2019) and fitted well sub-daily leaf scale observations; however, this still needs to be tested for longer term in situ ecosystem droughts. This could not be done in this study as leaf and soil water potentials were lacking. It does, however, highlight a promising research path for the future.

5. Conclusion

In this study, we used a big leaf framework to investigate the origin of edaphic drought impacts on GPP (stomatal origin limitation and non-stomatal origin limitation) in European forest ecosystems during the 2018 drought. In agreement with Granier *et al.* (2007a), we found that GPP and G_s were both greatly affected by soil moisture depletion at many sites. We went a step further by showing that these reductions could be faithfully modelled by decreasing $V_{cmax,app}$ (NSOL) when the REW dropped below around 0.4 while keeping the G_1 (SOL) parameter from the USO model (Medlyn *et al.*, 2011a) constant. These results were rather unexpected as it would suggest that stomatal closure was not responsible for GPP reductions with drought. We argue that this was caused by the fact that G_1 was not representative of stomatal behaviour during drought because GPP was not only regulated by stomatal closure but also by NSOL. Nevertheless, these results strengthen the increasing evidence that NSOL should be included in stomatal conductance/photosynthesis models to faithfully simulate both GPP and water fluxes in forest ecosystems.

CRediT authorship contribution statement

L.G.dlM. was the leader of the data analysis and writing of the paper. Q.B. and B.H. participated in the design of the study, gave intellectual inputs and feedbacks to the paper. B.L. designed the study and followed the data analyses and writing process closely. All the other co-authors were involved in the data acquisition as principal investigators for each site and actively contributed to the paper by commenting on intermediate versions.

Declaration of Competing Interest
We declare we have no competing interests

Data availability
Data will be made available on request.

Acknowledgments The study has been performed thanks to the European Fluxes database cluster. The authors would like to thank all the persons that contributed to this study. We would also like to thank all the financial support provided for sites. We thank the administration of the Hainich National Park for the opportunity for research in the National Park. Data from the Sorø beech forest site (DK-Sor) have been measured, evaluated and provided by Kim Pilegaard and Andreas Ibrom and the station team. We acknowledge the support of successive European projects, by European regional development programs with the Region Lorraine, by GIP Ecofor and SOERE F-ORE-T, by ADEME and by the INRA Department of Forest, Grassland and Freshwater Ecology (EFPA). Finally, we would also like to thank Carsten Gruening for his technical assistance.
Supplementary material Electronic supplementary material is available online at https://doi.org/10.6084/m9.figshare.c.5077590.

4

Non-stomatal processes are responsible for the decrease in gross primary production of a potato crop during edaphic drought

This paper has been published as:

Beauclaire, Q., Heinesch, B., Longdoz, B., 2023. Non-stomatal processes are responsible for the decrease in gross primary production of a potato crop during edaphic drought. Agricultural and Forest Meteorology 343, 109782. https://doi.org/10.1016/j.agrformet.2023.109782

1. Personal contributions

The maintenance of the EC site has been carried out by the technical team of the Lonzée ICOS station, namely Henri Chopin and Gaëtan Bogaerts. The Ecosystem Thematic Centre (ETC) performed the data processing and quality control of the EC site of Lonzée. The EC data used in this study is available on the ICOS Carbon Portal (see references in the paper below). I performed the data analysis and wrote the manuscript. Bernard Longdoz supervised the research, helped in interpreting the results and reviewed the different versions of the manuscript. Bernard Heinesch participated to the reviewing processes and helped in interpreting the results.

2. Abstract

Soil water stress is one of the main constraints on agrosystem functioning, causing a reduction in GPP. It is a key factor for the selection of drought-tolerant plant varieties and the adaptation of irrigation management strategies. Therefore, identifying the physiological factors limiting GPP is crucial. LSMs commonly implement a beta (β) stress function to reproduce the effects of drought on GPP. It is still unclear whether GPP limitations originate from a direct stomatal response (SOL) or from other non-stomatal causes (NSOL). Moreover, the shape and thresholds of the β function are a major cause of uncertainty in LSMs. This study investigated the effects of edaphic drought on GPP limitations of a potato crop by using eddy covariance data from the Lonzée ICOS station (BE-Lon) in Belgium for four years (2006, 2010, 2014 and 2018) and by calibrating the β function on NSOL and SOL. The decrease in the REW in the soil induced a decline in the apparent maximum carboxylation rate (NSOL) from similar REW thresholds for all growing seasons of potato crops. A sensitivity analysis showed that the non-inclusion of REW decrease on NSOL in the modeling of GPP led to important overestimations of carbon sequestration from a threshold corresponding to 46% of the maximum available soil water. The stomatal sensitivity to photosynthesis (SOL) remained constant or even increased in 2010 and 2018. The carbon and water fluxes were decoupled when REW decreased, exhibiting a strict control of NSOL on hourly dynamics of GPP. This study provides REW thresholds to identify drought stress episodes and to help for designing irrigation management strategies. Our results advocate for a better representation of the influence of drought on photosynthesis processes of potato crops to improve the accuracy of model predictions during drought.

3. Introduction

Many regions across the world are facing more intense and frequent episodes of water stress due to climate change (Chiang *et al.*, 2021). Edaphic drought has become a major limiting abiotic stress for agricultural production (Fahad *et al.*, 2017). It is also known to cause restrictions in carbon assimilation, impacting the photosynthetic capacities of terrestrial ecosystems, especially those located in the mid-latitude region of the Northern Hemisphere (Yu *et al.*, 2017). Consequently, severe water stress events reduce crop yield and sometimes offset carbon sinks or cause shifts from sink to source, inducing a positive feedback effect on global warming (Reichstein *et al.*, 2013). Predicting and anticipating the impacts of drought on ecosystems' abilities to store carbon requires a detailed understanding of the physiological processes involving CO_2 uptake through photosynthesis and their interconnections.

Plants respond to low soil water content through a complex chain of mechanisms constituting their adaptation strategies (see Harper *et al.* (2021) for a review). For example, plants usually close their stomata when the atmospheric demand for water (represented by the VPD) overcomes the supply capacity from the soil, which prevents cavitation in the plants' hydraulic transfer system (Hetherington & Woodward, 2003). A consequence of stomatal closure is the reduction of CO_2 diffusion from the leaf-surrounding atmosphere to sub-stomatal cavities, which leads to a decrease in carbon assimilation (Flexas *et al.*, 2004). Moreover, is it well known that stomatal conductance to CO_2 transfer (G_s) is highly correlated to GPP under stable vapor pressure deficit and soil water status (Wong *et al.*, 1979). These findings have been the basis of the empirical parametrization of G_s using carbon assimilation as a key element in addition to environmental factors (see Damour *et al.* (2010) for a review). Within this framework, any decrease of G_s can be caused either by a modification of the environmental conditions or by an inhibition of photosynthetic capacities. The USO model (Medlyn *et al.*, 2011a) reconciled this empirical approach with the optimality theory of Cowan & Farquhar (1977), which states that a plant should adjust its stomatal opening to maximize carbon assimilation while minimizing water losses over a constant time interval. In this USO framework, the G_1 parameter represents the slope of the linear relationship between G_s and carbon assimilation normalized by VPD and CO_2 concentration and is related to the marginal carbon gain per unit of water transpired (Medlyn *et al.*, 2011a). A reduction of carbon assimilation resulting from a decrease in G_1 corresponds to a direct stomatal control of CO_2 diffusion and will be referred in this paper to as a SOL. Carbon assimilation can also be impacted through the inhibition of photosynthetic capacities in two possible ways: changes in mesophyll conductance restricting CO_2 diffusion from sub-stomatal cavities to the carboxylation sites in the chloroplast (Flexas *et al.*, 2008), and modification of the biochemical reaction activities in the chloroplast. Both are generally implemented in photosynthesis modeling by a reduction of the apparent maximum carboxylation rate $V_{cmax,app}$ as in the FvCB

model of photosynthesis (Farquhar *et al.*, 1980; Flexas *et al.*, 2004). This origin of CO_2 assimilation limitation is further associated in this paper to a NSOL. It should be noted that NSOL also induces a diminution of G_s as carbon assimilation is recognized to be one of the variables influencing stomatal opening. The comparison between $V_{cmax,app}$ and G_1 dynamics during stressed periods gives insights on the importance of each cause of carbon photosynthesis perturbation (respectively NSOL and SOL). Using G_1 instead of G_s as an indicator of SOL allows to partition the coupling between G_s and GPP into changes in photosynthetic capacities and marginal water cost of carbon gain (Zhou *et al.*, 2013, 2014).

LSMs commonly implement a beta (β) stress function to account for soil water stress effects on carbon and water fluxes. This function uses the SWC normalized by the difference between the field capacity and the wilting point in the root layer (Egea *et al.*, 2011) to characterize the amount of water available for plant uptake. When SWC is below the field capacity, the β factor directly downregulates $V_{cmax,app}$ and/or G_1 (Egea *et al.*, 2011; Verhoef & Egea, 2014) to reproduce drought effects on carbon and water fluxes originating from respectively NSOL and SOL. However, Granier *et al.* (1999a) and Gourlez de la Motte *et al.* (2020) showed that plants can maintain a high level of carbon and water flux even when SWC is below the field capacity, leading to potential underestimations in carbon and water flux estimates from LSMs. Vidale *et al.* (2021) and Trugman *et al.* (2018) underlined this aspect by identifying that this stress function was one of the key uncertainties in photosynthesis and transpiration predictions in LSMs. Moreover, there is no consensus in the scientific community on whether soil water stress should impact stomatal functioning, photosynthetic capacities, or both, to accurately predict carbon and water fluxes during drought (Zhou *et al.*, 2013; Peters *et al.*, 2018). Therefore, the determination of the β stress factor (corresponding to a REW function) representing NSOL and SOL for different PFTs is a key factor for improving model predictions (Rogers *et al.*, 2017; Li *et al.*, 2022b).

Potato (*Solanum tuberosum*) is the third most important crop in the world in terms of food production, with more than 370 million metric tons produced in 2019 (FAOSTAT, 2021). In Europe, most potato crops are cultivated on loam soils with a predominance of clay, which allows the soil to hold an important amount of water for plant uptake. Potatoes cultivated on these soils represent more than 400 000 hectares of arable lands in Europe (Goffart *et al.*, 2022). Known to be a drought sensitive crop because of its shallow root system, potato yield and the quality of the tuber can be dramatically impacted by water stress (Obidiegwu, 2015). Therefore, any limitation on its production threatens food supply, impacting more than one billion people around the world (Lutaladio & Castaldi, 2009).

Up to now, no studies have investigated which processes are at the origin of the effects of drought on potato photosynthesis limitations estimated from eddy covariance data (EC). In this paper, we aimed at investigating the effects of drought on potato car-

bon assimilation by analyzing the data collected by the Lonzée flux tower and meteorological station (BE-Lon) located in central Belgium, which is part of the Integrated Carbon Observation System (ICOS – Franz et al., 2018). More specifically, this paper aims at: (i) partitioning the impacts of REW on GPP between SOL (G_1) and NSOL ($V_{cmax,app}$) and (ii) defining a REW threshold below which these two limitations occurred.

4. Material and methods

4.1. Site description

The Lonzée ICOS flux tower (Level 2 ICOS station) is installed in the middle of a cropland plot located in Lonzée, about 50 km SE of Brussels in Belgium (50° 33′ 5.71"N, 4°44′ 46.07"E, 167 m asl). It has been equipped with an eddy covariance (EC) system and a meteorological station since 2004 and is integrated into the CarboEurope-IP and FLUXNET networks. The cropland plot has an area of 12 hectares. The EC system has a fetch of 240 m and 200 m in the directions of the prevailing winds which are SW and NE (Buysse *et al.*, 2017). For any atmospheric conditions, the cropland area contribution to the EC footprint fluxes was large (91.1% in 2006, 90.5% in 2010, 90.7% in 2014, 93.3% in 2018, data not shown). The climate is temperate oceanic, with mean annual temperature and precipitation of respectively 10.2°C and 743 mm. The soil is a Luvisol (FAO classification) divided into two horizons (one plough layer from 0 to 35 cm and one layer enriched in clay particles from 35 to 100 cm – Table 4.1).

Table 4.1: Soil physical proprieties at BE-Lon: field capacity (θ_{fc}), wilting point (θ_{wp}), sand, silt, clay content and bulk density for the two soil horizons (0-35 cm and 35-100 cm). Field capacities and wilting points were measured by the WPC4 and HYPROP2 sensors (Meter environment., Hopkins Ct, NE, US) on soil samples collected in 2019.

Depth (cm)	θ_{fc} (cm^{-3} cm^{-3})	θ_{wp} (cm^{-3} cm^{-3})	Sand (%)	Silt (%)	Clay (%)	Bulk density (g cm^{-3})
0–35	45.3	11.7	8.4	80.5	11.2	1.3
35–85	40.4	13.0	6.1	75.7	18.2	1.5

4.2. Crop management

The Lonzée station has been cultivated for more than 80 years, with cropping management based on a 4-year rotation. For at least the past 20 years (Aubinet *et al.*, 2009), the rotation has been: winter wheat (*Triticum aestivum*) / sugar beet (*Beta vulgaris*) / winter wheat (*Triticum aestivum*) / seed potato (*Solanum tuberosum*). Potatoes

were cultivated in 2006, 2010, 2014 and 2018. The farming operations during the four growing seasons are described in Table 4.4. The tubers were planted in ridges with a space of 60 to 70 cm between the ridges and of 30 to 40 cm between the tubers.

4.3. Meteorological and fluxes measurements

Micrometeorological measurements were collected at the half-hourly timescale, including air humidity and air temperature (RHT2, Delta-T Devices Ltd., Cambridge, UK) at 1.3 m height (and 2.8 m height in 2018), incident photosynthetic photon flux density (PAR Quantum sensor SKP 215, Skye Instruments Limited, Llandrindod Wells, UK) and SWC (EnviroSCAN Probe, Sentek Sensor Technologies, Stepney, SA, AU) at five different depths in 2018 (5, 15, 25, 55 and 85 cm). In 2006, 2010 and 2014, SWC was measured using time domain reflectometers (ML2 ThetaProbe, Delta-T Devices Ltd, Cambridge, UK) at three different depths (5, 20 and 40 cm). For all years, the soil water sensors were located at the middle of the plot near the EC station.

The net CO_2 (F_c) and water vapor (LE) fluxes between the ecosystem and the atmosphere were determined on a half-hourly basis by the EC technique (Aubinet et al., 2012) using high frequency data of vertical wind speed, CO_2 and water vapor concentrations at the ecosystem-atmosphere interface. These variables were measured at 20 Hz by respectively a sonic anemometer (Solent Research R3, Gill Instruments Lymington, UK) placed at a height of 2.93 m on a mast located at the center of the field, and an infrared gas analyzer (LI-7000 before 2014 and LI-7200 after, LI-COR, Lincoln, NE, US) placed close to the anemometer. Half-hourly fluxes of F_c and LE were determined by postprocessing raw 20 Hz data by the ICOS Ecosystem Thematic Center using the ONEFlux pipeline (Pastorello *et al.*, 2020) and are available in the ICOS Carbon Portal (Dumont *et al.*, 2023a). More precisely, the storage flux was neglected (i.e., F_c corresponds to the net ecosystem exchange NEE) and GPP was obtained from the partitioning of NEE using the nighttime method (NT, Reichstein *et al.* (2002)). Moreover, data characterized by weak atmosphere turbulence level (low friction velocity u^*) using the variable u^* threshold method (VUT) were discarded. The variables GPP_NT_VUT_REF and LE_F_MDS with quality flags of 0 were selected from the dataset. Data was not gapfilled because only measurements can be used to study ecosystem functioning and no flux value cumulated over time were necessary.

4.4. Measurements of vegetation growth

Vegetation growth is commonly measured by the LAI which corresponds to the ratio of leaf area to unit ground surface area (Breda, 2003). However, the LAI does not allow to separate the green photosynthetic components (including chlorophyll cells) from the rest of the canopy structure. The Green Area Index (GAI), which corresponds to the green surface area of the vegetation, is a better proxy to assess the photosynthetically active component of the ecosystem. In this study, the GAI of the potato crop was mea-

sured six times during each growing season by a destructive sampling method. These measurements have been linked to the growing degree-days which is a main climatic driver of crop development (Mcmaster, 1997). The base temperature (temperature required for crop growth) was set to 7 ∘C (Sands *et al.*, 1979). A third-order polynomial function was fitted to GAI and growing-degree-days to model GAI dynamics and get a continuous function for each growing seasons.

In the results section, the timescale will be further expressed as Day after Emergence (DAE), which counts the number of days after the emergence of the first leaves of the crop, this latter corresponding to the date when GAI changed from a null to a positive value. The growing seasons were divided into two stages: the vegetative stage when GAI increased (leaf development and period before tuber development, roughly between DAE 0 and 40), and the reproductive stage when GAI decreased (tuber multiplication and elongation, roughly after DAE 40). This definition slightly differs from the reality since tuber growth initiation is expected to start before GAI reaches its maximum value (Obidiegwu, 2015). However, this assumption will not affect the results of this study since this denomination was only used for a descriptive purpose.

4.5. Quantification of soil water availability

TheREW for plant uptake is a drought index which corresponds to the fraction of available water for plant uptake from the soil surface up to the maximum rooting depth. REW is expressed as a fraction of the maximum available water calculated by the difference between field capacity and wilting point (Granier *et al.*, 1999a). The maximum rooting depth was estimated by analyzing the dynamics of SWC within each soil horizon during periods of potato crop development without precipitation. The decrease in SWC was observed only within the first soil horizon (0–35 cm, Table 4.1), suggesting that root water uptake only occurred in surface soil layers. Therefore, we assumed that the roots can uptake soil water only up to 35 cm depth (Table 4.1). This assumption could lead to REW overestimation at the beginning of the growing season as most roots are located within shallow soil layers. However, SWC data showed a rapid extension of the water uptake into deeper soil layers and the beginning of the growing season is not a drought-prone period. REW was calculated as follows (Granier *et al.*, 1999a):

$$REW = \frac{\overline{\theta} - \theta_{fc}}{\theta_{fc} - \theta_{wp}} \tag{4.1}$$

where θ_{wp}, θ_{fc} and θ are respectively the wilting point, the field capacity and the average of SWC measurements in the first soil horizon (Table 1). The units and a description of the variables used in this study can be found in Table 4.5. REW ranges from 1 ($\theta = \theta_{fc}$) to 0 ($\theta = \theta_{wp}$), even if values higher than 1 can be observed just

after a rainfall event, when soil water content is above field capacity. REW is directly related to the water stress β factor used in many LSMs (Verhoef & Egea, 2014):

$$\beta = \begin{cases} 1 & \overline{\theta} > \theta_{fc} \\ REW^p & \theta_{wp} < \theta_{fc} \\ 0 & \overline{\theta} < \theta_{wp} \end{cases} \tag{4.2}$$

with p the exponent allowing to implement a non-linear dependence of model parameters on REW. However, many species can maintain constant photosynthetic parameters even when $\theta < \theta_{fc}$ (Granier *et al.*, 1999a; Gourlez de la Motte *et al.*, 2020). Investigating the effects of drought on SOL and NSOL to determine specific REW thresholds from which model parameters linked to stomatal opening and apparent carboxylation rate are impacted by water stress is pivotal to avoid the propagation of uncertainties in models. This study focused on the characterization of these threshold by assuming that $p = 1$, as implemented in many LSMs (Vidale *et al.*, 2021; Oliver *et al.*, 2022).

4.6. "big leaf" approach

The "big leaf" is a concept where the canopy is simplified as a single leaf at the interface with the surrounding atmosphere. It is used to infer ecosystem physiological proprieties from flux tower measurements (Knauer *et al.*, 2018a). The air characteristics over the "big leaf" surface and the conductance related to the transfer of water vapor through respectively the stomata of the "big leaf" (named canopy conductance to water vapor G_{sw}) and the boundary layer (named aerodynamic conductance to water vapor G_{aw}) can be inferred from the micro-meteorological measurements performed above the canopy.

4.6.1. Determination of the "big leaf" surface conditions and aerodynamic conductance

Following the Thom model (Thom, 1972), G_{aw} is equivalent to the aerodynamic conductance for sensible heat (G_{ah}) and can be determined by:

$$G_{aw} = G_{ah} = \left(\frac{u}{u_*^2} + 6u_*^{-0.667} \right) \tag{4.3}$$

where u_* is the friction velocity and u the wind speed above the canopy. G_{ah} was used to calculate the H_2O concentration (e_s) and the CO_2 concentration (C_s) at the "big leaf" surface as follows (Knauer *et al.*, 2018a):

$$e_s = e_a + \frac{LE\gamma}{\rho_a G_{aw} c_p} \tag{4.4}$$

$$C_s = C_a + \frac{NEE}{G_{aw}} \frac{RT_a}{p} \tag{4.5}$$

with LE the latent heat flux (measured by the EC system), ρ_a the air density, c_p the heat capacity of dry air, γ the psychrometric constant and R is the perfect gas constant. e_a, C_a, T_a and p correspond respectively to the air vapor pressure, the CO_2 concentration, the air temperature and the air pressure measured above the canopy. $\frac{RT_a}{p}$ in Eq. (4.5) converts G_{aw} from m s^{-1} to mol m^{-2} s^{-1}.

The canopy temperature was determined from the longwave fluxes at the canopy surface (Knauer *et al.*, 2018a):

$$T_s = \sqrt[4]{\frac{LW_{out} - (1-\epsilon)LW_{in}}{\epsilon\sigma}} \tag{4.6}$$

with LW_{in} and LW_{out} the longwave downward and outgoing fluxes measured by the meteorological station, ϵ the emissivity of the canopy and σ the Stefan-Boltzmann constant. Missing T_s values due to lack of longwave fluxes measurements were gap filled with T_a. The vapor pressure deficit at the "big leaf" surface (VPD_s) was calculated as the difference between the saturated vapor pressure and the air vapor pressure at the canopy surface (e_s).

4.6.2. Canopy conductance

G_{sw} was computed by inverting the Penman-Monteith equation (Monteith, 1965):

$$G_{sw} = \frac{G_{ah}\gamma LE}{\Delta(R_n - G - S) + \rho_a c_p G_{ah} VPD_s - (\Delta + \gamma)LE} \tag{4.7}$$

where Δ is the slope of the saturated vapor pressure curve at T_a calculated from Allen & of the United Nations (1998), R_n is the net radiative flux and G the ground heat flux (both measured). The flux corresponding to the energy stored in the canopy (S) was neglected. Inferring G_{sw} from Eq. (4.7) is only possible when LE corresponds to the transpiration flux of the ecosystem (i.e., when soil and canopy evaporation are negligible comparing to transpiration). Therefore, the analysis focused only on the growing season and data during precipitation events and the subsequent 48 h (when evaporation is significant) were discarded. To ensure the selection of data with meaningful LE values, periods with low photosynthetic photon flux density (PPFD< 200 μmol m^{-2} s^{-1}), low surface temperature (<5 °C), high relative humidity (RH>95 %), LE < 0 and $Rn - G$ < 0 were also discarded (Knauer et al., 2018b). Moreover, the violation of the energy balance closure assumption in Eq. (4.7) may affect the interpretability of G_{sw} (Knauer *et al.*, 2018b). This issue was addressed by computing the slope of the regression between the sum of the turbulent fluxes and available energy

and by discarding half hourly data when the standardized residuals from the linear regression between were superior to 3.

4.6.3. Maximum apparent carboxylation rate

Under high irradiance, photosynthesis is limited by the activity of the RuBisCO enzyme (Farquhar *et al.*, 1980). In this case, the FvCB model applied at the "big leaf" surface estimates GPP under high irradiance (GPP_{sat}) from the apparent maximum carboxylation rate ($V_{cmax,app}$), the intracellular CO_2 concentration (C_i), the CO_2 compensation (Γ^*) point and the effective Michaelis-Menten coefficient for RuBisCO kinetics (K_m):

$$GPP_{sat} = \frac{V_{cmax,app}(C_i - \Gamma^*)}{C_i + K_m} \tag{4.8}$$

Both K_m and Γ^* were determined following an air temperature-based dependence (Bernacchi *et al.*, 2001). Eq. (4.8) assumes that leaf photorespiration is negligible under high irradiance. $V_{cmax,app}$ was calculated by inverting Eq. (4.8):

$$V_{cmax,app} = \frac{GPP_{sat}(C_i + K_m)}{C_i - \Gamma^*} \tag{4.9}$$

where GPP_{sat} is the GPP when PPFD is higher that a threshold ($PPFD_{sat}$) from which GPP saturated. This threshold was calculated from the light response curves of GPP for each growing season. The Mitscherlich model was used to mathematically describe the relationship between GPP and PPFD. Data was averaged within classes with a constant width of 200 μmol m^{-2} s^{-1} (respectively $\overline{GPP}$ and $\overline{PPFD}$):

$$\overline{GPP} = a(1 - e^{-b(\overline{PPFD} - c)}) \tag{4.10}$$

with a, b and c three parameters to adjust. The PPFD threshold was defined as the PPFD value when GPP deviated from the asymptote of the model (a) as follows:

$$PPFD_{sat} = c - \frac{ln(\frac{SE_a}{a})}{b} \tag{4.11}$$

with SE_a the standard deviation around a. In Eq. (4.9), C_i was determined following a Fick diffusive law (Farquhar & Sharkey, 1982), representing the CO_2 diffusion through stomata:

$$C_i = C_s - \frac{1.6 GPP_{sat}}{G_{sw}} \tag{4.12}$$

where G_{sw} is determined by Eq. (4.7), 1.6 is the ratio between H_2O and CO_2 conductances and C_s is the CO_2 concentration at the leaf surface, determined based on Eq.

(4.5). $V_{cmax,app}$ values were further normalized at 25 °C ($V_{cmax,app,25}$) by adjusting the Arrhenius model on $V_{cmax,app}$ and T_s data averaged within T_s classes with a width of 2 °C (Medlyn *et al.*, 2002).

4.7. NSOL during drought

The effects of drought on NSOL can be characterized only if the influence of other factors on the dynamics of $V_{cmax,app}$ is discarded from the analysis. The impact of u_* is limited by selecting fluxes during low turbulence periods, while $V_{cmax,app}$ was normalized at 25 °C to account for temperature effects on NSOL. Moreover, only half-hourly data at high irradiance (PPFD higher than $PPFD_{sat}$) were selected. The only remaining potential influence (besides REW) comes from the GAI variability which can be observed only for a study of the seasonal dynamics of GPP_{sat}. Therefore, the analysis should be focused on periods with relatively low variations of the phenological development of the crop. To overcome this potential influence, data with GAI above a threshold (GAI_{sat}) were selected to ensure that the amount of green area is high enough so that any increase in the green canopy cover had a negligible effect on GPP_{sat} dynamics. GAI_{sat} was determined by the same method as $PPFD_{sat}$ using Eqs. (4.10) and (4.11) by replacing PPFD by GAI. Days when GAI<GAI_{sat} were discarded since it may induce a bias in the analysis of the influence of REW on SOL and NSOL. The impact of edaphic drought on GPP originating from NSOL was assessed by studying the influence of REW on $V_{cmax,app,25}$ using the data selected.

4.8. SOL during drought

SOL was defined in this paper as a decrease in G_1, the slope parameter of the USO model which was adapted from the leaf to the canopy level by using the "big leaf" framework(Medlyn *et al.*, 2017b; Knauer *et al.*, 2018a):

$$G_{sw} = G_0 + 1.6\left(1 + \frac{G_1}{\sqrt{VPD_s}}\right)\frac{GPP_{sat}}{C_s} \tag{4.13}$$

where G_0 is the minimum stomatal conductance which was set to 0 (Medlyn *et al.*, 2017b) and G_1 represents the ecosystem stomatal sensitivity to GPP at high irradiance normalized by VPD_s and C_s. G_1 was calculated by combining Eqs. (4.12) and (4.13):

$$G_1 = \frac{\frac{C_i}{C_s}\sqrt{VPD_s}}{1 - \frac{C_i}{C_s}} \tag{4.14}$$

The impact of edaphic drought on GPP_{sat} originating from SOL was assessed by studying the influence of REW on G_1.

4.9. Detection of REW threhsolds

A linear segmented model including one breakpoint and one segment at a constant value for high REW (asymptote) was adjusted between half-hourly $V_{cmax,app,25}$ or G_1 and REW. The asymptote of the model characterizes the unstressed $V_{cmax,app,25}$ and G_1 values, respectively named $V_{cmax,app,25}*$ and G_1*. This procedure allows the detection of a breakpoint, below which SOL and NSOL increase or decrease linearly with REW. A Fisher F-test was conducted to verify if this segmented model was significantly different from a linear regression with no breakpoint. The quality of the segmented regressions was also assessed by the p-values of the adjusted coefficients and the R^2 of the model.

4.10. Sensitivity analysis

A sensitivity analysis was performed by calculating the ratio between theoretical GPP_{sat} values that would be modeled without accounting for water stress effect on $V_{cmax,app,25}$ and G_1 ($GPP_{Vcmax,app,25}*$ and $GPP_{G1}*$), with observed GPP_{sat} values. $GPP_{Vcmax,app,25}*$ was determined by using Eq. (4.8) where $V_{cmax,app,25}$ was replaced by $V_{cmax,app,25}*$ and by assuming that G_0 and ecosystem respiration are negligible. C_i in Eq. (4.8) was deduced from $GPP_{Vcmax,app,25}*$, C_a, G_{aw}, G_1 and VPD_s by combining Eqs. (4.12), (4.5) and (4.13):

$$C_i = \left(C_a - \frac{GPP_{Vcmax,app,25}*}{G_{aw}}\right)\left(1 - \frac{1}{(1+\frac{G_1}{\sqrt{VPD_s}})}\right) \tag{4.15}$$

Inserting Eq. (4.15) in Eq. (4.8) gives the following equation:

$$GPP_{Vcmax,app,25}* = V_{cmax,app,25}* \frac{\left(C_a - \frac{GPP_{Vcmax,app,25}*}{G_{aw}}\right)\left(1 - \frac{1}{1+\frac{G_1}{\sqrt{VPD_s}}}\right) - \Gamma^*}{\left(C_a - \frac{GPP_{Vcmax,app,25}*}{G_{aw}}\right)\left(1 - \frac{1}{1+\frac{G_1}{\sqrt{VPD_s}}}\right) + K_m} \tag{4.16}$$

which was solved for $GPP_{Vcmax,app,25}*$. In a similar way, $GPP_{G1}*$ was determined by solving Eq. (4.16) where $V_{cmax,app,25}*$ was replaced by observed$V_{cmax,app,25}$ and G_1 by G_1*. The comparison between $GPP_{Vcmax,app,25}*$ (or $GPP_{G1}*$) and the measured GPP_{sat} estimates the bias induced by the non-inclusion of NSOL (or SOL) in the modeling of GPP_{sat} . More precisely, a ratio $GPP_{G1} * /GPP_{sat}$ or $GPP_{Vcmax,app,25} * /GPP_{sat}$ higher than 1 indicates an overestimation of GPP_{sat} when REW effects on G_1 or $V_{cmax,app,25}$ are not considered.

4.11. Coupling between transpiration and photosynthesis

Stomata opening regulates both CO_2 and water vapor fluxes and is affected by the evaporative demand of the atmosphere. This leads to a high degree of coupling at the hourly timescale between $GPP\sqrt{VPD_s}$ and LE (Nelson *et al.*, 2018). Changes in environmental conditions may affect this level of coupling. Temperature variations, or appearance of cloud cover (decrease of PPFD) may induce a decoupling between $GPP\sqrt{VPD_s}$ and LE (Reinhardt & Smith, 2008; Urban *et al.*, 2017a; Krich *et al.*, 2022; Marchin *et al.*, 2022). Moreover, as drought intensifies and affects biochemical factors, carbon fixation may be inhibited independently of LE. Therefore, avoiding the potential effects of PPFD and T_s is required to investigate the effects of drought on the coupling between $GPP\sqrt{VPD_s}$ and LE. This has been realized by regrouping many days with large ranges of T_s and PPFD daily variations.

The level of coupling was quantified by the Spearman's rank correlation coefficient (Spearman, 1904) between LE and normalized carbon assimilation ($GPP\sqrt{VPD_s}$) (Nelson *et al.*, 2018):

$$DWCI = \rho(LE, GPP\sqrt{VPD_s}) \tag{4.17}$$

with $DWCI$ the Diurnal Water-Carbon Index (Nelson *et al.*, 2018). The fluxes were normalized by their maximum value for each day before using Eq. (4.17), which allowed for using fluxes measurements across growing seasons. The data already discarded for the G_{sw} calculation process was removed, and the period of analysis was restricted to the growing seasons. A linear segmented regression was adjusted on the $DWCI$ dependence on REW (all years regrouped) following the method presented in 2.9 to detect if the decrease in REW impacted the degree of coupling between carbon and water fluxes.

5. Results

5.1. Ancillary data and photosynthesis dynamics

5.1.1. Crop characteristics and pedo-climatic conditions

The maximum GAI value was measured in 2010 (5.02) while other years showed relatively similar maximum values between 3 and 4 (Fig. 4.1, Table 4.2). The year 2006 had the longest growing season with 74 days, compared to the three other years, which had a growing season of 71 days in 2010, 64 days in 2014 and 66 days in 2018 (Table 2). These differences are explained by farming activities and haulm killing dates that change throughout the years. The 2018 growing season had the lowest rainfall, with cumulative precipitation of 68.4 mm, slightly lower than 2010 (76.6 mm), and considerably below 2006 (186.2 mm) and 2014 (222.4 mm) (Table 4.2). In 2018,

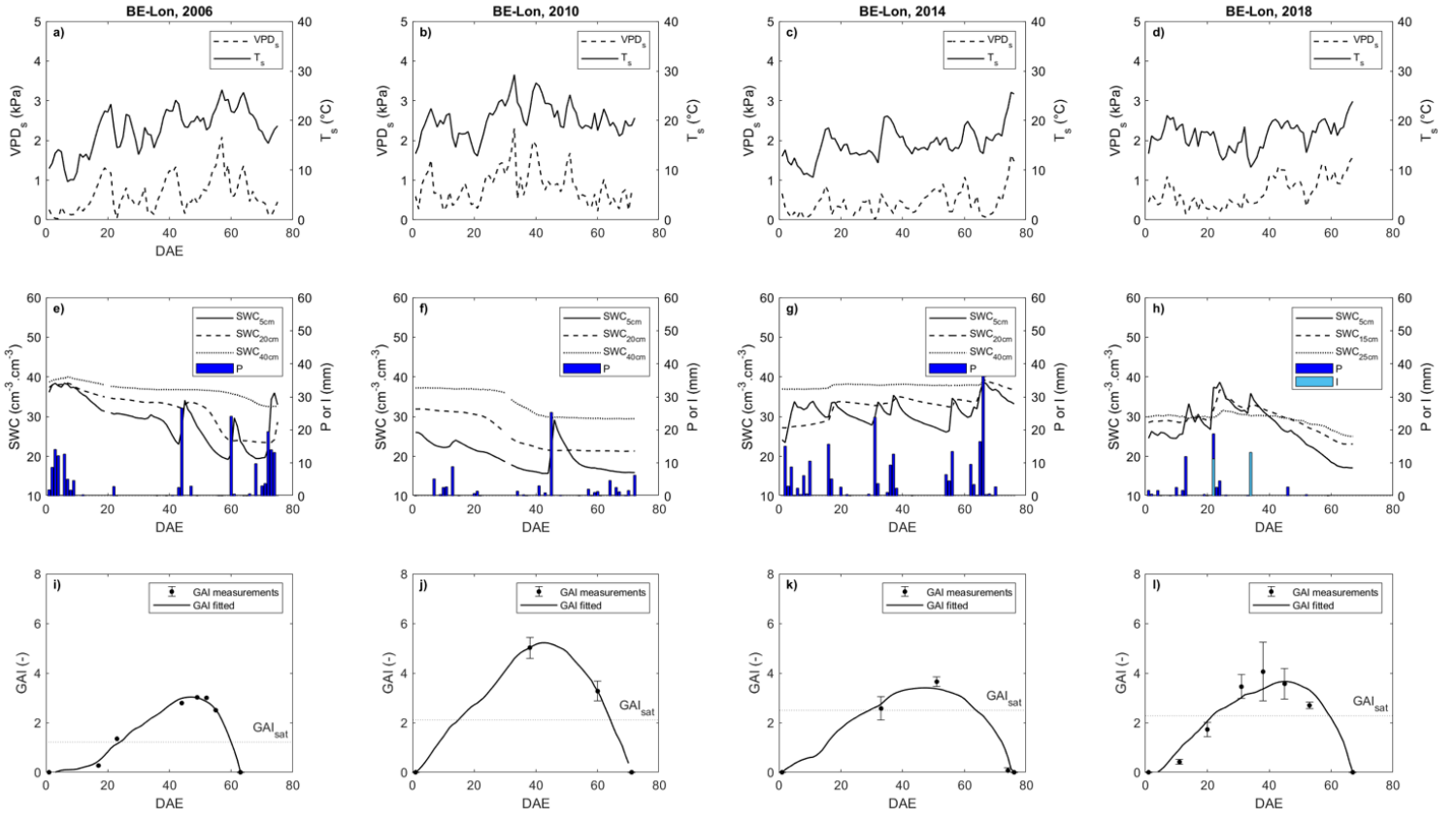

Figure 4.1: Vapor pressure deficit at the canopy surface (VPD_s), canopy temperature (T_s) (subplots a to d) and soil water content (SWC) (subplots e to h) daily means. Daily sums of precipitation (P) and irrigation (I) are displayed on the second line (subplots e to h). Interpolated green area index GAI (GAI fitted) and measurements (GAI measurements) with their standard deviation are shown on the third line (subplots i to l). DAE corresponds to days after emergence.

the site was irrigated two times (24.5 mm) by the aspersion technique (Fig. 4.1), for a total amount of water received by the crop of about 92.9 mm (precipitation and irrigation). SWC at 5 cm depth decreased with the lack of precipitation and reached approximately 16 % in 2018 and 2010 (Fig. 4.1), which was slightly higher than the wilting point (θ_{wp} =11.7 between 0 and 35 cm depth – Table 4.1). The minimum SWC values at deeper depths remained close to 25 %, suggesting that deeper soil layers in the first horizon were able to hold water above the wilting point during the growing seasons. The periods of lack of precipitation were associated to an increase in VPD_s and T_s (regularly in 2010, in late 2006 and 2018) when their daily averaged values both reached respectively about 1.5 kPa and 25 °C (Fig. 4.1. The trends in VPD_s, T_s and SWC illustrated that climate conditions generated periods with potential conditions for both atmospheric and edaphic droughts during the vegetative stage in 2010 and during the reproductive stage in 2006 and 2018. The lowest REW values were quite similar in 2006, 2010 and 2018 growing seasons at respectively 0.40, 0.31 and 0.30 (Fig. 4.2). In 2014, REW was always higher than 0.60 due to favorable weather conditions.

Table 4.2: Crop characteristics: growing season (from emergence to haulm killing), cumulative precipitation (P_{cum}), irrigation (I), maximum green area index (GAI_{max}) and variety.

	Growing season	P_{cum}	I	GAI_{max}	Variety
	(days)	(mm)	(mm)	(-)	(% of total area)
2006	74	186.2	-	3.02	Spunta (62.8 %) / Primura (11.6 %) / Kondor (11.6 %) / Draga (14 %)
2010	71	76.6	-	5.02 ± 0.42	Draga (100 %)
2014	64	222.4	-	3.55 ± 0.19	Draga (72.8 %) / Bianchidea (20 %) / Kennebec (7.2 %)
2018	66	68.4	24.5	4.05 ± 1.18	Agria (53.9 %) / Unidea (26.4 %) / Draga (19.7 %)

5.1.2. Photosynthesis and canopy conductance dynamics

A deviation from the expected bell-shape GPP_{sat} curve following GAI dynamics can be observed in 2018 and 2006 (during the reproductive stage) and in 2010 (during the vegetative stage) where GPP_{sat} dropped from 25 to 35 μmol m^{-2} s^{-1} to 5–15 μmol m^{-2} s^{-1} (Fig. 4.2). These sharp declines coincided with the decrease in REW (roughly from 0.65 to 0.45 in 2006, and from 0.60 to 0.30 in 2010 and 2018) and G_{sw} (roughly from 0.60 to 0.25 mol m^{-2} s^{-1} in 2006 and from 0.25 to 0.10 mol m^{-2} s^{-1} in 2010 and 2018, Fig. 4.2), which corresponded to the closure of the stomata when REW values were low. The relatively small amount of data recorded in 2014 (due to numerous precipitation events, and important gaps in the shortwave and longwave flux measurements) and 2006 (due to numerous days when cumulative precipitation was very low; e.g., <0.3 mm day^{-1} on DAE 39, 41, 56 or 64) explain that very few G_{sw} data points were available for the analysis. These observations highlighted two different

timings in drought appearance with varying amplitude and intensity, characterized by a decrease in GPP_{sat} and G_{sw}.

5.2. Drought impact on SOL and NSOL at the seasonal scale

5.2.1. Impact of drought on $V_{cmax,app,25}$

$V_{cmax,app,25}$ decreased with the decline in REW. The linear segmented model significantly described the dependence between $V_{cmax,app,25}$ and REW in 2018, 2010 and 2006 (Table 4.3 – Fig. 4.2). REW breakpoints ranging between 0.58 ± 0.01 and 0.45 ± 0.02 were found whatever the development stages of the crop when drought occurred, indicating a relatively uniform tipping point below which the photosynthetic capacities of the canopy decrease due to edaphic drought (Table 4.3). The asymptote of the model ($V_{cmax,app,25}*$) or averaged value was in a narrow range (from 98.7 ± 1.69 μmol m^{-2} s^{-1} in 2018 to 128 ± 6.11 μmol m^{-2} s^{-1} in 2010 – Table 4.3). In 2014, no effect of REW on $V_{cmax,app,25}$ was observed due to recurrent precipitation events and reduced amount of data (see explanation above). The slopes of the linear segmented model ranged from 324 ± 36.2 μmol m^{-2} s^{-1} in 2018 to 821 ± 137 μmol m^{-2} s^{-1} in 2010). The systematic pattern of decreasing $V_{cmax,app,25}$ with REW with quite similar unstressed values and breakpoints whatever the years demonstrated the existence of a clear uniform dependence of photosynthetic capacities on soil water availability either during the vegetative (2010) or reproductive stage (2006 and 2018).

5.2.2. Impact of drought on G_1

G_1 was significantly impacted by REW in 2010 and 2018. More precisely, G_1 increased during respectively the vegetative and reproductive stages (Fig. 4.3). The REW breakpoints were very similar for these two years (0.44 ± 0.05 in 2010 and 0.45 ± 0.03 in 2018, Table 4.3, Fig. 4.3). The asymptote value was slightly higher in 2010 (1.69 ± 0.24 kPa$^{0.5}$) compared to 2018 (2.37 ± 0.05 kPa$^{0.5}$). No significant effect of REW on G_1 was observed in 2006 and 2014. The averaged G_1 values in 2006 and 2014 (4.35 ± 0.80 kPa$^{0.5}$ and 4.44 ± 1.45 kPa$^{0.5}$ respectively, Table 4.3) were clearly higher than the asymptote of the segmented model in 2010 and 2018.

5.2.3. Impact of drought on GPP modeling

$GPP_{Vcmax,app,25}*/GPP_{sat}$ increased when REW passed below a REW breakpoint of 0.46 ± 0.01 for all years when edaphic drought induced NSOL, which is logically a similar breakpoint compared to those for $V_{cmax,app,25}$ (Fig. 4.4- Table 4.3). This ratio even exceeded 2 in 2010 and 2018 when the REW reached its minimum values during water stress events (Fig. 4.4). In opposition, the ratio $GPP_{G1} * /GPP_{sat}$ remained relatively constant for all the years and whatever the soil water availability. (Fig. 4.4). The REW breakpoint of the sensitivity analysis characterizes a tipping point illustrating the importance of including NSOL of GPP for potatoes during edaphic drought.

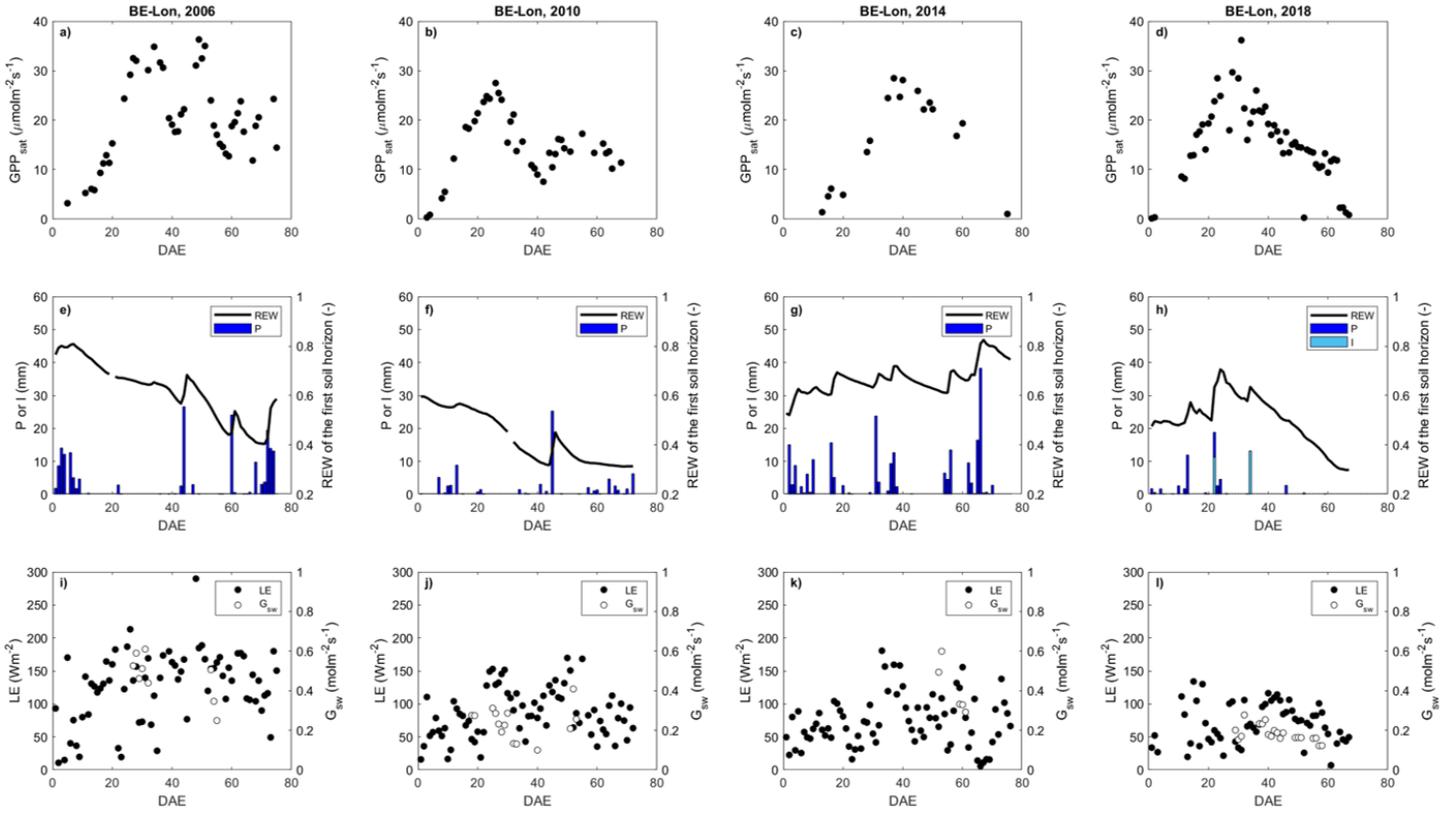

Figure 4.2: Gross primary production under high irradiance (GPP_{sat}; subplots a to d), relative extractable water (REW; subplots e to h), latent heat flux (LE) and canopy conductance to water vapor (G_{sw}; subplots i to f) daily means. Daily sums of precipitation (P) and irrigation (I) are displayed on the second line (subplots e to h). DAE corresponds to days after emergence.

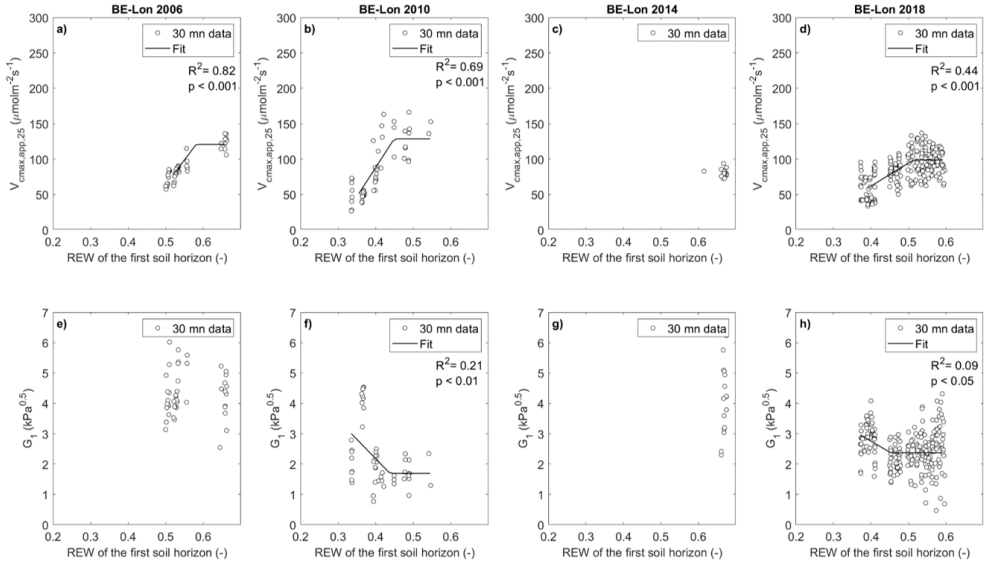

Figure 4.3: Apparent maximum carboxylation rate at 25°C ($V_{cmax,app,25}$; subplots a to d) and slope parameter of the USO model (G_1; subplots e to h) dynamics in function of the REW for the years studied. p refers to the p-value comparing the segmented model to a linear model (p-val$_{\text{mod}}$ in Table 4.3).

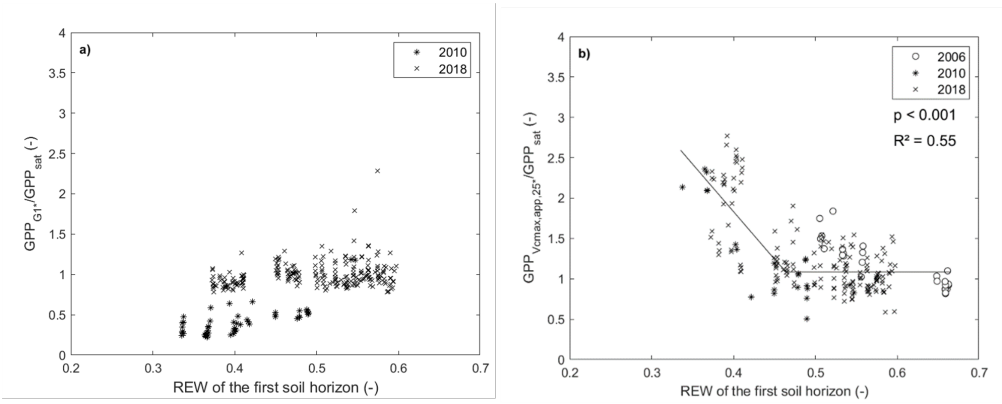

Figure 4.4: Sensitivity analysis for the modeling of GPP by setting $V_{cmax,app,25}$ and G_1 to a constant value when REW is non limiting (respectively ($GPP_{Vcmax,app,25}*$ and $GPP_{G1}*$). The ratios $GPP_{Vcmax,app,25} * /GPP_{sat}$ (subplot a) and $GPP_{G1} * /GPP_{sat}$ (subplot b) were only calculated for the years when a decrease in $V_{cmax,app,25}$ and/or an increase in G_1 were observed. p refers to the p-value comparing the segmented model to a linear model (p-val$_{\text{mod}}$ in Table 4.3).

	$V_{cmax,app,25}$					G_1				
	REW breakpoint	Asymptote ($V_{cmax,app,25}$*) or averaged value	Slope	$pval_{mod}$	R^2	REW breakpoint	Asymptote (G_1*) or averaged value	Slope	$pval_{mod}$	R^2
	(-)	(µmol m^{-2} s^{-1})	(µmol m^{-2} s^{-1})	(-)	(-)	(-)	($kPa^{0.5}$)	($kPa^{0.5}$)	(-)	(-)
2006	0.58 ± 0.01 ***	121 ± 2.93 ***	704 ± 94.1 ***	< 0.001	0.82	/	4.35 ± 0.80	/	/	/
2010	0.45 ± 0.02 ***	128 ± 6.11 ***	821 ± 137 **	< 0.001	0.69	0.44 ± 0.05 ***	1.69 ± 0.24 ***	-12.7 ± 5.63*	< 0.01	0.21
2014	/	80.2 ± 5.25	/	/	/	/	4.44 ± 1.45	/	/	/
2018	0.51 ± 0.01 ***	98.7 ± 1.69 ***	324 ± 36.2 ***	< 0.001	0.44	0.45 ± 0.03 ***	2.37 ± 0.05***	-7.27 ± 3.41*	< 0.05	0.09
Sensitivity analysis on $V_{cmax,app,25}$										
	REW breakpoint	Asymptote	Slope	$pval_{mod}$	R^2					
	(-)	(-)	(-)	(-)	(-)					
2006, 2010, 2018	0.46 ± 0.01 ***	1.08 ± 0.02 ***	-11.8 ± 1.31 ***	< 0.001	0.55					
DWCI										
	REW breakpoint	Asymptote	Slope	$pval_{mod}$	R^2					
	(-)	(-)	(-)	(-)	(-)					
2006, 2010, 2018	0.45 ± 0.04 ***	0.91 ± 0.01 ***	2.04± 0.95 **	< 0.01	0.41					

Table 4.3: Statistical proprieties of the regressions: REW breakpoint, asymptote (or averaged value), slope, model p-value ($pval_{mod}$) and R^2 for $V_{cmax,app,25}$, G_1, sensitivity analysis on $V_{cmax,app,25}$ and for the DWCI. Parameters are given with their standard deviation. For the p-values, $***$: <0.001, $**$: <0.01, $*$: <0.05 , ns : >0.05.

5.2.4. Coupling between carbon and water fluxes

In 2010 and 2018, NSOL induced a decoupling between $GPP\sqrt{VPD_s}$ and LE, characterized by a shift of the $GPP\sqrt{VPD_s}$ maximum toward morning hours (Fig. 4.5). During these years, a clear change in the $GPP\sqrt{VPD_s}$ dynamics was observed, with a maximum value being reached in the early morning (Fig. 4.6). This decoupling between carbon and water fluxes was not observed in 2006 and 2014, which can be explained by favorable weather conditions in 2014 (absence of water stress) and probably the relatively low intensity of the drought effect on $V_{cmax,app,25}$ in 2006 ($V_{cmax,app,25}$ remained higher than 50 μmol m^{-2} s^{-1}). DWCI decreased when REW passed below a threshold of 0.45 ± 0.04 (Fig. 6) which was similar to the thresholds for the $GPP_{Vcmax,app,25} * /GPP_{sat}$ ratio and $V_{cmax,app,25}$ dependence on REW (Table 4.3).

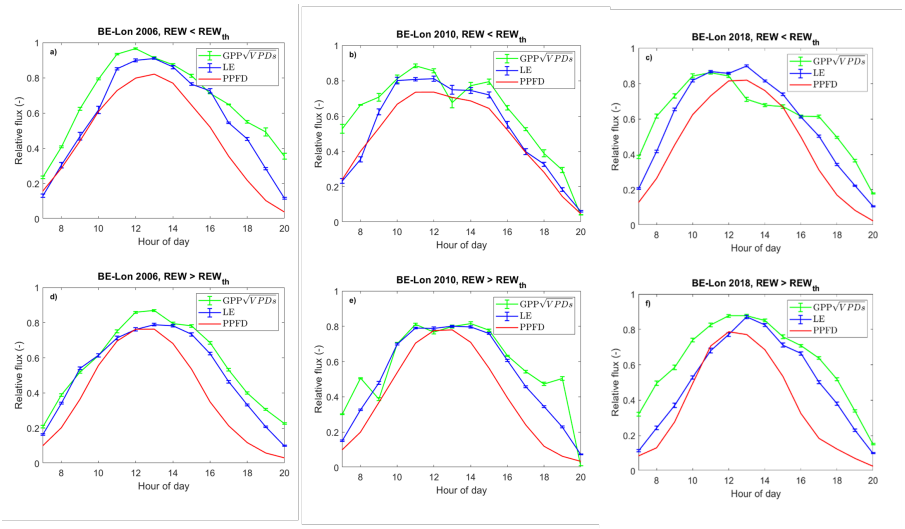

Figure 4.5: Latent heat flux (LE), photosynthetic photon flux density (PPFD) and normalized GPP ($GPP\sqrt{VPD_s}$) hourly means and standard deviation when REW is lower than REW breakpoints of segmented linear regressions for $V_{cmax,app,25}$ (subplots a to c) or when REW is not limiting (subplots d to f) for the three years when non-stomatal limitations were observed (Table 4.3).

6. Discussion

6.1. Photosynthesis limitations and methodological considerations

Whatever the year analyzed, we found a global pattern of reduction of photosynthesis capacities due to the influence of soil water availability. Only $V_{cmax,app,25}$ decreased

with REW, which suggests that the β stress function should only be applied when REW passes below the breakpoint of 0.46 ± 0.01 (for the varieties of potatoes cultivated at BE-Lon and the soil type present on this site). Not implementing water stress effect on $V_{cmax,app,25}$ would significantly overestimate GPP. This provides strong evidence that NSOL played a major role (or even unique because SOL has not been observed) in carbon assimilation dynamics of potato under high irradiance and during edaphic drought during the four years studied. Moreover, our study was performed at the canopy level which is representative of the physiological reaction of the entire ecosystem to drought since the "big leaf" approach includes all the leaves within the footprint of the EC tower. These conclusions are in accordance with previous studies carried out on forests Gourlez de la Motte *et al.* (2020) and on various non-cropland ecosystems (Chen *et al.*, 2019a), tending to show that NSOL should not be neglected for many plant functional types. At the leaf-level, numerous studies have evaluated the importance of NSOL on photosynthesis using coupled gas-exchange and fluorescence measurements for various crop (Flexas *et al.*, 2008; Wang *et al.*, 2018a) and tree species (Grassi & Magnani, 2005; Perez-Martin *et al.*, 2014; Zait & Schwartz, 2018; Zhu *et al.*, 2021).

While most of the studies conducted on potato aimed at identifying the physiological response to imposed drought through the dynamics of photosynthetic capacities or stomatal closure (Ramírez *et al.*, 2016; Li *et al.*, 2017; Boguszewska-Mańkowska *et al.*, 2018; Silva-Díaz *et al.*, 2020; Aliche *et al.*, 2020), the calibration of the β stress function during edaphic water stress for this crop is lacking. Our study provides a function of REW that can be directly translated to models of photosynthesis in LSMs.

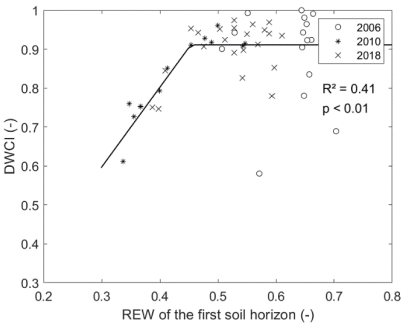

Figure 4.6: Diurnal water carbon index (DWCI) daily dynamics in function of the relative extractable water (REW). p refers to the p-value comparing the segmented model to a linear model ($p\text{-val}_{mod}$ in Table 4.3).

The decrease in $V_{cmax,app,25}$ illustrates an alteration of the photosynthesis capacities of the crop, either by a restriction of CO_2 diffusion through the mesophyll, real biochemical alteration of the photosynthetic apparatus, or both. Excessive diffusive limitation of CO_2 by the mesophyll may lead to an accumulation of ATP and NADPH which can no longer used by the Calvin cycle, causing energy imbalance, oxidative stress and damage to cell components (Pinheiro & Chaves, 2011). Moreover, biochemical alteration of photosynthetic capacities can be caused by photo-inhibition and/or irreversible inactivation of PSII, as has been identified during prolonged water stress (Obidiegwu, 2015). Our study did

not allow the identification of the NSOL causes as techniques used to quantify mesophyll conductance (involving carbon isotopes or fluorescence) were not tested. No global application of a model would require a heavy calibration for all plant functional types, a procedure that has not yet been achieved. Future studies should focus on continuous measurements of water extraction, photosynthetic capacities, mesophyll and stomatal conductance during dry periods and subsequent recovery episodes, so drought impacts on ecosystems can be fully understood and mechanistically modeled (Flexas *et al.*, 2018b). The relatively similar REW breakpoints for all growing seasons suggests that the same amount of water in the root zone was required to ensure that saturated photosynthesis remained unaffected by drought, whatever the timing of drought appearance or the potato varieties. This also indicates that the water needs for potato crops were similar during the vegetative (2006) or reproductive (2010, 2018) stages. This observation coincides with early studies stating that "soil moisture should never be allowed to drop below 50 % of the available range of moisture" for potato crop (Singh, 1969), confirming that potato is sensitive to water stress. Models such as Aquacrop usually calibrate similar functions of REW to simulate drought stress on crop physiology with upper thresholds of 0.6 for canopy expansion, 0.7 for canopy senescence, or 0.55 for stomatal control (Raes *et al.*, 2009). The degree of calibration of these thresholds is defined as minimum and requires further investigations for potatoes (Montoya *et al.*, 2016; Raes *et al.*, 2009). The REW breakpoint of 0.46 proposed by this study could be used to design irrigation management strategies from SWC measurements in surface soil layers to avoid the risk of crop abiotic damage. This information is complementary to high-throughput phenotyping techniques (Musse *et al.*, 2021) for selecting drought-tolerant varieties from the criteria of the lowest REW threshold for maintaining an optimum photosynthetic rate. The generalization of our results could be enhanced by applying the procedure and analysis proposed in this paper on other crop sites of the ICOS network where potato was cultivated, which could provide complementary REW thresholds for other soil types. The method used for calculating REW considers that all the roots have the same ability to extract water from the first soil horizon, whatever their age, diameter, architecture, location, or function. This assumption can be challenged, as it has been shown that the root water uptake can be dependent on root density, morphology, and physiology (Kumar *et al.*, 2015). For example, Stalham & Allen (2004) showed that 5 % of the deepest roots can account for a half of the total water uptake for the potato cultivar Cara. Some models do consider these dependences but are difficult to implement at a plot scale due to the high number of inputs and parameters required. Nonetheless, REW remains a useful indicator to determine the amount of available water in the soil from soil hydraulic or granulometric properties that are available for all the ICOS sites.

Some bias in the results can originate from errors in the estimation of C_i (Eq. (4.12)), and in the calculation of G_{sw} by Eq. (4.7). The Penman- Monteith equation assumes that the minimal gas diffusion through stomatal apertures (G_0) is set to zero and that

no transfer through the cuticle (in parallel with diffusion through stomata) is considered. However, as the cuticle may represent the main pathway for transpiration during drought (Boyer, 2015a; Duursma *et al.*, 2019), these assumptions could possibly lead to an underestimation of G_{sw} and then C_i by Eq. (4.12) (Boyer, 2015a). To counter this potential drawback, C_i could be directly measured at the leaf level by a gas(Wang *et al.*, 2018b). However, estimating G_0 by data adjustment on the USO model remains challenging due to statistical considerations (Duursma *et al.*, 2019), which explains that G_0 is often set to zero or to a constant value in coupled photosynthesis-stomatal conductance models (Medlyn *et al.*, 2017b; Duursma *et al.*, 2019).

6.2. Stomatal conductance modeling during drought

While the empirical Ball-Berry (Ball *et al.*, 1987) stomatal conductance model has been used as a baseline in climate models since the mid-1990s (Bonan *et al.*, 2014), many LSMs currently use the USO model (Eq. (4.13)) to estimate G_{sw} (Kala *et al.*, 2015a; Lawrence *et al.*, 2019). However, the calibration of the response of G_1 to edaphic water stress remains a key element for improving model predictions in a climate change context. Although most models downregulate G_1 with soil moisture (following the stomatal optimality theory; Mäkelä (1996)), numerous studies have observed a different G_1 dependance to soil moisture using leaf-level or ecosystem fluxes data (Zhou *et al.*, 2013; Chen *et al.*, 2019a; Gourlez de la Motte *et al.*, 2020). In line with these studies, our results showed that G_1 remained constant (or even increased) with the decrease in REW for potato. This observation suggests the absence of regulation of stomata opening during drought and indicates a deviation from the optimality theory as the increase of G_1 for low REW corresponds to a rise of the water cost of carbon gain. This behavior can be explained by a decrease in $V_{cmax,app,25}$ (inducing a decline of the carbon gain through the alteration of efficiency of RuBisCO to fix CO_2 in the Calvin cycle) more important than the corresponding increase in the water transport capacity. This hypothesis is supported by Aliche *et al.* (2020), who observed an adaptation of the hydraulic architecture of four potato cultivars in response to dehydration through and an increase in xylem flux density and an increase in the ratio between small and large xylem vessels, preventing from cavitation and facilitating the transport of water and assimilates. When $V_{cmax,app,25}$ was relatively low, NSOL induced a reduction of GPP_{sat} leading to a decrease in G_{sw} computed by Eq. (4.13), but partly compensated by an increase in G_1. This may explain the decoupling between $GPP\sqrt{VPD_s}$ and LE intra-day dynamics with decreasing REW and emergence of NSOL which induced an inhibition of photosynthetic capacities independently from transpiration. Similar results were presented by Nelson *et al.* (2018), who reported a decrease of DWCI during the 2003 drought in Puéchabon and for dry savanna/grassland plant functional types during dry episodes.

7. Conclusion

In this study, a "big leaf" approach including the FvCB model for photosynthesis and the USO model for stomatal conductance was used to infer the physiological properties of a potato crop for four consecutive growing seasons at the ICOS site of Lonzée in Belgium. Drought induced a decrease in $V_{cmax,app,25}$ with similar REW breakpoints and unstressed values for all years, which highlighted a uniform pattern of drought effects on GPP. A global value of 46 % of available soil water was obtained from a sensitivity analysis, which highlights the importance of implementing REW effects on $V_{cmax,app,25}$ to reproduce drought effects on GPP. The coupling of this representation with a constant value or a linear increase with REW of the slope parameter (G_1) in USO model was sufficient to simultaneously reproduce both carbon and water flux dynamics at seasonal and diurnal scales during drying-up episodes. The inclusion of the effects of drought on NSOL in LSMs for potatoes is recommended to properly implement the effects of drought on water and carbon cycles.

CRediT authorship contribution statement

Quentin Beauclaire: Conceptualization, Formal analysis, Software, Writing – original draft, Writing – review and editing, Validation. **Bernard Heinesch**: Resources, Writing – review and editing. **Bernard Longdoz**: Resources, Validation, Supervision, Writing – review and editing.

Declaration of Competing Interest

The authors declare that they have no known competing financial interests or personal relationships that could have appeared to influence the work reported in this paper.

Data availability

Data will be made available on request.

Acknowledgments and funding

This research was conducted within the framework of the ICOS Wallonia project, which is supported by the Service Public de Wallonie, Belgium [1217769]. The researchers were funded by the Federation Wallonie Bruxelles (FWB).

8. Supplementary materials

Date	Farming activities	
11-Apr-06	Application	Asparagite (0N/0P/25K +10% calcium oxide + 30% sulphuric oven-dry)
1-May-06	Planting	Potato: Spunta/Primura/Kondor/Draga
2-May-06	Application	Liquid Nitrogen (117 Units ha^{-1})
	Weeding + Pre emergence treatment	Defi (4l ha^{-1}) + Linuron (1l ha^{-1})
13-May-06	Earthing up	
14-May-06	Weeding + Pre emergence treatment	Defi (4l ha^{-1}) + Linuron (1l ha^{-1})
1-Jun-06	Application	Insecticide and fungicide treatments
9-Jun-06		
15-Jun-06		
20-Jun-06		
27-Jun-06		
3-Jul-06		
8-Jul-06		
19-Jul-06		
6-Aug-06	Topkilling	Purivel (2.5 kg ha^{-1}) + Spotlight (0.25 l ha^{-1})
13-Aug-06	Topkilling	Purivel (2.5 kg ha^{-1}) + Reglone (2 l ha^{-1})
15-Sep-06	Harvest	Spunta/Primura/Kondor/Draga
12-Apr-10	Application	Asparagite (0N/0P/25K +10% calcium oxide + 30% sulphuric oven-dry)
24-25-Apr-10	Planting	Potatoes : Draga
5-May-10	Application	Liquid Nitrogen (97.5 Units ha^{-1})
8-May-10	Definitive ridging	
11-May-10	Weeding + Pre emergence treatment	Defi (4l ha^{-1}) + Linuron (1l ha^{-1})
3-Jun-10	Weeding	Sencor (0.15 kg)
3/7/13/22/29-Jun10	Insecticide and Fungicide treatments	Sumi Alfa (Insect.) / Revus (Fung.) + Sumi Alfa (Insect.) / Mancozeb (Fung.) + Tepeki

		(Insect) / Dequiman (Fung.) + Sumi Alfa (Insect.) / Tepeki (Insect.)
6/13/23-Jul-10	Insecticide and Fungicide treatments	Tepeki (Insect.) / Karaté (Insect) + Acrobat (Fung) / Ninja (Insect.)
3-Aug-10	Insecticide treatment	Fastac
10-Aug-10	Chemical haulm destruction	Reglone + Spotlight
13-Aug-10	Chemical haulm destruction	Reglone + Spotlight
3-4-5-Sept-10	Harvest	
2-Apr-14	Application	Liquid Nitrogen (183.3 l ha^{-1}, 71.5 Units N ha^{-1})
5-7- Apr -14	Soil preparation, planting and earthing up	Potato : Draga/Bianchidea/Kennebec
5-7- Apr -14	Disinfection	Monarch (0.2 l t^{-1}) + Mirador (2.22l ha^{-1})
8- Apr -14	Weeding	Sencor (0.4 l ha^{-1}) + Centium (0.25 l ha^{-1}) + Reglone (on Fumaria officinalis) (1.5 l ha^{-1})
12-May-14	Insecticide	Lambda 50 EC (0.2 l ha^{-1}) + Mineral Oil (5l ha^{-1})
12-May-14	Weeding	Titus (40 g ha^{-1})
17-May-14	Insecticide	Lambda 50 EC (0.2 l ha^{-1}) + Mineral Oil (5l ha^{-1})
23-May-14	Insecticide	Lambda 50 EC (0.2 l ha^{-1}) + Mineral Oil (5l ha^{-1})
29-May-14	Insecticide	Lambda 50 EC (0.2 l ha^{-1}) + Mineral Oil (5l ha^{-1})
29-May-14	Fungicide	Mancozèbe (2 kg ha^{-1})
6-Jun-14	Fungicide	Acrobat (2kg ha^{-1}) + Mineral Oil (5 l ha^{-1})
6- Jun -14	Insecticide	Sumi Alpha (0.2 l ha^{-1})
11- Jun -14	Fungicide	Acrobat (2.5 kg ha^{-1}) + Mineral Oil (5 l ha^{-1})
11- Jun -14	Insecticide	Sumi Alpha (0.2 l ha^{-1})
11- Jun -14	Fungicide	Manfil (2.5 kg ha^{-1})
17- Jun -14	Fungicide	Acrobat (2 kg ha^{-1}) + Mineral Oil (5 l ha^{-1})
17- Jun -14	Insecticide	Sumi Alpha (0.2 l ha^{-1})
23- Jun -14	Fungicide	Acrobat (2 kg ha^{-1}) + Mineral Oil (5 l ha^{-1})

23- Jun -14	Insecticide	Okapi (1 l ha^{-1})
30- Jun -14	Fungicide	Ranman (Component A: 0.2 l ha^{-1}, Component B: 0.15 l ha^{-1}) + Mineral Oil (5 l ha^{-1})
30- Jun -14	Insecticide	Okapi (1 l ha^{-1})
7-Jul-14	Fungicide	Ranman (Component A: 0.2 l ha^{-1}, Component B: 0.15 l ha^{-1}) + Mineral Oil (5 l ha^{-1})
15-Jul-14	Topkilling	Reglone (2 l ha^{-1})
15-Jul-14	Fungicide	Shirlan (0.5 l ha^{-1})
19-Jul-14	Topkilling	Spotlight (1 l ha^{-1})
19-Jul-14	Fungicide	Ranman (Component A: 0.2 l ha^{-1}, Component B: 0.15 l ha^{-1}) + Mineral Oil (5 l ha^{-1})
21-22-Aug-14	Harvest	Draga/Bianchidea/Kennebec
12-Apr-18	Application	Solid (N 0, P 7, K 36 à 350 kg/ha + 5 MGO)
22-23-Apr-18	Planting	Potato: Agria/Unidea/Draga
9-10-May-18	Earthing up	
9-10-May-18	Application	Liquid Nitrogen (200 l ha^{-1})
13-May-18	Weeding	Promane (2 l ha^{-1}) + Défi (4 l ha^{-1}) + Centium (0.135 l ha^{-1})
23-May-18	Treatment	Mineral oil (3 l ha^{-1})
26-May-18	Treatment	Mineral oil (4 l ha^{-1})
31-May-18	Treatment	Mineral oil (8 l ha^{-1})
31-May-18	Insecticide	Teppeki (0.15 l ha^{-1})
1-2-Jun-18	Irrigation	Cv. Draga and Unidea
4-Jun-18	Treatment	Mineral oil (8 l ha^{-1})
4-Jun-18	Fungicide	Mancozeb (2 kg ha^{-1})
8-9-10-Jun-18	Irrigation	Draga/Unidea/Agria
13-Jun-18	Treatment	Mineral oil (8 l ha^{-1})
13-Jun-18	Fungicide	Prozeb (1.7 kg ha^{-1}) + Revus (0.4 l ha^{-1})
13-Jun-18	Insecticide	Sumi-alpha (0.2 l ha^{-1})
19-Jun-18	Treatment	Mineral oil (8 l ha^{-1})

19-Jun-18	Fungicide	Cymopur (0.25 l ha^{-1}) + Ranman (0.4 l ha^{-1})
19-Jun-18	Insecticide	Karaté (0.07 l ha^{-1})
20-21-Jun-18	Irrigation	Cv. Unidea
26-Jun-18	Treatment	Mineral oil (8 l ha^{-1})
26-Jun-18	Fungicide	Cymopur (0.2 l ha^{-1}) + Prozeb (2 kg ha^{-1})
26-Jun-18	Insecticide	Teppeki (0.15 l ha^{-1})
7-Jul-18	Treatment	Mineral oil (10 l ha^{-1})
7-Jul-18	Insecticide	Teppeki (0.15 l ha^{-1})
19-Jul-18	Treatment	Mineral oil (10 l ha^{-1})
19-Jul-18	Fungicide	Prozeb (2 kg ha^{-1})
21-Jul-18	Topkilling	Reglone (1.5 l ha^{-1}) + Spotlight (0.8 l ha^{-1})
26-Jul-18	Topkilling	Reglone (1.5 l ha^{-1}) + Spotlight (0.8 l ha^{-1})
3-Aug-18	Crushing	Cv. Agria
4-Aug-18	Topkilling	Reglone (1 l ha^{-1}) + Spotlight (0.8 l ha^{-1}) : Agria and Unidea
8-Aug-18	Topkilling	Reglone (1 l ha^{-1}) + Spotlight (0.8 l ha^{-1}) : Agria, Unidea and Draga
22-Aug-18	Harvest	Draga/Unidea
11-Sep-18	Harvest	Agria

Table 4.4: Farming activities during the 2006, 2010, 2014 and 2018 growing seasons of potato crop at BE-Lon.

Symbol	Description	Value [Units]
REW CALCULATION		
$\bar{\theta}$	Averaged soil water content	[-]
θ_{wp}	Soil water content at the wilting point	[-]
θ_{fc}	Soil water content at the field capacity	[-]
REW	Relative extractable water	[-]
EDDY COVARIANCE FLUXES AND "BIG-LEAF" MODEL		
GPP	Gross Primary Production	[µmol $m^{-2}s^{-1}$]
LE	Latent heat flux	[W m^{-2}]
H	Sensible heat flux	[W m^{-2}]
G	Ground heat flux	[W m^{-2}]
NEE	Net Ecosystem Exchange	[µmol $m^{-2}s^{-1}$]
G_{ah}	Aerodynamic conductance for sensible heat transfer	[m s^{-1}]
G_{aw}	Aerodynamic conductance for water vapor	[m s^{-1}]
C_s	CO_2 concentration in the air at the canopy surface	[µmol mol^{-1}]
C_i	CO_2 concentration in the substomatal cavities	[µmol mol^{-1}]
G_{sw}	Canopy conductance to water vapor transfer	[mol $m^{-2}s^{-1}$]
K_m	Michaelis-Menten coefficient	[µmol mol^{-1}]
Γ^*	CO_2 compensation point	[µmol mol^{-1}]
$V_{cmax,app,25}$	Apparent carboxylation rate of the Rubisco at 25°C	[µmol $m^{-2}s^{-1}$]
$V_{cmax,app,25}{}^*$	Apparent carboxylation rate of the Rubisco at 25°C in absence of water stress	[µmol $m^{-2}s^{-1}$]
G_1	Slope parameter in the USO model	[$kPa^{0.5}$]
G_0	Minimum canopy conductance in the USO model (neglected)	[mol $m^{-2}s^{-1}$]
$G_1{}^*$	Slope parameter in the USO model in absence of water stress	[$kPa^{0.5}$]
GAI_{sat}	Threshold for the non-influence of GAI on GPP under high irradiance	[-]

$PPFD_{sat}$	Threshold for the non-influence of PPFD on GPP	[µmol $m^{-2}s^{-1}$]
$DWCI$	Diurnal water-carbon index	[-]
ENVIRONMENTAL CONDITIONS		
R_n	Net radiation	[W m^{-2}]
C_a	CO_2 concentration in the air	[µmol mol^{-1}]
e_a	Air vapor pressure	[kPa]
e_s	Canopy vapor pressure	[kPa]
T_a	Air temperature	[K]
T_s	Canopy temperature	[K]
u^*	Air friction velocity	[m s^{-1}]
u	Wind speed	[m s^{-1}]
VPD_s	Vapor pressure deficit at the canopy surface	[kPa]
Δ	Slope of saturated vapor pressure curve	[kPa K^{-1}]
p	Air pressure	[kPa]
CONSTANTS		
c_p	Heat capacity of dry air	$c_p = 1005$ [J kg^{-1} K^{-1}]
ρ_a	Air density	$\rho_a = 1.23$ [kg m^{-3}]
γ	Psychrometric constant	$\gamma = 0.067$ [kPa K^{-1}]
ε	Emissivity of the canopy in the infrared	$\varepsilon = 0.97$ [-]
σ	Stefan-Boltzmann constant	$\sigma = 5.67\ 10^{-8}$ [W m^{-2} K^{-1}]
R	Perfect gas constant	$R = 8.314$ [J mol^{-1} K^{-1}]
ACRONYMS		

DAE	Day after emergence	[-]
GAI	Green leaf area index	[-]
SWC	Soil water content	[-]

Table 4.5: List of variables used in this study

5

New method to partition the origin of photosynthesis limitations of potato under soil water availability-limiting conditions

1. Personal contributions

The setup of the drought experiment was realized by myself, with the help of Alain Debacq (former ICOS station technical team) and the AgricultureIsLife (AIL) research platform of the University of Liege. Leaf-level measurements were collected by myself with the help of Florian Vanden Brande during his master thesis. Soil samples for building soil water retention curves were collected by the EnvironmentIsLife (EIL) research platform of the University of Liege. The manuscript was reviewed by Bernard Longdoz, who also actively helped in setting the experiment and interpreting the results. Florian Vanden Brand also reviewed the manuscript. This manuscript is in preparation.

2. Abstract

The identification of the physiological processes limiting carbon assimilation under water stress is crucial for selecting drought-tolerant varieties and ensuring crop productivity. However, the influence of soil water availability on the limitation of photosynthesis is still not fully understood. This study aimed to investigate the origins of photosynthesis limitations for potato (*Solanum Tuberosum*) during a field drought experiment. Gas exchange and chlorophyll fluorescence measurements were performed at the leaf level on irrigated and non-irrigated plants to determine the response of CO_2 assimilation processes to the decrease in the REW in the soil. For the first time, a limitation analysis was performed to quantitatively assess the importance of each factor in limiting photosynthesis and stomatal conductance of potato. The decrease in REW induced a closure of stomata and a restriction of CO_2 diffusion by the mesophyll, which explained the early reduction of light-saturated photosynthesis. Biochemical capacities decreased only from severe soil water restrictions, which led to an increase in the CO_2 concentration in substomatal cavities and an increase in the stomatal conductance sensitivity to photosynthesis. We revisited the limitation analysis equations and showed that mesophyll conductance was the most important constraint on carbon and water exchanges regardless of soil water conditions. We emphasize the need to modify the partitioning methods to fully unravel the physiological controls on photosynthesis and stomatal conductance under water stress.

3. Introduction

European ecosystems are facing more intense and frequent water stress events due to altered rainfall patterns and rising temperature induced by anthropogenic climate change (Samaniego *et al.*, 2018). Precipitation shortage episodes perturbate plant water status and induce disruptions of the water and carbon cycles through the inhibition of carbon assimilation and transpiration (Bertolino *et al.*, 2019; Fahad *et al.*, 2017;

Trenberth *et al.*, 2014). As a result, ecosystems services such as food production and carbon storage are strongly impacted by lack of soil water (Chang & Bonnette, 2016; Hendrawan *et al.*, 2022; Kang *et al.*, 2021). Land-atmosphere feedbacks originating from the perturbation of such processes such as drought and heatwave may exacerbate climate change through water stress intensification (Anderegg *et al.*, 2019; Hartick *et al.*, 2022). An in-depth understanding of the effects of drought on ecosystems physiological functioning is required to predict future ecosystem service capacities and to improve climate models predictions (Ryu *et al.*, 2019).

Photosynthesis is the process by which plants convert CO_2 into carbohydrates. CO_2 supply to the photosynthetic system is a key factor influencing carbon assimilation and is strongly impacted by the physiological barriers on its diffusional pathway such as stomatal opening and diffusion within the mesophyll (Gago *et al.*, 2020; Nadal & Flexas, 2018). In addition, light-saturated photosynthesis is constrained by the efficiency of the Rubisco enzyme for fixing CO_2 in the Calvin cycle (Farquhar *et al.*, 1980). Uncertainties remain on the importance of each limiting factor under soil water-limiting conditions across PFTs (Rogers *et al.*, 2017).

Quantifying the limitations of drought on photosynthesis is also pivotal for assessing phenotype plasticity and for serving as a guide for the selection of drought-tolerant varieties (Lupo & Moshelion, 2024; Nguyen *et al.*, 2023). To that end, mechanistic modeling can be used for disentangling the complexity of the mechanisms regulating plant response to water stress (Stirbet *et al.*, 2020). In the FvCB model (Farquhar *et al.*, 1980), carbon assimilation under high irradiance (A_{sat}) is mediated by the response of stomatal conductance (g_s), mesophyll conductance (g_m), and the maximum carboxylation rate of Rubisco (V_{cmax}). The quantitative contribution of each of these factors in limiting photosynthesis under water stress can be estimated by first, developing the total derivative of A_{sat} as a sum of the total derivative of these factors and second, by estimating the dependence of these terms to soil water availability. This method, also known as limitation analysis (Grassi & Magnani, 2005; Jones, 1985), can be used to partition photosynthesis limitations between stomatal (i.e., a decrease in A_{sat} originating from g_s) and non-stomatal factors (i.e., a decrease in A_{sat} originating from g_m and/or V_{cmax}).

Stomata are the gates of CO_2 diffusion and water transpiration at the leaves surface, whose opening is regulated by a complex interplay of abiotic and biotic factors. For instance, it is well known that an increase in VPD drives the closure of stomata through the evaporation of water in the guard cells (McAdam & Brodribb, 2016). In addition, carbon assimilation regulates stomatal opening to balance the CO_2 diffusion with the efficiency of the Calvin cycle (Lemonnier & Lawson, 2023; Wong *et al.*, 1979). An mechanistic formulation of these dependencies has been proposed by Cowan & Farquhar (1977) who hypothesized that stomatal opening is regulated to maximize carbon gains and minimize water losses over a constant time interval under non-limiting soil

water conditions. This optimization theory is at the basis of the USO model where g_s is a function of VPD, CO_2 concentration at the leaf surface, carbon assimilation and the stomatal sensitivity to photosynthesis (Medlyn *et al.*, 2011a). This latter, which is the slope of USO model (g_1), is linked to the water use strategy of the plant by being inversely proportional to the marginal carbon cost of water (Medlyn *et al.*, 2011a). During drying-up episodes, short timescales variations of g_1 can be used as an indicator of plants adaptation strategy. In the framework of the optimality theory, plants can maximize carbon gains (increase in g_1), minimize water losses (decrease in g_1) or keep the same balance between carbon gains and water losses stable (constant g_1). The sensitivity of g_1 to soil water availability strongly depends on plant species and PFTs (Héroult *et al.*, 2013; Beauclaire *et al.*, 2023b; Gourlez de la Motte *et al.*, 2020; Zhou *et al.*, 2013). Although the formulation of the relationship between g_s and A_{sat}, and the water cost associated with the opening of stomata are still active research topics in the scientific community (Lamour *et al.*, 2022; Mrad *et al.*, 2019), the USO model has become a reference for representing stomatal behavior in LSMs (Kala *et al.*, 2015b; Lawrence *et al.*, 2019; Sabot *et al.*, 2022).

As g_s is mediated by carbon assimilation, a decrease in g_s can also be induced by biochemical or mesophyll limitations which regulate stomatal opening with the mesophyll demand for CO_2 (Lemonnier & Lawson, 2023; Medlyn *et al.*, 2011a; Zhou *et al.*, 2013). As a result, g_s and A_{sat} are strongly coupled and stomatal closure can either originate from an optimal stomatal adaptation, or from a disguised effect of mesophyll conductance and/or carboxylation rate of Rubisco (Zhou *et al.*, 2013; Medlyn *et al.*, 2011a). This complicates the identification of the origins of stomatal closure and photosynthesis limitations under water stress. Using g_1 as the key variable for highlighting a stomatal control on photosynthesis allows to identify the feedback effect of non-stomatal factors on stomatal closure by linking photosynthesis limitations to the stomatal optimality theory (Zhou *et al.*, 2013). In addition, coupling the USO and FvCB models in the limitation analysis enables for a quantitative assessment of the effects of g_1, VPD, g_m and V_{cmax} on g_s and A_{sat}. To our knowledge, this study is the first to develop this approach. Both limitation schemes (i.e., either using g_1 or g_s as the key variable for stomatal limitation) will be compared and discussed. In this paper, the limitations of photosynthesis originating from stomatal closure induced by a decrease in g_1 or g_s are referred to as a SOL while an effect of g_m and/or V_{cmax} is referred to as a NSOL (Beauclaire *et al.*, 2023b; Gourlez de la Motte *et al.*, 2020).

SWC is a key eco-hydrological parameter impacting plant metabolism and more globally carbon and water fluxes (Zhou *et al.*, 2021). In particular, lack of soil water triggers complex mechanisms which regulate the water flow in the plant to avoid hydraulic failure (Martínez-Vilalta *et al.*, 2014). When the soil edaphic proprieties are known, SWC can be used to determine the REW for plant uptake (Granier *et al.*, 2007a), which is often used in LSMs as a drought index to implement water stress effects originating either from SOL and/or NSOL on photosynthesis (Vidale *et al.*,

2021). The response of FvCB and USO model parameters to decreasing soil water availability is likely species and PFTs-specific, which makes REW a critical variable for modeling the response of terrestrial ecosystems to drought (Peters *et al.*, 2018; Rogers *et al.*, 2017; Vidale *et al.*, 2021; Zhou *et al.*, 2013).

Potato is one of the most important crops, providing food for more than one billion people around the world (Lutaladio & Castaldi, 2009). In Europe, more than 400 000 hectares of arable lands are used for potato cultivation (Goffart *et al.*, 2022). This crop is highly sensitive to water stress because of its shallow root system and its inability to extract water from deeper soil layers (Obidiegwu, 2015). In particular, tuber bulking is a critical stage of potato growth as it determines the yield and quality of the harvest (Gervais *et al.*, 2021). Partitioning the limitation components of the photosynthetic flux is crucial for selecting drought-tolerant varieties and ensuring food security. We have implemented this approach during a drought experiment on field-grown potatoes. The goals of this study were: (i) to describe the response of A_{sat}, g_s, g_m, g_1 and V_{cmax} to the decrease in REW, (ii) to perform a limitation analysis on A_{sat} by using g_s or g_1, g_m, V_{cmax} and VPD as explanatory variables and finally (iii) to define REW thresholds from which each of these limitations occurred.

4. Material and methods

4.1. Plant materials and experimental setup

Potato plants were grown on a 4-ha experimental plot located in Belgium, about 50 km southeast of Brussels (50° 33′ 47.77"N, 4°42′ 46.403"E). This cropland has been used for cultivating chicory, sugar beet and winter wheat. In total, 88 tubers of potato (*Solanum tuberosum*, cv Agria) were planted under a plastic polytunnel greenhouse of 12 m long and 5 m large.

SWC and soil temperature were measured by time domain reflectometers (ML3 ThetaProbe, Delta-T Devices Ltd, Cambridge, UK) placed at 10 cm and 30 cm depth. Under the plastic tunnel, air humidity and air temperature were measured by a resistive platinum thermometer and electrical capacitive hygrometer (HMP155, Vaisala Oyj, Helsinki, FI) at 1.5 m height. The tubers were planted on May 15, 2020, and the first leaves appeared on June 4, 2020, which was considered as the emergence (i.e. DAE of 0). Soil water availability was quantified by calculating the REW of the first soil horizon, where most of the root water uptake of potato is expected to occur (Beauclaire *et al.*, 2023b):

$$REW = \frac{\theta_{H1} - \theta_{wp,H1}}{\theta_{fc,H1} - \theta_{wp,H1}} \tag{5.1}$$

where $\theta_{wp,H1}$ = 15.6 and $\theta_{fc,H1}$ = 35.01 are respectively the wilting point and the field capacity of the first horizon (H_1: 0-30 cm) and θ_{H1} is the SWC measured in H1,

which was considered as the weighted mean of SWC measurements measured at 10 cm and 30 cm depth (with a weight of 2/3 and 1/3 respectively). $\theta_{wp,H1}$ and $\theta_{fc,H1}$ were estimated from soil water retention curves by using the VG model (van Genuchten, 1980). Soil samples were collected before the experiment at 15 cm depth (3 replicates) and were saturated for at least 24h in distilled water. The pressure plates method (Richards (1948) – by the ISO 11274 standard) was applied and the measurements of suction head and SWC were recorded. $\theta_{wp,H1}$ and $\theta_{fc,H1}$ were estimated as the SWC at a pF (log of the suction head) respectively of 4.2 and 2.0. VG model parameters and retention curves of the three soil samples are given in the supplementary material (Fig. 5.6).

Over a first period of 35 days, all the plants were hand-watered to ensure that θ_{H1} remained near field capacity. The drought treatment consisted in withholding irrigation to reproduce a long-term precipitation deficit on half of the plants. The other half was hand-watered during the experiment. The drought treatment started on DAE 40 (corresponding to the beginning of the tuber bulking stage) and stopped on DAE 74 (corresponding to the appearance of the first signs of senescence on the irrigated potato plants). All the plants have experienced the same PAR, temperature and VPD conditions under the plastic tunnel.

4.2. Leaf-level measurements

Gas exchange and chlorophyll fluorescence measurements were conducted during the tuber bulking stage at 14 different dates (between DAE 35 to DAE 74, Fig. 5.1) from 10 am to 4 pm. Only the youngest leaves in the upper part of the plant were selected by randomly sampling irrigated and non-irrigated plants. Measurements were performed by using a LI-COR LI-6400 equipped with a LI-6400-40 fluorescence chamber (LI-COR Inc., Lincoln, NE, USA). The following procedure was applied to each leaf sample. The CO_2 concentration in the chamber (C_s) was set to 400 μmolmol^{-1}, the PPFD in the PAR at 1200 μmolm^{-2}s^{-1} and the air humidity and temperature were maintained at ambient levels. After stabilization of the steady state fluorescence signal (F_s), a multiphase flash with a saturation light of 9 000 μmolm^{-2}s^{-1} was applied, and the maximum fluorescence intensity under the light (F'_m) was measured. In addition, A_{sat}, leaf temperature, stomatal conductance to water vapor (g_{sw}), CO_2 concentration in sub-stomatal cavities (C_i) and the vapor pressure deficit at the leaf surface (VPD_{leaf}) were recorded. Stomatal conductance to CO_2 (g_s) was determined by dividing g_{sw} by 1.6.

4.2.1. Non-stomatal limitations: V_{cmax} and g_m

V_{cmax} was determined by using a single measurement of gas exchanges at light saturation (Wilson *et al.*, 2000; De Kauwe *et al.*, 2016):

$$V_{cmax} = A_{sat}\frac{C_c + K_m}{C_c - \Gamma^*} \tag{5.2}$$

with K_m the Michaelis-Menten coefficient, Γ^* the CO_2 compensation point and C_c the CO_2 concentration in the chloroplast. Eq. 5.2 is based on a single measurement of CO_2 assimilation at light saturation instead of using CO_2-response curves where V_{cmax} retrieval is impacted by the sensitivity of the fitting method (Miao *et al.*, 2009). Moreover, the leaf respiration (R_d) was neglected, as it is much smaller compared to A_{sat} (Knauer *et al.*, 2018a; Von Caemmerer, 2013). K_m and Γ^* were estimated by using C3 plant-based temperature response curves (Bernacchi *et al.*, 2001). C_c was calculated by using the Fick law (Farquhar & Sharkey, 1982)x:

$$C_c = C_i - \frac{A_{sat}}{g_m} \tag{5.3}$$

where g_m is determined by using the "variable electron transport" method (Harley *et al.*, 1992):

$$g_m = \frac{A_{sat}}{C_i - \frac{\Gamma^*(J_F + 8A_{sat})}{J_F - 4A_{sat}}} \tag{5.4}$$

with J_F the electron transport rate estimated from PAR, leaf absorptance in the PAR (α) photochemical efficiency of PSII open centers ϕ_{PSII}, and the fraction of the absorbed PAR allocated to PSII (β) (Genty *et al.*, 1989; Valentini *et al.*, 1995):

$$J_F = \alpha\beta\phi_{PSII}PAR \tag{5.5}$$

In Eq. 5.5, ϕ_{PSII} was determined from $F_m^{'}$ and F_s (Kramer *et al.*, 2004):

$$\phi_{PSII} = \frac{F_m^{'} - F_s}{F_m^{'}} \tag{5.6}$$

and $\alpha\beta$ was determined from the linear relationship between ϕ_{PSII} and the apparent quantum efficiency of the linear electron transport ϕ_{e-} (Valentini *et al.*, 1995):

$$\alpha\beta = \frac{4}{k} \tag{5.7}$$

where 4 is the number of electrons needed per CO_2 molecule fixed and k the slope of the linear relationship between ϕ_{e-} and ϕ_{PSII}. Under non-photorespiratory conditions, ϕ_{e-} can be estimated by the apparent quantum efficiency of CO_2 uptake ϕ_{CO2}, which is obtained by dividing the measured CO_2 assimilation by the incident PPFD (Genty *et al.*, 1989). Non-photorespiratory conditions were set by adding pure N2

(1% O2) to the LI-COR LI-6400 chamber. The meteorological conditions were maintained at ambient levels and the incoming PPFD was set to the following values: 2000, 1500, 1200, 1000, 800, 600, 400, 200, 100 and 0 μmolm^{-2}s^{-1}. Gas exchanges and fluorescence intensities were measured for each PPFD value and ϕ_{CO2} was calculated as the ratio of net carbon assimilation to PAR. The slope of fitted linear relationship between ϕ_{e-} and ϕ_{CO2} (k) was used to determine $\alpha\beta$ using Eq. 5.7. These measurements were conducted on three leaf samples for irrigated and non-irrigated potato plants and were repeated three times during the drought treatment (i.e., DAE 42, 64 and 73).

4.2.2. Stomatal limitations: g_1

In the USO model, g_{sw} is a function of VPD_{leaf}, C_s and A_{sat} (Medlyn *et al.*, 2011a):

$$g_{sw} = 1.6\left(1 + \frac{g_1}{\sqrt{VPD_{leaf}}}\right)\frac{A_{sat}}{C_s} \tag{5.8}$$

where the minimum stomatal conductance is neglected under high irradiance (Medlyn *et al.*, 2017b), and g_1 is the stomatal sensitivity to photosynthesis, which is inversly related to the marginal WUE. g_1 can be determined by combining the Fick law describing the CO_2 diffusion through stomata with Eq. 5.8, which gives (Medlyn *et al.*, 2017b):

$$g_1 = \frac{\frac{C_i}{C_s}\sqrt{VPD_{leaf}}}{1 - \frac{C_i}{C_s}} \tag{5.9}$$

4.3. Statistical analysis

g_m was discarded when C_i was without the range 150-350 μmolmol^{-1}, which minimizes errors in R_d and Γ^*, and by extension in g_m (Harley *et al.*, 1992; Niinemets *et al.*, 2006; Veromann-Jürgenson *et al.*, 2017). Moreover, V_{cmax} and g_m were normalized at 25°C ($V_{cmax,25}$, $g_{m,25}$) by using an Arrhenius temperature response function parameterized on tobacco (Bernacchi *et al.*, 2001, 2002). Gas exchange and chlorophyll fluorescence-related variables (i.e., A_{sat}, g_s, $g_{m,25}$, g_1 and $V_{cmax,25}$) were averaged for each day of measurement and drought treatment (irrigated and non-irrigated), thus regrouping measurements performed under similar meteorological and edaphic conditions.

The response of A_{sat}, g_s, $g_{m,25}$, g_1 and $V_{cmax,25}$ to the decrease in REW was assessed by using a linear-plateau model which consists in a constant value (y_{max}) and a linear segment (with slope a and intercept b) on either sides of a threshold (REW_{th}). Such model has already been used to describe the response of SOL and NSOL to soil

water availability of potato crops at the ecosystem scale (Beauclaire *et al.*, 2023b), and is used to implement the response of LSMs parameters to drought (Vidale *et al.*, 2021). The statistical significance of the linear-plateau model was achieved by comparing its Akaike Information Criterion (AIC) corrected for low sample size (AICc, Burnham *et al.* (2011)) to the one of a higher parsimonious model (i.e., a linear model with one slope and intercept). The model with the lowest AICc was selected (Burnham *et al.*, 2011; Scoffoni *et al.*, 2012). Differences between models were considered as meaningful when their AICc differed by at least 7 (Burnham *et al.*, 2011). If the difference was less than 7, the segmented model was selected as such pattern has already been observed for potato (Beauclaire *et al.*, 2023b). Model performance was assessed by the R^2 and the standard deviation of fitted parameters. The linear-plateau regression was fitted using the "nlsm" function from the "nlraa" package in R Studio (Archontoulis & Miguez, 2015; Miguez, 2023; R Core Team, 2020). Statistical difference between REW_{th} parameters was tested by calculating the p-value of a t-test using the fitted values and their corresponding standard deviation (Clogg *et al.*, 1995; Paternoster *et al.*, 1998).

4.4. Limitation analysis

The first limitation scheme used in this study has been proposed by Jones (1985) where SOL were associated to a decrease in g_s either caused by a decrease in V_{cmax} or g_m. The relative variation of A_{sat} compared to its maximum value (dA_{sat}/A_{sat}) is written as the sum of the relative variations of g_s, g_m and V_{cmax} following (Grassi & Magnani, 2005; Jones, 1985):

$$\frac{dA_{sat}}{A_{sat}} = \frac{dg_s}{g_s} l_{gs} + \frac{dg_m}{g_m} l_{gm} + \frac{dV_{cmax}}{V_{cmax}} l_{Vcmax} = L_{gs} + L_{gm} + L_{Vcmax} \tag{5.10}$$

$$l_{gs} = \frac{\frac{g_t}{g_s}\frac{\delta A_{sat}}{\delta C_c}}{g_t + \frac{\delta A_{sat}}{\delta C_c}} \tag{5.11}$$

$$l_{gm} = \frac{\frac{g_t}{g_m}\frac{\delta A_{sat}}{\delta C_c}}{g_t + \frac{\delta A_{sat}}{\delta C_c}} \tag{5.12}$$

$$l_{Vcmax} = \frac{g_t}{g_t + \frac{\delta A_{sat}}{\delta C_c}} \tag{5.13}$$

where l_{gs}, l_{gm} and l_{Vcmax} are respectively the relative stomatal, mesophyll and biochemical limitations (corresponding to dimensionless quantity between 0 and 1 that gives the proportion of the total limitation) while L_{gs}, L_{gm} and L_{Vcmax} are the contributions of respectively the stomatal, mesophyll and biochemical limitations to the relative variation of A_{sat}. g_t is the total conductance to CO_2 ($(g_t)^{-1} = (g_s)^{-1} + (g_m)^{-1}$)

and $\delta A_{sat}/\delta C_c$ is the partial derivative of A_{sat} with respect to C_c using Eq. 5.2. In this study, Eq. 5.10 has been further normalized by dA_{sat}/A_{sat} to improve the interpretation of the data. The temporal dynamics of these relative variations can be explained solely by REW and VPD as the relationship to temperature has already been considered by normalizing V_{cmax} and g_m at 25°C, as well as the one to solar radiation by collecting the data at light saturation.

This approach has two drawbacks. First, the decrease in A_{sat} originating from stomatal closure through a decrease in g_s can be induced by g_m and V_{cmax}, which may result in the underestimation of the contribution of non-stomatal factors in limiting photosynthesis. Second, identifying the contribution of REW to the variation in L_{gs} is complex as VPD has varied during the experiment. To tackle these issues, we used g_1 instead of g_s as SOL which allows, first to separate the feedback effect of NSOL on stomatal conductance, and second to consider the effect of VPD on stomatal closure (Zhou *et al.*, 2013). As a result, Eq. 5.10 has been modified by calculating the total derivative of g_s using the USO model, which gives (derived in Text S1):

$$\frac{dA_{sat}}{A_{sat}} = \frac{dg_1}{g_1}\left(\frac{l_{gs}}{1-g_s}\frac{C_i}{C_s}\right) + \frac{dg_m}{g_m}\left(\frac{l_{gm}}{1-g_s}\right) + \frac{dV_{cmax}}{V_{cmax}}\left(\frac{l_{Vcmax}}{1-g_s}\right) - \frac{dVPD}{VPD}\left(\frac{1}{2}\frac{l_{gs}}{1-l_{gs}}\frac{C_i}{C_s}\right) \quad (5.14)$$

$$\frac{dA_{sat}}{A_{sat}} = \frac{dg_1}{g_1}l_{g1,USO} + \frac{dg_m}{g_m}l_{gm,USO} + \frac{dV_{cmax}}{V_{cmax}}l_{Vcmax,USO} + \frac{dVPD}{VPD}l_{VPD,USO} \quad (5.15)$$

$$\frac{dA_{sat}}{A_{sat}} = L_{g1,USO} + L_{gm,USO} + L_{Vcmax,USO} + L_{VPD,USO} \quad (5.16)$$

where $L_{g1,USO}$, $L_{gm,USO}$, $L_{Vcmax,USO}$ and $L_{VPD,USO}$ are the contributions of respectively the optimal stomatal, mesophyll, biochemical and VPD limitations to the relative variation of A_{sat} using the USO model of stomatal conductance. Eq. 5.14 shows that dA_{sat}/A_{sat} can be written as the sum of the relative variations of g_1, g_m, V_{cmax} and VPD. Combining Eq. 5.10 and Eq. 5.16 allows to identify the effect of g_m, V_{cmax}, g_1 and VPD on the contribution of stomatal closure to photosynthesis as follows:

$$L_{gs} = L_{gm,USO} - L_{gm} + L_{Vcmax,USO} - L_{Vcmax} + L_{VPD,USO} + L_{g1,USO} \quad (5.17)$$

$L_{gm,USO} - L_{gm} + L_{Vcmax,USO} - L_{Vcmax}$ is the effect of NSOL on stomatal closure while $L_{VPD,USO} + L_{g1,USO}$ is the effect of VPD and g_1 on stomatal closure according to the USO model. The relative variations in Eq. 5.15 and Eq. 5.10 are calculated from the difference between the value of the variable at a specific REW and the asymptote of the linear-plateau using $\frac{dy}{y} = \frac{y_{max}-y}{y_{max}-y_{min}}$ with y being the ordinate at a specific

REW value and y_{max} the plateau of the segmented regression. In a similar fashion, $dVPD/VPD$ is determined from the VPD-REW relationship. During precipitation shortage episodes, this relationship is decreasing (i.e., increase in VPD when REW decrease), which has been observed during the experiment for non-irrigated plants (Fig. 5.8). This relationship was confirmed by the data of the nearby eddy covariance station of Lonzée for similar edaphic proprieties (data not shown). Therefore, this linear relationship has been used to determine $dVPD/VPD$ at each REW value.

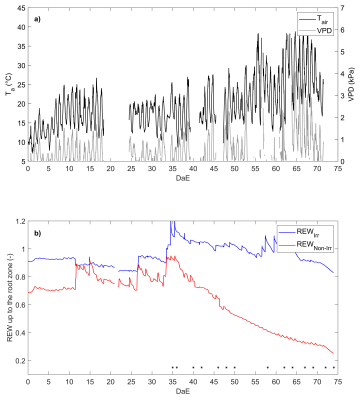

Figure 5.1: Temporal evolution of air temperature (T_a) and VPD under the plastic polytunnel greenhouse (panel a), and REW of the irrigated plot (REW_{irr}) and non-irrigated plot ($REW_{non-irr}$) (panel b). The asterisk indicates the days when leaf level measurements were conducted.

In Eq. 14, the ratio C_i/C_s also plays an important role in the limitation analysis as it directly influences $L_{g1,USO}$ and $L_{VPD,USO}$. Using g_1 as SOL implies that any stomatal constraint on A_{sat} should be associated to an increase of the ratio A_{sat}/g_s. Indeed, following the USO model framework, this constraint corresponds to a maximization of photosynthesis while minimizing water losses. As g_s and A_{sat} both regulate CO_2 diffusion through stomatal apertures and CO_2 fixation in the chloroplasts, the increase in A_{sat}/g_s is linked to a decrease in C_i/C_s illustrating an optimal stomatal control ($C_i/C_s \sim 1 - A_{sat}/g_s$). The relationship between C_i/C_s and REW was also evaluated by fitting a linear-plateau model as described in 2.4. Note that $L_{VPD,USO}$ is per essence negative because of the partial derivative of VPD with respect to A_{sat} as they are inversely related (i.e., VPD at the denominator in the USO model, Eq. 5.8). As a result, any increase in VPD induces a closure of stomata and a decrease in A_{sat}. For all the other terms of Eq. 16, a decrease in V_{cmax}, g_m or g_1 induces a decrease in A_{sat}.

5. Results

5.1. Meteorological and edaphic conditions

The decline in soil water availability was synchronized with a period of progressive increase in VPD and air temperature under the plastic polytunnel greenhouse (Fig. 5.1a) up to a maximum value of 4.10 kPa and 39.02 °C respectively (Fig. 5.1a) . Both irrigated and non-irrigated plants faced an increase in atmospheric dryness and air temperature. The REW of the non-irrigated plants decreased after stopping the

irrigation and reached 0.24 at the end of the experiment while the REW of the irrigated plants remained higher than 0.83 due to continuous hand watering (Fig. 5.1-b).

5.2. Effect of decreasing REW on the dynamics of gas-exchange and fluorescence traits

$\alpha\beta$ was not significantly different between irrigated and non-irrigated leaf samples at each DAE, and during the experiment (Fig. 5.7). Therefore, the mean of all $\alpha\beta_{PSII}$ values was used in Eq. 5.5 (i.e. $\alpha\beta_{PSII}$=0.73 $\pm$ 0.08). The linear-plateau model had the lowest AICc representing the dependence of $V_{cmax,25}$, g_1 and C_i/C_s on REW. For g_s, $g_{m,25}$ and A_{sat}, the difference between the AICc of the linear-plateau and the linear model was less than 5.67 (Table 5.3). These differences were not considered as evidence for selecting a model over another (Burnham *et al.*, 2011). Therefore, the segmented model was chosen for reproducing the response of A_{sat}, C_i/C_s, g_s, $g_{m,25}$ to REW (Fig. 5.2, Table 5.1). The REW threshold at which A_{sat}, g_s, $g_{m,25}$ started to decrease were higher than those of $V_{cmax,25}$, g_1 and C_i/C_s (Fig. 5.2, Table 5.1), which is confirmed by the p-values comparing these parameters (Table 5.2). Overall, CO_2 diffusion factors (i.e., $g_{m,25}$ and g_s) were the first variables to decrease with REW. Becauase of a non-significance difference, the REW thresholds for g_s and $g_{m,25}$ were averaged, corresponding to $REW_{th,gs,gm}$= 0.72 ± 0.12. Biochemical limitation ($V_{cmax,25}$) was only negatively impacted by severe soil water restrictions ($REW_{th,Vcmax}$= 0.43 $\pm$ 0.04). g_1 and C_i/C_s increased from a smaller REW threshold compared to $V_{cmax,25}$ ($REW_{th,g1,CiCs}$= 0.37 $\pm$ 0.02; Fig. 5.2, Table 5.1, Table 5.2).

	A_{sat} (µmol m^{-2} s^{-1})	$V_{cmax,25}$ (µmol m^{-2} s^{-1})	g_s (mol m^{-2} s^{-1})	$g_{m,25}$ (mol m^{-2} s^{-1})	g_1 (kPa$^{0.5}$)	C_i/C_s (-)
	$y = \begin{cases} y_{max}, & x > REW_{th} \\ ax + b, & x \leq REW_{th} \end{cases}$					
y_{max}(± SD)	18.74 ± 1.00	328.04 ± 14.85	0.10 ± 0.01	0.15 ± 0.01	1.39 ± 0.17	0.48 ± 0.02
a (± SD)	35.22 ± 8.38	1391.7 ± 494.5	0.18 ± 0.06	0.29 ± 0.11	-52.67 ± 9.83	-2.59 ± 1.12
b (± SD)	-6.73 ± 3.86	-268.4 ± 163.4	-0.03 ± 0.03	-0.06 ± 0.05	20.15 ± 3.06	1.43 ± 0.35
REW_{th} (± SD)	0.72 ± 0.08	0.43 ± 0.04	0.73 ± 0.12	0.72 ± 0.13	0.36 ± 0.01	0.37 ± 0.03
R^2	0.70	0.63	0.55	0.63	0.77	0.47

Table 5.1: Statistics of the linear-plateau regressions for the response of A_{sat}, $V_{cmax,25}$, g_s, $g_{m,25}$, g_1 and C_i/C_s to REW. Parameters are given with their standard deviation (SD).

5.3. Limitation analysis

The first limitation analysis scheme used in this study consists in partitioning photosynthesis limitations under high irradiance between L_{gm}, L_{Vcmax}, and L_{gs} (Jones, 1985). L_{gm} was always higher than L_{gs} above REW$\sim$0.28 where L_{gm} became pre-

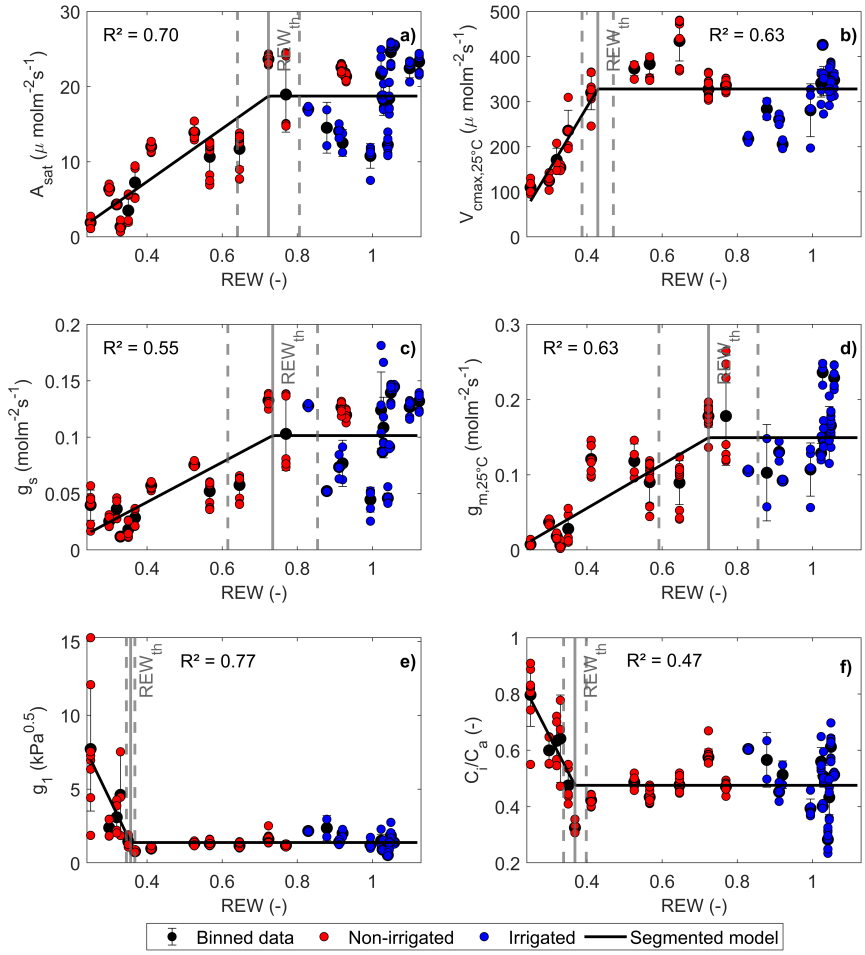

Figure 5.2: Response of A_{sat} (panel a), $V_{cmax,25}$ (panel b), g_s (panel c), $g_{m,25}$ (panel d), g_1 (panel e) and C_i/C_s (panel f) to relative extractable water (REW). Red and blue dots indicate respectively non-irrigated and irrigated potato plants. The fitted curve represents the linear-plateau regression $y = \begin{cases} y_{max}, & x > REW_{th}, \\ ax + b, & x \leq REW_{th} \end{cases}$. Binned data is shown with the corresponding standard deviation (SD). The grey vertical lines indicate $REW_{th} \pm$ SD.

dominent over L_{gs} (i.e., intersection of L_{gs} and L_{gm}, Fig. 5.3-b). When REW was minimum, 34% of the decrease in A_{sat} was explained by L_{gs}, 20% by L_{Vcmax} and 56% by L_{gm} (Fig. 5.3-a,b). This limitation scheme indicated that CO_2 diffusion factors (i.e., L_{gm} and L_{gs}) explained most of the decrease in A_{sat} with a similar contribution.

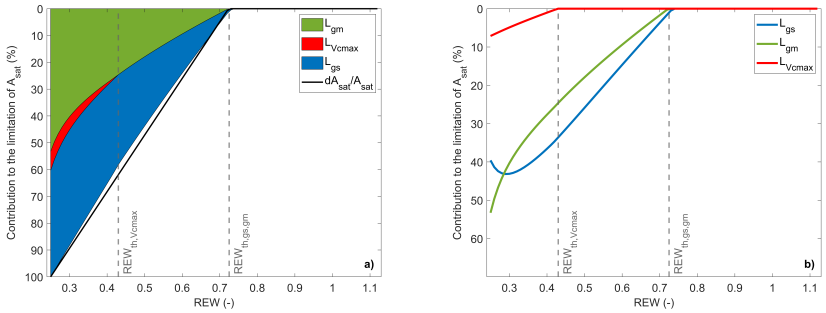

Figure 5.3: Partitioning of A_{sat} limitations between L_{gs}, L_{gm} and L_{Vcmax} in response to REW. Panel a) shows stacked limitation curves and panel b) shows unstacked limitation curves. The black line is the relative variation of A_{sat} compared to its maximum value (i.e., y_{max} of the segmented regression) and the grey vertical lines indicates REW_{th} ± SD.

However, using g_s, g_m, and V_{cmax} in the partitioning analysis does not allow to fully identify the origin of the early stomatal closure, as g_s itself can be influenced by V_{cmax} and g_m through A_{sat} (Eq. 5.8). This hypothesis is supported by the similar REW threshold for g_s and $g_{m,25}$, which suggests that the two variables are closely related. Combining Eq. 16 and Eq. 10 showed that the increase in L_{gs} is mostly caused by g_m and VPD especially under mild soil water conditions ($REW > REW_{th,CiCs}$, Fig. 5.4).In particular, $L_{gm,USO}$ was always higher than $L_{VPD,USO}$ and $L_{Vcmax,USO}$ (Fig. 5.4). Moreover, g_1 had a positive contribution to L_{gs} (Fig. 5.4), which indicates that the increase in g_1 (Fig. 5.2-e) promoted the opening of stomata to sustain CO_2 diffusion to the fixation sites. When implemented in the limitation analysis on A_{sat}, it can be shown that $L_{gm,USO}$was predominant over $L_{VPD,USO}$ regardless of soil water conditions (Fig. 5.5-a). When REW was minimum, 69% of the decrease in A_{sat} was explained by $L_{gm,USO}$, 31% by $L_{Vcmax,USO}$ and 20% by $L_{VPD,USO}$ (Fig. 5.5-a). In these conditions, $L_{g1,USO}$ was positive and reached 40%. The positive contribution of g_1 can be explained by the increase in

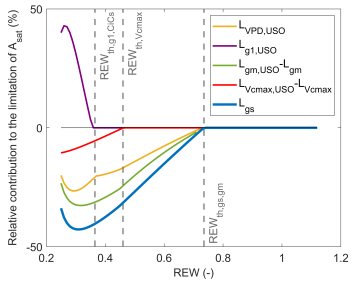

Figure 5.4: Partitioning of L_{gs} into $L_{g1,USO}$, $L_{gm,USO} - L_{gm}$, $L_{Vcmax,USO} - L_{Vcmax}$ and $L_{VPD,USO}$ in response to REW. The grey vertical lines indicatesREW_{th} ± SD.

dg_1/g_1 (Fig. 2-e), which resulted in an increase in $L_{g1,USO}$ (Eq. 15). Such increase in $L_{g1,USO}$ was observed from $REW_{th,g1,CiCs}$=0.37 $\pm$ 0.02 (Table 5.1, Table 5.2) which corresponded to low A_{sat} (6.8 μmol^{-2}s^{-1}) and g_s (0.04 mol^{-2}s^{-1}). Note that the sum of all curves in Fig. 5.5-b may not necessary equal 1 as the sum of limiting components when using the USO partitioning scheme did not exactly correspond to dA_{sat}/A_{sat} because of the uncertainties associated with the fitting of the linear-plateau segmented model on measurements (Fig. 5.2, Fig. 5.5-a).

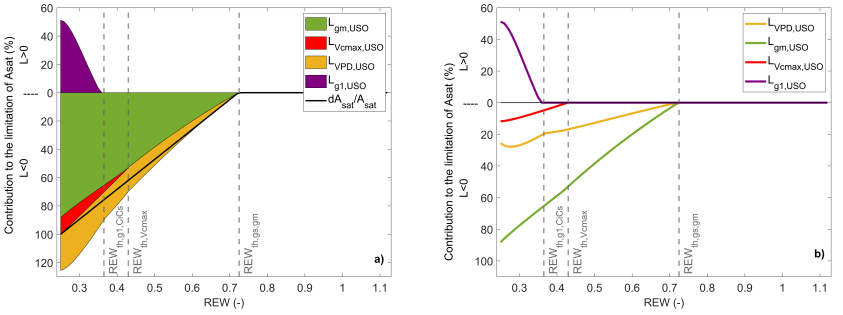

Figure 5.5: Partitioning of A_{sat} limitations between $L_{g1,USO}$, $L_{gm,SUO}$, $L_{Vcmax,USO}$ and $L_{VPD,USO}$ in response to REW. Panel a) shows stacked limitation curves and panel b) shows unstacked limitation curves. The black line is the relative variation of A_{sat} compared to its maximum value (i.e., y_{max} of the segmented regression) and the grey vertical lines indicates REW_{th} ± SD.

6. Discussion

The determination of thresholds of soil water availability impacting CO_2 assimilation is pivotal for calibrating the response of photosynthesis model parameters during drying-up episodes (Vidale *et al.*, 2021). The results of this study showed that soil water-limiting conditions induced a two-stage response of potato to water stress, with g_s and g_m being the first variables impacted by the decrease in REW followed by biochemical limitations through the decrease in V_{cmax} from a lower REW threshold. In addition, we used a new partitioning scheme where the total derivative of g_s was written as a function of its explanatory variables in the USO model (i.e., g_1, V_{cmax}, VPD and A_{sat}). This method allowed to quantify the origins of the decrease in A_{sat} in response to changes in g_m, V_{cmax}, g_1 and VPD. This partitioning was compared to the original formulation of photosynthesis limitations of Jones (1985) which attributed the origins of the reduction of A_{sat} to the relative variations of g_m, V_{cmax} and g_s. The comparison between the two schemes provides an estimation of the importance of the factors influencing g_s and A_{sat}.

6.1. Limitation on CO_2 diffusion as a major constraint of photosynthesis

Stomatal closure is a well-known mechanism of potato to reduce transpiration under water stress (Gerhards *et al.*, 2016; Gordon *et al.*, 1997; Obidiegwu, 2015; Romero *et al.*, 2017; Vos & Oyarz n, 1987). Stomatal closure dynamics are complex and can be directly caused by the evaporation of the water held by guard cells, or by the loss of turgor pressure induced by sensing of signaling molecules (Bharath *et al.*, 2021; Ding & Chaumont, 2020; Obidiegwu, 2015; Pirasteh-Anosheh *et al.*, 2016; Zhang *et al.*, 2022a).

These mechanisms seem to be synchronized with those influencing the mesophyll conductance as evidenced by a similar REW threshold for g_s and g_m (Fig. 5.2). In particular, mesophyll and stomatal conductance share similar responses to abscisic acid (Flexas *et al.*, 2012; Li *et al.*, 2021a; Sorrentino *et al.*, 2016), internal CO_2 concentration (Engineer *et al.*, 2016; Tan *et al.*, 2017) or starch-derived molecules (Lawson *et al.*, 2014), which leads to similar responses during water stress (Flexas *et al.*, 2004; Wang *et al.*, 2018a; Xiong *et al.*, 2018). L_{gm} became predominant over L_{gs} under severe water stress, which was associated to a very low g_m and a strong restriction of CO_2 diffusion to chloroplasts (Fig. 5.2, Fig 5.3). While this partitioning scheme indicated that photosynthesis limitations originated from g_s across most of the range of REW, it did not highlight the influence of non-stomatal factors on stomatal conductance. The origins of the decrease in g_s and A_{sat} can be identified by using the USO model equation in the limitation analysis. In particular, the USO partitioning scheme showed that most of stomatal closure dynamics can be attributed to a combined effect of g_m and VPD (Fig. 5.4). More specifically, $L_{gm,USO}$ was always higher than the other limiting components (Fig. 5.4-b) which highlights the strong control of mesophyll conductance on stomatal closure through its influence on A_{sat} regardless of REW values. These results confirm the importance of the mesophyll constraint is numerous species in many PFTs (Cano *et al.*, 2013; Flexas *et al.*, 2009; Galmés *et al.*, 2007; Grassi & Magnani, 2005; Limousin *et al.*, 2010; Perez-Martin *et al.*, 2014; Wang *et al.*, 2018b; Zait & Schwartz, 2018; Zhu *et al.*, 2021), and emphasize the importance of including the effect of REW on g_m in LSMs (Knauer *et al.*, 2020). This study also provides a calibration of the water stress factor for potato and contributes to reducing the uncertainties when estimating carbon assimilation and transpiration under water stress (Vidale *et al.*, 2021).

p-value REW_{th}	A_{sat}	$V_{cmax,25}$	g_s	$g_{m,25}$	g_1	C_i/C_s
A_{sat}	-					
$V_{cmax,25}$	0.000^{***}	-				
g_s	0.89^{ns}	0.000^{***}	-			
$g_{m,25}$	0.99^{ns}	0.000^{***}	0.92^{ns}	-		
g_1	0.00^{***}	0.000^{***}	0.000^{***}	0.000^{***}	-	
C_i/C_s	0.00^{***}	0.000^{***}	0.000^{***}	0.000^{***}	0.5^{ns}	-

Table 5.2: p-value of the t-test comparing REW_{th} between A_{sat}, $V_{cmax,25}$, g_s, $g_{m,25}$, g_1 and C_i/C_s.*** indicates when the p-value is <0.001, ** : <0.01, * : <0.05 and ns : >0.05

Additional information on the description of the physiological effects of mesophyll on stomatal closure can be found in (Lemonnier & Lawson, 2023). Since disentangling the primary metabolisms which synchronously control photosynthesis, stomatal and mesophyll conductance remains challenging, future studies would benefit from additional molecular or anatomical measurements to unravel the interplays between stomatal and non-stomatal factors (Gago *et al.*, 2020).

6.2. Severe restrictions in REW change the relationship between photosynthesis and stomatal conductance

Severe restrictions in soil water availability induced a decrease in V_{cmax} as well as an increase in g_1 and C_i/C_s (Fig. 5.2). An increase in C_i/C_s can be observed under strong limitations in CO_2 diffusion and decreasing photosynthetic activity (Bermúdez-Cardona *et al.*, 2015; Brodribb, 1996; Huang, 2020; Tan *et al.*, 2017). In particular, C_i/C_s increased when g_s was lower than 0.04 molm^{-2} s^{-1}, which was already reported as a stomatal conductance threshold for such C_i-inflexion point in various species (Blankenagel *et al.*, 2018; Brodribb, 1996; Flexas & Medrano, 2002; Martin & Ruiz-Torres, 1992; Rouhi *et al.*, 2007) including potato (Ramírez *et al.*, 2016). In these conditions of photosynthesis inhibition, the excess of energy carried by sun irradiance must be metabolized by alternative processes such as the xanthophyll (Demmig-Adams *et al.*, 2012), lutein (García-Plazaola *et al.*, 2003) and photorespiratory cycles (Osmond *et al.*, 1980). This latter may contribute to the increase in C_i/C_s by emitting CO_2 through the glycine decarboxylase enzyme which is not totally fixed by Rubisco (Busch *et al.*, 2017; Shi & Bloom, 2021).

The increase in g_1 induced an increase in dg_1/g_1 andL_{g1} when $REW < REW_{th,g1,CiCs}$ (Fig. 5.2, Fig. 5.4-a,b). g_1 is inversely related to the marginal carbon cost of water, which corresponds to the change in carbon gained per unit of water transpired, also known as marginal WUE (Medlyn *et al.*, 2011a). The increase in g_1 can be explained either by: (1) an increase in transpiration per unit of carbon gained by photosynthesis, or (2) a decrease in photosynthesis per unit of water transpired (Medlyn *et al.*, 2011a). For example, increasing stomatal conductance to promote transpiration may help in cooling down leaves surface during heatwaves at the expanse of increasing mortality risks through hydraulic vulnerability and cavitation (Marchin *et al.*, 2022; Urban *et al.*, 2017b). Numerous studies have highlighted such cooling effect on potato (Sprenger *et al.*, 2016; Zhang *et al.*, 2022b), which can ultimately lead to an increase in g_1 (Marchin *et al.*, 2023). A decoupling between stomatal conductance and photosynthesis may be the consequence of an adaptive strategy (i.e., sacrificing water for leaf survival and future carbon gains), or the increasing viscosity of water at high temperatures which facilitates the transport of water in the vascular system (Marchin *et al.*, 2023). In our experiment, the lowest measurement of g_s was 0.011 molm^{-2}s^{-1}, which is higher than the reported value of minimum stomatal conductance for CO_2 transfer

across plant species (i.e., g_s = 0.008 molm^{-2}s^{-1}, Duursma *et al.* (2019)) and suggests that stomata might not be fully closed. It is however unlikely that potato plants had access to water to sustain transpiration through stomata or cuticle because of the low REW values that were observed in these conditions (Fig. 5.2). Alternatively, the increase in g_1 may be caused by a decrease in photosynthesis through the additional effect of NSOL on A_{sat} (Beauclaire *et al.*, 2023b; Gourlez de la Motte *et al.*, 2020), which intensifies the decoupling between carbon assimilation and stomatal conductance by decreasing WUE (Manzoni *et al.*, 2011). This hypothesis is supported by previous studies which have shown that irrigation enhances WUE for potato (Akkamis & Caliskan, 2023; Ati *et al.*, 2012).

The increase in g_1 induced a positive contribution to dA_{sat}/A_{sat} (Fig. 5.5), suggesting that potato plants promoted the loss of water to the benefit of CO_2 diffusion despite the risks for the hydraulic system and carbon apparatus when photosynthesis reached critical levels (Deva *et al.*, 2020; Reynolds-Henne *et al.*, 2010). However, this behavior contradicts with the optimality theory, which assumes that the curvature of photosynthesis versus transpiration is negative (Buckley *et al.*, 2017). this hypothesis is challenged when mesophyll conductance strongly constrains CO_2 diffusion, resulting in an increasing sensitivity of photosynthesis to changes in g_m compared to g_s (Cowan & Farquhar, 1977). Therefore, low REW may induce a violation of the optimality theory which can be evidenced by an increase in g_1 (Buckley *et al.*, 2017; Zenes *et al.*, 2020).

6.3. Methodological considerations

g_m was determined by the 'variable J' method (Harley *et al.*, 1992) which is sensitive to variation in R_d and Γ^*. These two variables can be impacted by drought and heat, which was not considered in the method part. First, it has been shown that R_d can increase under water stress due to the additional release of CO_2 from mitochondria by the photorespiratory cycle (Busch *et al.*, 2017; Pinheiro & Chaves, 2011; Schmiege *et al.*, 2023). Second, the sensitivity of Γ^* to temperature can change under critical levels (usually above 30°C, Walker *et al.* (2017)), invalidating the Bernacchi *et al.* (2001) parameterization on leaf temperature. Measuring the CO_2 compensation point (Walker & Ort, 2015) and leaf respiration (Yin & Amthor, 2024) under drought could help resolving these uncertainties.

Lastly, the diffusion of water vapor through cuticle and epidermis may become significant compared to stomatal diffusion under water stress (Boyer, 2015a,b; Boyer *et al.*, 1997). As the transpiration flux measured by gas exchange measurement systems correspond to the sum of the diffusion through stomatal and cuticle conductance, strong overestimations of C_i can occur as the Fick law considers an identical gas phase path for CO_2 and H_2O. Direct measurements of C_i by a modified gas exchange (BOYER & KAWAMITSU, 2011) or a modification of the Fick law by quantifying the

cuticle conductance (Wang *et al.*, 2018b) could increase the accuracy of C_i estimates under water stress.

7. Acknowledgements and fundings

This study was conducted with the support of the CAREs EnvironmentIsLife and AgricultureIsLife of Gembloux Agro-Bio Tech, ULiege, Belgium. The researchers were funded by the Federation Wallonie Bruxelles (FWB).

8. Supplementary materials

8.1. Mathematical development of the partitioning scheme using the USO and FvCB models

The mathematical development of the limitation analysis using the USO model (Medlyn *et al.*, 2011a) and the FvCB model (Farquhar *et al.*, 1980) can be demonstrated by starting from the equation describing the limitation of carbon assimilation under high irradiance (A_{sat}) by Rubisco as:

$$A_{sat} = V_{cmax} \frac{C_c - \Gamma^*}{C_c + K_m} \tag{5.18}$$

where V_{cmax} is the maximum carboxylation rate of Rubisco, C_c the CO_2 concentration in the chloroplast, Γ^* the CO_2 compensation point, K_m the Michaelis-Menten coefficient of Rubisco kinetics and R_d is the leaf respiration. At 25°C (i.e., no effects of temperature on model parameters) and neglecting leaf respiration variations, the total derivative of A_{sat} is:

$$dA_{sat} = \frac{\delta A_{sat}}{\delta V_{cmax}} dV_{cmax} + \frac{\delta A_{sat}}{\delta C_c} dC_c \tag{5.19}$$

with $\frac{\delta A_{sat}}{\delta V_{cmax}} = \frac{A_{sat}}{V_{cmax}}$ and $\frac{\delta A_{sat}}{\delta C_c} = V_{cmax} \frac{K_m + \Gamma^*}{(C_c + K_m)^2}$. The total derivative of C_c can be determined using the Fick's law (Farquhar & Sharkey, 1982) as:

$$C_c = c_s - \frac{A_{sat}}{g_s} - \frac{A_{sat}}{g_m} \tag{5.20}$$

with C_s the CO_2 concentration at the leaf surface, g_s and g_m the stomatal and mesophyll conductance to CO_2 transfer. When the dependance of g_s to VPD, CO_2 concentration and carbon assimilation is not considered (i.e., the USO model not implemented in the limitation analysis), the total derivative of C_c is:

$$dC_c = \frac{\delta C_c}{\delta A_{sat}} dA_{sat} + \frac{\delta C_c}{\delta g_s} dg_s + \frac{\delta C_c}{\delta g_m} dg_m \tag{5.21}$$

$$dC_c = \left(-\frac{1}{g_m} - \frac{1}{g_s} \right) dA_{sat} + \frac{A_{sat}}{(g_s)^2} dg_s + \frac{A_{sat}}{(g_m)^2} dg_m \tag{5.22}$$

Combining Eq. 5.22 and Eq. 5.19 gives:

$$dA_{sat} = \frac{A_{sat}}{V_{cmax}} dV_{cmax} + \frac{\delta A_{sat}}{\delta C_c} \left[\left(-\frac{1}{g_m} - \frac{1}{g_s} \right) dA_{sat} + \frac{A_{sat}}{(g_s)^2} dg_s + \frac{A_{sat}}{(g_m)^2} dg_m \right] \tag{5.23}$$

Simplifying Eq. 5.23 and writing dA_{sat} on the left-hand side gives:

$$dA_{sat} + \frac{\delta A_{sat}}{\delta C_c} \left(\frac{1}{g_m} + \frac{1}{g_s} \right) dA_{sat} = \frac{A_{sat}}{V_{cmax}} dV_{cmax} + \frac{\delta A_{sat}}{\delta C_c} \frac{A_{sat}}{(g_s)^2} dg_s + \frac{\delta A_{sat}}{\delta C_c} \frac{A_{sat}}{(g_m)^2} dg_m \tag{5.24}$$

$$dA_{sat} = \frac{A_{sat} \dfrac{dV_{cmax}}{V_{cmax}}}{1 + \dfrac{\delta A_{sat}}{\delta C_c} \left(\dfrac{1}{g_s} + \dfrac{1}{g_m} \right)} + \frac{\dfrac{\delta A_{sat}}{\delta C_c} \dfrac{dA_{sat}}{g_s} \dfrac{dg_s}{g_s}}{1 + \dfrac{\delta A_{sat}}{\delta C_c} \left(\dfrac{1}{g_s} + \dfrac{1}{g_m} \right)} + \frac{\dfrac{\delta A_{sat}}{\delta C_c} \dfrac{dA_{sat}}{g_m} \dfrac{dg_m}{g_m}}{1 + \dfrac{\delta A_{sat}}{\delta C_c} \left(\dfrac{1}{g_s} + \dfrac{1}{g_m} \right)} \tag{5.25}$$

Finally, simplifying Eq. 5.25 in terms of relative changes in A_{sat} and implementing the total conductance to CO_2 transfer $g_t = ((g_s)^{-1} + (g_m)^{-1})^{-1}$ gives:

$$\frac{dA_{sat}}{A_{sat}} = \frac{g_t \dfrac{dV_{cmax}}{V_{cmax}}}{g_t + \dfrac{\delta A_{sat}}{\delta C_c}} + \frac{\dfrac{g_t}{g_s} \dfrac{dg_s}{g_s} \dfrac{\delta A_{sat}}{\delta C_c}}{g_t + \dfrac{\delta A_{sat}}{\delta C_c}} + \frac{\dfrac{g_t}{g_m} \dfrac{dg_m}{g_m} \dfrac{\delta A_{sat}}{\delta C_c}}{g_t + \dfrac{\delta A_{sat}}{\delta C_c}} \tag{5.26}$$

$$\frac{dA_{sat}}{A_{sat}} = \frac{dg_s}{g_s} l_{gs} + \frac{dg_m}{g_m} l_{gm} + \frac{dV_{cmax}}{V_{cmax}} l_{Vcmax} = L_{gs} + L_{gm} + L_{Vcmax} \tag{5.27}$$

with:

$$l_{gs} = \frac{\dfrac{g_t}{g_s} \dfrac{\delta A_{sat}}{\delta C_c}}{g_t + \dfrac{\delta A_{sat}}{\delta C_c}} \tag{5.28}$$

$$l_{gm} = \frac{\dfrac{g_t}{g_m} \dfrac{\delta A_{sat}}{\delta C_c}}{g_t + \dfrac{\delta A_{sat}}{\delta C_c}} \tag{5.29}$$

$$l_{Vcmax} = \frac{g_t}{g_t + \frac{\delta A_{sat}}{\delta C_c}} \tag{5.30}$$

where L is the limitation component and l the relative limitation component. Eq. 5.27 is the limitation analysis scheme described in Grassi & Magnani (2005).

The second partitioning scheme considered in this study is obtained by implementing the USO model (Eq. 5.31) for calculating the total derivative of g_s (dg_s, Eq. 5.27) as:

$$g_s = \left(1 + \frac{g_1}{\sqrt{VPD}}\right)\frac{A_{sat}}{C_s} \tag{5.31}$$

$$dg_s = \frac{\delta g_s}{\delta g_1}dg_1 + \frac{\delta g_s}{\delta A_{sat}}dA_{sat} + \frac{\delta g_s}{\delta VPD}dVPD + \frac{\delta g_s}{\delta C_s}dC_s \tag{5.32}$$

Calculating the partial derivatives of each term and considering C_s as constant gives:

$$dg_s = \frac{A_{sat}}{C_s\sqrt{VPD}}dg_1 + \frac{\left(1 + \frac{g_1}{\sqrt{VPD}}\right)}{C_s}dA_{sat} - \frac{1}{2}\frac{A_{sat}g_1}{C_s VPD^{3/2}}\frac{dVPD}{VPD} \tag{5.33}$$

Writing Eq. 5.33 in terms of relative changes in g_s gives:

$$\frac{dg_s}{g_s} = \frac{g_1}{g_1 + \sqrt{VPD}}\frac{dg_1}{g_1} + \frac{dA_{sat}}{A_{sat}} - \frac{1}{2}\left(\frac{g_1}{g_1 + \sqrt{VPD}}\right)\frac{dVPD}{VPD} \tag{5.34}$$

Eq. 5.34 gives the relative variation of g_s with respect to the relative variations of g_1, A_{sat} and VPD. Moreover, it can be shown that $\frac{g_1}{g_1+\sqrt{VPD}} = \frac{C_i}{C_s}$:

$$\frac{C_i}{C_s} = 1 - \frac{\sqrt{VPD}}{\sqrt{VPD} + g_1} = \frac{g_1}{g_1 + \sqrt{VPD}} \tag{5.35}$$

which gives, after combining Eq. 5.34 into Eq. 5.35:

$$\frac{dg_s}{g_s} = \frac{C_i}{C_s}\frac{dg_1}{g_1} + \frac{dA_{sat}}{A_{sat}} - \frac{1}{2}\frac{C_i}{C_s}\frac{dVPD}{VPD} \tag{5.36}$$

Finally, combining Eq. 5.36 and Eq. 5.27 gives after simplification:

$$\frac{dA_{sat}}{A_{sat}} = \frac{dg_1}{g_1}\left(\frac{l_{gs}}{1-l_{gs}}\frac{C_i}{C_s}\right) + \frac{dg_m}{g_m}\left(\frac{l_{gm}}{1-l_{gs}}\right) + \frac{dV_{cmax}}{V_{cmax}}\left(\frac{l_{Vcmax}}{1-l_{gs}}\right) - \left(\frac{1}{2}\frac{l_{gs}}{1-l_{gs}}\frac{C_i}{C_s}\right)\frac{dVPD}{VPD} \tag{5.37}$$

$$\frac{dA_{sat}}{A_{sat}} = \frac{dg_1}{g_1} l_{g1,USO} + \frac{dg_m}{g_m} l_{gm,USO} + \frac{dV_{cmax}}{V_{cmax}} l_{Vcmax,USO} + \frac{dVPD}{VPD} l_{VPD,USO} \quad (5.38)$$

$$\frac{dA_{sat}}{A_{sat}} = L_{g1,USO} + L_{gm,USO} + L_{Vcmax,USO} + L_{VPD,USO} \quad (5.39)$$

Eq. 5.38 and Eq. 5.38 link the relative variation of A_{sat} to the relative variations of VPD, g_1, g_m and V_{cmax} (Farquhar *et al.*, 1980; Medlyn *et al.*, 2011a).

8.2. Figures and tables

ΔAICc= AICc-min(AICc)	ΔAICc Linear model	ΔAICc Segmented model
A_{sat}	0	-3.36
$V_{cmax,25}$	-7.45	0
g_s	0	4.72
$g_{m,25}$	0	5.67
g_1	23	0
C_i/C_s	6.22	0

Table 5.3: Akaike information criterion corrected for small sample size (AICc) of the linear and linear-plateau models describing the response of A_{sat}, $V_{cmax,25}$, g_s, $g_{m,25}$, g_1 and C_i/C_s to REW. ΔAICc is the difference between the lowest AICc and the linear or segmented model for each variable.

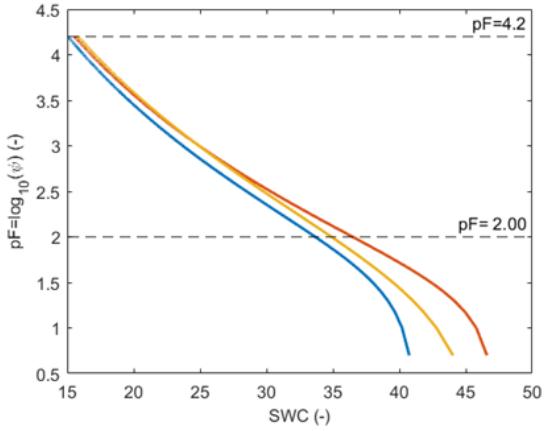

Figure 5.6: SWRC of the three soil samples collected at 15 cm depth. The field capacity and wilting point were calculated as the average values of soil water content SWC at a pF (log(ψ), with ψ the suction head) of respectively 2 and 4.2. SWRC were obtained from the van Genuchten model (van Genuchten, 1980) : $SWC = SWC_r + \frac{SWC_r - SWC_s}{|1 + (\alpha|\psi|^n|)^m|}$ with SWC_r the residual SWC, SWC_s the saturated SWC, ψ the suction head, α related to the inverse of the air entry suction, n and m are empirical parameters. The parameters of the three SWRC are SWC_s=0.412, SWC_r=0, α=0.028, n=1.27, m=0.13 (blue curve), SWC_s=0.471, SWC_r=0, α=0.04, n=1.45, m=0.118 (orange curve), and SWC_s=0.460, SWC_r=0, α=0.037, n=0.84, m=0.20 (yellow curve).

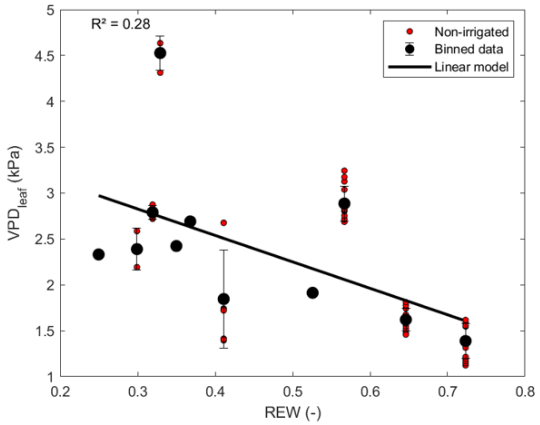

Figure 5.7: Relationship between VPD at the leaf surface (VPD_{leaf}) and REW for non-irrigated plants

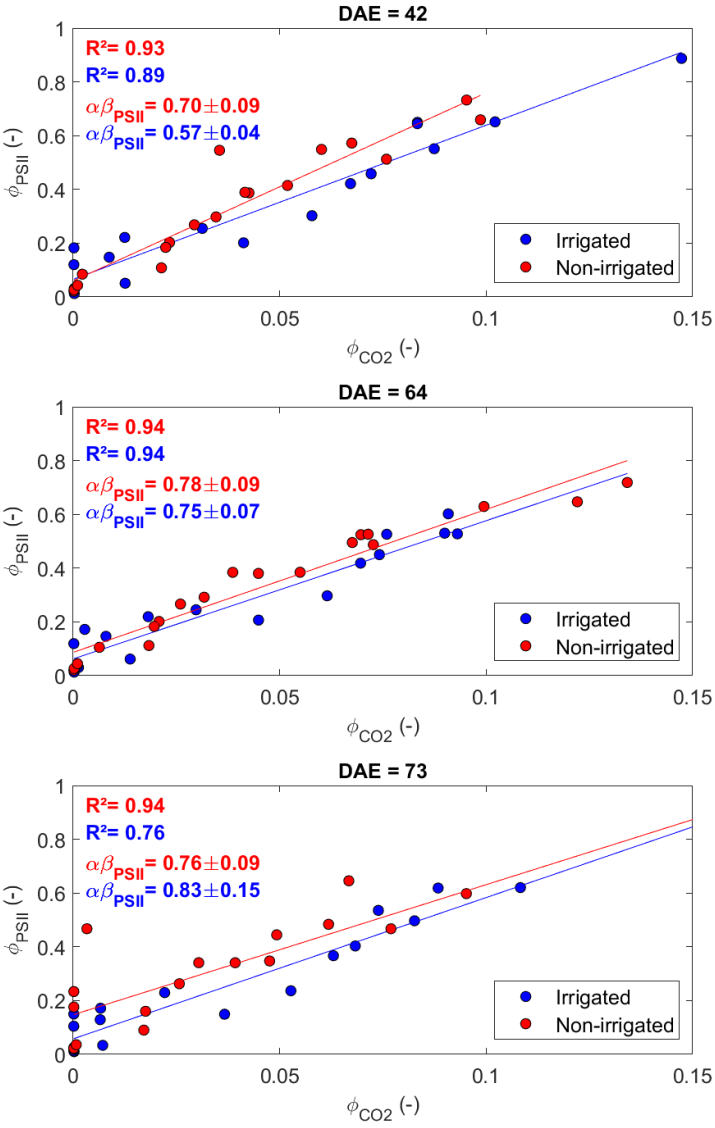

Figure 5.8: Relationship between the fluorescence quantum yield of PSII (ϕ_{PSII}) and the apparent quantum yield of CO_2 assimilation (ϕ_{CO2}) for three different DAE during the drought experiment. For each DAE, a linear regression ($\phi_{PSII} = k\phi_{CO2} + k'$) was fitted for irrigated (blue) and non-irrigated (red) data and the product of leaf absorptance to the fraction of the absorbed PAR allocated to PSII ($\alpha\ \beta_{PSII}$) was calculated as $4/k$.

6

Modeling gross primary production and transpiration from sun-induced chlorophyll fluorescence using a mechanistic light-response approach

This paper has been published as:

Beauclaire, Q., De Cannière, S., Jonard, F., Delhez, L., Pezzetti, N., Longdoz, B., 2024. Modeling gross primary production and transpiration from sun-induced chlorophyll fluorescence using a mechanistic light-response approach. Remote Sensing of Environment .
https://doi.org/10.1016/j.rse.2024.114150

1. Personal contributions

The installation of the spectrometer has been carried out by the technical team of the Lonzée ICOS station, namely Henri Chopin and Gaëtan Bogaerts. The Ecosystem Thematic Centre (ETC) performed the data processing and quality control of the EC site of Lonzée. The EC data is available on the ICOS Carbon Portal (see references in the paper below). Leaf-level measurements were collected by myself with the help of Natacha Pezzetti during her master thesis. Root biomass measurements were collected by Laura Delhez. The spectrometer was provided by the Forschungszentrum Jülich and Simon De Cannière, who also participated to the installation of the sensor. SIF data processing and quality control were performed by myself. The manuscript was reviewed by Bernard Longdoz, who also actively participated to the thesis by helping in setting the sensor installation and interpreting the results. Simon De Cannière and François Jonard helped in interpreting SIF data, discussing the results and reviewing the manuscript. Natacha Pezzetti and Laura Delhez reviewed the manuscript.

2. Abstract

SIF is a promising optical remote sensing signal which is directly linked to photosynthesis, allowing for the monitoring of GPP. Although empirical relationships between these variables have demonstrated the potential of SIF for site-specific GPP estimations, a better physiological understanding of the link between SIF and GPP would pave the way for a more robust model of photosynthesis. The MLR model is a novel approach which determines GPP from SIF by using only a small set of equations and parameters with physiological significance. This study combines the MLR model with the USO model to estimate both GPP and Tr at the ecosystem scale. Top-of-canopy SIF measurements were collected over a winter crop with a field spectrometer installed next to an eddy covariance station. MLR-USO model parameters were determined from gas exchange and active chlorophyll fluorescence measurements at the leaf level and interpolated on a half-hourly basis using solar irradiance and canopy temperature. GPP and Tr estimated by the MLR-USO model and eddy covariance measurements were highly correlated at half-hourly and daily timescales ($R^2 \geq 0.91$, rRMSE$\leq$13.7 %) under a wide range of environmental conditions, including soil water stress. These results highlight the potential of the MLR-USO model as an important step towards

an improvement of our understanding of the coupling between the water and carbon cycles at the ecosystem scale and beyond.

3. Introduction

Each year, terrestrial ecosystems uptake approximately one-third of the carbon emitted by human activities (Friedlingstein *et al.*, 2022). GPP of terrestrial ecosystems represents the most important flux in the global carbon cycle (Beer *et al.*, 2010) and plays a central role in regulating atmospheric CO_2 concentration (Sha *et al.*, 2022).

Anthropogenic climate change increases the occurrence of climate extremes such as droughts or heatwaves, which causes a reduction in GPP (Williams *et al.*, 2014; Reichstein *et al.*, 2013). Whether terrestrial ecosystems will keep removing as much CO_2 from the atmosphere or become CO_2 sources is highly uncertain as most LSMs predict various future ecosystem uptake abilities in a climate change context (Ryu *et al.*, 2019). Quantifying and modeling GPP at global scales is therefore crucial to better understand how climate extremes constrain primary production in climate modeling.

GPP is the total amount of carbon fixed by ecosystems and originates from complex photosynthetic processes that cannot be directly measured. The standard approach for estimating GPP at the ecosystem scale is the measurement of the NEE with the eddy covariance (EC) technique, and its partitioning between ecosystem respiration (R_{ECO}) and GPP. More than 200 EC sites are currently part of the FLUXNET network, which regroups over 1500 site-years of data (Baldocchi, 2014; Pastorello *et al.*, 2020). However, flux towers are unevenly distributed across the globe, which explains that the temporal and spatial representativeness of flux measurements (the extrapolation of flux information to extended spatial and timescales) has become an increasingly important issue for the scientific community to provide flux information "everywhere and all the time" (Chu *et al.*, 2017, 2021). In addition, the size and shape of flux tower footprints (the source areas of EC fluxes) are directly affected by meteorological variables (such as wind direction or air turbulence) and surface roughness, which complicates the interpretation of GPP from local to global scales (Kong *et al.*, 2022). Most of the recent approaches for upscaling carbon assimilation to large scales use machine learning to build empirical models between remote sensing (RS) data and ground observations of GPP (Jung *et al.*, 2020)).

Photosynthesis is a complex chain of photochemical and enzymatical reactions, which are commonly categorized between the light reactions (which generate ATP and NADPH from light and water) and the dark reactions (which transform CO_2 into carbohydrates using ATP and NADPH). SIF originates from the emission of photons in the red and far-red regions, after the absorption of a fraction of PAR by chlorophyll a pigments during the light reactions of photosynthesis. Although SIF quantum yield is very low (1 to 2 %; Maxwell & Johnson (2000)) compared to PQ and thermal energy dissipa-

tion (i.e., NPQ), it is tightly coupled to GPP as these three processes are in competition for PAR. In particular, SIF is linked to the electron transport rate which fuels ATP and NADPH to the fixation sites in the chloroplasts (Gu *et al.*, 2019). While the relationship between SIF and PQ quantum yields at the leaf level is highly nonlinear on short timescales (Porcar-Castell *et al.*, 2014), large temporal and spatial scales data show a strong linearity between SIF and carbon assimilation (Lee *et al.*, 2015; Damm *et al.*, 2010; Li *et al.*, 2018b; Chen *et al.*, 2019a). Such relationship has been the basis of the calibration of empirical models between ground-based GPP and remotely sensed SIF for estimating GPP at global scale using the LUE approach (Porcar-Castell *et al.*, 2014; Jonard *et al.*, 2020; Li *et al.*, 2018b; Xiao *et al.*, 2019). However, this concept does not allow to identify the actual mechanistic link between SIF and GPP, and there is a lack of knowledge about the influence of physiological and environmental factors on these relationships. A decoupling between SIF and GPP can be observed during stress episodes such as heatwaves (Wohlfahrt *et al.*, 2018; Martini *et al.*, 2022), drought (Helm *et al.*, 2020; Marrs *et al.*, 2020; Chen *et al.*, 2021), light-limiting conditions (Chen *et al.*, 2019a), or for heterogeneous canopies (van der Tol *et al.*, 2009; Gu *et al.*, 2019). These examples illustrate the limits of using this approach across spatial scales and climate conditions.

A model must consider two aspects to estimate GPP from SIF with a mechanistic approach. First, the relationship between fluorescence and photochemistry must be characterized at the photosystem level. Second, the scattering and absorption effects of overlying leaves should be considered when the fluorescence photons travel through the canopy (Yang *et al.*, 2019). The Soil Canopy Observation, Photochemistry and Energy fluxes (SCOPE) model (van der Tol *et al.*, 2009) integrates both the physiological and the canopy structural aspects of the SIF emission in separate sub-models. These aspects are highly dynamic and change in function of the plant water status (De Cannière *et al.*, 2022; Wang *et al.*, 2022). Although the SCOPE model is often used in a reduced form when coupled to other models, it is computationally intensive and requires numerous parameters, forcing the user to make a series of assumptions (e.g., Lee *et al.* (2015); De Cannière *et al.* (2021)).

An alternative approach to link SIF and GPP is the MLR model (Gu *et al.*, 2019). While the SCOPE model uses sub-models to integrate the physiological and structural aspects of SIF emission, the MLR model only considers few parameters which describe the energy partitioning at the PSII level (e.g., the fraction of open PSII center q_L and the maximum photochemical quantum yield $\phi_{PSII,max}$) and leaf-to-canopy radiative transfer processes (i.e., the escape probability factor f_{esc}) to determine the actual electron transport rate between the two photosystems (PSII and PSI). This mechanistic representation of the light reactions contrasts with the FvCB model of photosynthesis (Farquhar *et al.*, 1980) where the potential electron transport rate is determined from PAR by an empirical relationship. The FvCB model requires numerous parameters that are highly variable across PFT and environmental conditions; such uncertainty

causes important disagreements in LSMs which use the FvCB model to estimate carbon assimilation (Walker *et al.*, 2021; Rogers *et al.*, 2017). By taking advantage of the physiological information carried by SIF, MLR model equations mechanistically describe photosynthetic processes while reducing the impact of parameter uncertainty (Han *et al.*, 2022b; Gu *et al.*, 2019). With this approach, GPP can be estimated from electron requirements for carboxylation and oxygenation regardless of carboxylation limiting stages (Gu *et al.*, 2019).

Stomatal opening controls both water and carbon exchanges at the leaf surface. Through stomatal regulation, plants balance water loss and carbon uptake (Cowan & Farquhar, 1977), leading to a close coupling between GPP and Tr. Recent models simulating stomatal behavior such as the USO model (Medlyn *et al.*, 2011a) are based on the optimization of the ratio between benefit (i.e., carbon gain) and cost (i.e., water loss) of stomatal opening and on environmental variables such as VPD, GPP and CO_2 concentration at the leaf surface. Coupling the MLR and USO models (MLR- USO) provides a new, process-based approach for the modeling of carbon and water fluxes from SIF.

SIF can be retrieved by high-resolution measurements of vegetation spectral proprieties from sensons on masts; aircrafts or satellites (Mohammed *et al.*, 2019; Jonard *et al.*, 2020). For instance, spaceborne spectrometers such as the TROPOMI or the NASA's Orbiting Carbon Observatory Orbiting Carbon Observatory-2 (OCO-2) measure SIF emission at a specific wavelength (e.g., 740 nm for TROPOMI) from kilometer-scale footprints. These data have been used for training machine learning algorithms linking SIF and GPP with empirical linear regressions (Jung *et al.*, 2020) or for investigating water and light limiting conditions on photosynthesis at large scales (Jonard *et al.*, 2022). The upcoming FLEX tandem mission with Sentinel-3 will enable the quantification of unique products related to SIF and surface temperature at a high spatial resolution (300 × 300 m; Drusch *et al.* (2017)). Such improvement will reduce the current mismatch between flux tower footprint and RS products. Moreover, many studies have been designed to validate future FLEX products by measuring SIF with top-of-canopy (TOC) sensors such as the FloX (JB Hyperspectral, Düsseldorf, Germany), whose development has been supported by the European Space Agency (ESA) (Schuttemeyer *et al.*, 2018). The MLR- USO model must be first evaluated at the ecosystem scale using TOC SIF measurements before future applications with RS SIF data at larger scales.

The MLR- USO model relies on a straightforward methodology for improving our understanding of the photosynthetic and transpiration processes by exploiting the physiological message carried by the SIF signal. To date, no studies have tested such a model. In this perspective, we used the MLR- USO model to estimate GPP and Tr from TOC SIF. This study focused on wheat, which is the most widely planted crop (Erenstein *et al.*, 2022) and an important crop functional type in climate models (Lu

et al., 2017; Boas *et al.*, 2021). Our approach aimed at: (1) characterizing the relationship between SIF and GPP at the ecosystem scale for winter wheat, (2) measuring MLR- USO model parameters and assessing their dependence on meteorological variables and (3) validating MLR-USO model outputs with EC data.

4. Material and methods

4.1. Study site

All the measurements presented in this study were collected at the ICOS station of Lonzée (BE-Lon, Level 2 ICOS station), located in the Wallonia region in Central Belgium (50° 33' N, 4°44' E, 167 m asl). The period studied is the 2022 growing season dedicated to winter wheat (*Triticum aestivum* cv. Skyscraper). The Lonzée experimental site has been cultivated for more than 80 years based on a typical 4-year rotation: winter wheat / sugar beet (*Beta vulgaris*) / winter wheat / seed potato (*Solanum tuberosum*). The climate in Lonzée is temperate oceanic, with mean annual air temperature and cumulative precipitation of about 10.2 °C and 743 mm respectively. The soil is silty clay, with two main horizons: a ploughed layer from 0 to 35 cm (FAO classification Ap) and a layer enriched in clay (FAO classification Bt) from 35 to 100 cm depth (Table 6.1). This study exclusively focused on the 2022 growing season dedicated to winter wheat (*Triticum aestivum* cv. Skyscraper), which was sown on October 28, 2021 and harvested on July, 24 2022. No irrigation was applied during the growing season. Farming activities are summarized in Table 6.2.

4.2. Eddy covariance fluxes and meteorological measurements

The contribution of the target cropland to the EC fluxes was large regardless of the atmospheric condition (more than 90% on average during the last 13 years, data not shown). The prevailing winds are SW and NE with a cropland fetch of respectively 240 m and 200 m. The sonic anemometer (Solent Research R3, Gill Instruments Lymington, UK) and gas analyzer (LI-7200, LI-COR, Lincoln, NE, US) of the EC station were selected following ICOS guidelines (Rebmann *et al.*, 2018). Half-hourly fluxes of net CO_2 and LE (from which Tr is thereafter determined) were computed from high frequency measurements (20 Hz) of vertical wind speed, CO_2 and H_2O concentrations at 2.93 m above the ground. These raw data were processed by the ICOS Ecosystem Thematic Center (ETC) using the ONEFlux pipeline (Pastorello *et al.*, 2020) and are available in the ICOS Carbon Portal (Dumont *et al.*, 2023a). R_{ECO} and GPP were determined from NEE by using the nighttime partitioning method (Reichstein *et al.*, 2005). Storage CO_2 fluxes were neglected owing to the short measurement height. Flux data corresponding to low turbulence conditions (with low friction velocity u_*) were discarded from the analysis using the variable u_* threshold method (VUT; Pastorello *et al.* (2020)), which is preferred when canopy cover changes throughout the

years such as crops. Moreover, no gap-filled fluxes were selected (i.e., quality flag of 0). The variables GPP_NT _VUT_REF for GPP and LE_F_MDS for LE were selected from the dataset. These fluxes are referred to in this paper as GPP_{EC} and LE_{EC}.

Micrometeorological measurements were collected on a half-hourly basis, including incoming photosynthetic photon flux density in the PAR (photodiode-based sensor - PAR Quantum sensor SKP 215, Skye Instruments Limited, Llandrindod Wells, UK), precipitation (weighing rain gauge - TRwS415, MPS system sro, Bratislava, SK), air temperature and relative humidity (resistive platinum thermometer and electrical capacitive hygrometer - HMP155, Vaisala Oyj, Helsinki, FI), soil heat flux (self-calibrating soil heat flux plate- HFP01SC, Hukseflux Thermal Sensors B.V., Delft, NL), longwave downward and outgoing fluxes, net radiation (pyradiometer – CNR 4, Kipp and Zonen, Delft, NL) and SWC at three different locations and at five different depths (5, 15, 25, 55 and 85 cm) using silicon bandgap temperature and capacitance sensors (EnviroSCAN Probe, Sentek Sensor Technologies, Stepney, SA, AU).

4.3. Spectral measurements of SIF

Solar irradiance and reflected radiance from the canopy were measured by the FloX (JB Hyperspectral, Düsseldorf, Germany), which consists of two spectrometers: a QE Pro and a FLAME-S spectrometer (Ocean Optics, Inc., USA). QE Pro measures downwelling irradiance and upwelling radiance covering the range between 650 and 800 nm to observe the SIF signal in the O_2-A (760 nm) and O_2-B (687 nm) absorption bands while FLAME-S covers a wider range from 400 to 1000 nm including both visible and NIR wavelengths. The QE-Pro and FLAME-S spectrometers have a spectral sampling interval and spectral resolution of respectively 0.17 nm, 0.3 nm and 0.65 nm, 1.5 nm. The spectrometers are housed in a thermally regulated box which keeps temperature below 25°C to avoid spectral shifts and dark current drifts. The optical fibers were installed on a mast at 2 m height, at approximately 20 m from the center of the plot, and 5 m from the location where one of the three soil water content sensor profiles was installed. The downward looking bare fibers have an opening angle of 23° which allows to measure the canopy reflectance and SIF emission over a footprint of approximately 1.5 m². The receptor of the upward looking fiber measuring the downwelling irradiance has a hemispherical field of view of 180°. The FloX was installed on February 24, 2022 and removed on July 18, 2022, few days before the harvest of winter wheat.

SIF was retrieved using the SFM from the canopy reflectance spectrum in the O_2-A band which provides the most reliable SIF measurements (Cendrero-Mateo *et al.*, 2019; Chang *et al.*, 2020). The O_2-A band was preferred over the O_2-B band as it enables to track photosynthesis dynamics and limits the reabsorption effects within the canopy structure (Cendrero-Mateo *et al.*, 2019; Martini *et al.*, 2022). Moreover, dense cloud cover may complicate the retrieval of SIF. Therefore, days with a clearness index (i.e., the ratio between net radiation at the top of the canopy and extraterrestrial

net radiation,Chang *et al.* (2020)) lower than 0.3 were discarded from the analysis (Chen *et al.*, 2020; Yang *et al.*, 2021), as well as data when solar radiation is too low (before 9 am and after 3 pm; UTC+1). Nonlinearity and spectral shift corrections on raw FloX measurements were applied. A threshold of solar zenithal angle of 70° was set to avoid detector saturation (Chang *et al.*, 2021). TOC SIF retrieved with the SFM method within the O_2-A band is further referred to as $SIF_{TOC,760}$.

4.4. Downscaling of SIF from top-of-canopy to photosystem level

As SIF is affected by re-absorption and scattering effects of the canopy, $SIF_{TOC,760}$ is indirectly related to the SIF emitted by leaves. Estimating GPP with the MLR model requires the determination of the SIF signal emitted only from PSII at the leaf level over the broadband spectrum emission of fluorescence (Gu *et al.*, 2019). Therefore, $SIF_{TOC,760}$ values must be multiplied by three conversion factors representing (i) the fraction of PSII fluorescence emission contributing to the total SIF emission of the leaf (f_{PSII}), (ii) the integration of the SIF signal at 760 nm over the broadband spectrum emission of fluorescence (f_λ), and (iii) the effects of absorption and re-scattering by the canopy structure (f_{esc}^{-1}). Total SIF (SIF_{TOT}) was therefore calculated from$SIF_{TOC,760}$ by (Liu *et al.*, 2022c):

$$SIF_{TOT} = \frac{SIF_{TOC,760}\ f_{PSII}\ f_\lambda}{f_{esc}} \tag{6.1}$$

The calculation steps of the three factors are detailed below.

4.4.1. Separating the contribution of PSII to SIF measurement

Both PSI and PSII contribute to the emission of SIF in the NIR. Therefore, the influence of PSI on $SIF_{TOC,760}$ must be considered before applying the MLR model which is valid only for PSII SIF emission. Therefore, f_{PSII} was calculated as the ratio of chlorophyll fluorescence quantum yields at the leaf level, while accounting for the contribution of PSI (Jia *et al.*, 2023). The detailed procedure of leaf-level measurements is given in section 4.9.

4.4.2. From top-of-canopy to leaf surface

f_{esc} is the escape probability that SIF photons emitted by PSII reach the top of the canopy. f_{esc} was determined as the ratio of NIR light originating from vegetation NIR_v to the fraction of incident PAR absorbed by the canopy f_{APAR} under the assumption of high leaf area index and low contribution of soil reflectance (Zeng *et al.*, 2019):

$$f_{esc} = \frac{NIR_v}{f_{APAR}} \tag{6.2}$$

NIR_v was calculated from the Normalized Difference Vegetation Index (NDVI) and the canopy reflectance in the NIR (R_{NIR}; Badgley *et al.* (2017)):

$$NIR_v = (NDVI - NDVI_0) R_{NIR} = \left(\frac{R_{NIR} - R_{RED}}{R_{NIR} + R_{RED}} - NDVI_0 \right) R_{NIR} \quad (6.3)$$

Where R_{RED} is the canopy reflectance in the red and $NDVI_0$ is the minimum NDVI and accounts for the effects of bare soil on NIR_v (Badgley *et al.*, 2017). R_{NIR} and R_{RED} were measured by the FloX at respectively 760 nm and 680 nm. f_{APAR} was determined from NDVI by using a linear model which has already been used to estimate wheat crop yields (Moriondo *et al.*, 2007; Myneni & Williams, 1994):

$$f_{APAR} = 1.16\, NDVI - 0.14 \quad (6.4)$$

$NDVI_0$ was set to 0.12, which is the NDVI value when f_{APAR} (Eq. 6.4) equals 0 (Myneni & Williams, 1994).

4.4.3. Integrating the SIF signal over the broadband fluorescence emission spectrum

The final step of the conversion of $SIF_{TOC,760}$ into SIF_{TOT} consists in integrating the SIF signal emitted by PSII at 760 nm over the broadband chlorophyll fluorescence emission spectrum, which requires broadband theoretical fluorescence emission spectrum of PSII. The SCOPE model (version 1.73; van der Tol *et al.* (2009)) was used to simulate a total of 6720 chlorophyll fluorescence spectra between 650 and 840 nm from a canopy with different leaf biochemical and structural proprieties, sun-canopy sensor geometry and structure. The fluorescence spectrum that provided the most meaningful representation of the dataset was retrieved by the Singular Vector Decomposition (SVD) technique (Liu *et al.*, 2022b; Zhao *et al.*, 2014). The first principal component explained more than 99% of the variance of the dataset (data not shown), which allowed to estimate the broadband SIF emitted from PSII at all wavelengths ($SIF_{TOT,\lambda}$) by:

$$SIF_{TOT,\lambda} = \frac{SIF_{TOC,760}\, f_{PSII}}{f_{esc}} \frac{v_1(\lambda)}{v_1(760)} = \frac{SIF_{TOC,760}\, f_{PSII}\, f_\lambda}{f_{esc}}, \lambda \in [650, 840] \quad (6.5)$$

with λ the wavelength, $v_1(\lambda)$ is the first right singular vector from the SVD and $f_\lambda = \frac{v_1(\lambda)}{v_1(360)}$. Eq. 6.5 becomes, after integration over the broadband range of SIF emission and unit conversion:

$$SIF_{TOT} = \pi \sum_{640}^{850} SIF_{TOT,\lambda} \frac{10^6\ 10^{-9}\ 10^{-3}}{h\ c\ N_a} \quad (6.6)$$

with h the Planck constant, c the light velocity, N_a the number of Avogadro, $SIF_{TOT,\lambda}$ in mWm$_{-2}$nm$_{-1}$sr$_{-1}$, and SIF_{TOT}=in μmolm$_{-2}$s$_{-1}$. The factor 10^{-3} converts from milliwatt to watt, 10^{-9} from nanometers to meters, 10^{6} from moles to μmoles and π integrates the signal over the hemispherical space.

4.5. Relationship between SIF and GPP

The relationship between measured GPP and total SIF (i.e., GPP_{EC} and SIF_{TOT}) was characterized by fitting a linear and a linear-plateau segmented model (Jonard *et al.*, 2022). This latter allows to identify a breakpoint in the relationship between two variables. Above the threshold, GPP is constant while SIF increases. Below the threshold, GPP and SIF are positively related. The most significant model was selected by using the lowest AIC, which avoids overfitting (Burnham *et al.*, 2002). Moreover, the SIF yield ($SIF_y = \frac{SIF_{TOT}}{APAR}$ and the light-use efficiency of GPP $LUE = \frac{GPP_{EC}}{APAR}$, where $APAR = f_{APAR}PAR$ is the absorbed irradiance), were calculated to reduce the effect of canopy structure and to provide a more physiological interpretation of the variability of GPP_{EC} and SIF_{TOT} throughout the growing season (Martini *et al.*, 2022).

4.6. GPP modeling

The MLR model calculates the actual electron transport rate (J_{SIF}) from SIF_{TOT} by Gu *et al.* (2019):

$$J_{SIF} = q_L \frac{\phi_{PSII,max}(1 + k_{DF})SIF_{TOT}}{1 - \phi_{PSII,max}} \tag{6.7}$$

with q_L the fraction of PSII centers that are opened, $\phi_{PSII,max}$ the maximum photochemical quantum yield, and k_{DF} equal to the ratio between k_D (representing the rate of constitutive heat thermal dissipation) and k_F (representing the rate of fluorescence emission), set to 19 as in Gu *et al.* (2019). q_L and $\phi_{PSII,max}$ were calculated from leaf level measurements (see section 4.9).

Modeled GPP (GPP_{SIF}) was determined from J_{SIF} based on the electron requirements for carboxylation and oxygenation processes (Gu *et al.*, 2019; Farquhar *et al.*, 1980):

$$GPP_{SIF} = J_{SIF}\frac{C_i - \Gamma^*}{C_i + K_m} = q_L\frac{\phi_{PSII,max}(1 + k_{DF})SIF_{TOT}}{1 - \phi_{PSII,max}}\frac{C_i - \Gamma^*}{4C_i + 8\Gamma^*} \tag{6.8}$$

with C_i CO_2 concentration in substomatal cavities directly measured at the leaf level (details in section 4.9) and Γ^* the CO_2 compensation point. Γ^* was estimated from the canopy surface temperature (T_{can}) (Bernacchi *et al.*, 2001):

$$\Gamma^* = 42.75 \exp \frac{37830(T_{can} - 278.15)}{298.15\ R\ (T_{can} + 273.15)} \tag{6.9}$$

where T_{can} was determined from the longwave fluxes:

$$T_{can} = \sqrt[4]{\frac{LW_{out} - (1-\epsilon)LW_{in}}{\epsilon\ \sigma}} \tag{6.10}$$

with LW_{in} and LW_{out} the longwave downward and outgoing fluxes, ϵ the far-infrared emissivity equal to 0.97 and σ the Stefan-Boltzmann constant.

4.7. Transpiration modeling

The most widely used equation to estimate LE at the ecosystem scale is the PM equation (Monteith, 1965; Maes *et al.*, 2019). This equation models LE under the hypothesis that ecosystem fluxes originate from a single homogeneous plane (i.e., a single 'big-leaf', Knauer *et al.* (2018a)):

$$LE = \Delta\ (R_n - G) + \rho_a\ c_p\ VPD_{can}\ G_{ah}\Delta + \gamma(1 + \frac{G_{aw}}{G_{sw}} \tag{6.11}$$

with Δ the slope of the saturated pressure curve, R_n the net radiation, G the ground heat flux, ρ_a the air density, c_p the heat capacity of dry air, VPD_{can} the vapor pressure deficit at the canopy surface and γ the psychrometric constant. G_{aw} is the aerodynamic conductance for water vapor transport and G_{sw} refers to the canopy surface conductance to water vapor, which includes evaporation from the soil and transpiration from wet vegetation surfaces. VPD_{can} was determined from T_{can} and air relative humidity. The Thom equation (Thom, 1972) was used to determine G_{aw} was determined from wind speed (u) and air friction velocity (u_*):

$$G_{aw} = \left(\frac{u}{u_*^2} + 6u_*^{-0.667}\right)^{-1} \tag{6.12}$$

G_{sw} (Eq. 6.11) was determined by using the USO model while neglecting the minimum stomatal conductance (Medlyn *et al.*, 2017b, 2011a):

$$G_{sw} \sim g_{sw} = 1.6\left(1 + \frac{g_1}{\sqrt{VPD_{leaf}}}\right)\frac{A_n}{C_s} \tag{6.13}$$

with g_1 the slope parameter also related to the marginal water cost of carbon gain (Medlyn *et al.*, 2011a), g_{sw} the stomatal conductance to water vapor and A_n the net photosynthesis. VPD_{leaf} and C_s are respectively the VPD and CO_2 concentration at the leaf surface (i.e., within the boundary layer). All variables in Eq. 6.13 were

measured at the leaf level. g_1 was determined by adjusting a nonlinear regression on leaf-level measurements of A_n, C_s, VPD_{leaf} and g_{sw} (see section 4.9), giving g_1=2.28 ± 0.09 kPa$^{0.5}$ (Fig. S1). The combination of Eq. 6.11 to Eq. 6.13 with A_n replaced by GPP_{SIF} from Eq. 6.8 and VPD_{leaf} replaced by VPD_{can}, gives G_{sw} and Tr (Tr_{SIF}) from SIF measurements, under the assumption of dry canopy surface. Therefore, days when precipitation was measured and the subsequent 48h were discarded from the analysis (Knauer *et al.*, 2018b). In these conditions, it is assumed that the evaporation is negligible and that LE only corresponds to Tr. Tr_{SIF} was converted from Wm^{-2} to mmolm^{-2}s^{-1} using the latent heat of vaporization and the molar mass of H_2O.

4.8. Assessment of edaphic water stress

4.8.1. Relative extractable water

SWC was used to calculate the REW which represents the amount of water available for plant uptake in the root zone (Granier *et al.*, 1999a). The original equation of (Granier *et al.*, 1999a) has been modified to weight the amount of available water by the rooting depth within each soil layer, therefore providing a more realistic estimation of the soil water availability in the root zone. The detail of the calculation of REW can be found in the supplementary materials.

4.8.2. Relationship with ecosystem physiology

Physiological processes such as carbon assimilation, stomatal closure or SIF emission often show a two-steps response to the decrease in soil water avialbaility with a clear transition from non-limiting to limiting soil water conditions from a threshold (Beauclaire *et al.*, 2023b; Gourlez de la Motte *et al.*, 2020; Jonard *et al.*, 2022). In this study, soil water-limiting conditions were defined by using the REW threshold from which a decrease in LUE was observed (Reitz *et al.*, 2023). As any other response ration, LUE is strongly affected by changes in the denominator ($APAR$) especially when it small. Therefore, a logarithmic transformation was used to avoid skewness in the sampling distribution and to linearize the ratio so that LUE is affected equally by changes in $APAR$ or GPP_{EC} (Hedges *et al.*, 1999). A linear and a linear-plateau segmented model were fitted to the log10-transformed daily means of LUE and daily means of REW, and statistical selection was made according to the lowest AIC similarly to the GPP_{EC} - SIF_{TOT} relationship (Stocker *et al.*, 2018; Jonard *et al.*, 2022; Reitz *et al.*, 2023). The linear-plateau segmented model had the lowest AIC and the REW threshold (REW_{th}) was determined as the corresponding REW below which a decrease in REW induced a decrease in LUE . A threshold of 0.57±0.06 was found (Fig. 6.13). This lower limit of this threshold (i.e., REW_{th}=0.51) was used to discuss the impact of non-limiting (i.e., REW>REW_{th}) or limiting (i.e., REW<REW_{th}) soil water conditions on MLR- USO model robustness and on the GPP_{EC} - SIF_{TOT} relationship.

4.9. Gas exchange and fluorescence measurements at the leaf level

q_L, $\phi_{PSII,max}$, C_i and f_{PSII} used in Eq. 6.1 and Eq. 6.8, as well as A_n, C_s, and VPD_{leaf} in Eq. 6.13 were determined from active fluorescence and gas exchange measurements at the leaf level by using a LICOR LI-6400 device and a LI-6400-40 fluorescence chamber (LI-COR Inc., Lincoln, NE, USA). The following procedure was applied to each measurement. Only the youngest and most exposed leaves on the upper part of the canopy were selected, considering that they mostly contributed to the total emitted SIF signal due to their very large role in PAR interception, and their high content in chlorophyll and nitrogen (Li *et al.*, 2015). In the chamber, the CO_2 concentration was set to 400 ppm, and the air humidity and temperature were maintained at ambient level. For the measurements on dark-adapted materials, the actinic light was turned off for at least 20 minutes. A multiphase fluorescence flash of 9 000 µmol m^{-2} s^{-1} was then applied to measure the maximum and minimum fluorescence intensities in the dark (F_m and F_0). After this, the actinic light was turned on and the PAR in the chamber (PAR_{leaf}) was set to ambient level. After stabilization of the fluorescence and gas exchange signal, the steady state fluorescence intensity (F_s) was measured before the application of the same multiphase fluorescence flash to measure the maximum fluorescence intensity under the light ($F_m^{'}$). The minimum fluorescence of a light-adapted sample ($F_0^{'}$) was measured after the application of a far-red pulse to excite PSI and draw the electrons from PSII to ensure that reaction centers remain fully oxidized. In addition, A_n, leaf transpiration, leaf temperature (T_{leaf}) and C_s were measured. These variables were used to calculate g_{sw}, C_i and VPD_{leaf} (Eq. 6.13). Leaf-level measurements were performed at different locations within the FloX footprint between 7 am and 5 pm. A total of 387 measurements were collected between April 14 and June 30, 2022 (Fig. 2). These fluorescence intensities should correspond only to PSII emission. This has been considered by hypothesizing that steady-state PSI fluorescence represents 24% of F_s (i.e., $F_{s,PSI} = 0.24F_s$ when performing active fluorescence measurements at the leaf level Pfündel *et al.* (2013)). This contribution reaches 45% in the NIR for SIF in the O_2-A band (i.e., $F_{s,PSI,NIR} = 0.45F_s$, Pfündel (2021)). Therefore, q_L; $\phi_{PSII,max}$ and f_{PSII} were calculated as following (Kramer *et al.*, 2004; Jia *et al.*, 2023)

$$q_L = \frac{F_m^{'} - F_{s,PSI}}{F_m^{'} - F_0^{'}} \frac{F_0^{'}}{F_{s,PSI}} \tag{6.14}$$

$$\phi_{PSII,max} = \frac{F_m - F_0}{F_m - F_{s,PSI}} \tag{6.15}$$

$$f_{PSII} = \frac{F_s - F_{s,PSI,NIR}}{F_s} = 1 - \frac{F_{s,PSI,NIR}}{F_s} \tag{6.16}$$

It is necessary to interpolate MLR model parameters determined by leaf-level measurements campaigns (q_L, $\phi_{PSII,max}$, C_i and f_{PSII}) to calculate GPP_{SIF} (Eq. 6.8) and Tr_{SIF} (Eq. 6.11) at a half-hourly timescale before validation. This temporal interpolation has been carried out using the relationship between model parameters and potential environmental drivers (VPD_{leaf}, PAR_{leaf}, T_{leaf}, REW). An exponential model was used to represent the relationship between q_L and PAR_{leaf} (Chang *et al.*, 2021). As C_i is sensitive to leaf temperature with a peak between 20 °C and 30 °C for wheat (Huang *et al.*, 2021), a second-order polynomial model was used to interpolate C_i with T_{leaf}. f_{PSII} was linearly related to PAR_{leaf} by a first-order linear function. The equations are:

$$q_L = a_{qL}\, e^{-b_{qL}\, PAR_{leaf}} + c_{qL} \tag{6.17}$$

$$f_{PSII} = a_{fPSII}\, PAR_{leaf} + b_{fPSII} \tag{6.18}$$

$$C_i = a_{Ci}\, T_{leaf}^2 + b_{Ci}\, T_{leaf} + c_{Ci} \tag{6.19}$$

q_L, f_{PSII} and C_i were grouped in PAR_{leaf}, T_{leaf} and VPD_{leaf} classes with an interval of respectively 50 μmolm^{-2}s^{-1}, 2°C and 0.1 kPa before fitting the exponential and polynomial models. Statistical significance of models was evaluated by comparing the AIC of the exponential (Eq. 6.17) and polynomial (Eq. 6.18, Eq. 6.19) models with the AIC of a linear (for Eq. 6.17, Eq. 6.19) and a zero-slope model (for Eq. 6.18). Only models with the lowest AIC are presented. The relationship between model parameters and other potential drivers (i.e., REW, PAR_{leaf}, T_{leaf} and VPD_{leaf}) was also tested (Fig. S3, Table 6.3).

4.10. Energy partitioning at the leaf level

As mentioned in the introduction, NPQ, SIF and PQ are in competition for the incoming irradiance. Therefore, the sum of the three corresponding quantum yields (ϕ_{NPQ}, ϕ_{SIF} and ϕ_{PQ}) equals 1 (Porcar-Castell *et al.*, 2014) and the relationship between carbon assimilation and fluorescence at the leaf level is tightly coupled to the dissipation of excessive energy by heat. It is then expected that the partitioning between ϕ_{NPQ}, ϕ_{SIF} and ϕ_{PQ} at the leaf level directly impacts the relationship between SIF_{TOT} and GPP_{SIF}. The quantum yields were calculated following (Gu *et al.*, 2019; Kramer *et al.*, 2004; Jia *et al.*, 2023):

$$\phi_{PQ} = \frac{F_m^{'} - F_s}{F_m^{'} - F_{s,PSI}} \tag{6.20}$$

$$\phi_{NPQ} = \frac{F_s - F_{s,PSI}}{F'_m - F_{s,PSI}} - \frac{F_s - F_{s,PSI}}{F_m - F_{s,PSI}} \tag{6.21}$$

$$\phi_{SIF} = \frac{1 - \phi_{PSII,max}}{(1 + k_{DF}) \left(\left(1 + \frac{F_m - F'_m}{F'_m} \right) (1 - \phi_{PSII,max}) + q_L \, \phi_{PSII,max} \right)} \tag{6.22}$$

where $NPQ = (F_m - F_m^{'})/(F_m^{'} - F_(s, PSI))$ is the NPQ parameter. Note that ϕ_{NPQ} and ϕ_{PQ} were corrected for PSI emission and that ϕ_{SIF} corresponds to the SIF quantum yield of PSII (Gu *et al.*, 2019) .The relationship between ϕ_{NPQ}, ϕ_{PQ}, ϕ_{SIF} and environmental drivers was evaluated using the correlation coefficients, and their corresponding p-values

4.11. Statistical analysis

The performance of the MLR- USO model was evaluated by calculating the R² and the relative root mean square error (rRMSE) between GPP_{SIF}-GPP_{EC} and between Tr_{SIF}-Tr_{EC}, at both daily and half-hourly timescales. The rRMSE was calculated by dividing the root mean square error by the amplitude of EC data (i.e., the difference between the maximum and minimum value). The heteroskedasticity was assessed by calculating the p-value of the Breusch-Pagan test (Breusch & Pagan, 1979) to characterize a potential trend in residuals variability with GPP_{SIF} or Tr_{SIF}. Finally, the relationship between model residuals and potential drivers (REW, VPD_{can}, T_{can}, f_{esc}) was evaluated using the correlation coefficients, and their corresponding p-values.

5. Results

5.1. Meteorological conditions and EC fluxes

CO_2, H_2O fluxes and meteorological variables in 2022 were compared to the previous winter wheat growing seasons at BE-Lon by combining the FLUXNET2015 and the ICOS Carbon Portal datasets over the years 2005, 2007, 2009, 2011, 2013 and 2019 (Dumont *et al.*, 2023a; Pastorello *et al.*, 2020). The temporal evolution of cumulative precipitation, VPD_{can}, PAR and T_{can} in 2022 is presented in Fig. 6.1 and was compared to the average values over the reference period 2005-2019. In 2022, several episodes with very low precipitation can be observed, as highlighted by numerous horizontal lines on the cumulative precipitation curve (Fig. 6.1-a). At the harvest, the total cumulative precipitation in 2022 was about 251 mm, which is not significantly lower than the average cumulative precipitation for the reference period 2005-2019 (361 ± 153 mm).

Four peaks of VPD_{can} were observed in 2022 around DOY 83, 135, 169, 194, clearly above the average values of the reference period (Fig. 1-b). These sharp increases in VPD_{can} also corresponds to an increase in T_{can} and PAR (Fig. 6.1-c,d). The lack of precipitation during spring and summer 2022 caused a decrease in REW between DOY 55 to 85, DOY 98 to 139, and DOY 160 to 173 (Fig. 6.2-c). The most severe precipitation shortage episode was between DOY 98 to 139, which corresponds to more than 40 days without precipitation. During this period, REW decreased to a minimum value of 0.24. The lowest REW value was 0.14 at DOY 197 (Fig. 6.2-c). GPP_{EC} and LE_{EC} showed a strong seasonal pattern with a typical bell-shape curves in parallel with canopy cover development and NDVI dynamics (Fig. 6.2-a,b; Fig. 6.3-a). Maximum values of 55.0 μmolm^{-2}s^{-1} for $GPP_{EC}$and 419 Wm^{-2} for LE_{EC} were observed at DOY 133 (Fig. 6.2-a,b).

5.2. Temporal evolution of spectral data

Due to a malfunction of the QEPro spectrometer after DOY 175, only SIF data from DOY 55 to DOY 175 were analyzed. Moreover, data gaps between DOY 141-152 and 159-166 were caused by sensor maintenance (Fig. 6.3), and errant NDVI data between DOY 98 and 110 were replaced by data from the NDVI sensor installed on the EC station (laboratory-made sensor, see Soudani *et al.* (2012) for references). NDVI, NIR_v and f_{APAR} followed vegetation development with a gradual increase from DOY 55 to DOY 130 and a maximum value of respectively 0.89, 0.50 and 0.89 (Fig. 6.3-a,b), which characterizes the full development of the canopy. A progressive decrease due to senescence and yellowing can be observed from DOY 182 to DOY 198. The variability of f_{esc} was high before DOY 80, corresponding to the beginning of the growing season. Indeed, f_{esc} is very sensitive to short scale variations of NDVI (Eq. 6.2). This latter showed a strong variability in the early stage of vegetation growth, which can be

explained by the impact of soil reflectance and canopy scattering on the NDVI measurements. Therefore, NDVI measurements are very sensitive to changes in canopy structural proprieties (i.e., such as leaf angle inclination) when vegetation cover is low (Atherton *et al.*, 2022). This might explain the erratic pattern of f_{esc} before DOY 80. From DOY 80, f_{esc} followed crop phenology as NDVI and NIR_v increased, with values stabilizing between 0.50 and 0.39 (Fig. 6.3-b), which has already been observed in similar crops (Dechant *et al.*, 2020). SIF_{TOT} was impacted by both canopy cover development and half-hourly variations of meteorological conditions (Fig. 6.3-c). In particular, SIF_{TOT} gradually increased from DOY 55 to a maximum value of 9.34 μmolm^{-2}s^{-1} observed at DOY 123 (Fig. 6.3-c). The relationship between GPP_{EC} and SIF_{TOT} was characterized by an increase in GPP_{EC} for SIF_{TOT} $\leq$6.90 μmolm^{-2}s^{-1} before a progressive stabilization of GPP_{EC} at $\sim$ 45.6 μmolm^{-2}s^{-1} for SIF_{TOT} $\geq$ 6.90 μmolm^{-2}s^{-1} (Fig. 6.4-a). The nonlinearity was observed at very high $APAR$ ($\sim$ 1500 μmolm^{-2}s^{-1}, corresponding to 3.6% of the $APAR$ dataset) which may suggest a decoupling between GPP_{EC} and SIF_{TOT} induced by light absorption and/or canopy structure effects. The relationship between LUE and SIF_y was linear (Fig. 6.4-b), which highlights that the saturating shape was explained by light absorption rather than structural changes (Fig. 6.4-b). Finally, soil water-limiting conditions (i.e., REW$\leq$ REW_{th}) did not induce a nonlinear pattern between SIF_y and LUE (Fig. 6.5).

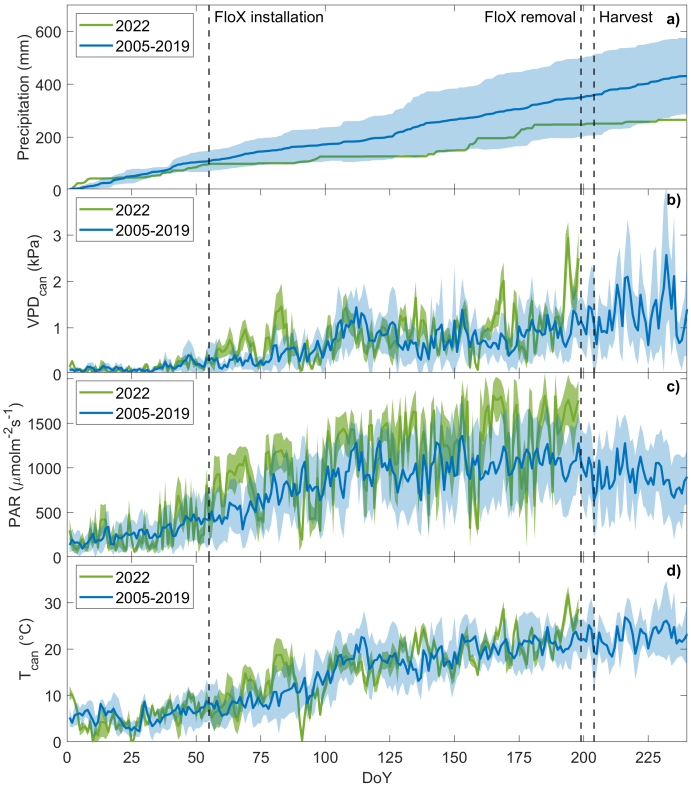

Figure 6.1: Temporal evolution in 2022 of daily cumulative precipitation (panel a), canopy vapor pressure deficit at the canopy surface (VPD_{can} - panel b), photosynthetic active radiation (PAR – panel c) and canopy temperature (T_{can} – panel d) compared to previous winter wheat growing seasons (2005-2019). Shaded areas correspond to the standard deviation around the daily means.

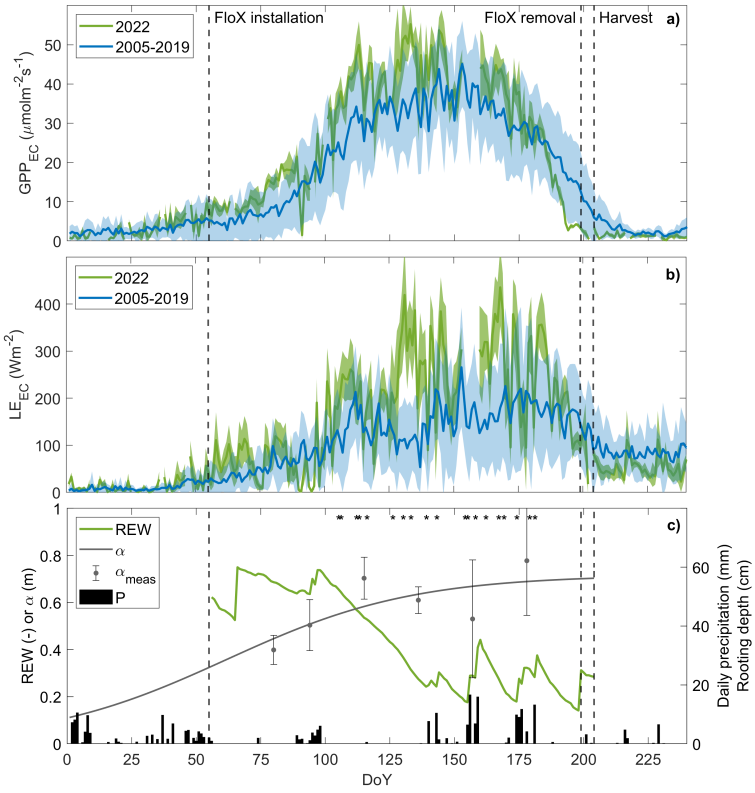

Figure 6.2: Temporal evolution in 2022 of gross primary production (GPP_{EC} – panel a), latent heat flux (LE_{EC} - panel b) and relative extractable water (REW- panel c). Subplot c) also displays maximum rooting depth measurements (α_{meas}) and extrapolated values (α), as well as daily cumulative precipitation (P) and days when leaf level measurements were performed (*). In addition, panels a) and b) also display GPP_{EC} and LE_{EC} over the previous winter wheat growing seasons (2005-2019). Shaded areas correspond to the standard deviation around the daily means. The details of the calculation of REW are given in Text S1.

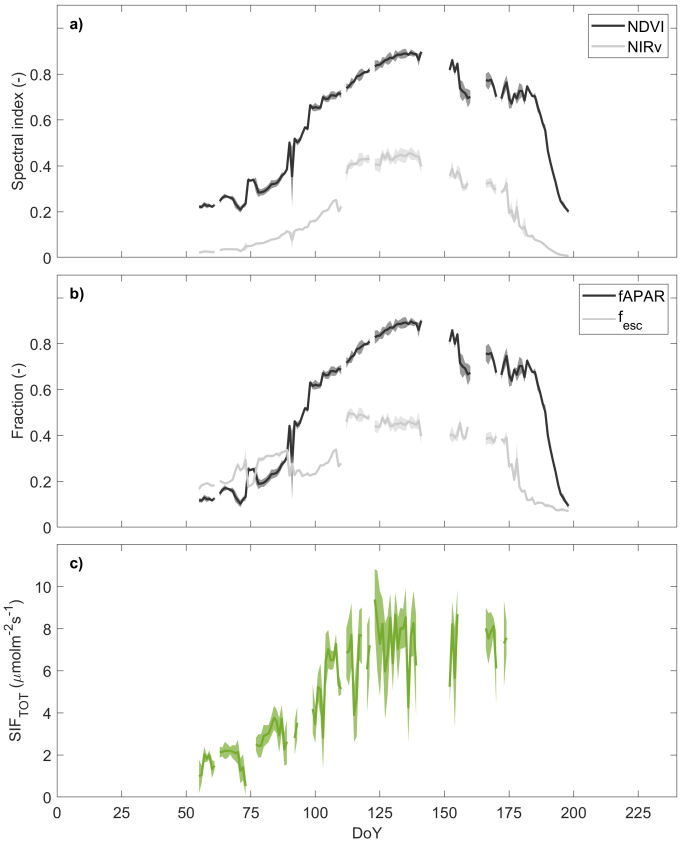

Figure 6.3: Temporal evolution in 2022 of daily means of normalized difference vegetation index (NDVI) and near-infrared reflectance of vegetation (NIR_v – panel a), fraction of absorbed irradiance (f_{APAR}), escape probability (f_{esc}- panel b), and total sun-induced chlorophyll fluorescence (SIF_{TOT} – panel c). Shaded areas correspond to the standard deviation around the daily means.

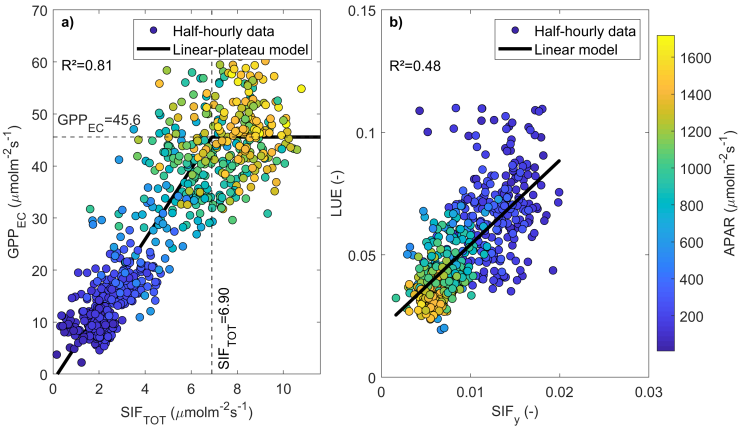

Figure 6.4: Relationship between gross primary production (GPP_{EC}) and total sun-induced fluorescence (SIF_{TOT} - panel a), and between LUE and SIF yield (SIF_y - panel b). The color map indicates the range of absorbed PAR (APAR). R² is the coefficient of determination of the linear or linear-plateau segmented model. The selected model was the one with the lowest AIC.

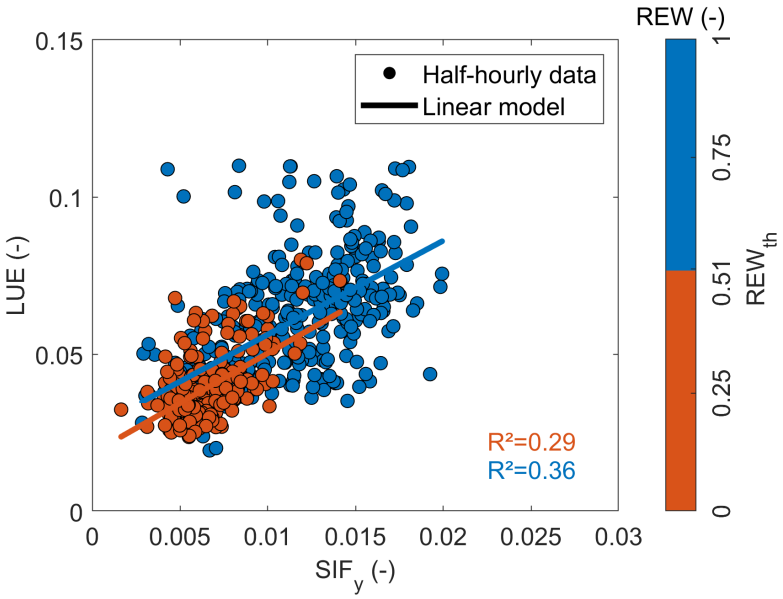

Figure 6.5: Relationship between LUE and SIF yield (SIF_y) with relative extractable water (REW). R² is the coefficient of determination of the linear model. The color map indicates the range of REW and is defined according to the REW threshold characterizing soil water-limiting conditions (REW_{th})

5.3. Leaf-level measurements

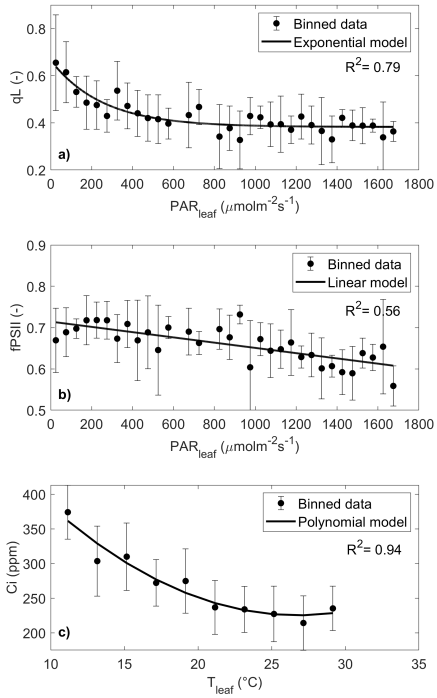

Figure 6.6: Relationship between the fraction of open PSII centers (q_L) and the fraction of PSII fluorescence emission (f_{PSII}) with photosynthetic active radiation at the leaf level (PAR_{leaf} - panels a and b). Panel c) displays the relationship between CO_2 concentration in sub-stomatal cavities (C_i) and leaf temperature (T_{leaf}). Measurements are grouped into PAR_{leaf} or T_{leaf} classes with an interval of respectively 50 μmolm^{-2}s^{-1} and 2°C. The error bars show the standard deviation around the mean for each class. R² is the coefficient of determination of the exponential or polynomial models.

T_{leaf} explained a larger part of the variability of C_i compared to VPD_{leaf} and PAR_{leaf} (i.e., highest R², Fig. 6.6, Fig. 6.14, Table 6.2). $\phi_{PSII,max}$ remained constant and was not affected by any environmental variables ($\phi_{PSII,max}$=0.81, Fig. S3). q_L exponentially decreased from 0.63 before stabilizing to 0.38 when PAR exceeded ∼500 μmolm^{-2}s^{-1} (Fig. 6.6-a), and f_{PSII} linearly decreased between 0.71 and 0.60 (Fig. 6.6-b). C_i decreased with increasing T_{leaf} up to ∼20°C before stabilizing above ∼20°C (Fig. 6.6-c). Fitted coefficients and R² of the regressions (Eq. 6.17,6.18 and 6.19) are given in Table S3. No significant relationship between q_L, f_{PSII} and other environmental drivers was observed (Fig. 6.14). These equations were used to calculate q_L, C_i and f_{PSII} at the half-hourly timescale using T_{can} (Eq. 6.10) and PAR for estimating GPP_{SIF} and SIF_{TOT}. Time series of leaf-level measurements is shown in Fig. 6.15.

A positive correlation between PAR and ϕ_{NPQ} was observed (Fig. 6.7), where ϕ_{NPQ} increased with PAR from ∼0 to ∼0.6. On the other hand, ϕ_{PQ} decreased with increasing PAR from ∼0.8 to ∼0.3, which resulted in a negative correlation (Fig. 6.7). A weaker negative correlation between ϕ_{SIF} and PAR was also evidenced (Fig. 6.7). A significant correlation was also observed between leaf-level quantum yields and T_{leaf} and VPD_{leaf} (Fig. S5). In particular, the decrease in ϕ_{SIF} and ϕ_{PQ} with T_{leaf} and VPD_{leaf} was associated to the corresponding increase in ϕ_{NPQ}. Moreover, the decrease in REW did not affect leaf-level quantum yields (Fig. 6.16).

5.4. MLR- USO model performances for estimating GPP and transpiration

The MLR- USO model reproduced a large proportion of the temporal variability of GPP_{EC} and Tr_{EC} throughout the growing season and under various meteorological conditions (Fig. 6.8). These results are confirmed by the direct comparison between modeled GPP and Tr (GPP_{SIF} and Tr_{SIF}) and EC measurements (Fig. 6.9 and Fig. 6.10). The MLR- USO model explained 95% of the variance of GPP_{EC} at the half-hourly timescale (R^2=0.95) with a rRMSE of 13.7% and a slope of the linear regression between GPP_{EC}C and GPP_{SIF} close to 1 (Fig. 6.9-a). At the daily timescale, the rRMSE was slightly lower, while the other statistics remained very similar (R^2=0.95, rRMSE=11.5%, slope=0.97 ± 0.04) (Fig. 6.9-b). At the half-hourly timescale, 95% of the variance of Tr_{EC} was explained by the model (R^2=0.95) with a rRMSE of 9.1% and a slope of 0.89 ± 0.02 (Fig. 6.10-a). Similar statistics were observed at the daily timescale (Fig. 6.10-b). Low REW induced an underestimation of Tr_{SIF} compared to Tr_{EC}, which was more pronounced at the half-hourly timescale (Fig. 6.10). No deviation from the 1:1 line as $APAR$ increased can be observed for both GPP and Tr (Fig. 6.9 and Fig. 6.10). The mean of residuals was very close to 0 for GPP (0.36 μmolm^{-2}s^{-1} half-hourly / 0.63 μmolm^{-2}s^{-1} daily) and Tr (-0.11 mmolm^{-2}s^{-1} half-hourly / -0.15 mmolm^{-2}s^{-1} daily). An increase in residuals variability as GPP_{SIF} and Tr_{SIF} increased was observed, but only at the half-hourly timescale for GPP (i.e., p<0.05, Fig. 6.9 and Fig. 6.10). GPP residuals were significantly correlated with REW, T_{can} and VPD_{can} but not with f_{esc} (Fig. 6.11-a,b,c,d). Similar correlations are observed for Tr residuals (Fig. 6.11-e,f,g,h). More specifically, the correlation was positive between model residuals and REW, and negative for T_{can} and VPD_{can}. A more important trend towards negative residuals for Tr was observed when REW was lower than REW_{th}, which can explain the slight underestimation of Tr_{SIF} compared to Tr_{EC} (Fig. 6.10). No correlation was observed at the daily timescale for any GPP or Tr residuals.

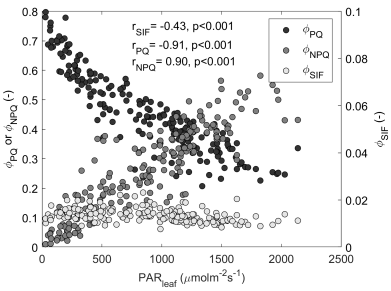

Figure 6.7: Relationship between quantum yields of fluorescence (ϕ_{SIF}), non-photochemical quenching (ϕ_{NPQ}) and photochemical quenching (ϕ_{PQ}) with photosynthetic active radiation at the leaf level (PAR_{leaf}). r is the correlation coefficient and p is the corresponding p-value.

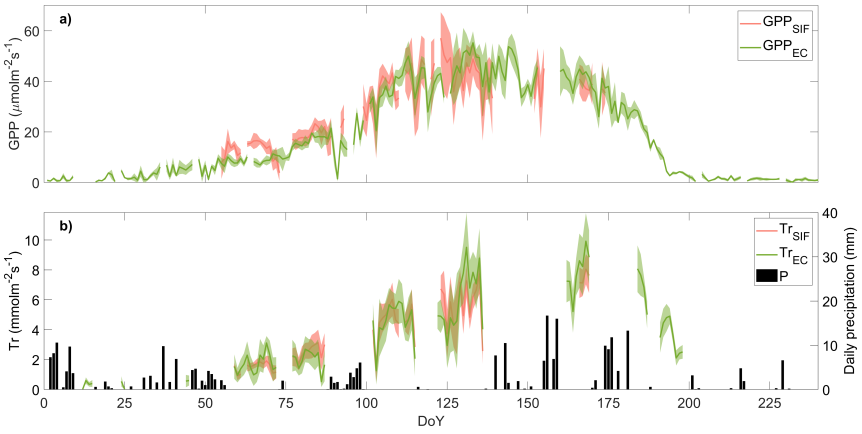

Figure 6.8: Temporal evolution in 2022 of gross primary production from eddy covariance (GPP_{EC}) and estimated by the MLR- USO model (GPP_{SIF} - panel a). Panel b) shows the temporal evolution of daily transpiration from eddy covariance (Tr_{EC}) and estimated by the MLR- USO model (Tr_{SIF}), as well as the daily cumulative precipitation (P). Shaded areas correspond to the standard deviation around the daily means

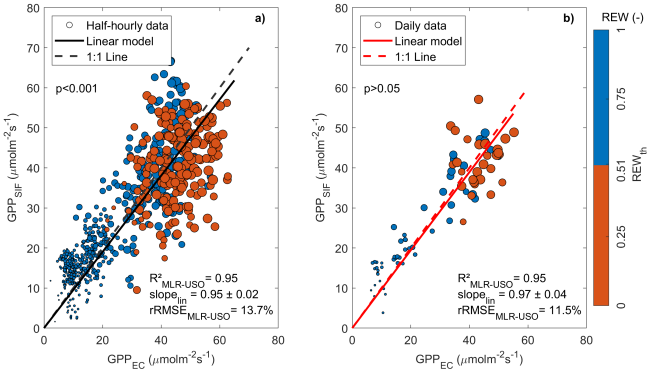

Figure 6.9: Scatterplot between gross primary production from eddy covariance (GPP_{EC}) and gross primary production estimated by the MLR- USO model (GPP_{SIF}) at the half-hourly (panel a) and daily (panel b) timescales. Dot size is proportional to the absorbed photosynthetic active radiation (APAR). The color map indicates the range of relative extractable water (REW) and is defined according to the REW threshold characterizing soil water-limiting conditions (REW_{th}). $R^2_{MLR\text{-}USO}$ and $rRMSE_{MLR\text{-}USO}$ are respectively the coefficient of determination and the relative root mean squared error calculated from GPP_{SIF} and GPP_{EC}. slopelin is the slope of the linear relationship between GPP_{SIF} and GPP_{EC}. p is the p-value of the Breusch-Pagan test for heteroskedasticity

6. Discussion

6.1. Relationship between MLR- USO model parameters and environmental drivers

A key step for applying the MLR model is the determination of the factors for estimating SIF_{TOT} from $SIF_{TOC,760}$. This step includes the conversion of photosystem-level SIF emission to canopy level, the conversion of narrowband SIF to broadband SIF considering a physiological and structural component, and finally the exclusion of PSI fluorescence. f_λ is constant and does not vary with meteorological variables while f_{esc} integrates the structural changes in the canopy and was retrieved from NIR_v and f_{APAR}, which are both reflectance-based measurements available at local and large scales (Zeng *et al.*, 2019; Dechant *et al.*, 2022). As the SIF signal includes the contribution of both photosystems in the O_2-A band, the effect of PSI cannot be neglected. f_{PSII} was estimated by excluding the contribution of PSI to leaf-level fluorescence intensities which was set to 45% of F_s (Pfündel, 2021). Although this value is higher than previous observations (e.g., Genty *et al.* (1990); Franck *et al.* (2002); Pfündel *et al.* (2013)), it can be used to consider PSI contribution in the O_2-A band as it was calculated from selective fluorescence measurements above 700 nm (Pfündel, 2021; Jia *et al.*, 2023). f_{PSII} moderately decreased with PAR, while being not affected by the increase in VPD_{leaf}, T_{leaf} or REW (Fig. 6.6, Fig. S3). This dynamic is similar to the PAR-ϕ_{SIF} relationship which showed a week negative correlation (Fig. 6.7) and can be explained by a strong coupling between F_s and PQ quantum yield under high irradiance when NPQ is limiting (Maguire *et al.*, 2020; Liu *et al.*, 2022c). This contrasts with other studies which modeled the fluorescence quantum yields ratio (Eq. 6.16) with temperature, PAR and CO_2 availability, making f_{PSII} highly sensitive to other environmental conditions (Liu *et al.*, 2022c; Bacour *et al.*, 2019; van der Tol *et al.*, 2014). Disentangling the importance of PSI contribution in the total SIF signal is one important issue to be considered in future studies (Porcar-Castell *et al.*, 2021), as it directly influences the magnitude of SIF_{TOT} especially in the O_2-A band.

Given the wide diversity in physiological mechanisms across ecosystems, it is expected that the parameters of the MLR- USO model (i.e., $\phi_{PSII,max}$,q_L,C_i and g_1) are to be determined from a PFT-based calibration. We tackled this problem by taking in-situ measurements at the leaf level. T_{leaf} explained the most important part of C_i variability (highest R^2, Fig. 6.6, Table 6.3) which is explained by the temperature response of stomata and Rubisco (Warren, 2006a). This combined effect leads to a temperature optimum for photosynthesis, typically around 25°C (Crous *et al.*, 2022), with some variability between species (Marchin *et al.*, 2022). Such relationship was also observed in other studies conducted on winter wheat (Urban *et al.*, 2018; Huang *et al.*, 2021).

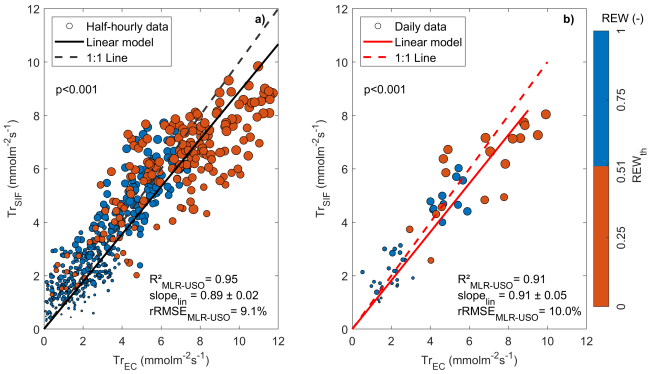

Figure 6.10: Scatterplot between transpiration from eddy covariance (Tr_{EC}) and gross primary production estimated by the MLR-USO model (Tr_{SIF}) at the half-hourly (panel a) and daily (panel b) timescales. Dot size is proportional to the Absorbed Photosynthetically Active Radiation (APAR). The color map indicates the range of REW and is defined according to the REW threshold characterizing soil water-limiting conditions (REW_{th}). $R^2_{MLR\text{-}USO}$ and $rRMSE_{MLR\text{-}USO}$ are respectively the coefficient of determination and the relative root mean squared error calculated from Tr_{SIF} and Tr_{EC}. $slope_{lin}$ is the slope of the linear relationship between Tr_{SIF} and Tr_{EC}. p is the p-value of the Breusch-Pagan test for heteroskedasticity

The exponential decrease in q_L with PAR illustrates the closure of PSII centers when solar irradiance increases (Cendrero-Mateo *et al.*, 2015; Zivcak *et al.*, 2014; Flexas & Medrano, 2002; Broddrick *et al.*, 2022; Ouzounis *et al.*, 2015). We did not observe an effect of other environmental variables on q_L besides PAR (Fig. 6.14), in contrast with previous studies which showed a significant effect of heat and atmospheric dryness on this parameter (Han *et al.*, 2022b; Shin *et al.*, 2021; Zhou *et al.*, 2019a; Cano *et al.*, 2013). However, it might be possible that our experimental set-up didn't allow the identification of such effects as chlorophyll fluorescence measurements were carried out along with gas exchanges, which limited the number of measurements throughout the day and the growing season. Expanding the range of environmental variables under controlled conditions could uncover such additional effects (e.g., Han *et al.* (2022b)).

6.2. SIF-GPP relationship

The saturation of GPP_{EC} at high SIF_{TOT} (Fig. 6.4-a) and the linearity between LUE and SIF_y (Fig. 6.4-b) indicates that APAR is an important driver of the dynamics of GPP_{EC} and SIF_{TOT}. Such relationship has also been observed for croplands, savannas (Yao *et al.*, 2022) or needleleaf forests (Yao *et al.*, 2022; Kim *et al.*, 2021). This nonlinearity can be explained by the competitive mechanism between ϕ_{NPQ}, ϕ_{PQ} and ϕ_{SIF} at the leaf level for the incoming irradiance. We found an asymmetric pattern of ϕ_{PQ} and ϕ_{NPQ} dynamics with PAR (Fig. 6.7) as highlighted by numerous

studies (Baker, 2008; van der Tol *et al.*, 2014; Chen *et al.*, 2019b; Gu *et al.*, 2019). In light-limiting conditions, most of the incoming PAR is used for fueling the dark reactions of photosynthesis by carrying the energy through the electron transport chain to produce ATP and NADPH, resulting in a high PQ at low PAR. As more energy is received by chlorophyll molecules, PSII reaction centers close (decrease in q_L) and the rate of absorbed photons decreases (decrease in ϕ_{PQ}). In these conditions, numerous regulatory mechanisms are used to dissipate the excess energy as heat to prevent the formation of reactive oxygen species (see Demmig-Adams & Adams III (2006) for a review), resulting in an increase in ϕ_{NPQ} with increasing PAR. As ϕ_{SIF} depends on ϕ_{NPQ} and q_L (Eq. 6.22), the opposite behavior of these two parameters with PAR explains the weaker sensitivity of ϕ_{SIF} to PAR (Fig. 6.7), and the nonlinearity between GPP_{EC} and SIF_{TOT} at high APAR (Fig. 6.4-a, Gu *et al.* (2019)).

The linearity between SIF_y and LUE was also observed under soil water-limiting conditions (i.e., REW$\leq$REW$_{\text{th}}$, Fig. 6.5). Similar results were shown in deciduous forests (He *et al.*, 2019; Yang *et al.*, 2015), winter wheat crop (Shen *et al.*, 2022) or natural grassland (Verma *et al.*, 2017). A key factor impacting SIF_y and LUE is the maximum carboxylation rate of Rubisco (V_{cmax}). A decrease in V_{cmax} is often observed in crops during drought (e.g., Beauclaire *et al.* (2023b); Zhou *et al.* (2013)), which could explain the decrease in LUE with REW as highlighted in this study (Fig. S2). Moreover, numerous studies using the SCOPE model (van der Tol *et al.*, 2009) have shown that SIF is sensitive to V_{cmax} (Zhang *et al.*, 2018, 2014; Koffi *et al.*, 2015; Wang & Xiao, 2021; Zhang *et al.*, 2016; Camino *et al.*, 2019), suggesting that SIF_y may decrease as well when soil water availability is reduced. Therefore, the linearity between SIF_y and LUE could be explained by a similar sensitivity of LUE and SIF_y to V_{cmax} during water stress.

Unlike the saturation of GPP_{EC} at high APAR and SIF_{TOT} (Fig. 6.4-a), a linear relationship between GPP_{SIF} and SIF_{TOT} was observed (Fig. 6.16-d). This suggests that the model did not capture the saturation of GPP_{EC} at high APAR. However, the corresponding impact on model performance was limited as only 3.6% of the APAR data was above the saturation point of $\sim$1500 μmolm^{-2}s^{-1} (Fig. 6.4-a). In the MLR model, the influence of PAR on GPP_{SIF} is implemented through the effects of q_L on J_{SIF} (Eq. 1.42, Eq. 6.14). This sensitivity is explained by the coupling between the dark and light reactions of photosynthesis. In particular, the production of energy-carrier molecules (i.e., ATP and NADPH) by the electron transport chain (which depends on q_L) must balance carbon uptake, itself regulated by the stomatal dynamics (Gu *et al.*, 2019). As SIF_{TOT} is the product of ϕ_{SIF} , f_{esc}, and $APAR$ (Gu *et al.*, 2019) it is expected that SIF_{TOT} increases with PAR. On the other hand, the decrease in q_L (Eq. 6.14, Fig. 6.6-a) compensates for the corresponding increase in SIF_{TOT} in the MLR model (i.e., $GPP_{SIF} \simeq q_L SIF_{TOT}$, Eq. 1.43). As a result, the shape of the $PAR - q_L$ relationship modulates the sensitivity of GPP_{SIF} to SIF_{TOT} (Gu *et al.*, 2019).

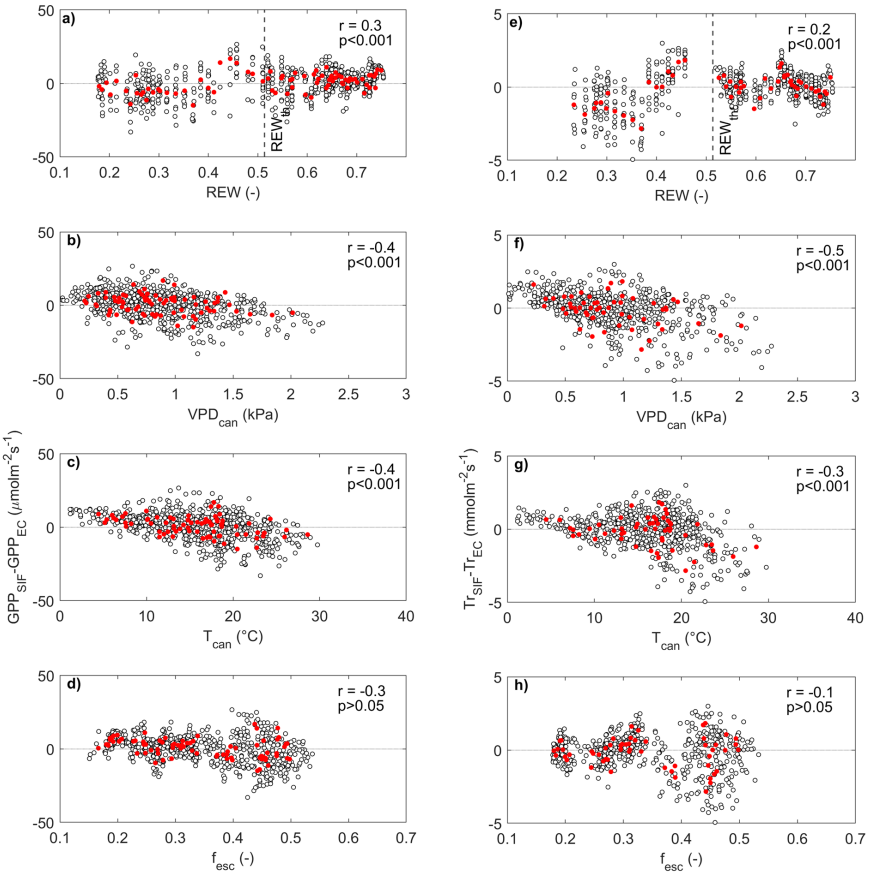

Figure 6.11: Scatterplot of MLR USO model residuals of gross primary production ($GPP_{SIF} - GPP_{EC}$) and transpiration ($Tr_{SIF} - Tr_{EC}$) compared to relative extractable water (REW- panels a, e), canopy vapor pressure deficit (VPD_{can} - panels b, f), canopy temperature (T_{can} - panels c, g) and escape probability (f_{esc} - panels d, h). Dark dots correspond to half-hourly data and red dots to daily data. r is the correlation coefficient and p is the corresponding p-value

The importance of the $PAR - q_L$ relationship on GPP_{SIF} can be assessed by simulating q_L light-response curves based on the 95% confidence intervals of the fitted parameters (Eq. 6.17, Table 6.2, Fig. 6.17-a). These data are then fed into the MLR model (Eq. 6.8), which gives a modeled GPP ($GPP_{SIF,mod}$) using modeled SIF determined from the light-use efficiency model (i.e., $SIF_{TOT,mod}$=$\phi_{SIF}.f_{esc}.f_{APAR}.PAR$, where f_{esc} and f_{APAR} are set to constant, and ϕ_{SIF} is estimated from a linear relationship between ϕ_{SIF} and PAR at the leaf level - Fig. 6.7, Fig. S6). This sensitivity analysis showed that the variability of the $PAR - q_L$ model did not change the pattern of the light response curve of $GPP_{SIF,mod}$, which remained very similar to the $PAR - SIF_{TOT,mod}$ relationship (Fig. 6.17-b). This similar sensitivity to PAR explained the strong linearity between the two variables regardless of the $PAR - q_L$ response curves (Fig. 6.17-c). This suggests that the nonlinearity between SIF_{TOT} and GPP_{SIF} is not likely to be related to the measurements and parametrization of q_L as performed in this study.

One possible explanation of such discrepancy lies in the location of leaf-level measurements within the canopy. In particular, only sunlit leaves at the top of the canopy were selected for active fluorescence measurements, thus implicitly neglecting the contribution of the lower parts of the canopy to the SIF signal. However, wheat canopies can be characterized by leaves with various nitrogen content and structure (Furbank *et al.*, 2015; Chang *et al.*, 2022), and can have an heterogeneous contribution to the observed SIF signal. For instance, while sunlit leaves receive both diffuse and direct light, the proportion of absorbed diffuse light is higher for shaded leaves, which impacts their light absorption proprieties. In-situ measurements have shown that the sensitivity of q_L to PAR changes with the sunlit-shaded status of the leaf (Chang *et al.*, 2021; Zivcak *et al.*, 2014), which is also supported by model simulations on evergreen needleleaf forests (Chen *et al.*, 2024c) . Such variability could explain the observed saturation of GPP_{SIF} at high PAR at the ecosystem scale. This hypothesis is supported by the sensitivity analysis on q_L conducted beyond the 95% confidence interval of $PAR - q_L$ model parameters (Fig. 6.18), which shows that q_L is a key parameter for reproducing the SIF-GPP relationship. Neglecting such complexity in the response of a canopy-scale q_L to irradiance may explain the linearity between SIF_{TOT} and GPP_{SIF} at high APAR. This is even more relevant for dense canopies where the performances of the MLR USO model might be significantly affected under non-limiting light conditions. Future examination of the dependence of q_L on environmental conditions while differentiating light distribution through the canopy is needed (Chen *et al.*, 2024c; Chang *et al.*, 2021).

6.3. Performance of the model

The MLR model was used to determine GPP from TOC SIF measurement over a winter wheat crop. For the first time, this model has been coupled with the USO model

for stomatal conductance (Medlyn *et al.*, 2011a) to use both stomatal optimality theory and the MLR approach to estimate carbon and water fluxes with a single SIF measurement above the canopy. These findings should be considered in the light of previous studies, which already highlighted the promising capacities of the MLR model for predicting GPP at the canopy scale of an irrigated winter wheat crop (Liu *et al.*, 2022c), at the leaf scale for a grass and two tree species (Shi *et al.*, 2022), or for winter wheat grown under controlled conditions (L. Jia et al., 2023). Another recent study of Han *et al.* (2022a) evaluated the robustness of the MLR model at the leaf level for 29 C3 and C4 plant species (not including winter wheat) representative of the major PFT across the globe and demonstrated that the MLR model was also capable of estimating net assimilation rate under diverse light and temperature conditions. The direct use of SIF to model Tr was also tested by (Feng *et al.*, 2021) who coupled the MLR model with the Ball-Woodrow-Berry (BWB) parametrization for stomatal conductance (Ball *et al.*, 1987). Although Tr estimated from the MLR BWB model was in a good agreement with EC data for one maize site and two forest sites, the results might have been impacted by neglecting the effects of changes in canopy structure (i.e., setting f_{esc} to constant, Feng *et al.* (2021)). Our study shows that accounting for canopy structural changes and model parameters dependence on environmental variables is critical for estimating GPP and Tr from SIF.

6.3.1. Robustness of the model during dry conditons

The decrease in LUE from REW_{th} (Fig. 6.13) highlights that winter wheat photosynthesis is sensitive to the decrease in soil water availability (Li *et al.*, 2023a; Yang *et al.*, 2023) , which can lead to yield losses (Riedesel *et al.*, 2023). Statistical metrics indicated that the MLR USO model performed well even when soil water was limiting (i.e., REW$\leq REW_{th}$), or when T_{can} and VPD_{can} were high. The slopes of the linear regressions between MLR USO model estimates (GPP_{SIF}, Tr_{SIF}) and EC measurements (GPP_{EC}, Tr_{EC}) were very close to one (Fig. 6.9, Fig. 6.10), which indicates that the influence of meteorological conditions and changes in canopy structure were reproduced by the model through: (i) the dependence of model parameters on PAR and T_{can}, and (ii) the sensitivity of SIF_{TOT} to VPD_{can} and REW.

However, the correlation between model residuals and environmental drivers (T_{can}, VPD_{can} and REW) suggests that soil water-limiting conditions and high T_{can} and VPD_{can} increased the error term of the MLR USO model. The cone-shaped scatterplot between model residuals and REW (Fig. 6.11) can be explained by uncertainties in the partitioning of NEE between GPP_{EC} and R_{ECO}. For instance, the partitioning of carbon fluxes from EC data relies on the accuracy of the relationship between T_{air} and R_{ECO} (i.e., nighttime method), which can be affected by soil water availability, diffuse radiation, soil temperature (Wohlfahrt & Galvagno, 2017) or the inhibition of daytime respiration (Keenan *et al.*, 2019). Although GPP_{EC} was retrieved using the OneFlux pipeline which uses relatively short moving windows to establish the relation-

ship between T_{air} and R_{ECO} (Pastorello *et al.*, 2020; Reichstein *et al.*, 2005), rapid changes in climate conditions such as rewetting after precipitation shortage episodes may induce a strong variability in this relationship, therefore impacting the accuracy of NEE partitioning (Tramontana *et al.*, 2020). This may explain the larger variability and the decreasing trend of the residuals for REW$\leq REW_{th}$, as numerous rainfall events were observed around DOY 150 after a constant reduction of soil water availability during the 40-days precipitation shortage period. In addition, MLR-USO parameters and VPD_{can} were determined using T_{can} from far-infrared radiation measurements at the canopy surface. While this approach has the advantage of increasing the versatility of the MLR USO model for a use at larger scales with RS of land surface temperature (Hulley *et al.*, 2019; Li *et al.*, 2013), the nighttime partitioning method uses T_{air} instead of T_{can} to determine ecosystem respiration and GPP_{EC} from NEE (Reichstein *et al.*, 2005). This difference may increase model residuals, especially when drought affects the coupling between T_{can} and T_{air} (Aprile *et al.*, 2013; Pradhan *et al.*, 2022). The choice of the driving temperature for R_{ECO} and the partitioning of NEE has been discussed in many studies and is still under debate in the scientific community (Lasslop *et al.*, 2012; Wohlfahrt & Galvagno, 2017). A recent paper of Kira *et al.* (2021) has explored the possibility to use SIF to empirically model GPP to improve the partitioning of NEE. In this perspective, the MLR model also represents a promising perspective to improve the partitioning of NEE by modeling GPP independently from NEE.

Finally, differences between Tr_{SIF} and Tr_{EC} may originate from the calibration of the USO model. g_1 was estimated by using leaf-level measurements of gas exchanges, and the value of 2.28 kPa$^{0.5}$ was in the range of the results of the study of (Medlyn *et al.*, 2017b) for crops, who calibrated the USO model from EC and leaf-level measurements .In our study, leaf-level measurements were conducted on sunlit leaves at the top of the canopy, which do not integrate the whole canopy variability of plant functional traits and meteorological conditions. In particular, canopy architecture induces variability in sun exposure, resulting in within-canopy gradients of meteorological conditions (Coble *et al.*, 2017) or plant traits (Niinemets *et al.*, 2004). Maximum stomatal conductance and stomatal sensitivity to PAR may be higher in the upper part of the canopy (Van Wilder *et al.*, 2022; Tarvainen *et al.*, 2013) whereas C_i is substantially lower in the deep canopy layers (Niinemets *et al.*, 2006). Therefore, the stomatal sensitivity to photosynthesis (i.e., the parameter g_1) can be influenced by within-canopy variations in environmental conditions (Miner *et al.*, 2017), which ultimately results in uncertainties when scaling from leaves to the canopy. Limiting leaf-level measurements to sunlit leaves in the upper layers of the canopy may not capture such variability, and the potential effect of REW on g_1. In particular, it has been shown that g_1 may increase under soil water-limiting conditions at the canopy scale (e.g., Beauclaire *et al.* (2023b); Gourlez de la Motte *et al.* (2020)), which could lead to an underestimation of canopy conductance during soil water stress. Considering this within-canopy variability might be important to model biosphere-atmosphere fluxes

for more dense and complex ecosystems such as forests (Bonan *et al.*, 2021). Future efforts should be focused on elucidating the relationship between model parameters and environmental conditions in dense canopies before testing the MLR USO model over a wider variety of ecosystems.

Despite this uncertainty in the calibration, the MLR USO model still reproduced a very high proportion of GPP_{EC} and Tr_{EC} variability while no parameters were downregulated by REW. It indicates that SIF_{TOT} was sensitive to the decrease in soil water availability either through changes in the physiological (i.e., $SIF_{TOC,760}$) or structural (i.e., f_{esc}) component of SIF_{TOT}. Although $SIF_{TOC,760}$ may decrease due to an increase in NPQ (Porcar-Castell *et al.*, 2014; Xu *et al.*, 2021a), canopy structure through f_{esc} can also be affected by changes in leaf angle distribution usually caused by leaf rolling (Dechant *et al.*, 2020; Xu *et al.*, 2021a; Lu *et al.*, 2020) which is a common adaptative response of winter wheat for reducing transpiration and lowering leaf surface temperature during water stress (Ali *et al.*, 2022; Blum & Tuberosa, 2018). Disentangling drought effects between structural or physiological changes would require additional measurements of morphological traits such as leaf angle distribution (Kattenborn *et al.*, 2022; Zou *et al.*, 2014).

7. Conclusion

This study provides a method which combines existing mechanistic modeling frameworks for estimating GPP and Tr from SIF observations. The novelty of this approach lies in the joint representation of stomatal optimality and light use partitioning processes in a small set of mechanistically-based equations. Our results show that model parameters can be retrieved from canopy temperature and solar irradiance, which are available at large scales from RS data. A high correlation between MLR-USO model estimates and eddy covariance measurements was observed, with more than 90% of variance in observed GPP and Tr explained by the model ($R^2 \geq 0.91$, rRMSE$\leq$13.7% at all timescales) across a wide range of environmental conditions, including light-limiting and soil water-limiting conditions. We also showed that the sensitivity of the fraction of open PSII centers to PAR plays a key role in regulating the response of GPP to SIF. This study confirms that the MLR-USO model can be used for estimating carbon and water fluxes from TOC SIF. More ecosystem-scale studies are needed to fully assess the potential of such model before an application at larger scales with satellite data. This study contributes to paving the way towards an improvement of the modeling of carbon and water fluxes across scales.

8. Acknowledgments and fundings

This research was conducted within the framework of the ICOS Wallonia project, which is supported by the Service Public de Wallonie, Belgium [1217769]. Simon

De Cannière was funded by the Deutsche Forschungsgemeinschaft (DFG, German Research Foundation) under Germany's excellence strategy-EXC 2070-390732324. The other researchers were funded by the Federation Wallonie Bruxelles (FWB). The Fluorescence boX (FloX) was provided by the Forschungszentrum Jülich.

9. Supplementary materials

9.1. Calculation of the REW

The REW (Granier *et al.*, 1999a) was calculated from SWC measurements and maximum rooting depth following:

$$REW = \begin{cases} \dfrac{\theta_{z0} - \theta_{wp,z0}}{\theta_{fc,z0} - \theta_{wp,z0}} & if\ \alpha \leq z_0 \\ \dfrac{z_{i-1}\left(\theta_{z_{i-1}} - \theta_{wp,z_{i-1}}\right) + |\alpha - z_i|\left((\theta_{z_i} - \theta_{wp,z_i}\right)}{z_{i-1}\left(\theta_{fc,z_{i-1}} - \theta_{wp,z_{i-1}}\right) + |\alpha - z_i|\left((\theta_{fc,z_i} - \theta_{wp,z_i}\right)} & if\ z_{i-1} \leq \alpha \leq z_i \\ & i \in [1:4] \end{cases} \tag{6.23}$$

where θ_{z_i}, θ_{wp,z_i} and θ_{wp,z_i} are respectively the measured soil water content, the wilting point and field capacity at the soil depth z_i, and α is the maximum rooting depth. z_0 corresponds to the depth of the first SWC sensor at 5 cm depth while i ranges from 1 to 4 (i.e., corresponding to the depths of SWC sensors at 15, 25, 55 and 85 cm). These depths were weighted by $\pm$ 5 cm to account for a zone of influence around the sensor. The wilting point and field capacity at each depth are shown in Table S1. α was determined from root biomass, which was measured six times during the experiment (α_{meas}, at day of year DOY 80, 94, 115, 136, 157 and 178) with samples taken within six soil layers (0-15 cm, 15-30 cm, 30-45 cm, 45-60 cm, 60-80 cm and 80-100 cm) across the field and soil horizons following a random sampling method. For each day of measurements, the cumulative RBD was calculated from biomass measurements and was extrapolated for all soil depth using a sigmoidal function $y = \frac{a}{1+\exp -b(z-c)}$ with y the cumulative RBD, a the asymptote of the model, b the soil depth corresponding to $y = \frac{a}{2}$, z the soil depth, and c a curvature parameter. For each day of measurement, a continuous RBD profile was calculated. α was defined as the soil depth at which the root density does no longer significantly increase. Therefore, α was calculated as the corresponding soil depth when $y = a - \sigma_a$ with σ_a the standard deviation of a:

$$\alpha = c - \frac{\log \frac{\sigma_a}{a - \sigma_a}}{b} \tag{6.24}$$

α was calculated for each day of the soil sampling campaign and was extrapolated from the date of sowing ($\alpha = 0$ on October 21, 2021) to the date of harvest (July 24, 2022) with a sigmoidal function.

9.2. Calibration of the USO model on leaf-scale measurements

The USO model (Medlyn *et al.*, 2011a) was calibrated by adjusting a nonlinear regression between Eq. 6.25 and leaf-level measurements of stomatal conductance to water vapor (g_{sw}), CO_2 concentration at the leaf surface (C_s), leaf vapor pressure deficit (VPD_{leaf}) and net photosynthesis (A_n) following:

$$g_{sw} = 1.6 \left(1 + \frac{g_1}{\sqrt{VPD_{leaf}}}\right) \frac{A_n}{C_s} \tag{6.25}$$

The relationship between g_{sw} and $\frac{A_n}{C_s\sqrt{VPD_{leaf}}}$, as well as predicted values of g_{sw} using Eq. 6.25 are shown in Fig. 6.12.

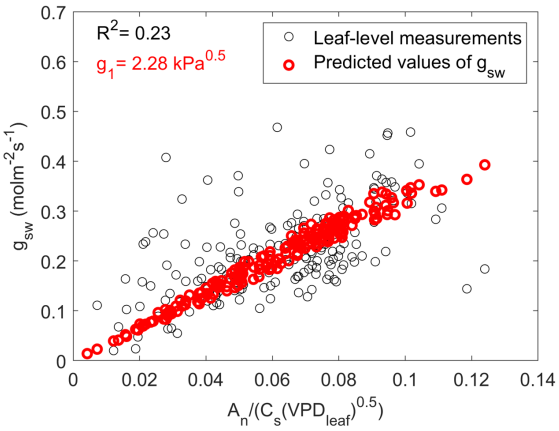

Figure 6.12: Relationship between stomatal conductance to water vapor (g_{sw}), net photosynthesis (A_n), CO_2 concentration at the leaf surface (C_s) and leaf vapor pressure deficit (VPD_{leaf}). The R^2 is the coefficient of determination of the nonlinear regression of the USO model and g_1 is the calibrated value. Red dots show the predicted values of g_{sw} using g_1=2.28 $kPa^{0.5}$

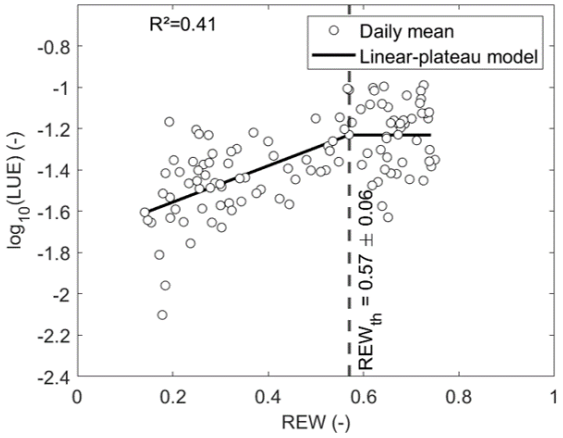

Figure 6.13: Relationship between the log10-transformed LUE ($LUE = GPP_{EC}/APAR$) and the REW. R² is the coefficient of determination of the two-regime model and REW_{th} is the REW threshold where a shift from soil water-limiting to non-limiting conditions is observed.

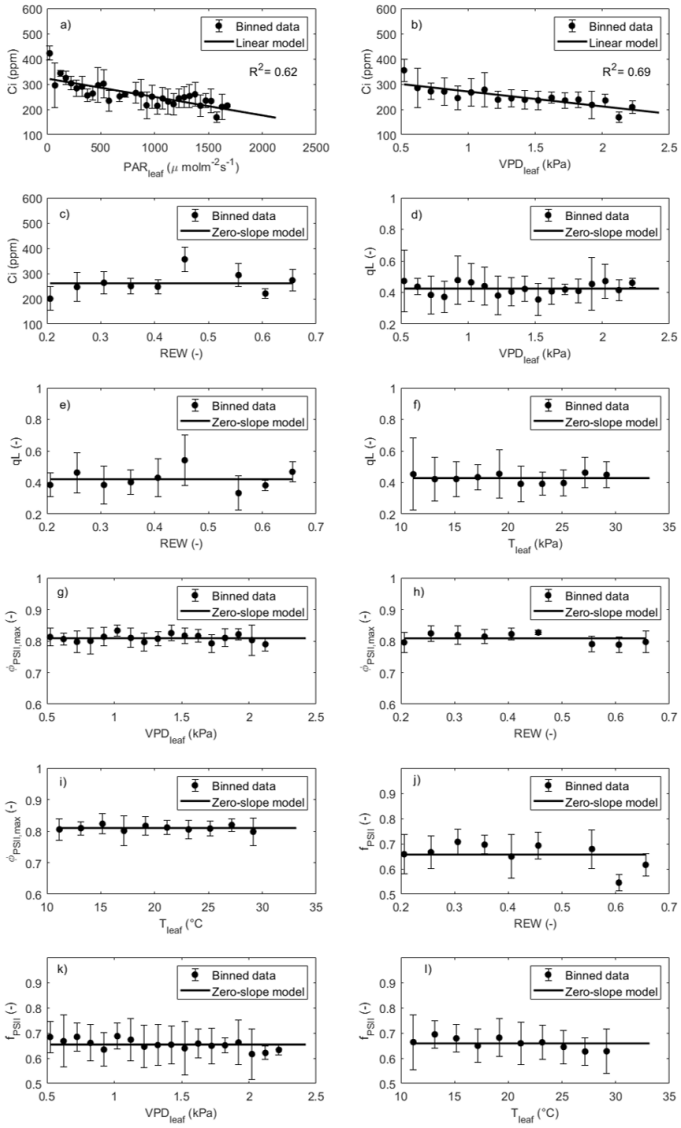

Figure 6.14: Relationship between MLR-USO model parameters (CO_2 concentration in sub-stomatal cavities - C_i, fraction of open PSII centers - q_L, maximum photochemical quantum yield $\phi_{PSII,max}$, and fraction of fluorescence attributed to PSII - f_{PSII}) and meteorological variables (leaf incoming irradiance - PAR_{leaf}, leaf vapor pressure deficit - VPD_{leaf} and relative extractable water - REW). Measurements are grouped into REW, PAR_{leaf}, VPD_{leaf} or T_{leaf} classes with an interval of respectively 0.05, 50 μmolm^{-2}s^{-2}, 0.1 kPa and 2°C. Only models with the lowest AIC are shown. The error bars show the standard deviation around the mean for each data class. Statistical metrics are given in Table 6.14.

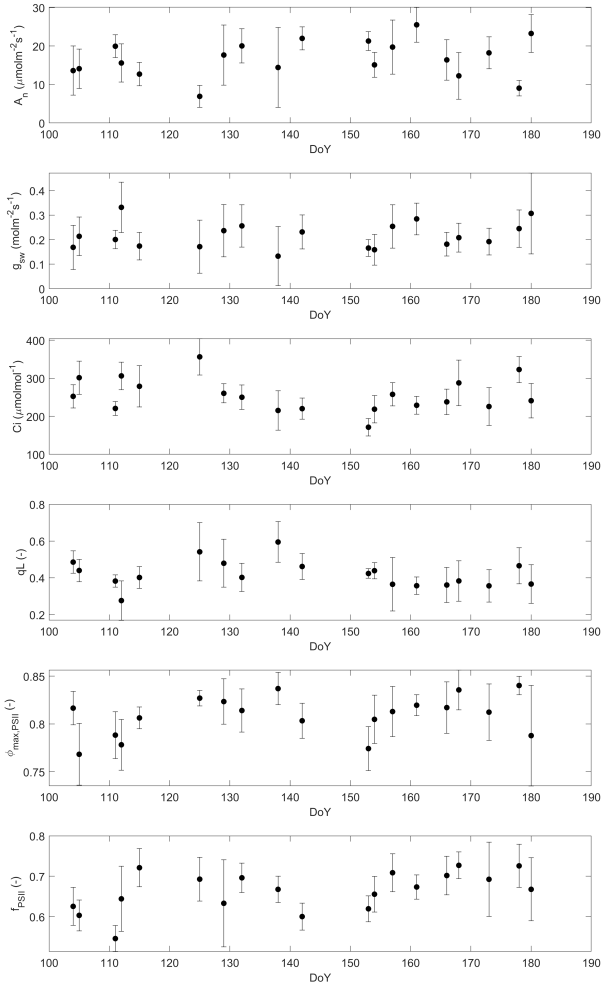

Figure 6.15: Time series of daily means of leaf-level measurements of net photosynthesis (A_n), stomatal conductance to water vapor (g_{sw}), CO_2 concentration in the substomatal cavities (C_i), fraction of open PSII centers (q_L), maximum photochemical quantum yield ($\phi_{PSII,max}$) and fraction of emitted fluorescence attributed to PSII (f_{PSII}). The error bars show the standard deviation around the daily means.

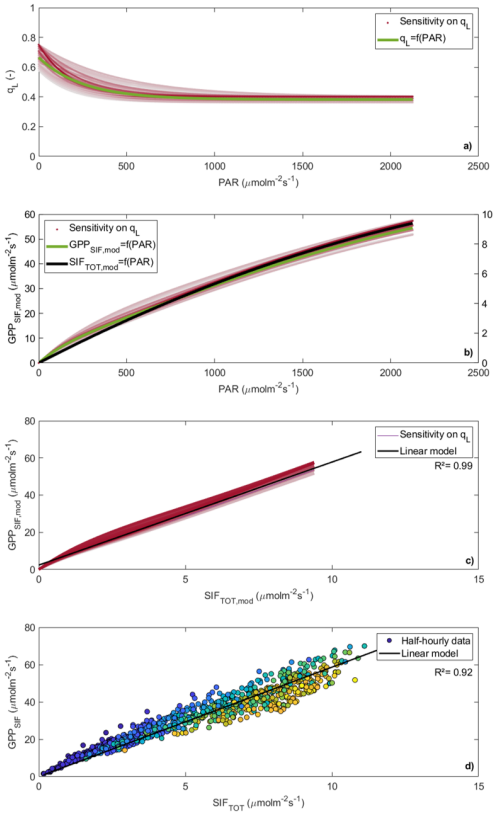

Figure 6.17: Response of the relationship between fraction of the open PSII centers (q_L) and solar irradiance (PAR) to changes in regression parameters (Eq. 6.17 – Table 6.3) within their observed variability (i.e., ± 95% confidence interval – panel a). Panel b shows the corresponding impact on the relationship between modeled GPP($GPP_{SIF,mod}$) and PAR. $GPP_{SIF,mod}$ was estimated using the MLR model (Eq. 6.8) and total sun-induced chlorophyll fluorescence ($SIF_{TOT,mod}$) simulated using $SIF_{TOT,mod} = \phi_{SIF} f_{APAR} PAR f_{esc}$ (Gu *et al.*, 2019). ϕ_{SIF} is the PSII fluorescence quantum yield which was estimated using a first-order polynomial model from the negative correlation between ϕ_{SIF} measurements and PAR (Fig. 6.7). All the other parameters are kept constant, with values of C_i=265 ppm, Γ*=30 ppm (temperature = 20°C), f_{esc}=0.5, f_{APAR}=0.7. PAR ranged from 0 to the maximum PAR measured with a step of 5 μmolm^{-2}s^{-1}. The green curve is the relationship between PAR and q_L measurements (panel a, Fig. 6-a), and between PAR and $GPP_{SIF,mod}$ (panel b). The black curve is the relationship between $SIF_{TOT,mod}$ and PAR (panel b). Panel c) shows the relationship between simulated $GPP_{SIF,mod}$ and $SIF_{TOT,mod}$, and the corresponding linear regression. Each color from red to light-red is associated to a q_L-PAR curve with combination of regression parameters. Panel d) shows the relationship between GPP estimated by the MLR-USO model (GPP_{SIF}- Eq. 6.8) and measured total SIF (SIF_{TOT} - Eq. 6.1).

Horizon	Depth (cm)	θ_{fc} (cm^{-3} cm^{-3})	θ_{wp} (cm^{-3} cm^{-3})	Sand (%)	Silt (%)	Clay (%)	Bulk density (g cm^{-3})
H_1	0-35	45.3	11.7	8.35	80.5	11.2	1.27
H_2	35-85	40.4	13.01	6.1	75.7	18.2	1.52

Table 6.1: Soil physical proprieties in the ICOS Lonzée site: field capacity (θ_{fc}), wilting point (θ_{wp}), sand, silt, clay content and bulk density for the two soil horizons (H1: 0-35 cm and H2: 35-100 cm). Field capacities and wilting points were measured by the WPC4 and HYPROP2 sensors (Meter environment., Hopkins Ct, NE, US) on soil samples collected in 2019.

Date	Activities	Product
28/10/21	Sowing	*Triticum aestivum* cv. Skyscraper
24/03/22	Fertilizer	Liquid Nitrogen 39/0/0 (150 l ha^{-1})
13/04/22	Weeding	Capri Duo (200 g ha^{-1}) + Accurate (10 g ha^{-1})
13/04/22	Growth regulator	Cycocel (1 l ha^{-1})
13/04/22	Biostimulating fertilizer	Amino Mag (2 l ha^{-1})
14/048/22	Fertilizer	Liquid Nitrogen 39/0/0 (100 l ha^{-1})
12/05/22	Fungicide	Aquino (1,2 l ha^{-1}) + Protendo (0,4 l ha^{-1})
17/05/22	Fertilizer	Nitrate 27 (200 kg)
31/05/22	Fungicide	Ascra (1,2 l ha^{-1}) + Protendo (0,5 l ha^{-1})
24/07/22	Harvest	*Triticum aestivum* cv. Skyscraper

Table 6.2: Farming activities in the ICOS Lonzée site during the 2022 winter wheat growing season

MLR model parameters	a ± $CI_{95\%}$	b ± CI_{95}	c ± CI_{95}	R^2
$C_i = a_{Ci} \cdot T_{leaf}^2 + b_{Ci} \cdot T_{leaf} + c_{Ci}$	0.55 ± 0.36	-26 ± 14.8	626 ± 141	0.94
$C_i = a_{Ci} \cdot PAR_{leaf} + b_{Ci}$	-0.07 ± 002	332 ± 21	-	0.62
$C_i = a_{Ci} \cdot VPD_{leaf} + b_{Ci}$	-58.2 ± 21.1	330 ± 31	-	0.68
$f_{PSII} = a_{fPSII} \cdot PAR_{leaf} + b_{fPSII}$	(-6.77 ± 2.25)·10^{-5}	0.72 ± 0.02	-	0.56
$q_L = a_{qL} \cdot exp^{-b_{qL} \cdot PAR_{leaf}} + c_{qL}$	0.28 ± 0.07	0.004 ± 0.002	0.38 ± 0.02	0.79

Table 6.3: Statistics of the regressions between MLR model parameters (CO_2 concentration in substomatal cavities - C_i, fraction of open PSII centers - q_L and fraction of emitted fluorescence attributed to PSII - f_{PSII}) and meteorological variables (leaf temperature T_{leaf}, vapor pressure deficit VPD_{leaf}, and solar irradiance PAR_{leaf}). Regression parameters are given with their 95% confidence intervals.

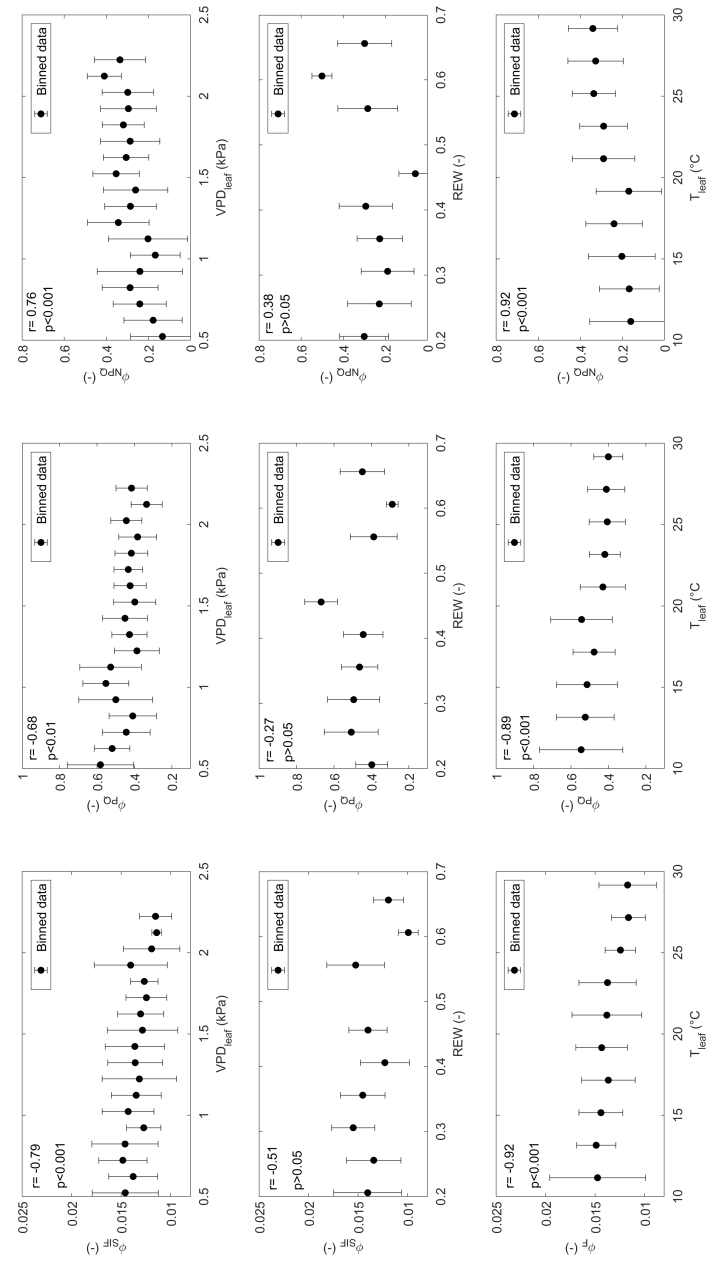

Figure 6.16: Relationship between leaf-level quantum yields (photochemistry - ϕ_{PQ}, non-photochemical quenching - ϕ_{NPQ} and chlorophyll fluorescence - ϕ_{SIF}) and meterological variables (leaf vapor pressure deficit - VPD_{leaf}, REW and leaf temperature T_{leaf}). Measurements are grouped into REW, VPD_{leaf} or T_{leaf} classes with an interval of respectively 0.05, 0.1 kPa and 2°C. The error bars show the standard deviation around the mean for each data class. r is the correlation coefficient and p is the corresponding p-value.

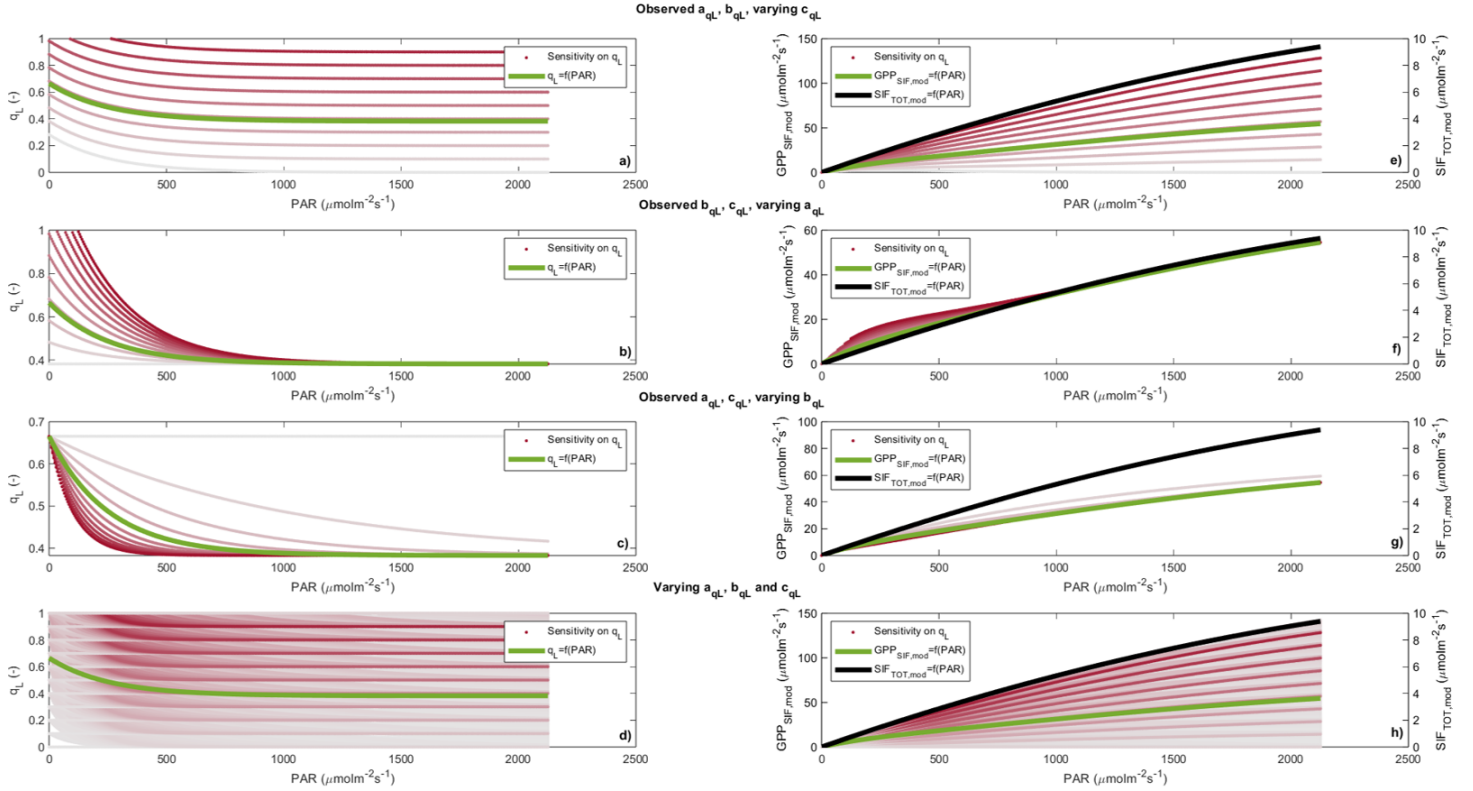

Figure 6.18: Response of the relationship between fraction of the open PSII centers (q_L) and solar irradiance (PAR) to changes in regression parameters (Eq. 17 – Table 6.3) beyond their 95% confidence interval (panels a to d). In panel a), c_{qL} varies between 0 and 1. In panel b), a_{qL} varies between 0 and 1. In panel c), b_{qL} varies between 0 and 0.01. All the other parameters are taken from Table 6.3 if not specified otherwise. Panels e) to h) shows the corresponding relationship between $GPP_{SIF,mod}$ and $SIF_{TOT,mod}$. Details about the sensitivity analysis calculation steps can be found in the legend of Fig. 6.17 .

7

Thesis achievements, methodological considerations and perspectives

1. Thesis achievements

Improving the understanding of the effects of soil water stress on photosynthetic processes is one of the main challenges in photosynthesis research. By using a collection of gas exchange and ChlF measurement techniques at the leaf and ecosystem scales, this thesis contributed to advance representation of photosynthesis in LSMs (Rogers *et al.*, 2017) by : (i) the identification of the constraints on photosynthesis originating from non-stomatal factors and the calibration of their response to soil water availability, (ii) the development of a new partitioning method to emphasize the key role played by mesophyll conductance on limiting carbon assimilation and transpiration, and (iii) the use of RS data to improve the modeling of carbon assimilation and transpiration at the ecosystem scale.

1.1. The constraints on photosynthesis originating from non-stomatal factors under soil water stress

One of the objectives of this thesis was to determine which parameter of the USO and FvCB models should be modified to consider the effect of decreasing soil water availability on physiological processes. This approach was tested on potato and forest ecosystems (dominated by European beech (*Fagus sylvatica*), European spruce (*Picea abies*), European red pine (*Pinus sylvestris*) and maritime pine (*Pinus pinaster*)) either at the ecosystem scale (for forests and potato) or at the leaf scale (for potato solely) (Gourlez de la Motte *et al.*, 2020; Beauclaire *et al.*, 2023b). The limitations on photosynthesis originating from a stomatal control were associated to an effect of the parameter g_1 of the USO model (or G_1 at the ecosystem scale) while the limitations of photosynthesis originating from other non-stomatal factors were associated to V_{cmax} and g_m (or apparent $V_{cmax,app}$ at the ecosystem scale) of the FvCB model. These models are used as sub-models to simulate leaf carbon and water exchanges in LSMs and provide insights on the effects of water stress on the whole plant functioning (Rogers *et al.*, 2017).

How to consider the effects of soil water stress on fluxes remains an important issue in modeling. Most LSMs use an empirical multiplier (i.e., the β factor determined from soil water availability, Eq. 1.49) which directly affects FvCB or USO model parameters when SWC drops below field capacity (i.e., REW<1). This induces abrupt transitions and neglects any plasticity of the physiological response of ecosystems to lack of soil water, ultimately leading to unrealistic drought responses (Zhou *et al.*, 2019b). These abrupt transitions and the uncertainty on which variable should be affected by β are key issues when modeling drought response of terrestrial ecosystems. As highlighted by Vidale *et al.* (2021), "The treatment of β (...) represents a key structural uncertainty in contemporary LSMs, in terms of predictions of gross primary productivity, energy fluxes and soil moisture evolution (...)".

Different approaches are implemented in LSMs for integrating β. For instance, β is

applied on g_1 in CABLE (Wang *et al.*, 2011; De Kauwe *et al.*, 2015a), while in JULES and in JSBACH, β is used on A_n and g_s (Harper *et al.*, 2021; Knauer *et al.*, 2015). In ORCHIDEE V_{cmax} is decreased by β (Krinner *et al.*, 2005). Other approaches use β to affect biochemical signaling such as ABA synthesis, root growth or leaf senescence (see Harper *et al.* (2021) for references). These differences in the treatment of β largely originate from a poor description of the response of plant gas exchanges to drought due to a lack of model-oriented experiments or field studies (Powell *et al.*, 2013; Zhou *et al.*, 2019b).

In this thesis, we used gas exchange and leaf-level ChlF measurements to calibrate β on NSOL and SOL for forest and potato ecosystems, either at the canopy scale (chapter 4 and 3), or at the leaf scale (chapter 5). One important finding of this thesis is the consistent relationship between NSOL, SOL and REW. In particular, canopy-scale measurements of EC showed that the decrease in REW induced a decrease in $V_{cmax,app}$ while G_1 remained constant or slightly increased under severe water stress. It highlights that NSOL was the main constraint on GPP, a pattern which is likely to be consistent in C3 plant species (e.g., Zhou *et al.* (2013); Zait & Schwartz (2018); Wang *et al.* (2018b)). Neglecting the dependence of $V_{cmax,app}$ to REW resulted in strong overestimation of GPP in temperate forest ecosystems (chapter 3), and potato (chapter 4). These results reflect that β should be applied on $V_{cmax,app}$ to reproduce drought effects on GPP. The increase in G_1 when REW $\sim$0.40 is more likely to be a consequence of high NSOL constraints, and can be interpreted in terms of water use strategy.

While it provides large datasets of gas exchanges data at the ecosystem scale, the EC technique does not allow the identification of the true origin of the decrease in $V_{cmax,app}$. Was it caused by an alteration of biochemical capacities (i.e., a decrease in V_{cmax}) or by a strong restriction of CO_2 diffusion to the chloroplasts by the mesophyll (i.e., a decrease in mesophyll conductance g_m) ? This issue is critical as numerous studies have shown that g_m is sensitive to water stress (see chapter 5). LSMs typically model g_m at the leaf level by considering the effects of temperature and water stress through empirical multipliers similar to β (Knauer *et al.*, 2019b). Therefore, realistic drought responses of photosynthesis and transpiration also rely on calibrating β on g_m (as it regulates CO_2 diffusion to chloroplasts (Eq. 1.27), and g_s through A_{sat} (Eq. 1.35)). We tackeld this issue by setting-up a drought experiment on field-grown potatoes and by conducting joint measurements of gas exchange and actively-induced ChlF at the leaf level using a LI-COR LI-6400XT (Chapter 5). We showed that water stress induced a two-stage response of physiological processes with constraints on CO_2 diffusion (i.e., related to conductances) being the first reaction of potato plants to soil drought. Although this approach is essential to analyze the temporal dynamics of model parameters and their dependence to soil water conditions, it does not indicate which model parameters had the most important impact on photosynthesis. To do so, we first started by calculating the total derivative of A_{sat} as a function of g_s,

g_m and V_{cmax} to quantitatively assess the importance of each parameter in explaining the response of photosynthesis to water stress. This method is not new and has been already applied in numerous studies to decipher the importance of stomatal and non-stomatal constraints on photosynthesis (e.g., Grassi & Magnani (2005); Zait & Schwartz (2018); Wang *et al.* (2018b)). The novelty of the method proposed in chapter 5 is the coupling of the USO and FvCB models in the limitation analysis to identify the origins of the limitations on A_{sat} and g_s. The basis of this method is the partitioning of stomatal conductance into relative variations of VPD, g_1 and A_{sat} as described in the USO model (Medlyn *et al.*, 2011b). The mathematical development is given in the supplementary material in chapter 5. The two partitioning schemes (with or without the implementation of the USO model) showed that mesophyll conductance was the most important constraint on A_{sat} and g_s (Fig. 5.5). These results go further than the studies presented in chapter 4 and chapter 3, and provide a quantitative analysis of the role played by mesophyll conductance on the decrease in photosynthesis and stomatal conductance under water stress. In addition, the importance of VPD in regulating stomatal conductance and photosynthesis can be quantitatively assessed.

Another interesting result is the consistent decrease in WUE (increase in g_1) under severe drought, which contradicts with the expected increase in WUE in particular for crops (Yu *et al.*, 2020a), and suggests that extreme dry conditions altered the ability of potato to maintain a constant water use for a given carbon gained. This increase in g_1 highlights the strong effect of NSOL on the decoupling between photosynthesis and transpiration (see chapter 4), almost solely driven by g_m (see chapter 5). In particular, it suggests that improving CO_2 diffusion to chloroplasts can increase WUE. This result is consistent with other studies which showed that g_m is a key limiting factor for WUE for crops (Leakey *et al.*, 2019) or for tree species (Zhu *et al.*, 2021). Engineering anatomical and biochemical factors associated to g_m such as cell wall thickness, porosity, the surface of chloroplasts exposed to the intercellular air spaces, aquaporins or carbonic anhydrase activity could increase CO_2 diffusion and by extension WUE (Petrík *et al.*, 2023). Additional measurements of cells anatomy, molecular signaling and water transport in plants would help in understanding the mechanisms driving the response of mesophyll and WUE to water stress.

Not only the role played by NSOL in limiting photosynthesis under water stress was highlighted, but a similar REW threshold of $\sim$ 0.4 was found for forests and potato at the ecosystem scale. This result for forest ecosystems is in accordance with previous studies which have shown that a decrease in Tr and GPP of temperate forest stands was observed from a REW of $\sim$ 0.4 (Bernier *et al.*, 2002; Rambal *et al.*, 2003; Granier *et al.*, 2007b, 1999b; Bréda *et al.*, 2006, 1995) and confirm that the threshold at which β starts impacting NSOL should be lower than field capacity (Verhoef & Egea, 2014). This threshold of $\sim$ 0.4 is often used to separate stressed and unstressed conditions when interpreting tree gas exchanges (e.g., Xu *et al.* (2017); Van Sundert *et al.* (2020); Aguilos *et al.* (2019)). However, there is little information regarding

the REW thresholds for NSOL or SOL on potato. We found two contrasting results with different thresholds at the leaf scale for diffusive (REW=0.72 $\pm$ 0.12) and biochemical constraints (REW=0.43 $\pm$ 0.03). These discrepancies are further discussed in section 2.2.1. These results are nonetheless particularly useful in crop models such as Aquacrop where the calibration level for these thresholds is defined as minimum for potato (Raes *et al.*, 2009). More studies should be conducted to provide further analysis on the similarities between REW thresholds for forests and potato. Importantly, this method could be applied to select potato varieties which provides the best drought-resistant characteristics (i.e., the lowest REW threshold), thus potentially improving crop yields and irrigation scheduling. Perspectives are given in section 3.2.

1.2. Modeling of GPP from SIF by a mechanistic framework

For more than four decades, ChlF has been used to physiological processes and more specifically stress responses of plants (Baker, 2008; Genty *et al.*, 1989). To date, most of ChlF measurements are performed by active methods at the leaf scale. Because these sensors use an artificial light to drive the reduction of PSII centers, the application of such technique for remote sensing platforms is limited (Cendrero-Mateo *et al.*, 2015; Magney *et al.*, 2017). Spectrometers with sub-nanometer resolutions have enabled the development of passive methods for retrieving SIF in the O_2-A and O_2-B absorption bands using the FLD or SFM method (see chapter 1, section 3.2.2). The MLR model now provides a mechanistic framework for interpreting SIF temporal variability in terms of changes in carbon assimilation (Gu *et al.*, 2019). Yet it remained to be tested under natural conditions and under soil-water limiting conditions. We also added a transpiration module to the model by using the USO equation for stomatal conductance, thereby allowing to estimate both GPP and Tr from SIF.

This thesis have demonstrated the potential of the MLR-USO model for estimating GPP and Tr from SIF measurements at the ecosystem scale. In particular, MLR-USO model estimates were highly correlated to eddy covariance measurements (i.e., R^2>0.91, rRMSE<13.7%) across a wide range of environmental conditions, including high solar irradiance, atmospheric and edaphic dryness (chapter 5). The model relies only on the measurement of SIF, PPFD and surface temperature. However, major uncertainties still remain, especially when considering an application at larger scales or on other ecosystems where within-canopy gradients of environmental conditions are observed and cannot be neglected. In particular, selecting only top-of-canopy leaves for model parameterization may result in strong uncertainties as it is well known that the understorey and midstorey also strongly contribute to the total SIF signal in forests (Morozumi *et al.*, 2023a; Liu *et al.*, 2019). In addition, the response of GPP to PPFD varies with the location of the leaf within the canopy where top-of-canopy leaves are mostly light-saturated while shaded leaves are light-limited. Therefore, light availability must be characterized by distributing top-of-canopy PPFD into the different layers

of the canopy (Zhang *et al.*, 2023b). These aspects are not captured by 'big leaf' models which simplify the canopy as a single layer (already discussed in chapter 1 and in chapter 6). In this perspective, several research questions remain. Does the MLR-USO model requires a species-specific or PFTs-specific calibration? Does the hypothesis of a predominant contribution of top-of-canopy leaves to the SIF signal still hold for other PFTs ? These questions and the recent advances published in the literature are further detailed in section 3.7.

2. Methodological considerations

The results of this thesis were obtained by designing a framework which is based on several hypothesises and methodological choices. The main methodological considerations are : (i) the choice of the NT partitioning method for estimating GPP from NEE, the choice of REW as the explanatory variable for calibrating β, and (iii) the choice of joint measurements of gas exchanges and ChlF to calculate g_m.

2.1. GPP partitioning methods

EC products are determined by a series of post-processing methods which are implemented into a common data treatment pipeline within the ICOS and FLUXNET networks (i.e., the OneFlux pipeline, Pastorello *et al.* (2020)) which allows a harmonization of data treatment and facilitates the comparison of EC products across sites. One of the key steps is the separation of the contribution of ecosystem respiration R_{ECO} from NEE by either the DT or NT partitioning methods (Reichstein *et al.*, 2005; Lasslop *et al.*, 2010). This last remains the most widely used in the flux community (Trifunov *et al.*, 2021). Partitioning methods strongly rely on several underlying assumptions regarding the relationship between NEE and few environmental drivers (see chapter 1 and chapter 6). While both methods are relatively similar for estimating R_{ECO} (they only differ by how R_b (Eq. 1.17) is estimated either from NT or DT data), strong differences may be observed for GPP.

A practical example of these discrepancies can be found in the 2022 dataset of BE-Lon. Despite a strong correlation between DT and NT GPP (Fig. 7.1-a), a decoupling is observed at three specific periods during the growing season: between DoY 116-123, DoY 146-149 and DoY 176-177 (Fig. 7.1-b), which suggests an underestimation of DT GPP. This is confirmed by the light-response curve of the two GPP, highlighting a clear unexpected decrease in DT GPP (Fig. 7.2).

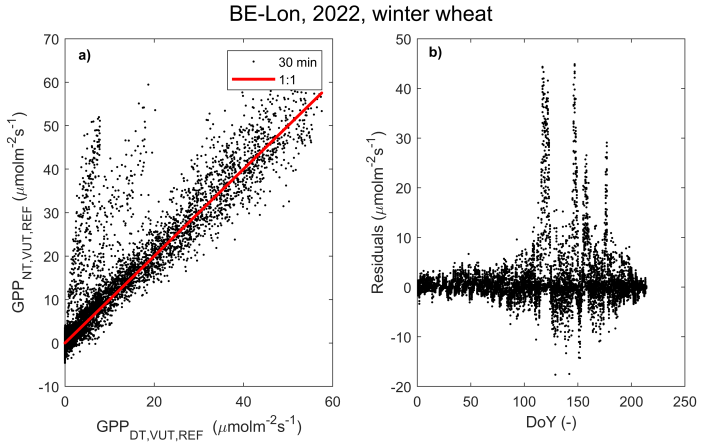

Figure 7.1: Difference between DT and NT GPP at BE-Lon in 2022. The names of the variables in the post-processed dataset (Dumont *et al.*, 2023b) are as in the legend.

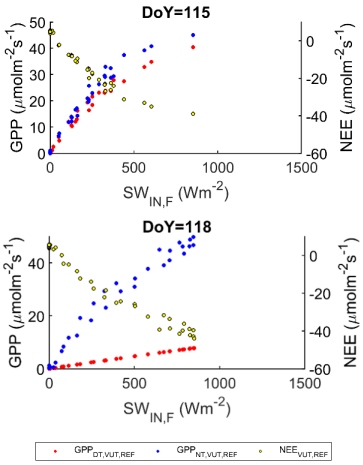

Figure 7.2: Light response curves of NT and DT GPP at BE-Lon in 2022 for two contrasting DoY. The names of the variables in the post-processed dataset (Dumont *et al.*, 2023b) are as in the legend.

These differences can only originate from the parameterization of the NEE light-response curve within a 4-days moving window leading to an unrealistic response to VPD (i.e., low β_{NEE}) or to R_g (i.e., low α_{NEE}). In the DT partitioning method, T_{ref} is first fixed as the median temperature of the moving window and T_0 is set to -46.02 °C. E_0 is then estimated from nighttime data for a shifting moving window of 4 days, before α_{NEE}, β_{NEE} and R_b (Eq. 1.18) are fitted using DT data. The 2022 dataset of BE-Lon did not show any unexpected low R_g or high VPD during the days when these anomalies were detected (as a recall the threshold VPD value for the DT approach is 1 kPa, (Wutzler *et al.*, 2018), Fig. 7.3). This issue still needs to be resolved. Therefore, the choice of the partitioning method for GPP may have strong implications in modeling or ecophysiological studies. For example, the use of DT GPP as validation dataset of MLR-USO would have weakened the performances of the model compared to NT GPP (data not shown). This uncertainty logically propagates to carbon budgets where a difference of $\sim$120 gCm^{-2}d^{-1} between DT and NT cumulative GPP was observed at harvest (data not shown).

In the perspective of evaluating the differences between NT and DT GPP, Jung *et al.* (2024) have proposed an algorithm for flagging these inconsistencies. Complementary consistency flags (C2F) revealed that GPP, R_{ECO} and radiation variables were the most flagged data across the FLUXNET2015 dataset (Jung *et al.*, 2024). This suggests that, despite recent development in data post-processing and quality check controls, a fine analysis of GPP time series is a prerequisite before interpreting EC data. Partitioning NEE remains an key research topic in the scientific community, and many alternatives for estimating R_{ECO} and GPP from NEE have been developed. Most of the recent methods for partitioning NEE use proxies of GPP, based, for instance, on SIF (Zhan *et al.*, 2022; Kira *et al.*, 2021), carbonyl sulfide (Kohonen *et al.*, 2022), machine learning algorithms (Chen *et al.*, 2024a) or stable isotopes (Lee *et al.*, 2020).

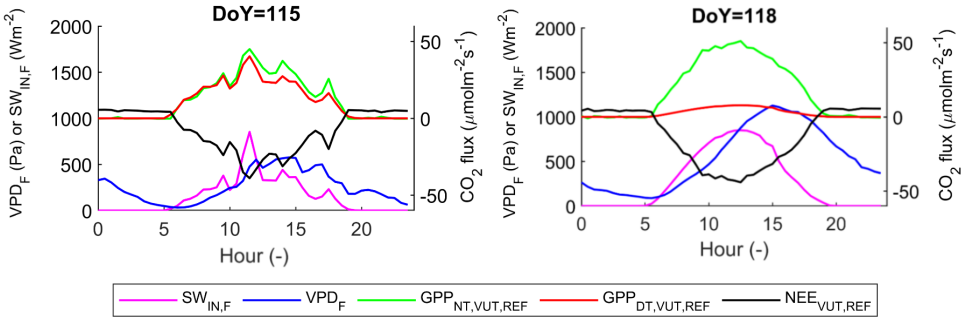

Figure 7.3: Meteorological conditions at BE-Lon in 2022 during two contrasting DoY for DT and NT GPP. The names of the variables in the post-processed dataset (Dumont *et al.*, 2023b) correspond to the legend. SW_{IN} is incoming shortwave radiation (i.e., $\sim R_g$).

2.2. On the choice of REW for modeling NSOL and SOL under water stress

Characterizing soil water status in ecophysiology requires the measurement of a physical variable which considers the water availability for plant uptake. In this thesis, we chose to combine SWC with SWRC to determine REW, which characterizes the fraction of available water for plant uptake. REW provides a better estimation of soil water holding capacities compared to SWC by integrating soil physical proprieties (through θ_{wp} and θ_{fc}) and roots water uptake capacities (through weighting β with root length or root biomass). In addition, field capacity and wilting point can be measured by a single soil sampling campaign and do not change over time (if no soil disturbances occur). As a result, this variable presents two key advantages: (i) it provides additional information regarding soil water availability to plant uptake compared to other approaches considering SWC solely, and (ii) it avoids the drawbacks of characterizing soil water status with SWP (see chapter 1). However, several uncertainties

and methodological considerations remain.

2.2.1. Diverging REW thresholds for similar ecosystems

The results of this thesis show that different REW thresholds were found for potato in chapter 4 and chapter 5 where leaf-level g_m decreased from a higher REW threshold than canopy-scale $V_{cmax,app}$ (i.e., respectively REW = 0.72 $\pm$ 0.12 and REW = 0.43 $\pm$ 0.03). Similar uncertainties were also observed for forest ecosystems although the confidence intervals of the thresholds were overlapping and were not significantly different from 0.4. These differences can be explained by the design of the drought experiment setup (chapter 5), the measurement of SWC, or to the calculation of REW.

First, similar potato varieties were selected for the drought experiment (chapter 5) compared to the main variety planted in Lonzée in 2018 (i.e., the variety Agria, chapter 4). This limits the differences in species-specific traits when comparing the results. However, no fertilizers, pesticides or fungicides were applied during the drought experiment while the EC site in Lonzée is managed by conventional farming practises. This could have weakened the photosynthetic apparatus during the drought experiment (by e.g., a lack of nutrients), resulting in an increasing sensitivity to soil drying and a higher REW threshold.

Second, we calculated REW by considering either a constant weighting scheme (i.e., REW weighted only with the depth of soil layers inferred from SWC temporal dynamics, chapter 3, chapter 4 and chapter 5), or a dynamic weighting scheme (i.e., REW weighted by a dynamic RBD determined from root biomass measurements, chapter 6). Assuming a constant rooting depth in the topsoil might be challenged for potato, where root water uptake can be observed in deep soil layers (Stalham & Allen, 2004, 2001). In particular, differences in root anatomy can lead to very different Root Water Uptake (RWU) capacities. For instance, species with a high fine root hair fraction can access water strongly held by adsorptive forces by finer pores, leading to an increasing capacity to sustain the water flow under high atmospheric pressure (e.g., Marin *et al.* (2021) for barley, or Duddek *et al.* (2023) for maize). Another example is the lateral root formation which facilitates root water uptake (Agee *et al.*, 2021). When the contribution of soil water adsorptive forces compared to capillarity increases in a specific soil layer, plants may also stimulate the production of fine roots to promote water uptake from deeper soil layers where water is mostly held by capillarity. Although these patterns have been highlighted in many tree species (e.g., Peek *et al.* (2006); Leonova *et al.* (2022); Zwetsloot & Bauerle (2021)) and crops (Li *et al.*, 2022a), intra-species uncertainties remain (Gessler *et al.*, 2022; Walthert *et al.*, 2021). Acclimation to local climate conditions seem to play a key role in the drought tolerance of an ecosystem (Puchi *et al.*, 2024; Fan *et al.*, 2017). Overall, a wide variety of water uptake depth across PFTs and climate conditions can be expected (Bachofen *et al.*, 2024). In this perspective, measurements of rooting depth or RBD provides key information but relies on time and labor-consuming destructive biomass sampling campaigns (as detailed

in chapter 6). Instead, RBD models could be used to determine the water uptake capacities profile in the soil and REW weighting factors at a finer temporal resolution (Perona *et al.*, 2022; Kumar *et al.*, 2015). Non-destructive methods for measuring root biomass are also detailed in Cabal *et al.* (2021). This aspect is critical, as REW is very sensitive to the factors used to weight the available water for plant uptake in each soil layer (Fig. 7.4).

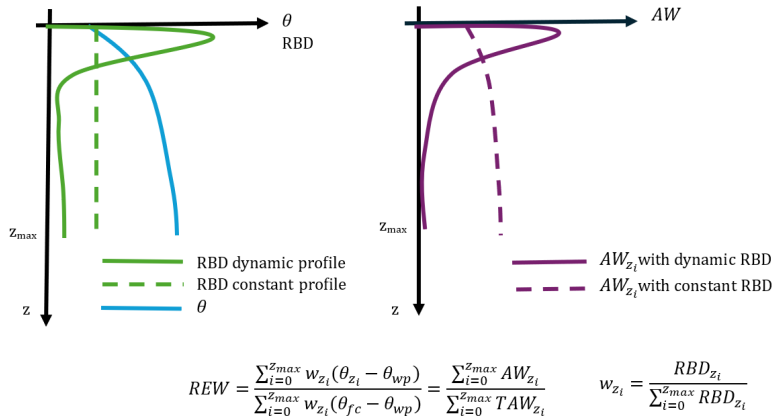

Figure 7.4: Conceptual illustration of a theoretical constant and dynamic RBD profile and the corresponding weighting factors (w_{z_i}) of REW for each soil layer (i) at a specific depth z_i. For simplification, the wilting point (θ_{wp}) and field capacity (θ_{fc}) are considered constant. REW is calculated as the ratio of available water (AW) to total available water (TAW) integrated over the root zone and weighted by w_{z_i}, which are calculated based on a proportion of the RBD profile.

Finally, differences in SWC measurements could originate from sensors calibration equations, which are pivotal for linking the raw measurement of soil dielectric permittivity to SWC (Cosh *et al.*, 2005; J. D. Jabro *et al.*, 2005; RoTimi Ojo *et al.*, 2015). As the sensors used in these two studies were not the same (i.e., EnviroScan sensor in the 2018 dataset, ML2 and ML3 sensors for the other years in chapter 4; ML2 sensor in chapter 5), the corresponding uncertainty could have been exacerbated. In addition, uncertainties remain when estimating field capacity and wilting point from either laboratory or field observation-based methods (Parker & Patrignani, 2021; Evett *et al.*, 2019; Kukal & Irmak, 2023). The measurement of SWC by TDR sensors can be also strongly overestimated in highly conductive soils such as loam and clay soils (Bittelli *et al.*, 2008). As a result, a series of uncertainties can be propagated throughout REW calculation. Comparing REW data across sites is therefore challenging (Ford & Quiring, 2019). These considerations advocate for a careful use of REW for characterizing water status.

2.2.2. From thresholds of REW to thresholds of SWP

Despite these methodological considerations which may explain the differences between REW thresholds, it is worth noting that these values remain in a narrow range when considering the lower limit of the leaf-scale and the upper limit of the ecosystem-scale thresholds (i.e., between 0.60 and 0.46). This range also includes most of thresholds found for forest ecosystems in chapter 3 (Fig. 3.2). This result can be interpreted in terms of water potentials. To this end, we built SWRCs by using VG model parameters of twelve typical soil types as defined by the United States Department of Agriculture (USDA) in the pedotransfer function Rosetta (Schaap *et al.*, 2001; Zhang & Schaap, 2017). These SWRCs were used to get the field capacity and wilting point of each soil textural class. REW was then reconstructed to interpret the thresholds in terms of SWP (Fig. 7.5). Importantly, it can be shown that the range of REW thresholds corresponds to a range of SWP between -19.6 kPa and -87.4 kPa for most of soil textural classes. Only sand soils had a smaller range of SWP thresholds between -12 kPa and -13.8 kPa (i.e., pF between 2.10 and 2.15, Fig. 7.5).

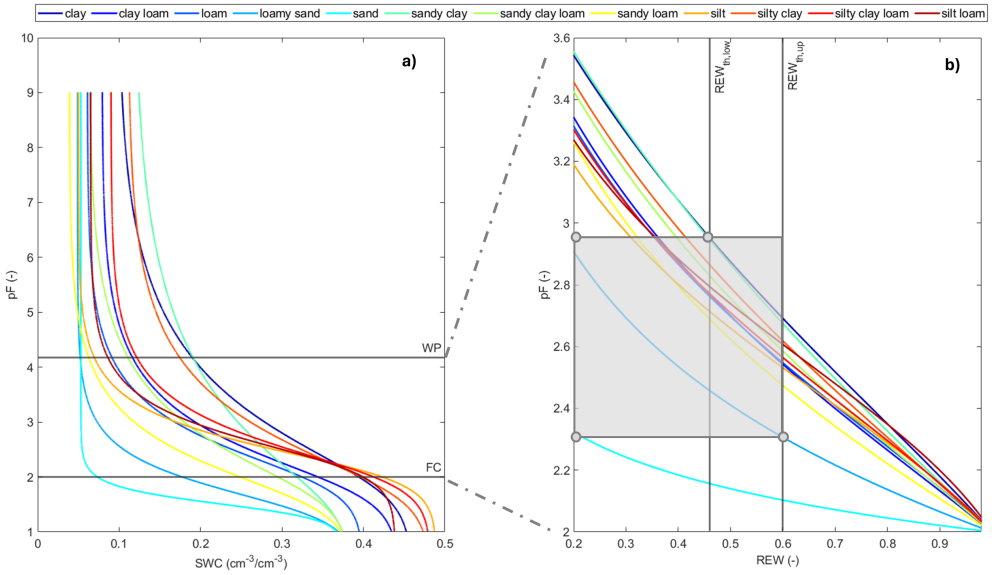

Figure 7.5: REW thresholds linked to SWP by SWRCs of twelve USDA soil textural classes. SWRCs were reconstruct by using VG model parameters from the Rosetta database (Schaap *et al.*, 2001; Zhang & Schaap, 2017). $pF = log_{10}(\psi)$ with ψ in cm. Panel a) shows the SWRCs of the twelve different soil types with field capacity (FC) and wilting point (WP). Panel b) shows the relationship between REW and pF. The shaded grey area illustrates the range of pF values corresponding to REW between 0.46 and 0.6 (i.e., the thresholds of NSOL found in this thesis for potato and forest ecosystems).

By comparison, other studies have found that the water transport in the roots is impeded from SWP thresholds ranging from -6 to -1000 kPa (Cai *et al.*, 2022). Although a SWP of -25 kPa has been reported as optimal growth conditions for potato (Wang *et al.*, 2007), data is still critically lacking. Much lower critical SWP values ranging from -470 kPa to -1200 kPa have been reported for tree species (Eckes-Shephard *et al.*, 2021; de Blécourt *et al.*, 2021; Schütt *et al.*, 2022). These values are however difficult to compare as they strongly differ by the choice of the response variable to changes in SWP. The results of this thesis underline two important outcomes: physiological processes through NSOL are impacted at a much smaller SWP than wilting point (pF=4.2 or ψ_{soil}=-1550 kPa) and calibrating β provides a relatively narrow range of SWP thresholds across soil types. Importantly, these values can also be used in models which uses β as a function of SWP or incorporates plant hydraulics (see section 3.4).

2.2.3. Downregulating NSOL with the β scalar

In this thesis, we chose to calibrate the response of photosynthesis limitations to soil water stress by adjusting β on field data. The main feature of this approach is the determine the shape of β (itself a function of REW) and the parameter on which it should be applied to capture plant response to drought (either on SOL and/or on NSOL). This assumes that REW is a bulk variable encompassing many other processes in the SPAC continuum such as hydraulic or physiological limitations. In addition to the uncertainties when calculating REW (as detailed in section 2.2), the shape of β, and the thresholds of REW are expected to vary in time, or across PFT (Robinson *et al.*, 2019; Teuling *et al.*, 2006). The lack of an universal β formulation is one primary source of uncertainties in carbon cycling modeling, representing between 40-50 % of inter-model variability in GPP predictions (Trugman *et al.*, 2018; Paschalis *et al.*, 2020). Although modifying β to consider plant-specific resistances to drought through a site calibration is possible and recommended (section 3.3, Fig. 7.6), this approach globally lacks from theoretical foundation which may ultimately leads to unrealistic drought responses of gas exchanges in LSMs. Calibrating β for different physiological stages, species, plant species or climate zones represents a huge effort with its share of uncertainty not to be overlooked. An alternative to these empirically-based approaches for reproducing vegetation responses to drought considers the explicit representation of plant hydraulics in coupled photosynthesis-stomatal conductance models (Eller *et al.*, 2020; Sabot *et al.*, 2020). This is further detailed in section 3.4.

2.3. Mesophyll conductance and carbon isotopes

Mesophyll conductance was estimated from joint measurements of gas exchange and chlorphyll fluorescence under natural conditions of CO_2 concentration (Harley *et al.*, 1992). Alternatively, g_m can also be determined by exploiting the fractionation of carbon isotopes naturally occurring during photosynthesis.

Atmospheric CO_2 contains about 1.1 % of ^{13}C (the heavier C isotope) and about 98.9 % of ^{12}C (the lighter C isotope). During photosynthesis, ^{13}C is discriminated against ^{12}C because of (i) its slower diffusion to chloroplasts and (ii) the reduced capacity of Rubisco to fix heavy ^{13}C (O'Leary, 1981). As a result, photosynthetic products are typically enriched in ^{12}C compared to ^{13}C. The deviation of the sample isotope ratio compared to a known standard (δ^{13}) is related to the carbon isotope discrimination (Δ_{iso}) by:

$$\Delta_{iso} = \frac{\zeta(\delta^{13}_{in} - \delta^{13}_{out})}{1 + \delta^{13}_{out} - \zeta(\delta^{13}_{out} - \delta^{13}_{in})} \tag{7.1}$$

$$\zeta = \frac{C_{in}}{C_{in} - C_{out}} \tag{7.2}$$

with δ^{13}_{in}, δ^{13}_{out}, C_{in} and C_{out} are the measured carbon isotope composition and CO_2 concentration inside and outside the measurement chamber (Evans *et al.*, 1986). The isotopic composition of leaf samples can be measured by laser absorption spectroscopy (Bowling *et al.*, 2003; TAZOE *et al.*, 2011; Holloway-Phillips *et al.*, 2019) which can be coupled to the LI-6400 for joint measurements with CO_2 concentration (Sonawane & Cousins, 2019; Holloway-Phillips *et al.*, 2019). The main advantage of these methods is the ability to measure carbon isotope composition in real-time under controlled conditions set in the chamber, therefore allowing to track carbon fractionation at the sub-daily timescale (Diao *et al.*, 2024). Mesophyll conductance can be determined by the difference between carbon isotope discrimination assuming that g_m is infinite ($\Delta_{iso,inf}$) and Δ_{iso} as follows (Busch *et al.*, 2020):

$$g_m = \frac{1+t}{1-t} \frac{b - a_m - \frac{1+b}{(1+e^{'})\alpha_R} e^{'} \frac{R_d}{A}}{\Delta_{iso,inf} - \Delta_{iso}} \frac{A}{C_a} \tag{7.3}$$

where a_m represents fractionation associated with CO_2 diffusion in water (1.8‰), b represents the fractionation during carboxylation (30‰), $e^{'}$ the fractionation during day respiration, t is the ternary effect (Farquhar & Cernusak, 2012) and $\alpha_R = 1 + \frac{R_d}{A} \frac{e^{'}}{(1+e^{'})}$. It has been shown that both methods (gas exchange - fluorometry or gas exchange - laser absorption spectroscopy) yielded similar results, highlighting that they all converge towards a uniform g_m estimate (Marino *et al.*, 2020; Kromdijk *et al.*, 2019; Flexas *et al.*, 2008; Warren, 2006b). Joint measurements of carbon and oxygen isotopes also showed promising perspectives to partition g_m components and assess their response to environmental drives (Barbour *et al.*, 2016; Xiao & Zhu, 2017). Nonetheless, each of these methods has its own limitations, and g_m measurements should be interpreted with caution (Sun *et al.*, 2014; Flexas *et al.*, 2008; Pons *et al.*, 2009). For instance, isotope methods requires a precise knowledge of isotopic fractionation factors and an expansive instrumentation. In this perspective, joint measurements gas exchange and ChlF (actively-induced or with SIF - see section 3.5) still

remains a widely used approach for characterizing the impact of edaphic drought on mesophyll conductance. The recent review of Cousins *et al.* (2020) gives a series of recommendations and discuss the recent advances for measuring g_m.

3. Perspectives

In this section, we draw some perspectives to this work which are summarized in Fig. 7.13.

3.1. Drought resistance of croplands from EC data

This thesis opens up new perspectives for the quantification of stomatal and non-stomatal responses of other crops or PFTs. The method proposed in chapter 4 (and originally developed in chapter 3) could be applied on other agricultural ecosystems of the ICOS and FLUXNET networks to determine whether SOL or NSOL control GPP under water stress, and to calibrate β to reduce uncertainties in LSMs. In particular, most of ICOS sites provide SWC measurements and a description of the soil profile with soil textural proprieties in each soil layer. Using such approach with EC fluxes can be used to determine crops drought tolerance and resistance, with the crop with the lowest REW threshold being the most resistant to water stress (e.g., Gholipoor *et al.* (2013)). This method could be directly tested on nearly 30 EC cropland sites of ICOS and FLUXNET (Pastorello *et al.*, 2020). Drought-resistant tree populations could also be identified by applying this method on other forest ecosystems.

3.2. REW thresholds as a tool for improving crop yields and irrigation scheduling

Reliable estimates of drought responses of physiological processes are also important for improving crop modeling. In particular, the Aquacrop model (Raes *et al.*, 2009) uses empirical factors to implement water stress effects on crop growth and simulate crop yield and irrigation scheduling. In a similar fashion to β in LSMs, these modifiers are either linear, concave or convex, and affect physiological processes when the soil water avilability is lower than a percentage of the total amount of water available for plant uptake in the root zone (i.e., also known as Total Available Water (TAW), the denominator of REW). In Aquacrop, five water stress coefficients are used to affect canopy expansion, transpiration, stomatal closure, canopy senescence and pollination (Raes *et al.*, 2009). A set of upper and lower limits (when the stress function starts/stops operating) are defined for each crop species. Not only impacting crop yield estimates, these thresholds also influence the design of irrigation scheduling, which is provided by Aquacrop through an irrgation module (Alvar-Beltrán *et al.*, 2023; Mwiya *et al.*, 2020). Among the different scheduling approaches, one particularly relies on thresholds of SWC (i.e., the 'soil moisture-based' approach (Gu *et al.*, 2020)). The

key feature of this method is to maintain the SWC in the root zone within an acceptable range for crop growth. This threshold is typically set to the field capacity, which implies that the root zone is refilled as soon as REW is lower than 1 (Wang *et al.*, 2017; Haley & Dukes, 2012). Another approach consists in using a depletion factor, which is a threshold of REW used to calculate the 'readily available water' from the TAW (Allen *et al.*, 1998). The amount of water to be added directly depends on the depletion factor (i.e., very similar to REW_{th}) which is often set to 0.5 (Allen *et al.*, 1998). For potato, existing irrigation scheduling strategies use a threshold of 0.70-0.85 which can vary at different growth stages (King *et al.*, 2020). We suggest that this threshold can be reduced to 0.46-0.6 for the potato plants studied in this thesis. Determining these thresholds is particularly important in the context of water scarcity, where every drop of water must be efficiently used for crop growth. These 'threshold-based' approaches can be used as a preventive tool to buffer the negative effects of drought on crop physiology. More studies based on the calibration of the response of physiological processes under water stress are needed.

3.3. Modifying β for implementing more realistic responses to drought in modeling

Instead of setting the starting point of the downregulation of NSOL by β to the field capacity (Eq. 1.49), we suggest to use more realistic SWC values from which model parameters should be impacted by water stress. In particular, we calibrated a linear-plateau model to characterize the response of NSOL and SOL to REW. This model has a simple linear segment below the REW threshold (REW_{th}), characterized by a slope (a) and an intercept (b). As β is an empirical scalar which affects model parameters when REW decrease, β should correspond to the relative variation of y compared to its maximum value y_{max}. In other words, if y has decreased by 50% compared to y_{max} because of REW, β should equal 0.5. This can be described mathematically as follows. The linear-plateau model is:

$$y = \begin{cases} y_{max}, & REW \geq REW_{th}, \\ aREW + b, & REW < REW_{th} \end{cases} \tag{7.4}$$

with $a = \frac{y_{max} - b}{REW_{th}}$. b, y_{max} and REW_{th} are fitted parameters. By considering that (i) β must be expressed as a function of REW, and (ii) β must equal the relative variation of y compared to y_{max}, one can write:

$$\beta = \frac{y}{y_{max}} = \frac{REW}{REW_{th}} \left(1 - \frac{b}{y_{max}}\right) + \frac{b}{y_{max}} \tag{7.5}$$

This equation shows that β is dependent on three fitted parameters which are species (or PFT)-specific. Eq. 7.5 can be written in an integrated form using REW or SWC:

$$\beta = \begin{cases} 1 & REW \geq REW_{th} \\ \dfrac{REW}{REW_{th}} \left(1 - \dfrac{b}{y_{max}}\right) + \dfrac{b}{y_{max}} & REW < REW_{th} \end{cases} \tag{7.6}$$

$$\beta = \begin{cases} 1 & \theta \geq REW_{th}(\theta_{fc} - \theta_{wp}) + \theta_{wp} \\ \dfrac{(\theta - \theta_{wp})}{REW_{th}(\theta_{fc} - \theta_{wp})} \left(1 - \dfrac{b}{y_{max}}\right) + \dfrac{b}{y_{max}} & \theta < REW_{th}(\theta_{fc} - \theta_{wp}) + \theta_{wp} \end{cases} \tag{7.7}$$

In total, Eq. 7.7 requires two additional parameters compared to Eq. 7.5 : the field capacity and wilting point (θ_{fc}, θ_{wp}), which allow to convert REW into SWC. As an example, a theoretical relationship between g_m and REW, and the corresponding β are given in Fig. 7.6.

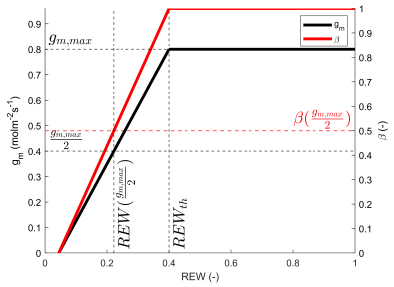

Figure 7.6: Example of a modified β factor considering a linear-plateau relationship between g_m and REW using $g_{m,max} = 0.8$ molm^{-2}s^{-1}, $REW_{th} = 0.4$ and $b = -0.1$ molm^{-2}s^{-1}.

Eq. 7.7 provides a more realistic calibration of the response of NSOL to the decrease in REW. Notably, Eq. 7.7 is very similar to the equation used in JULES (v4.6). In particular, a linear-plateau also describes the response of A_n to soil water availability, and β is operating only from an upper SWC threshold (θ_{upp}) which depends on a parameter (p_0) allowing to delay the decrease in carbon assimilation (Harper *et al.*, 2021):

$$\theta_{upp} = (1 - p_0)(\theta_{fc} - \theta_{wp}) + \theta_{wp} \tag{7.8}$$

By comparing Eq. 7.8 and Eq. 7.7, it can be show that p_0 is directly related to REW_{th} as:

$$p_0 = 1 - REW_{th} \tag{7.9}$$

In JULES, p_0 is set to 0.4, which means that β is operating from a REW_{th} of 0.6 (Harper *et al.*, 2021). Moreover, β equal zero when $\theta = \theta_{wp}$ (i.e., when REW=0), which also implies that the intercept b in Eq. 7.7 equal 0. It can be shown that the mathematical expression of β in JULES (Harper *et al.*, 2021) and Eq. 7.7 are exactly similar if $b = 0$. Therefore, Eq. 7.7 requires two more parameters compared to JULES (y_{max} and b), but will inevitably yield significant improvement for representing the response of physiological processes to water stress. These additional parameters can be determined from EC and leaf-level measurements. Modifying the weighting scheme

and assessing the impacts on LSMs estimates is currently explored in numerous studies. Future studies should focus on testing the implementation of a modified β factor accounting for RBD and RWU plant capacities in LSMs. For example, better estimates of Tr under water stress have been found when using RWU instead of rooting fraction (similarly to rooting depth) for β in the LSM CLM5 (Sulis *et al.*, 2019). It is also urgent to unify soil water availability metrics to facilitate the interpretation of drought experiment results (Vicca *et al.*, 2012).

3.4. The profit-based optimization: an alternative to empirical solutions for implementing plant responses to drought in modeling

One of the alternatives of β-based empirical approaches for modeling plant responses to drought is plant hydraulic models, which represent the water transport in vegetation using flux-gradient relationships. Incorporating plant hydraulics in photosynthesis models provides a mechanistic bridge between physiological regulation of leaf gas exchanges and environmental drivers. These models aim to capture plant responses to drought through the representation of stomatal responses to LWP, which is the most direct variable for assessing leaf water status (Brodribb *et al.*, 2003; Klein, 2014). The LWP sensitivity to stomata is tightly coupled to xylem anatomy and vulnerability to cavitation. Here we describe the 'loss-gain' theory, where plant hydraulics modeling is based on the supply of transpiration while considering a 'cost' and a 'gain' function (Sperry *et al.*, 2017).

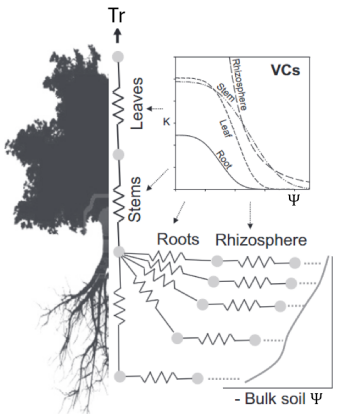

Figure 7.7: Conductance network linking bulk soil water potential (ψ) to sustain transpiration from the rhizosphere to the leaves. Each network component has a vulnerability curve (VC) describing the drop in hydraulic conductance k with increasing ψ (Sperry *et al.*, 2016).

The water flow is supplied to the leaves as transpiration by the tension-cohesion mechanism along the SPAC where water flows from low to high potentials (Fig. 7.7). Importantly, the transpiration stream is driver by total plant resistance, along with soil and atmospheric water deficits (Wolfe *et al.*, 2023). The supply function therefore describes the relation between transpiration (Tr) and xylem water potential at a specific soil water potential. It is calculated by integrating vulnerability curves within each component of the SPAC (i.e., the response of the hydraulic conductance k to the decrease in water potential ψ) following (Sperry *et al.*, 2017):

$$Tr = \int_{\Psi_{up}}^{\Psi_{down}} k(\Psi) d(\Psi) \tag{7.10}$$

where k is described with a two-parameter vulnerability curve for xylem components (Sperry *et al.*, 2016, 2017):

$$k(\Psi) = k_{max} e^{[(\frac{-\Psi}{b})^c]} \tag{7.11}$$

with k_{max} the maximum hydraulic conductance, b corresponding to Ψ when $\frac{k(\Psi)}{k_{max}} = 0.37$ and c controls the shape of the vulnerability curve. A vulnerability curve for rhizosphere is also proposed as a function of k_{max}, soil texture-specific parameters and SWP using a VG function. A common assumption of such model is the consideration of unsegmented xylem components (i.e., the same vulnerability curve for all xylem components) (Sperry *et al.*, 2017).

On the demand-side, the 'demand' function specifies the actual regulation of plant transpiration rate along the supply function, mostly achieved by stomatal movements. The role of the 'loss' function is to avoid a critical loss of hydraulic conductance leading to cavitation, and to utilize the full supply capacity of xylem for sustaining transpiration. As a result, the 'demand' and supply functions are mathematically dependant (Sperry & Love, 2015). The demand function characterizes the restrictive effect of increasing ψ on the transpiration flow as (Sperry *et al.*, 2017):

$$\Pi(\Psi) = \frac{k_{max} - k(\Psi)}{k_{max} - k_{crit}} \tag{7.12}$$

with k_{crit} the critical hydraulic conductance when $\Psi = \Psi_{crit}$ at dessication. While this approach clearly identifies the fitness cost of moving water (i.e., the loss of conductivity), it ignores the role played by stomata for regulating photosynthesis and the corresponding carbon gain. To that end, a 'gain' function has been added in the model of Sperry *et al.* (2017).

On the gain-side, the 'gain' function considers the carbon gain through photosynthesis related to stomatal opening defined as Sperry *et al.* (2017):

$$\Omega(\Psi) = \frac{A(\Psi)}{A_{max}} \tag{7.13}$$

where A is the gross assimilation rate, determined by a photosynthesis model similar to the FvCB model (Collatz *et al.*, 1991). This latter is determined by coupling the supply function (giving the plant conductance to water) to the Fick law representing CO_2 diffusion through stomata. A is evaluated at each Ψ and A_{max} is the maximum A over the full range of SWP.

For each supply function of Tr, the leaf temperature is calculated from radiation, wind speed and air temperature following a flux-gradient equation. The leaf to air vapor pressure deficit is then determined, followed by the canopy conductance, ultimately used for the internal CO_2 concentration in the gain function. Overall, the model requires environmental drivers, hydraulic cost and photosynthetic gain parameters (see Table 1 in Sperry *et al.* (2017)). Among the parameters specific to the hydraulic cost, only the shape of the vulnerability curve and k_{max} need to be set to a specific value (b is set by k_{max}, and k_{max} is set by V_{cmax}). No other parameters is specie or PFT-specific.

At each fixed instant for a given set of environmental drivers, a family of water potential response curves is generated by the model, representing steady state values. The plant can only be on one single point among all the possibilities. The profit (Pr) maximization criterion solve all these possibilities by maximizing the difference between the photosynthetic gain ($\Omega(\Psi)$) and the hydraulic cost ($\Pi(\Psi)$) (Wolf *et al.*, 2016; Sperry *et al.*, 2017):

$$Pr = max(\Omega(\Psi) - \Pi(\Psi)) \tag{7.14}$$

which occurs when the partial derivative of $\Omega(\Psi)$ and $\Pi(\Psi)$ are equal. This maximum difference occurs at a unique Ψ in the plant, which gives a set of model solutions at the corresponding instant and defines a hydraulic safety margin for maximizing carbon gains and minimizing hydraulic failure. The influence of soil water availability is considered in the model through changes in SWP which directly influences the rhizosphere water potential, resulting in a smaller optimal plant potential and a smaller stomatal conductance (Fig. 7.8).

The 'profit-maximization' approach applied to the 'cost-gain' theory in plant hydraulics does not require any calibration of empirical factors related to SWC on SOL or NSOL. Instead, only few plant traits (e.g., k_{max}) need to be calibrated on measurements of stomatal conductance, or determined by in situ measurements. SWC data can be converted into SWP by SWRC and fed in the model to predict plant response to drought. While the gain function is well identified (i.e., carbon gain through photosynthesis), many optimization models have been developed in the past years, where the 'cost' function has been associated to a parabola function of leaf water potential (Wolf *et al.*, 2016) or to a reduction of photosynthetic capacities (Dewar *et al.*, 2018). Finally, Joshi *et al.* (2022) set the profit-maximization hypothesis as the benefit from photosynthetic assimilation minus the costs of maintaining the photosynthetic capacities and the hydraulic pathway. This latter study yielded particularly good performances for predicting carbon assimilation, stomatal conductance and photosynthetic capacities under progressive soil drying (Joshi *et al.*, 2022).

These approaches provide undoubtedly a more realistic representation of plant responses to drought. However, do they outperform empirical approaches? In a broad review testing the performances of twelve empirical and optimization approaches, Sabot

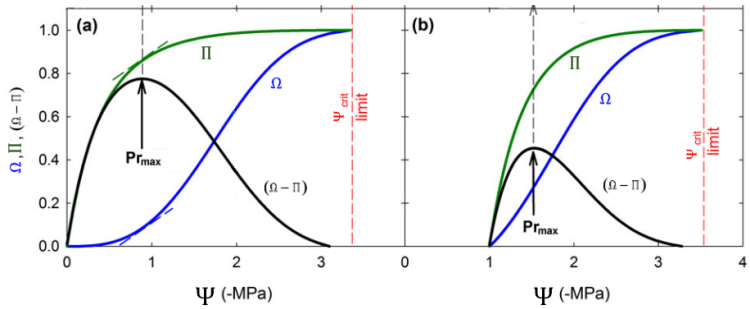

Figure 7.8: The hydraulic cost function (Ω, blue) is the fractional loss of hydraulic conductance that is calculated from the supply function $Tr(\Psi)$. The gain function (Π, green) is the fractional increase in A that is calculated from the $A(\Psi)$ curve. The maximum profit is reached when the derivative of $\Omega - \Pi$ function is null. At this point, stomata are assumed to maintain the plant at the optimum. The corresponding Ψ solution is used to calculate leaf temperature, leaf VPD, A, Tr, internal CO_2 concentration and stomatal conductance. The second panel (b) describes a situation when soil water potential shifts from 0 MPa (panel a) to -1 MPa (panel b). The optimal Ψ solution becomes more negative, and the six parameters mentioned previously decrese correspondingly. Adapted from Sperry *et al.* (2017).

et al. (2022) highlighted that five optimization schemes (including the profit maximization model described above) showed slightly better performances than the USO model for predicting leaf-level stomatal conductance. While the inclusion of plant hydraulics and the profit-maximization approach generally improves the modeling of vegetation gas exchanges (Bonan *et al.*, 2014; Eller *et al.*, 2020; Kennedy *et al.*, 2019; Sabot *et al.*, 2020), it comes at a high computational cost (Prentice *et al.*, 2015). In addition, the parameters of the vulnerability curves are difficult to measure because (i) they are typically measured at a single SPAC component and do not reflect the behavior of the whole plant, and (ii) they remain highly variable across species and PFTs (Couvreur *et al.*, 2018). Modifying g_1 of V_{cmax} by β, either as a function of SWC or SWP (TUZET *et al.*, 2003; Zhou *et al.*, 2013; Anderegg *et al.*, 2017), still remains the most widely used method while yielding reasonably good results (Blyth *et al.*, 2021; Paschalis *et al.*, 2020). More studies are needed to test and implement these novel approaches in LSMs (Blyth *et al.*, 2021; Sabot *et al.*, 2022).

3.5. Canopy-scale mesophyll conductance

Characterizing the response of mesophyll conductance to meteorological drivers remains an important model deficiency in LSMs (Knauer *et al.*, 2020). As g_m is related to the electron transport rate, it could be estimated by using the mechanistic representation of the light reactions of photosynthesis provided by the MLR model (Eq. 1.42, chapter 6). Therefore, joint measurements of SIF and GPP at the ecosystem scale holds great promises for estimating g_m at a high temporal and large spatial resolution.

In particular, G_m (canopy-scale g_m) could be estimated from SIF and GPP as follows:

$$G_m = \frac{GPP}{C_i - \frac{\Gamma^*(J_{SIF} + 8GPP)}{J_{SIF} - 8GPP}} \tag{7.15}$$

where C_i is canopy-scale CO_2 concentration in substomatal cavities and is a function of canopy conductance to water vapor and GPP (see chapter 4). Therefore, using joint measurements of GPP and SIF at the ecosystem scale could also provide REW-response curves of NSOL based on automatic SIF measurements. This would certainly help in disentangling the role of mesophyll conductance in limiting CO_2 supply, reducing LSMs uncertainties, and engineering mesophyll conductance to improve photosynthesis under water stress (Nguyen *et al.*, 2023; Lundgren & Fleming, 2020).

3.6. Estimating R_{ECO} from NEE and SIF

By relying solely on meteorological drivers and SIF, the MLR model also represents an interesting approach for separating NEE into GPP and R_{ECO}. For now, EC data post-processing pipelines use either the NT or DT partitioning methods to estimate R_{ECO} and GPP from NEE (Reichstein *et al.*, 2005; Lasslop *et al.*, 2012; Pastorello *et al.*, 2020). As detailed in chapter 6 and section 2.1, these methods present some key uncertainties. Recent studies have used either machine learning algorithms (Zhan *et al.*, 2022) or empirical methods (Kira *et al.*, 2021) to determine R_{ECO} from NEE and SIF, which led to a significant improvement of R_{ECO} estimates under water stress and high temperatures. By using the MLR model for GPP and NEE measurements, R_{ECO} can be determined as:

$$R_{ECO} = NEE + \frac{C_c - \Gamma^*}{4C_c + 8\Gamma^*} \frac{q_L \, SIF_{TOT} \, \phi_{PSII,max}(1 + k_{DF})}{1 - \phi_{PSII,max}} \tag{7.16}$$

3.7. Versatility of the MLR-USO model: integrating the complexity of heterogeneous canopies

As listed in section 1.2, several key limitations remain for a use of the MLR-USO model on other ecosystems and at larger scales. In a recent study, Chen *et al.* (2024c) proposed an adaptation of the MLR model on three evergreen needleleaf forests in Canada (site code CA-Obs), United States (US-NR1) and South Korea (KR-TCK). SIF observations were collected by a PhotoSpec spectrometer at 26 m height (at CA-Obs and US-NR1) and by a QE-Pro spectrometer at 40 m height (at KR-ICK). The MLR model was implemented into a layered, a two-leaf and a layered-two-leaf model.

In the MLR model (Eq. 1.43), several parameters are expected to show a strong spatial variability within the canopy, notably q_L (which is related to leaf light absorption proprieties) and C_i (which is related to both stomatal and photosynthetic dynamics).

The most straightforward approach consists in assuming that the q_L light-response curve is the same for all the leaves of the canopy whatever their light exposure. The alternative is to measure q_L light response curves at different depth within the canopy, or on sunlit and shaded leaves. In addition, the origin of the SIF signal must be attributed to each of these different canopy components. Overall, the light distribution and the SIF emission within the canopy must be described.

3.7.1. The layered MLR model

In the layered model, the PAR within each layer i is calculated from top-of-canopy PAR following Chen *et al.* (2024c):

$$PAR_i = PAR\, e^{-\frac{0.5\ \Omega_{Cl}\ LAI_{ai}}{\cos(SZA)}} \tag{7.17}$$

with SZA the solar zenith angle, LAI_{ai} the accumulated leaf area index from the top to layer i, and Ω_{Cl} the clumping index (i.e., characterizing the clumping of leaves within the canopy). These two parameters are related to canopy structure and are expected to be PFT-specific and to vary throughout the growing season. This model therefore requires time series of Ω_{Cl}, which can be retrieved from RS data (Chen *et al.*, 2024c) or measured at the field scale (Liang *et al.*, 2023). Eq. 7.17 can be used to determine q_L using either a single or multiple light-response curves. Instead of using a temperature-response curve, half-hourly C_i can be estimated from a PAR-based relationship as these two variables are expected to be strongly correlated (Beauclaire *et al.*, 2023a). The decomposition of SIF emission within the canopy is described by dividing top-of-canopy SIF_{TOT} as:

$$SIF_{TOT,i} = SIF_{TOT} \frac{APAR_i\ \phi_{SIF,i}}{\sum_i^n APAR_i\ \phi_{SIF,i}} \tag{7.18}$$

where n is the number of layers, $APAR_i$ is calculated as the difference between the PAR in layer $i+1$ and the PAR in the layer i (Eq. 7.17, and $\phi_{SIF,i}$ is determined from a nonlinear function with PAR_i (Liu *et al.*, 2021). This layered version requires measurements of PAR and SIF at the top-of-canopy, as well as of the clumping index Ω_{Cl} and the LAI. The total GPP is then calculated as the sum of all GPP in each i-th layer within the canopy.

3.7.2. The two-leaf MLR model

The two-leaf MLR model categorizes the leaves according to their light exposure (either shaded or sunlit) (Chen *et al.*, 2024c). The decomposition of the SIF signal is based on Eq. 7.18 with $APAR$ divided into a sun and a shade component:

$$APAR_{sun} = (1-a)\ PAR_{sun}\ LAI_{sun} \tag{7.19}$$

$$APAR_{shade} = (1-a)\ PAR_{shade}\ LAI_{shade} \tag{7.20}$$

with a the leaf albedo. The calculation of PAR_{shade},LAI_{shade}, PAR_{sun} and LAI_{sun} is detailed in Chen *et al.* (1999). The total GPP is then calculated as the sum of all GPP from sunlit and shaded leaves.

These models provide estimates of q_L that vary with leaf exposure or canopy depth (Fig. 7.9). Overall, these two models are expected to outperform the 'big leaf' model (Chen *et al.*, 2024c). Much work remains to be done, specifically for broadleaf forests typical of Western Europe. In addition, the understorey and midstorey are expected to strongly contribute to the measured SIF signal (Morozumi *et al.*, 2023b; Hornero *et al.*, 2021). This must be considered in the future versions of the model for a broader use on forest ecosystems.

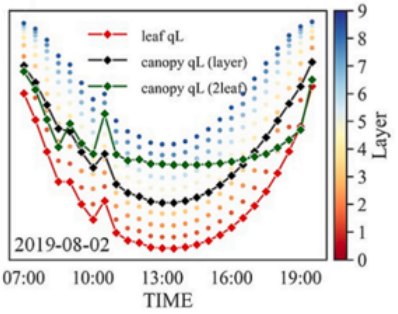

Figure 7.9: The diurnal patterns of 'big leaf' q_L (red lines), canopy-scale q_L from the layered model (black lines), canopy-scale q_L from the two-leaf model (green lines), and the q_L in different layers of the canopy (colored scatters). The colour of the dots represents the layer index, and the larger number represents the deeper location within the canopy. The LAI of each layer in this figure can be calculated as total LAI/10 with 10 being the total number of layers (Chen *et al.*, 2024c).

3.8. Versatility of the MLR-USO model: from the field to larger scales with RS SIF

3.8.1. The first global GPP product based on the MLR model

In the perspective of using the MLR model at larger scales with satellite-based SIF, very interesting results are provided by a recent study of Chen *et al.* (2024b) who applied the MLR model with TROPOSIF dataset (Guanter *et al.*, 2021) to estimate GPP (defined as the CMLR GPP product) from May 2018 to September 2021, and validated their estimates using ground-based GPP from 293 flux sites. The authors used the 'big leaf' version of the MLR model where q_L was parameterized by a machine learning techniques which consisted of (i) calculating q_L from Eq. 1.43 using measured ground based GPP and RS TROPOMI SIF, and (ii) taking 70% of the dataset to train a machine learning model using several explanatory variables such as VPD, NDVI, or PAR. The CMLR GPP dataset showed comparable performances when compared to other SIF-based GPP products. While relying on 'big leaf' assumptions and an empirical parameterization for q_L, their approach provides global maps of GPP with the MLR model at a 0.05° spatial resolution (Fig. 7.10). A significant improvement of the GPP product could be provided by sub-daily SIF data which would allow to track short-term responses of ecosystem functioning to climate drivers. In that case, the 'big leaf' underlying hypothesises are not likely to hold (Chen *et al.*, 2024b).

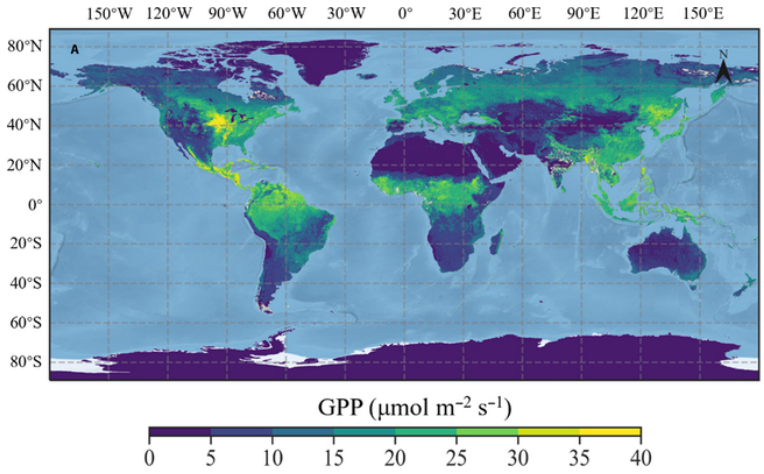

Figure 7.10: Global map of CMLR SIF-based GPP using the MLR model on 29 July 2019 at a 0.05° resolution (Chen *et al.*, 2024b).

3.8.2. Geostationary satellites for tracking sub-daily dynamics of plant gas exchanges

For now, the majority of RS SIF products are provided by satellites in sun-synchronous orbits. These data are either too coarse or with a long revisit time, which does not allow a detection of early stress responses of vegetation to drought. The most precise RS SIF measurement will be provided by FLEX (0.09 km² spatial resolution) but comes to an expanse of a long revisit time (27 days) (Fig. 7.11). The optimal temporal scale for an early detection of stress effects on vegetation is at the sub-daily timescale where short-term responses of plants to meteorological drivers can be monitored (e.g., midday stomatal closure, or day-to-day downregulation of photosynthetic capacities).

Alternatively, an existing fleet of satellites have the capability in studying plant functioning on a sub-daily basis (Xiao *et al.*, 2021). To date, a few of them sample the Earth reflectance in the far-red region, which is suitable for measuring SIF. These are: Orbiting Carbon Observatory-3 (OCO-3) (low-Earth orbit), Tropospheric Emission Monitoring of POllution (TEMPO) (geostationary) and Sentinel-4 (geostationary) (note that GeoCarb was supposed to be launched in 2024 but was cancelled by the NASA in November 2022). OCO-3 is currently onboard ISS and has been providing SIF measurements during the day above the tropics (i.e., between 52°N-52°S) since August 2019 (Taylor *et al.*, 2020). OCO-3 SIF strongly correlates with OCO-2 SIF, and therefore with tower-based GPP and SIF across multiple PFT and climate zones (Li *et al.*, 2018a). However, OCO-3 observations are not continuous for a given location (Taylor *et al.*, 2020). TEMPO has been originally designed for air pollution monitoring over North America and was launched in early 2022 (Zoogman *et al.*, 2017). Finally, ESA Sentinel-4 (embarked upon Meteosat Third Generation-Sounder (MTG-S)) is a pay-

load with an ultra-violet visible near infrared spectrometer providing hourly sampling over Europe (Quesada-Ruiz *et al.*, 2020) to be launched in September 2024. As being very new geostationary satellite missions, most of exploring results are not yet published. They however hold great hopes for understanding the diurnal cycling of plant functioning and ecosystem processes (Li *et al.*, 2023b; Zoogman *et al.*, 2017). These data will open up new perspectives for unravelling the responses of vegetation under edaphic droughts or heatwaves from satellite measurements. The MLR model is going to be play a key role for interpreting these data in the near future.

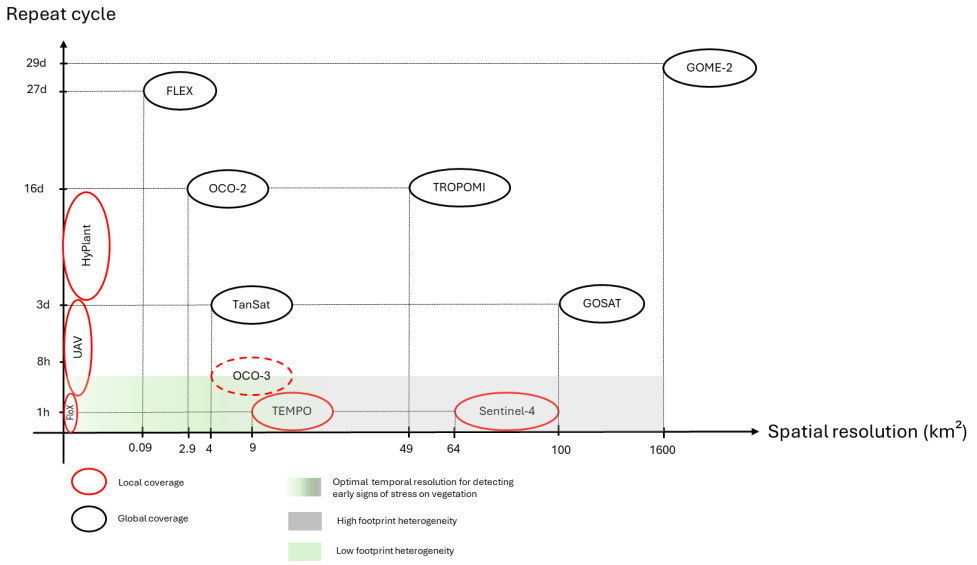

Figure 7.11: Spatial and temporal resolution of SIF measurement systems. The colorbar ranges from dark grey to light green representing high to low footprint heterogeneity. The optimal resolution range for capturing short-term responses of vegetation to stress is in the green area. The size of circles is indicative. The scale of the axes is not proportional. OCO-3 sampling at a particular geolocation varies across all hours of the day at absolute latitudes less than $\sim 52°$. Spatial resolutions and repeat cycles are taken from Mohammed *et al.* (2019) and Doughty *et al.* (2022).

3.8.3. Alternative RS products : monitoring vegetation temperature and heat dissipation

Within the infrared spectral regions, some other geostationary and low-Earth orbit satellites also have the capability for measuring the energy emitted by the Earth surface by sampling the 3-14 μm range (also known as Thermal InfraRed (TIR)). All bodies at a temperature above 273 K emit radiation which is related to their temperature (Liang & Wang, 2020). As a result, RS of TIR can be used to retrieve the Land Surface Temperature (LST), which is an important variable within the Earth's climate system

and an indicator of the energy and water exchange between the atmosphere and the land surface (Li *et al.*, 2023c). LST can be used to determine drought indexes such as the vegetation health index, which is very efficient for detecting vegetation droughts (Zeng *et al.*, 2023). Numerous applications in agricultural sciences also exist, such as monitoring of plant diseases and crop yields (Khanal *et al.*, 2017). The ECOsystem Spaceborne Thermal Radiometer Experiment on Space Station (ECOSTRESS) satellite provides LST with a pixel size 70 m several times a day. These measurements provide key information for farmers an forest managers such as a hourly monitoring of vegetation yellowing due to drought at an unprecedented precision, both in terms of spatial and temporal resolution (Xiao *et al.*, 2021). ECOSTRESS also provides estimates of evapotranspiration from energy budget-based models using LST (Kalma *et al.*, 2008). Recent studies have also applied a machine learning algorithm trained on meteorological variables and land cover to predict GPP from ECOSTRESS LST (Li *et al.*, 2021b), or to reconstruct global SIF datasets at a meter-range spatial resolution (Zhang *et al.*, 2023a). Nonetheless, SIF remains a better proxy of GPP as being directly related to carbon assimilation processes.

SIF is not the only hyperspectral variable to be strongly linked to short-term variations of GPP. In particular, the energy dissipated by heat through mostly the xantophyll cycle at hourly scales is an important element in the energy dissipation pathways. When plants experience very high sun irradiance, photochemical quenching solely is not sufficient for dissipating the incoming energy. This excessive amount is dissipated mostly by the de-epoxidation of violaxanthin into zeaxanthin via antheraxanthin in the xantophyll cycle (Demmig-Adams & Adams III, 2006), which is included into what is referred to as NPQ. The rapid response of the xantophyll cycle allows photochemistry to keep operating at very high PAR flux densities. For nearly three decades, it is known that the activity of the xantophyll cycle can be monitored by the Photochemical Reflectance Index (PRI), which is derived from reflectance at 531 nm (reduced by deepoxidation of xanthophyll pigments) and a reference wavelength (typically 570 nm) (Penuelas *et al.*, 1995). PRI is strongly correlated to vegetation LUE and GPP at the sub-daily timescale (Garbulsky *et al.*, 2011), and can capture a wide range of vegetation responses to environmental conditions (Yang *et al.*, 2020a; Mulero *et al.*, 2023; Zhang *et al.*, 2017; Magney *et al.*, 2016). However, interpreting PRI measurements at the seasonal scale might be complicated by its sensitivity to canopy structure or carotene content (Garbulsky *et al.*, 2011). Yet, PRI is very effective for capturing subdaily temporal dynamics of NPQ which reveals the control of abiotic stresses (e.g., soil moisture, or high irradiance) on GPP. As the response of SIF to water stress or heatwaves still remains unclear (see chapter 6), this specific characteristic of PRI has been exploited to improve empirical SIF-GPP models specifically under water stress (Ma *et al.*, 2022; Wang *et al.*, 2020a; Schickling *et al.*, 2016). The strong correlation between PRI and V_{cmax} has also been highlighted (Chou *et al.*, 2020; Yu *et al.*, 2020b) which opens up new perspectives for mapping this parameter at large scales

or for assimilating PRI in the FvCB model. Current RS products provide daily PRI from Moderate Resolution Imaging Spectroradiometer (MODIS) (Gamon *et al.*, 2016; Vanikiotis *et al.*, 2021) or Environmental Mapping and Analysis Program (EnMAP) (Dotzler *et al.*, 2015) with a spatial resolution of 1 km and 30 m respectively. Importantly, what is currently lacking is a mechanistic modeling framework for using both PRI and SIF to estimate GPP. While we showed that SIF was likely responsive to dry soil conditions (chapter 6), future studies should explore the possibility to use PRI as a stress indicator, notably in the MLR model.

3.9. Assessing vegetation water status with RS of microwave observations

Besides LWP, Vegetation Water Content (VWC) is also an important physiological indicators to assess plant water conditions. VWC can be measured either by destructive methods (e.g., by measuring the weight difference of the sample before and after drying in a heat chamber; Zhou *et al.* (2021)) or by non-destructive methods (e.g., terahertz radiation (Li *et al.*, 2020), electrical impedance spectroscopy (Serrano-Finetti *et al.*, 2023), hyperspesctral spectroscopy (Junttila *et al.*, 2022), or microwaves (Calla *et al.*, 2008)). Destructive methods are time-consuming, lead to perturbations of the vegetation as the leaf must be removed from the plant before being analyzed, and cannot provide an estimation of VWC of large patches of vegetation. Such approaches do not allow to track short-term variations of VWC at diurnal scales.

The mains advantage of VWC is its ability for being monitored by RS techniques. In particular, microwaves strongly interact with the dielectric proprieties of soil and vegetation (Jackson, 1993; Jackson & Schmugge, 1991). When considering remote sensing of soil and vegetation moisture, two types of sensors coexist. Radiometers measure the intensity of the natural thermal emission of a land surface (i.e., the emissivity - passive method) and have a coarse spatial resolution that increases with frequency. Typical radiometers spatial resolution is in the 10-100 km range. Radars measure the backscattering coefficient of a land surface from the power ratio between the emitted and returned electromagnetic wave (i.e., the reflectivity - active method). Synthetic aperture radars (SAR) use a radar technique that can provide finer spatial resolution (in the meter range). Such instruments only perform measurements during a very small fraction of their orbit around Earth because of the high energy demand of the SAR technique (Grasso *et al.*, 2021). Flying SAR instruments in tandem overcomes this issue (e.g., SAR onboard Sentinel-1). Dozens of passive and active microwave satellites have been operating over the past decades, with very different characteristics of band frequency, repeat cycle and spatial resolution (Mavrovic *et al.*, 2023). The most recent satellite microwave missions are Soil Moisture and Ocean Salinity (SMOS) and Soil Moisture Active Passive (SMAP) (passive only, the radar onboard SMAP experienced failure 208 days after launching), as well as Advanced SCATterometer (ASCAT) and

SAR-Sentinel (radar) (Mazzariello *et al.*, 2023).

The penetration of microwaves within the land surface depends on their band frequency (the longer the microwave, the deeper the penetration). Therefore, microwave measurements include the signal of different components such as vegetation, soil, snow and atmosphere (Kerr *et al.*, 2012). Disentangling the complexity of this raw signal requires the use of radiative transfer models which calculate scattering, reflection and attenuation of the electromagnetic waves of the different components of the surface. The degree of attenuation of the microwave by the vegetation (i.e., the Vegetation Optical Depth (VOD)) is related to various attenuation and scattering factors such as vegetation structure, water content or sensor wavelength (Jagdhuber *et al.*, 2019).

VOD was originally considered as a noise in the microwave signal, but it recently gained interest as a promising ecological indicator linked to plant hydraulics (Konings *et al.*, 2019). Spaceborne passive and active microwave sensors have been used to provide VOD at large scales since the 1970s (Owe *et al.*, 2008; Frappart *et al.*, 2020). Recent studies have derived long-term VOD products from multiple sensors in the Ku-band (19 GHz), X-band (10.7 GHz) and C-band (6.9 GHz) (Moesinger *et al.*, 2020; Hu *et al.*, 2023; Liu *et al.*, 2023). L-band VOD from SMAP and SMOS is expected to be more correlated with dense ecosystem physiology than X-band or C-band VOD (Chaparro *et al.*, 2019).

Early *in situ* measurements on soybean have highlighted a strong linearity between VOD and VWC (Jackson & Schmugge, 1991), later confirmed on many species at the diurnal scale (e.g., Xu *et al.* (2021b); van Emmerik *et al.* (2015)). However, the covariation of VOD with AboveGround Biomass (AGB) and Vegetation Relative Water Content (VRWC) complicates the interpretability of microwave measurements at large temporal and/or spatial scales. For instance, Tian *et al.* (2017) showed that seasonal variations in VOD were influenced by changes in forest phenology and vegetation water status. Therefore, the link between VOD and vegetation water status is strongly influenced by biomass changes (Konings *et al.*, 2019). However, the role of AGB in explaining VOD dynamics can be reduced at temporal scales when AGB variations are negligible. Many studies have used this approach to derive vegetation water status from VOD retrieved from tower-based or satellite microwave measurements (Momen *et al.*, 2017; Konings & Gentine, 2017; van Emmerik *et al.*, 2017). The reverse route (isolating the effect of vegetation water status for assessing biomass changes) is however more complicated (Konings *et al.*, 2019).

Notwithstanding the key recent advances in monitoring VOD, several limitations remain. First, the validation of RS VOD data has not yet been achieved as ground measurements are very limited. In this perspective, the use of affordable microwave sensors on the ground could be very helpful for validating satellite-based VOD products. For instance, Humphrey & Frankenberg (2023) and Yao *et al.* (2024) have shown that Global Navigation Satellite Systems (GNSS) can be used at the ecosystem scale

to capture sub-daily dynamics of VOD and canopy water content of forests. Such validation campaigns are required for assessing the accuracy of RS VOD products. In addition, the temporal and spatial frequency of microwave satellite measurements is one of main constraint on providing a VOD product that can be linked to plant physiology and to gas exchanges. For instance, satellites in sun-synchronous orbits such as SMOS provide a measurement at 6 AM and 6 PM (local time) every 3 days (Al-Yaari *et al.*, 2017). Assessing ecosystem responses to drought requires joint measurements of SIF and VOD at a sub-daily resolution to capture the dynamics of photosynthesis limiting factors such as stomatal closure through changes in LWP (Zhang *et al.*, 2019b). Monitoring such processes at a high frequency with radar geostationary satellites potentially has a direct implication for forecasting crop yields and forest fire risks (Nolan *et al.*, 2020; Konings *et al.*, 2021; Jackson *et al.*, 2004).

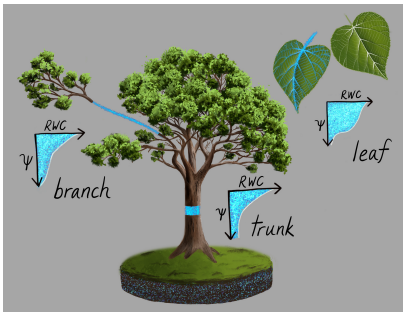

Figure 7.12: As VOD scales with VWC, retrieving plant water potential from VOD requires a vertical distributions of tissue-specific water retention properties through VRWC curves. ψ is the vegetation water potential within each tree structural units (Konings *et al.*, 2021).

Finally, linking VOD to trends in vegetation water status is not straightforward. In particular, the relationship between VOD and VWC actually varies with the time of day, the location of the emission source within the canopy (e.g., leaves, trunk or branches) and the water status of the vegetation. Most existing modeling approaches for retrieving VOD (e.g., zeroth-order radiative transfer model or water cloud models for radiometer and radar-based measurements, (Jagdhuber *et al.*, 2019)) represents the vegetation as a single water reservoir without disentangling the different structural units of the canopy. Future retrieval algorithms including a more mechanistic representation of microwave dynamics in vegetation with a description of ecosystem structure would help in estimating the VWC at different heights within the canopy (Konings *et al.*, 2021; Steele-Dunne *et al.*, 2017). This would be particularly helpful for describing the hydraulic constraints along the SPAC and deciphering the driving forces of the water flow under water stress (Konings *et al.*, 2021). Characterizing Vegetation Water Retention Curves (VWRC) which link VWC to plant water potential throughout the canopy is also needed (Fig. 7.12).

Importantly, the combination of SIF and VOD at the sub-daily timescale provides a window on the health of terrestrial ecosystems by combining information on photosynthetic activity and VWC, which are two major drivers of the carbon and water cycles. The MLR-USO model is placed at the core of this thematic as a key tool for linking plant hydraulics and carbon assimilation. By being a proxy of VWC and LWP, VOD can capture the diel cycle of stomatal conductance which directly influences the CO_2

availability to chloroplasts and the transpiration flux. Future studies should focus on adapting the MLR-USO model for assimilating SIF and VOD products at a sub-daily timescale.

4. General conclusion

The outcomes of this thesis show that, more than ever, delving into the complexity of the intertwined processes ruling ecosystem responses to a changing climate requires the coordination of different research teams involved in monitoring the soil and plant water status, performing flux analysis, characterizing root system, and collecting proximal/remote sensing measurements of hyperspectral variables. The development of these areas of research should be structured around EC stations, which provide the gold benchmark for greenhouse gases and energy fluxes measurements at the canopy level. We encourage the creation of a data portal where proximal sensing measurements are made available for researchers similarly to the ICOS network. This perspective is currently explored in the United States (Pierrat *et al.*, 2023) while China has moved forward with the creation in 2021 of the ChinaSpec network regrouping 26 sites (Zhang *et al.*, 2021). We also advocate for the constitution of complementary research teams and an improved cooperation between research centers. With several EC sites spanning across different PFTs, the BIODYNE department has a key role to play. Future research projects or equipment funds should be focused on measuring root biomass density, acquiring field spectrometers, microwave sensors or microtensiometers for durable, permanent installation at measurement sites. Future PhDs could be orientated towards these research topics. Considerable, but no less exciting challenges lie ahead.

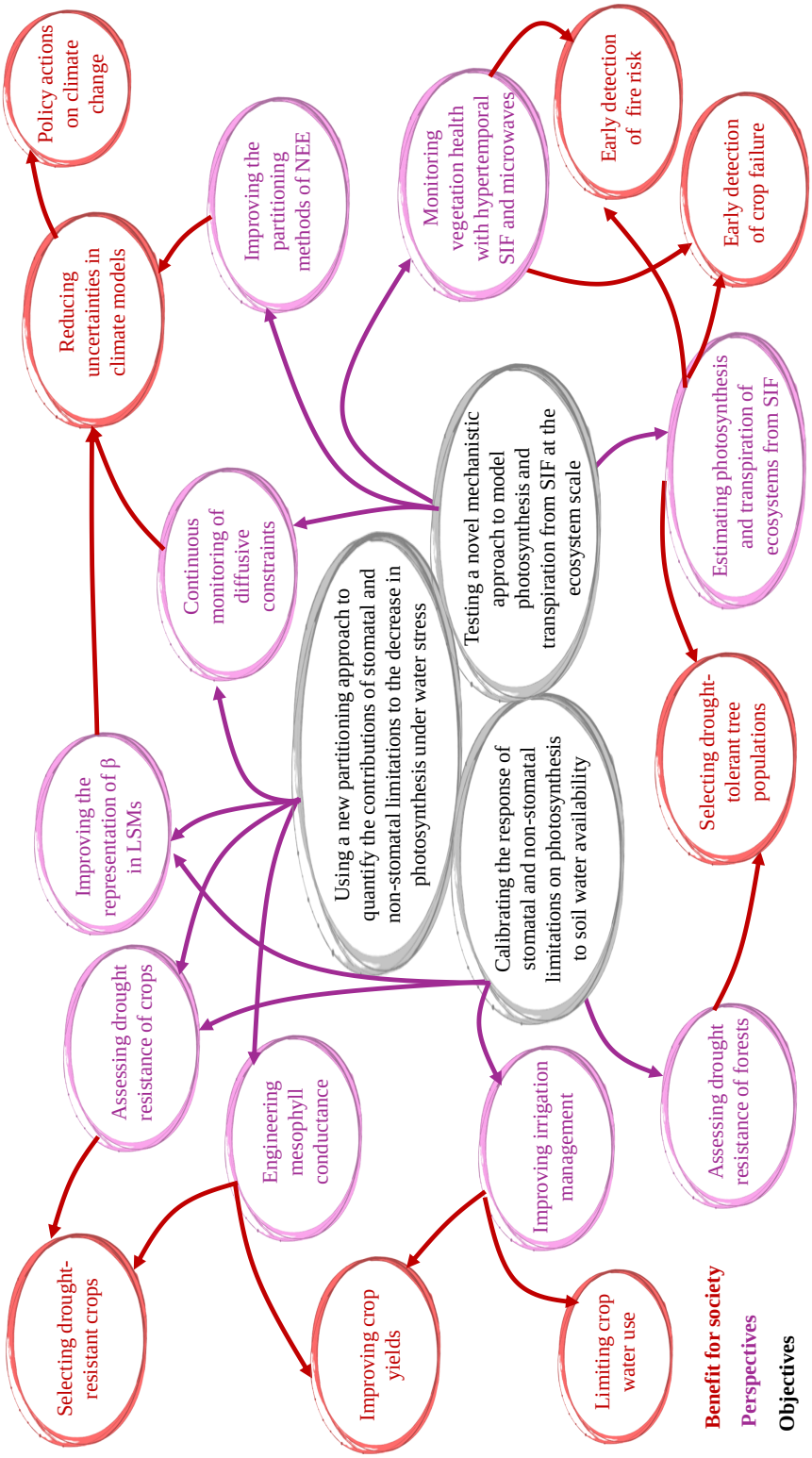

Figure 7.13: Perspectives of the thesis

Bibliography

AALBERS, E. E., VAN MEIJGAARD, E., LENDERINK, G., DE VRIES, H., & VAN DEN HURK, B. J. J. M. 2023. The 2018 west-central European drought projected in a warmer climate: how much drier can it get? *Natural Hazards and Earth System Sciences*, **23**(5), 1921–1946.

AGEE, ELIZABETH, HE, LINGLI, BISHT, GAUTAM, COUVREUR, VALENTIN, SHAHBAZ, PARISA, MEUNIER, FÉLICIEN, GOUGH, CHRISTOPHER M., MATHENY, ASHLEY M., BOHRER, GIL, & IVANOV, VALERIY. 2021. Root lateral interactions drive water uptake patterns under water limitation. *Advances in Water Resources*, **151**, 103896.

AGUILOS, MARICAR, STAHL, CLÉMENT, BURBAN, BENOIT, HÉRAULT, BRUNO, COURTOIS, ELODIE, COSTE, SABRINA, WAGNER, FABIEN, ZIEGLER, CAMILLE, TAKAGI, KENTARO, & BONAL, DAMIEN. 2019. Interannual and Seasonal Variations in Ecosystem Transpiration and Water Use Efficiency in a Tropical Rainforest. *Forests*, **10**(1).

AKKAMIS, MUSTAFA, & CALISKAN, SEVGI. 2023. Responses of yield, quality and water use efficiency of potato grown under different drip irrigation and nitrogen levels. *Scientific Reports*, **13**(1), 9911.

AL-YAARI, A., WIGNERON, J.-P., KERR, Y., RODRIGUEZ-FERNANDEZ, N., O'NEILL, P.E., JACKSON, T.J., DE LANNOY, G.J.M., AL BITAR, A., MIALON, A., RICHAUME, P., WALKER, J.P., MAHMOODI, A., & YUEH, S. 2017. Evaluating soil moisture retrievals from ESA's SMOS and NASA's SMAP brightness temperature datasets. *Remote Sensing of Environment*, **193**, 257–273.

ALI, ZULFIQAR, MERRIUM, SABAH, HABIB-UR RAHMAN, MUHAMMAD, HAKEEM, SADIA, SADDIQUE, MUHAMMAD ABU BAKAR, & SHER, MUHAMMAD ALI. 2022. Wetting mechanism and morphological adaptation; leaf rolling enhancing atmospheric water acquisition in wheat crop—a review. *Environmental Science and Pollution Research*, **29**(21), 30967–30985.

ALICHE, ERNEST B., PRUSOVA-BOURKE, ALENA, RUIZ-SANCHEZ, MARIAM, OORTWIJN, MARIAN, GERKEMA, EDO, VAN AS, HENK, VISSER, RICHARD G. F., & VAN DER LINDEN, C. GERARD. 2020. Morphological and physiological responses of the potato stem transport tissues to dehydration stress. *Planta*, **251**(2), 45.

ALLAN, RICHARD P., BARLOW, MATHEW, BYRNE, MICHAEL P., CHERCHI, ANNALISA, DOUVILLE, HERVÉ, FOWLER, HAYLEY J., GAN, THIAN Y., PENDERGRASS, ANGELINE G., ROSENFELD, DANIEL, SWANN, ABIGAIL L. S., WILCOX, LAURA J., & ZOLINA, OLGA. 2020. Advances in understanding large-scale responses of the water cycle to climate change. *Annals of the New York Academy of Sciences*, **1472**(1), 49–75. _eprint: https://nyaspubs.onlinelibrary.wiley.com/doi/pdf/10.1111/nyas.14337.

ALLEN, R. G., & OF THE UNITED NATIONS, FOOD AND AGRICULTURE ORGANIZATION (eds). 1998. *Crop evapotranspiration: guidelines for computing crop water requirements*. FAO irrigation and drainage paper, no. 56. Rome: Food and Agriculture Organization of the United Nations.

ALLEN, RICHARD, PEREIRA, L., RAES, DIRK, & SMITH, M. 1998. FAO Irrigation and drainage paper No. 56. *Rome: Food and Agriculture Organization of the United Nations*, **56**(01), 26–40.

ALVAR-BELTRÁN, JORGE, SATURNIN, COULIBALY, GRÉGOIRE, BAKI, CAMACHO, JOSE LUÍS, DAO, ABDALLA, MIGRAINE, JEAN BAPTISTE, & MARTA, ANNA DALLA. 2023. Using AquaCrop as a decision-support tool for improved irrigation management in the Sahel region. *Agricultural Water Management*, **287**, 108430.

AMOROS-LOPEZ, J., GOMEZ-CHOVA, L., VILA-FRANCES, J., ALONSO, L., CALPE, J., MORENO, J., & DEL VALLE-TASCON, S. 2008. Evaluation of remote sensing of vegetation fluorescence by the analysis of diurnal cycles. *International Journal of Remote Sensing*, **29**(17-18), 5423–5436.

ANDEREGG, WILLIAM R. L., WOLF, ADAM, ARANGO-VELEZ, ADRIANA, CHOAT, BRENDAN, CHMURA, DANIEL J., JANSEN, STEVEN, KOLB, THOMAS, LI, SHAN, MEINZER, FREDERICK, PITA, PILAR, RESCO DE DIOS, VÍCTOR, SPERRY, JOHN S., WOLFE, BRETT T., & PACALA, STEPHEN. 2017. Plant water potential improves prediction of empirical stomatal models. *PLOS ONE*, **12**(10), 1–17.

ANDEREGG, WILLIAM R. L., TRUGMAN, ANNA T., BOWLING, DAVID R., SALVUCCI, GUIDO, & TUTTLE, SAMUEL E. 2019. Plant functional traits and climate influence drought intensification and land–atmosphere feedbacks. *Proceedings of the National Academy of Sciences*, **116**(28), 14071–14076.

APRILE, ALESSIO, HAVLICKOVA, LENKA, PANNA, RICCARDO, MARÈ, CATERINA, BORRELLI, GRAZIA M, MARONE, DANIELA, PERROTTA, CARLA, RAMPINO, PATRIZIA, DE BELLIS, LUIGI, CURN, VLADISLAV, MASTRANGELO, ANNA M, RIZZA, FULVIA, & CATTIVELLI, LUIGI. 2013. Different stress responsive strategies to drought and heat in two durum wheat cultivars with contrasting water use efficiency. *BMC Genomics*, **14**(1), 821.

ARCHONTOULIS, SOTIRIOS V., & MIGUEZ, FERNANDO E. 2015. Nonlinear Regression Models and Applications in Agricultural Research. *Agronomy Journal*, **107**(2), 786–798.

AROCA, R., PORCEL, R., & RUIZ-LOZANO, J. M. 2012. Regulation of root water uptake under abiotic stress conditions. *Journal of Experimental Botany*, **63**(1), 43–57.

ATHERTON, JON, ZHANG, CHAO, OIVUKKAMÄKI, JAAKKO, KULMALA, LIISA, XU, SHAN, HAKALA, TEEMU, HONKAVAARA, EIJA, MACARTHUR, ALASDAIR, & PORCAR-CASTELL, ALBERT. 2022. What Does the NDVI Really Tell Us About Crops? Insight from Proximal Spectral Field Sensors. *Pages 251–265 of:* BOCHTIS, DIONYSIS D., LAMPRIDI, MARIA, PETROPOULOS, GEORGE P., AMPATZIDIS, YIANNIS, & PARDALOS, PANOS (eds), *Information and Communication Technologies for Agriculture—Theme I: Sensors*. Cham: Springer International Publishing.

ATI, ALAA S., IYADA, AMMAR DAHAM, & NAJIM, SALAH M. 2012. Water use efficiency of potato (Solanum tuberosum L.) under different irrigation methods and potassium fertilizer rates. *Annals of Agricultural Sciences*, **57**(2), 99–103.

AUBINET, M., MOUREAUX, C., BODSON, B., DUFRANNE, D., HEINESCH, B., SULEAU, M., VANCUTSEM, F., & VILRET, A. 2009. Carbon sequestration by a crop over a 4-year sugar beet/winter wheat/seed potato/winter wheat rotation cycle. *Agricultural and Forest Meteorology*, **149**(3-4), 407–418.

AUBINET, MARC. 2023. The known unknowns: Measurement techniques. *Pages 59–100 of: Conceptual Boundary Layer Meteorology*. Elsevier.

AUBINET, MARC, GRELLE, ACHIM, IBROM, ANDREAS, RANNIK, ÜLLAR, MONCRIEFF, JOHN, FOKEN, THOMAS, KOWALSKI, ANDY S, MARTIN, PHILIPPE H, BERBIGIER, PAUL, BERNHOFER, CH, *et al.* 1999. Estimates of the annual net carbon and water exchange of forests: the EUROFLUX methodology. *Pages 113–175 of: Advances in ecological research*, vol. 30. Elsevier.

AUBINET, MARC, VESALA, TIMO, & PAPALE, DARIO (eds). 2012. *Eddy Covariance: A Practical Guide to Measurement and Data Analysis*. Dordrecht: Springer Netherlands.

AUBINET, MARC, HURDEBISE, QUENTIN, CHOPIN, HENRI, DEBACQ, ALAIN, DE LIGNE, ANNE, HEINESCH, BERNARD, MANISE, TANGUY, & VINCKE, CAROLINE. 2018. Inter-annual variability of Net Ecosystem Productivity for a temperate mixed forest: A predominance of carry-over effects? *Agricultural and Forest Meteorology*, **262**, 340–353.

BACHOFEN, CHRISTOPH, TUMBER-DÁVILA, SHERSINGH JOSEPH, MACKAY, D. SCOTT, MCDOWELL, NATE G., CARMINATI, ANDREA, KLEIN, TAMIR, STOCKER, BENJAMIN D., MENCUCCINI, MAURIZIO, & GROSSIORD, CHARLOTTE. 2024. Tree water uptake patterns across the globe. *New Phytologist*, **242**(5), 1891–1910.

BACHY, A., AUBINET, M., SALERNO, G., SCHOON, N., AME-LYNCK, C., BODSON, B., MOUREAUX, C., & HEINESCH, B. 2013. Long-term measurements of volatile organic compounds exchanges above a maize field at Lonzee (Belgium). *Communications in agricultural and applied biological sciences*, **78**(1), 127–132. Place: Belgium.

BACOUR, C., MAIGNAN, F., MACBEAN, N., PORCAR-CASTELL, A., FLEXAS, J., FRANKENBERG, C., PEYLIN, P., CHEVALLIER, F., VUICHARD, N., & BASTRIKOV, V. 2019. Improving Estimates of Gross Primary Productivity by Assimilating Solar-Induced Fluorescence Satellite Retrievals in a Terrestrial Biosphere Model Using a Process-Based SIF Model. *Journal of Geophysical Research: Biogeosciences*, **124**(11), 3281–3306. Publisher: John Wiley & Sons, Ltd.

BADGLEY, GRAYSON, FIELD, CHRISTOPHER B., & BERRY, JOSEPH A. 2017. Canopy near-infrared reflectance and terrestrial photosynthesis. *Science Advances*, **3**(3), e1602244.

BAI, JIA, ZHANG, HELIN, SUN, RUI, LI, XING, XIAO, JINGFENG, & WANG, YAN. 2022. Estimation of global GPP from GOME-2 and OCO-2 SIF by considering the dynamic variations of GPP-SIF relationship. *Agricultural and Forest Meteorology*, **326**(Nov.), 109180.

BAILLIE, ALICE L., & FLEMING, ANDREW J. 2020. The developmental relationship between stomata and mesophyll airspace. *New Phytologist*, **225**(3), 1120–1126.

BAKER, NEIL R. 2008. Chlorophyll Fluorescence: A Probe of Photosynthesis In Vivo. *Annual Review of Plant Biology*, **59**(1), 89–113.

BALDOCCHI, DENNIS. 2014. Measuring fluxes of trace gases and energy between ecosystems and the atmosphere - the state and future of the eddy covariance method. *Global Change Biology*, **20**(12), 3600–3609.

BALDOCCHI, DENNIS, FALGE, EVA, GU, LIANHONG, OLSON, RICHARD, HOLLINGER, DAVID, RUNNING, STEVE, ANTHONI, PETER, BERNHOFER, CH, DAVIS, KENNETH, EVANS, ROBERT, FUENTES, JOSE, GOLDSTEIN, ALLEN, KATUL, GABRIEL, LAW, BEVERLY, LEE, XUHUI, MALHI, YADVINDER, MEYERS, TILDEN, MUNGER, WILLIAM, OECHEL, WALT, PAW, K. T., PILEGAARD,

KIM, SCHMID, H. P., VALENTINI, RICCARDO, VERMA, SHASHI, VESALA, TIMO, WILSON, KELL, & WOFSY, STEVE. 2001. FLUXNET: A New Tool to Study the Temporal and Spatial Variability of Ecosystem–Scale Carbon Dioxide, Water Vapor, and Energy Flux Densities. *Bulletin of the American Meteorological Society*, **82**(11), 2415–2434.

BALDOCCHI, DENNIS D. 2020. How eddy covariance flux measurements have contributed to our understanding of *Global Change Biology*. *Global Change Biology*, **26**(1), 242–260.

BALL, J. TIMOTHY, WOODROW, IAN E., & BERRY, JOSEPH A. 1987. A Model Predicting Stomatal Conductance and its Contribution to the Control of Photosynthesis under Different Environmental Conditions. *Pages 221–224 of:* BIGGINS, J. (ed), *Progress in Photosynthesis Research: Volume 4 Proceedings of the VIIth International Congress on Photosynthesis Providence, Rhode Island, USA, August 10–15, 1986*. Dordrecht: Springer Netherlands.

BARBOUR, MARGARET M., EVANS, JOHN R., SIMONIN, KEVIN A., & VON CAEMMERER, SUSANNE. 2016. Online CO2 and H2O oxygen isotope fractionation allows estimation of mesophyll conductance in C4 plants, and reveals that mesophyll conductance decreases as leaves age in both C4 and C3 plants. *New Phytologist*, **210**(3), 875–889.

BEAUCLAIRE, QUENTIN, DE CANNIÈRE, SIMON, JONARD, FRANÇOIS, & LONGDOZ, BERNARD. 2023a (May). *Mechanistic modelling of gross primary production and latent heat flux using SIF observations in different water and light limitation conditions*. other. display.

BEAUCLAIRE, QUENTIN, HEINESCH, BERNARD, & LONGDOZ, BERNARD. 2023b. Non-stomatal processes are responsible for the decrease in gross primary production of a potato crop during edaphic drought. *Agricultural and Forest Meteorology*, **343**(Dec.), 109782.

BEER, CHRISTIAN, REICHSTEIN, MARKUS, TOMELLERI, ENRICO, CIAIS, PHILIPPE, JUNG, MARTIN, CARVALHAIS, NUNO, RÖDENBECK, CHRISTIAN, ARAIN, M. ALTAF, BALDOCCHI, DENNIS, BONAN, GORDON B., BONDEAU, ALBERTE, CESCATTI, ALESSANDRO, LASSLOP, GITTA, LINDROTH, ANDERS, LOMAS, MARK, LUYSSAERT, SEBASTIAAN, MARGOLIS, HANK, OLESON, KEITH W., ROUPSARD, OLIVIER, VEENENDAAL, ELMAR, VIOVY, NICOLAS, WILLIAMS, CHRISTOPHER, WOODWARD, F. IAN, & PAPALE, DARIO. 2010. Terrestrial Gross Carbon Dioxide Uptake: Global Distribution and Covariation with Climate. *Science*, **329**(5993), 834–838.

BEILLOUIN, DAMIEN, SCHAUBERGER, BERNHARD, BASTOS, ANA, CIAIS, PHILLIPE, & MAKOWSKI, DAVID. 2020. Impact of extreme weather conditions on European crop production in 2018. *Philosophical Transactions of the Royal Society B: Biological Sciences*, **375**(1810), 20190510.

BELAL, ABDEL-AZIZ, EL-RAMADY, HASSAN R., MOHAMED, ELSAYED S., & SALEH, AHMED M. 2014. Drought risk assessment using remote sensing and GIS techniques. *Arabian Journal of Geosciences*, **7**(1), 35–53.

BERMÚDEZ-CARDONA, MARIA BIANNEY, FILHO, JOÃO AMÉRICO WORDELL, & RODRIGUES, FABRÍCIO ÁVILA. 2015. Leaf Gas Exchange and Chlorophyll *a* Fluorescence in Maize Leaves Infected with *Stenocarpella macrospora*. *Phytopathology®*, **105**(1), 26–34.

BERNACCHI, C., DIAZ-ESPEJO, A., & FLEXAS, J. 2012. Gas-exchange analysis: basics and problems. *Pages 115–130 of:* FLEXAS, JAUME, LORETO, FRANCESCO, & MEDRANO, HIPÓLITOEDITORS (eds), *Terrestrial Photosynthesis in a Changing Environment: A Molecular, Physiological, and Ecological Approach*. Cambridge University Press.

BERNACCHI, C. J., SINGSAAS, E. L., PIMENTEL, C., PORTIS JR, A. R., & LONG, S. P. 2001. Improved temperature response functions for models of Rubisco-limited photosynthesis: *In vivo* Rubisco enzyme kinetics. *Plant, Cell & Environment*, **24**(2), 253–259.

BERNACCHI, CARL J., PORTIS, ARCHIE R., NAKANO, HIROMI, VON CAEMMERER, SUSANNE, & LONG, STEPHEN P. 2002. Temperature Response of Mesophyll Conductance. Implications for the Determination of Rubisco Enzyme Kinetics and for Limitations to Photosynthesis in Vivo. *Plant Physiology*, **130**(4), 1992–1998.

BERNIER, P.Y., BRÉDA, N., GRANIER, A., RAULIER, F., & MATHIEU, F. 2002. Validation of a canopy gas exchange model and derivation of a soil water modifier for transpiration for sugar maple (Acer saccharum Marsh.) using sap flow density measurements. *Forest Ecology and Management*, **163**(1), 185–196.

BERTOLINO, LÍGIA T., CAINE, ROBERT S., & GRAY, JULIE E. 2019. Impact of Stomatal Density and Morphology on Water-Use Efficiency in a Changing World. *Frontiers in Plant Science*, **10**(Mar.), 225.

BEST, M. J., PRYOR, M., CLARK, D. B., ROONEY, G. G., ESSERY, R. L. H., MÉNARD, C. B., EDWARDS, J. M., HENDRY, M. A., PORSON, A., GEDNEY, N., MERCADO, L. M., SITCH, S., BLYTH, E., BOUCHER, O., COX, P. M., GRIMMOND, C. S. B., & HARDING, R. J. 2011. The Joint UK Land Environment Simulator (JULES), model description – Part 1: Energy and water fluxes. *Geoscientific Model Development*, **4**(3), 677–699.

BHARATH, PULIMAMIDI, GAHIR, SHASHIBHUSHAN, & RAGHAVENDRA, AGEPATI S. 2021. Abscisic Acid-Induced Stomatal Closure: An Important Component of Plant Defense Against Abiotic and Biotic Stress. *Frontiers in Plant Science*, **12**(Mar.), 615114.

BITTELLI, MARCO. 2010. Measuring Soil Water Potential for Water Management in Agriculture: A Review. *Sustainability*, **2**(5), 1226–1251.

BITTELLI, MARCO, SALVATORELLI, FIORENZO, & PISA, PAOLA ROSSI. 2008. Correction of TDR-based soil water content measurements in conductive soils. *Geoderma*, **143**(1), 133–142.

BLANKENAGEL, SONJA, YANG, ZHENYU, AVRAMOVA, VIKTORIYA, SCHÖN, CHRIS-CAROLIN, & GRILL, ERWIN. 2018. Generating Plants with Improved Water Use Efficiency. *Agronomy*, **8**(9), 194.

BLANKENSHIP, ROBERT E. 2002. *Molecular mechanisms of photosynthesis*. Oxford ; Malden, MA: Blackwell Science. OCLC: ocm49273347.

BLUM, ABRAHAM, & TUBEROSA, ROBERTO. 2018. Dehydration survival of crop plants and its measurement. *Journal of Experimental Botany*, **69**(5), 975–981.

BLYTH, ELEANOR M., ARORA, VIVEK K., CLARK, DOUGLAS B., DADSON, SIMON J., DE KAUWE, MARTIN G., LAWRENCE, DAVID M., MELTON, JOE R., PONGRATZ, JULIA, TURTON, RACHAEL H., YOSHIMURA, KEI, & YUAN, HUA. 2021. Advances in Land Surface Modelling. *Current Climate Change Reports*, **7**(2), 45–71.

BOAS, THERESA, BOGENA, HEYE, GRÜNWALD, THOMAS, HEINESCH, BERNARD, RYU, DONGRYEOL, SCHMIDT, MARIUS, VEREECKEN, HARRY, WESTERN, ANDREW, & HENDRICKS FRANSSEN, HARRIE-JAN. 2021. Improving the representation of cropland sites in the Community Land Model (CLM) version 5.0. *Geoscientific Model Development*, **14**(1), 573–601.

BOGUSZEWSKA-MAŃKOWSKA, D., PIECZYŃSKI, M., WYRZYKOWSKA, A., KALAJI, H. M., SIECZKO, L., SZWEYKOWSKA-KULIŃSKA, Z., & ZAGDAŃSKA, B. 2018. Divergent strategies displayed by potato (Solanum tuberosum L.) cultivars to cope with soil drought. *Journal of Agronomy and Crop Science*, **204**(1), 13–30. Publisher: John Wiley & Sons, Ltd.

BONAN, G. B., WILLIAMS, M., FISHER, R. A., & OLESON, K. W. 2014. Modeling stomatal conductance in the earth system: linking leaf water-use efficiency and water transport along the soil–plant–atmosphere continuum. *Geoscientific Model Development*, **7**(5), 2193–2222.

BONAN, GORDON B., PATTON, EDWARD G., FINNIGAN, JOHN J., BALDOCCHI, DENNIS D., & HARMAN, IAN N. 2021. Moving beyond the incorrect but useful paradigm: reevaluating big-leaf and multilayer plant canopies to model biosphere-atmosphere fluxes – a review. *Agricultural and Forest Meteorology*, **306**(Aug.), 108435.

BOWLING, DAVID R., SARGENT, STEVE D., TANNER, BERT D., & EHLERINGER, JAMES R. 2003. Tunable diode laser absorption spectroscopy for stable isotope studies of ecosystem–atmosphere CO2 exchange. *Agricultural and Forest Meteorology*, **118**(1), 1–19.

BOYER, J. S., WONG, S. C., & FARQUHAR, G. D. 1997. CO2 and Water Vapor Exchange across Leaf Cuticle (Epidermis) at Various Water Potentials. *Plant Physiology*, **114**(1), 185–191.

BOYER, JOHN S. 2015a. Impact of cuticle on calculations of the CO2 concentration inside leaves. *Planta*, **242**(6), 1405–1412.

BOYER, JOHN S. 2015b. Turgor and the transport of CO2 and water across the cuticle (epidermis) of leaves. *Journal of Experimental Botany*, **66**(9), 2625–2633.

BOYER, JOHN S., & KAWAMITSU, YOSHINOBU. 2011. Photosynthesis Gas Exchange System with Internal CO2 Directly Measured. *Environmental Control in Biology*, **49**(4), 193–207.

BREDA, N. J. J. 2003. Ground-based measurements of leaf area index: a review of methods, instruments and current controversies. *Journal of Experimental Botany*, **54**(392), 2403–2417.

BREUSCH, T. S., & PAGAN, A. R. 1979. A Simple Test for Heteroscedasticity and Random Coefficient Variation. *Econometrica*, **47**(5), 1287.

BRODDRICK, JARED T., WARE, MAXWELL A., JALLET, DENIS, PALSSON, BERNHARD O., & PEERS, GRAHAM. 2022. Integration of physiologically relevant photosynthetic energy flows into whole genome models of light-driven metabolism. *The Plant Journal*, **112**(3), 603–621.

BRODRIBB, T. 1996. Dynamics of Changing Intercellular CO2 Concentration (ci) during Drought and Determination of Minimum Functional ci. *Plant physiology*, **111**(1), 179–185. Place: United States.

BRODRIBB, T. J., HOLBROOK, N. M., EDWARDS, E. J., & GUTIERREZ, M. V. 2003. Relations between stomatal closure, leaf turgor and xylem vulnerability in eight tropical dry forest trees. *Plant, Cell & Environment*, **26**(3), 443–450.

BROOKS, ROYAL HARVARD, & COREY, ARTHUR T. 1966. Properties of porous media affecting fluid flow. *Journal of the irrigation and drainage division*, **92**(2), 61–88.

BRÁS, TERESA ARMADA, SEIXAS, JÚLIA, CARVALHAIS, NUNO, & JÄGERMEYR, JONAS. 2021. Severity of drought and heatwave crop losses tripled over the last five decades in Europe. *Environmental Research Letters*, **16**(6), 065012.

BRÉDA, N., GRANIER, A., BARATAUD, F., & MOYNE, C. 1995. Soil water dynamics in an oak stand: I. Soil moisture, water potentials and water uptake by roots. *Plant and Soil*, **172**(1), 17–27.

BRÉDA, NATHALIE, HUC, ROLAND, GRANIER, ANDRÉ, & DREYER, ERWIN. 2006. Temperate forest trees and stands under severe drought: a review of ecophysiological responses, adaptation processes and long-term consequences. *Annals of Forest Science*, **63**(6), 625–644.

BUCKLEY, THOMAS N. 2019. How do stomata respond to water status? *New Phytologist*, **224**(1), 21–36.

BUCKLEY, THOMAS N., & MOTT, KEITH A. 2013. Modelling stomatal conductance in response to environmental factors: Modelling stomatal conductance. *Plant, Cell & Environment*, **36**(9), 1691–1699.

BUCKLEY, THOMAS N, SACK, LAWREN, & FARQUHAR, GRAHAM D. 2017. Optimal plant water economy. *Plant, Cell & Environment*, **40**(6), 881–896.

BUMAN, BASTIAN, HUENI, ANDREAS, COLOMBO, ROBERTO, COGLIATI, SERGIO, CELESTI, MARCO, JULITTA, TOMMASO, BURKART, ANDREAS, SIEGMANN, BASTIAN, RASCHER, UWE, DRUSCH, MATTHIAS, & DAMM, ALEXANDER. 2022. Towards consistent assessments of in situ radiometric measurements for the validation of fluorescence satellite missions. *Remote Sensing of Environment*, **274**(June), 112984.

BURBA, G. 2021. *Eddy covariance method: for scientific, regulatory, and commercial applications*. Lincoln, Nebraska: LI-COR Biosciences. OCLC: 1378273189.

BURBA, G G, MCDERMITT, D K, ANDERSON, D J, FURTAW, M D, & ECKLES, R D. 2010. Novel design of an enclosed CO2/H2O gas analyser for eddy covariance flux measurements.

BURBA, GEORGE. 2019. Illustrative Maps of Past and Present Eddy Covariance Measurement Locations: II. High-Resolution Images. 08.

BURNHAM, KENNETH P., ANDERSON, DAVID RAYMOND, & BURNHAM, KENNETH P. 2002. *Model selection and multimodel inference: a practical information-theoretic approach*. 2nd ed edn. New York: Springer. OCLC: ocm48557578.

BURNHAM, KENNETH P., ANDERSON, DAVID R., & HUYVAERT, KATHRYN P. 2011. AIC model selection and multimodel inference in behavioral ecology: some background, observations, and comparisons. *Behavioral Ecology and Sociobiology*, **65**(1), 23–35.

BUSCH, FLORIAN A. 2020. Photorespiration in the context of Rubisco biochemistry, CO_2 diffusion and metabolism. *The Plant Journal*, **101**(4), 919–939.

BUSCH, FLORIAN A., SAGE, ROWAN F., & FARQUHAR, GRAHAM D. 2017. Plants increase CO2 uptake by assimilating nitrogen via the photorespiratory pathway. *Nature Plants*, **4**(1), 46–54.

BUSCH, FLORIAN A., HOLLOWAY-PHILLIPS, MEISHA, STUART-WILLIAMS, HILARY, & FARQUHAR, GRAHAM D. 2020. Revisiting carbon isotope discrimination in C3 plants shows respiration rules when photosynthesis is low. *Nature Plants*, **6**(3), 245–258.

BUYSSE, PAULINE, BODSON, BERNARD, DEBACQ, ALAIN, DE LIGNE, ANNE, HEINESCH, BERNARD, MANISE, TANGUY, MOUREAUX, CHRISTINE, & AUBINET, MARC. 2017. Carbon budget measurement over 12 years at a crop production site in the silty-loam region in Belgium. *Agricultural and Forest Meteorology*, **246**(Nov.), 241–255.

BYRNE, MICHAEL P., & O'GORMAN, PAUL A. 2015. The Response of Precipitation Minus Evapotranspiration to Climate Warming: Why the "Wet-Get-Wetter, Dry-Get-Drier" Scaling Does Not Hold over Land*. *Journal of Climate*, **28**(20), 8078–8092.

CABAL, CIRO, DE DEURWAERDER, HANNES PT, & MATESANZ, SILVIA. 2021. Field methods to study the spatial root density distribution of individual plants. *Plant and Soil*, **462**, 25–43.

CAI, GAOCHAO, AHMED, MUTEZ A., ABDALLA, MOHANNED, & CARMINATI, ANDREA. 2022. Root hydraulic phenotypes impacting water uptake in drying soils. *Plant, Cell & Environment*, **45**(3), 650–663.

CALLA, O.P.N., BOHRA, DINESH, VYAS, RAJESH, PUROHIT, BHAWANI SHANKAR, PRASHER, RAKESH, LOOMBA, ABHISHEK, & KUMAR, NAVEEN. 2008. Measurement of soil moisture using microwave radiometer. *Pages 621–624 of: 2008 International Conference on Recent Advances in Microwave Theory and Applications*. Jaipur, Rajasthan, India: IEEE.

CAMINO, CARLOS, GONZALEZ-DUGO, VICTORIA, HERNANDEZ, PILAR, & ZARCO-TEJADA, PABLO J. 2019. Radiative transfer Vcmax estimation from hyperspectral imagery and SIF retrievals to assess photosynthetic performance in rainfed and irrigated plant phenotyping trials. *Remote Sensing of Environment*, **231**(Sept.), 111186.

CANO, F. JAVIER, SÁNCHEZ-GÓMEZ, DAVID, RODRÍGUEZ-CALCERRADA, JESÚS, WARREN, CHARLES R., GIL, LUIS, & ARANDA, ISMAEL. 2013. Effects of drought on mesophyll conductance and photosynthetic limitations at different tree canopy layers: Limitations to carbon uptake into the canopy. *Plant, Cell & Environment*, May, n/a–n/a.

CARMINATI, ANDREA, & JAVAUX, MATHIEU. 2020. Soil Rather Than Xylem Vulnerability Controls Stomatal Response to Drought. *Trends in plant science*, **25**(9), 868–880. Place: England.

CENDRERO-MATEO, WIENEKE, DAMM, ALONSO, PINTO, MORENO, GUANTER, CELESTI, ROSSINI, SABATER, COGLIATI, JULITTA, RASCHER, GOULAS, AASEN, PACHECO-LABRADOR, & ARTHUR. 2019. Sun-Induced Chlorophyll Fluorescence III: Benchmarking Retrieval Methods and Sensor Characteristics for Proximal Sensing. *Remote Sensing*, **11**(8), 962.

CENDRERO-MATEO, M. PILAR, CARMO-SILVA, A. ELIZABETE, PORCAR-CASTELL, ALBERT, HAMERLYNCK, ERIK P., PAPUGA, SHIRLEY A., & MORAN, M. SUSAN. 2015. Dynamic response of plant chlorophyll fluorescence to light, water and nutrient availability. *Functional Plant Biology*, **42**(8), 746.

CHANG, CHRISTINE Y., GUANTER, LUIS, FRANKENBERG, CHRISTIAN, KÖHLER, PHILIPP, GU, LIANHONG, MAGNEY, TROY S., GROSSMANN, KATJA, & SUN, YING. 2020. Systematic Assessment of Retrieval Methods for Canopy Far-Red Solar-Induced Chlorophyll Fluorescence Using High-Frequency Automated Field Spectroscopy. *Journal of Geophysical Research: Biogeosciences*, **125**(7), e2019JG005533. _eprint: https://agupubs.onlinelibrary.wiley.com/doi/pdf/10.1029/2019JG005533.

CHANG, CHRISTINE Y., WEN, JIAMING, HAN, JIMEI, KIRA, OZ, LEVONNE, JULIE, MELKONIAN, JEFFREY, RIHA, SUSAN J., SKOVIRA, JOSEPH, NG, SHARON, GU, LIANHONG, WOOD, JEFFREY D., NÄTHE, PAUL, & SUN, YING. 2021. Unpacking the drivers of diurnal dynamics of sun-induced chlorophyll fluorescence (SIF): Canopy structure, plant physiology, instrument configuration and retrieval methods. *Remote Sensing of Environment*, **265**(Nov.), 112672.

CHANG, HEEJUN, & BONNETTE, MATTHEW RYAN. 2016. Climate change and water-related ecosystem services: impacts of drought in california, usa. *Ecosystem Health and Sustainability*, **2**(12), e01254.

CHANG, TIAN-GEN, SHI, ZAI, ZHAO, HONGLONG, SONG, QINGFENG, HE, ZHONGHU, VAN RIE, JEROEN, DEN BOER, BART, GALLE, ALEXANDER, & ZHU, XIN-GUANG. 2022. 3dCAP-Wheat: An Open-Source Comprehensive Computational Framework Precisely Quantifies Wheat Foliar, Non-foliar, and Canopy Photosynthesis. *Plant Phenomics*, **2022**(Jan.), 2022/9758148.

CHAPARRO, DAVID, DUVEILLER, GRÉGORY, PILES, MARIA, CESCATTI, ALESSANDRO, VALL-LLOSSERA, MERCÈ, CAMPS, ADRIANO, & ENTEKHABI, DARA. 2019. Sensitivity of L-band vegetation optical depth to carbon stocks in tropical forests: a comparison to higher frequencies and optical indices. *Remote Sensing of Environment*, **232**(Oct.), 111303.

CHAVARRIA, GERALDO, & DOS SANTOS, HENRIQUE PESSOA. 2012. Plant Water Relations: Absorption, Transport and Control Mechanisms. *Chap. 5 of:* MONTANARO, GIUSEPPE, & DICHIO, BARTOLOMEO (eds), *Advances in Selected Plant Physiology Aspects*. Rijeka: IntechOpen.

CHAVES, M M, FLEXAS, J, & PINHEIRO, CARLA. 2009. Photosynthesis under drought and salt stress: regulation mechanisms from whole plant to cell. *Annals of botany*, **103**(4), 551–560.

CHEN, BIN, CHEN, JING M., BALDOCCHI, DENNIS D., LIU, YANG, WANG, SHAOQIANG, ZHENG, TING, BLACK, T.A., & CROFT, HOLLY. 2019a. Including soil water stress in process-based ecosystem models by scaling down maximum carboxylation rate using accumulated soil water deficit. *Agricultural and Forest Meteorology*, **276-277**(Oct.), 107649.

CHEN, HAN, LI, HAN, WEI, YIZHAO, MCBEAN, EDWARD, LIANG, HONG, WANG, WEIMIN, & HUANG, JINHUI JEANNE. 2024a. Partitioning eddy covariance CO2 fluxes into ecosystem respiration and gross primary productivity through a new hybrid four sub-deep neural network. *Agriculture, Ecosystems Environment*, **361**, 108810.

CHEN, JIDAI, LIU, XINJIE, DU, SHANSHAN, MA, YAN, & LIU, LIANGYUN. 2020. Integrating SIF and Clearness Index to Improve Maize GPP Estimation Using Continuous Tower-Based Observations. *Sensors*, **20**(9), 2493.

CHEN, JIDAI, LIU, XINJIE, DU, SHANSHAN, MA, YAN, & LIU, LIANGYUN. 2021. Effects of Drought on the Relationship Between Photosynthesis and Chlorophyll Fluorescence for Maize. *IEEE Journal of Selected Topics in Applied Earth Observations and Remote Sensing*, **14**, 11148–11161.

CHEN, J.M, LIU, J, CIHLAR, J, & GOULDEN, M.L. 1999. Daily canopy photosynthesis model through temporal and spatial scaling for remote sensing applications. *Ecological Modelling*, **124**(2), 99–119.

CHEN, RUONAN, LIU, LIANGYUN, LIU, XINJIE, & RASCHER, UWE. 2024b. CMLR: A Mechanistic Global GPP Dataset Derived from TROPOMIS SIF Observations. *Journal of Remote Sensing*, **4**, 0127.

CHEN, RUONAN, LIU, LIANGYUN, LIU, XINJIE, LIU, ZHUNQIAO, GU, LIANHONG, & RASCHER, UWE. 2024c. Improving estimates of sub-daily gross primary production from solar-induced chlorophyll fluorescence by accounting for light distribution within canopy. *Remote Sensing of Environment*, **300**(Jan.), 113919.

CHEN, XUEJUAN, MO, XINGGUO, HU, SHI, & LIU, SUXIA. 2019b. Relationship between fluorescence yield and photochemical yield under water stress and intermediate light conditions. *Journal of Experimental Botany*, **70**(1), 301–313.

CHIANG, FELICIA, MAZDIYASNI, OMID, & AGHAKOUCHAK, AMIR. 2021. Evidence of anthropogenic impacts on global drought frequency, duration, and intensity. *Nature Communications*, **12**(1), 2754.

CHOU, SHUREN, CHEN, BIN, CHEN, JING, WANG, MIAOMIAO, WANG, SHAOQIANG, CROFT, HOLLY, & SHI, QIN. 2020. Estimation of leaf photosynthetic capacity from the photochemical reflectance index and leaf pigments. *Ecological Indicators*, **110**, 105867.

CHRISTENSON, CLAY G., GOHARDOUST, MOHAMMAD R., CALLEJA, SEBASTIAN, THORP, KELLY R., TULLER, MARKUS, & PAULI, DUKE. 2024. Monitoring cotton water status with microtensiometers. *Irrigation Science*, Apr.

CHU, HOUSEN, BALDOCCHI, DENNIS D., JOHN, RANJEET, WOLF, SEBASTIAN, & REICHSTEIN, MARKUS. 2017. Fluxes all of the time? A primer on the temporal representativeness of FLUXNET: FLUXES ALL OF THE TIME? *Journal of Geophysical Research: Biogeosciences*, **122**(2), 289–307.

CHU, HOUSEN, LUO, XIANGZHONG, OUYANG, ZUTAO, CHAN, W. STEPHEN, DENGEL, SIGRID, BIRAUD, SÉBASTIEN C., TORN, MARGARET S., METZGER, STEFAN, KUMAR, JITENDRA, ARAIN, M. ALTAF, ARKEBAUER, TIM J., BALDOCCHI, DENNIS, BERNACCHI, CARL, BILLESBACH, DAVE, BLACK, T. ANDREW, BLANKEN, PETER D., BOHRER, GIL, BRACHO, ROSVEL, BROWN, SHANNON, BRUNSELL, NATHANIEL A., CHEN, JIQUAN, CHEN, XINGYUAN, CLARK, KENNETH, DESAI, ANKUR R., DUMAN, TOMER, DURDEN, DAVID, FARES, SILVANO, FORBRICH, INKE, GAMON, JOHN A., GOUGH, CHRISTOPHER M., GRIFFIS, TIMOTHY, HELBIG, MANUEL, HOLLINGER, DAVID, HUMPHREYS, ELYN, IKAWA, HIROKI, IWATA, HIROKI, JU, YANG, KNOWLES, JOHN F., KNOX, SARA H., KOBAYASHI, HIDEKI, KOLB, THOMAS, LAW, BEVERLY, LEE, XUHUI, LITVAK, MARCY, LIU, HEPING, MUNGER, J. WILLIAM, NOORMETS, ASKO, NOVICK, KIM, OBERBAUER, STEVEN F., OECHEL, WALTER, OIKAWA, PATTY, PAPUGA, SHIRLEY A., PENDALL, ELISE, PRAJAPATI, PRAJAYA, PRUEGER, JOHN, QUINTON, WILLIAM L, RICHARDSON, ANDREW D., RUSSELL, ERIC S., SCOTT, RUSSELL L., STARR, GREGORY, STAEBLER, RALF, STOY, PAUL C., STUART-HAËNTJENS, ELLEN, SONNENTAG, OLIVER, SULLIVAN, RYAN C., SUYKER, ANDY, UEYAMA, MASAHITO, VARGAS, RODRIGO, WOOD, JEFFREY D., & ZONA, DONATELLA. 2021. Representativeness of Eddy-Covariance flux footprints for areas surrounding AmeriFlux sites. *Agricultural and Forest Meteorology*, **301-302**(May), 108350.

CIAIS, PH., REICHSTEIN, M., VIOVY, N., GRANIER, A., OGÉE, J., ALLARD, V., AUBINET, M., BUCHMANN, N., BERNHOFER, CHR., CARRARA, A., CHEVALLIER, F., DE NOBLET, N., FRIEND, A. D., FRIEDLINGSTEIN, P., GRÜNWALD, T., HEINESCH, B., KERONEN, P., KNOHL, A., KRINNER, G., LOUSTAU, D., MANCA, G., MATTEUCCI, G., MIGLIETTA, F., OURCIVAL, J. M., PAPALE, D., PILEGAARD, K., RAMBAL, S., SEUFERT, G., SOUSSANA, J. F., SANZ, M. J., SCHULZE, E. D., VESALA, T., & VALENTINI, R. 2005. Europe-wide reduction in primary productivity caused by the heat and drought in 2003. *Nature*, **437**(7058), 529–533.

CLEGG, ROBERT M. 2004. Nuts and Bolts of Excitation Energy Migration and Energy Transfer. *Pages 83–105 of:* PAPAGEORGIOU, GEORGE CHRISTOS, & GOVINDJEE (eds), *Chlorophyll a Fluorescence: A Signature of Photosynthesis*. Dordrecht: Springer Netherlands.

CLOGG, CLIFFORD C., PETKOVA, EVA, & HARITOU, ADAMANTIOS. 1995. Statistical Methods for Comparing Regression Coefficients Between Models. *American Journal of Sociology*, **100**(5), 1261–1293.

COBLE, ADAM P, FOGEL, MARILYN L, & PARKER, GEOFFREY G. 2017. Canopy gradients in leaf functional traits for species that differ in growth strategies and shade tolerance. *Tree Physiology*, **37**(10), 1415–1425.

COCHARD, HERVÉ, PIMONT, FRANÇOIS, RUFFAULT, JULIEN, & MARTIN-STPAUL, NICOLAS. 2020. SurEau.c : a mechanistic model of plant water relations under extreme drought. *bioRxiv*.

COGLIATI, S., VERHOEF, W., KRAFT, S., SABATER, N., ALONSO, L., VICENT, J., MORENO, J., DRUSCH, M., & COLOMBO, R. 2015. Retrieval of sun-induced fluorescence using advanced spectral fitting methods. *Remote Sensing of Environment*, **169**(Nov.), 344–357.

COLLATZ, G.JAMES, BALL, J.TIMOTHY, GRIVET, CYRIL, & BERRY, JOSEPH A. 1991. Physiological and environmental regulation of stomatal conductance, photosynthesis and transpiration: a model that includes a laminar boundary layer. *Agricultural and Forest Meteorology*, **54**(2), 107–136.

CORNIC, GABRIEL, & MASSACCI, ANGELO. 2004. Leaf Photosynthesis Under Drought Stress. *Pages 347–366 of:* BAKER, NEIL R. (ed), *Photosynthesis and the Environment*, vol. 5. Dordrecht: Kluwer Academic Publishers. Series Title: Advances in Photosynthesis and Respiration.

COSH, MICHAEL H., JACKSON, THOMAS J., BINDLISH, RAJAT, FAMIGLIETTI, JAMES S., & RYU, DONGRYEOL. 2005. Calibration of an impedance probe for estimation of surface soil water content over large regions. *Journal of Hydrology*, **311**(1-4), 49–58.

COUSINS, ASAPH B., MULLENDORE, DANIEL L., & SONAWANE, BALASAHEB V. 2020. Recent developments in mesophyll conductance in C3, C4, and crassulacean acid metabolism plants. *The Plant Journal*, **101**(4), 816–830.

COUVREUR, VALENTIN, LEDDER, GLENN, MANZONI, STEFANO, WAY, DANIELLE A., MULLER, ERIK B., & RUSSO, SABRINA E. 2018. Water transport through tall trees: A vertically explicit, analytical model of xylem hydraulic conductance in stems. *Plant, Cell & Environment*, **41**(8), 1821–1839.

COWAN, I.R. 1978. Stomatal Behaviour and Environment. Advances in Botanical Research, vol. 4. Academic Press.

COWAN, IR, & FARQUHAR, GD. 1977. Stomatal function in relation to leaf metabolism and environment. *Symposia of the Society for Experimental Biology*, **31**, 471–505.

CRAUSBAY, SHELLEY D., RAMIREZ, AARON R., CARTER, SHAWN L., CROSS, MOLLY S., HALL, KIMBERLY R., BATHKE, DEBORAH J., BETANCOURT, JULIO L., COLT, STEVE, CRAVENS, AMANDA E., DALTON, MELINDA S., DUNHAM, JASON B., HAY, LAUREN E., HAYES, MICHAEL J., MCEVOY, JAMIE, MCNUTT, CHAD A., MORITZ, MAX A., NISLOW, KEITH H., RAHEEM, NEJEM, & SANFORD, TODD. 2017. Defining Ecological Drought for the Twenty-First Century. *Bulletin of the American Meteorological Society*, **98**(12), 2543 – 2550.

CROUS, KRISTINE Y., UDDLING, JOHAN, & DE KAUWE, MARTIN G. 2022. Temperature responses of photosynthesis and respiration in evergreen trees from boreal to tropical latitudes. *New Phytologist*, **234**(2), 353–374.

CRUZ DE CARVALHO, MARIA HELENA. 2008. Drought stress and reactive oxygen species: production, scavenging and signaling. *Plant Signaling & Behavior*, **3**(3), 156–165.

DAMM, ALEXANDER, ELBERS, JAN, ERLER, ANDRÉ, GIOLI, BENIAMINO, HAMDI, KARIM, HUTJES, RONALD, KOSVANCOVA, MARTINA, MERONI, MICHELE, MIGLIETTA, FRANCO, MOERSCH, ANDRÉ, MORENO, JOSE, SCHICKLING, ANKE, SONNENSCHEIN, RUTH, UDELHOVEN, THOMAS, VAN DER LINDEN, SEBASTIAN, HOSTERT, PATRICK, & RASCHER, UWE. 2010. Remote sensing of sun-induced fluorescence to improve modeling of diurnal courses of gross primary production (GPP). *Global Change Biology*, **16**(1), 171–186. Publisher: John Wiley & Sons, Ltd.

DAMOUR, GAËLLE, SIMONNEAU, THIERRY, COCHARD, HERVÉ, & URBAN, LAURENT. 2010. An overview of models of stomatal conductance at the leaf level: Models of stomatal conductance. *Plant, Cell & Environment*, July, no–no.

DARCY, H. 1856. *Les fontaines publiques de la ville de Dijon: exposition et application des principes à suivre et des formules à employer dans les questions de distribution d'eau*. Victor Dalmont.

DASGUPTA, PRAGNA, DAS, BHABANI S., & SEN, SOUMITRA K. 2015. Soil water potential and recoverable water stress in drought tolerant and susceptible rice varieties. *Agricultural Water Management*, **152**, 110–118.

DAVIES, WILLIAM J., KUDOYAROVA, GUZEL, & HARTUNG, WOLFRAM. 2005. Long-distance ABA Signaling and Its Relation to Other Signaling Pathways in the Detection of Soil Drying and the Mediation of the Plant's Response to Drought. *Journal of Plant Growth Regulation*, **24**(4), 285–295.

DE BLÉCOURT, M., GRÖNGRÖFT, A., THOMSEN, S., & ESCHENBACH, A. 2021. Temporal variation and controlling factors of tree water consumption in the thornbush savanna. *Journal of Arid Environments*, **189**, 104500.

DE CANNIÈRE, S., HERBST, M., VEREECKEN, H., DEFOURNY, P., & JONARD, F. 2021. Constraining water limitation of photosynthesis in a crop growth model with sun-induced chlorophyll fluorescence. *Remote Sensing of Environment*, **267**(Dec.), 112722.

DE CANNIÈRE, SIMON, VEREECKEN, HARRY, DEFOURNY, PIERRE, & JONARD, FRANÇOIS. 2022. Remote Sensing of Instantaneous Drought Stress at Canopy Level Using Sun-Induced Chlorophyll Fluorescence and Canopy Reflectance. *Remote Sensing*, **14**(11), 2642.

DE KAUWE, M. G., ZHOU, S.-X., MEDLYN, B. E., PITMAN, A. J., WANG, Y.-P., DUURSMA, R. A., & PRENTICE, I. C. 2015a. Do land surface models need to include differential plant species responses to drought? Examining model predictions across a mesic-xeric gradient in Europe. *Biogeosciences*, **12**(24), 7503–7518.

DE KAUWE, M. G., KALA, J., LIN, Y.-S., PITMAN, A. J., MEDLYN, B. E., DUURSMA, R. A., ABRAMOWITZ, G., WANG, Y.-P., & MIRALLES, D. G. 2015b. A test of an optimal stomatal conductance scheme within the CABLE land surface model. *Geoscientific Model Development*, **8**(2), 431–452.

DE KAUWE, MARTIN G., LIN, YAN-SHIH, WRIGHT, IAN J., MEDLYN, BELINDA E., CROUS, KRISTINE Y., ELLSWORTH, DAVID S., MAIRE, VINCENT, PRENTICE, I. COLIN, ATKIN, OWEN K., ROGERS, ALISTAIR, NIINEMETS, ÜLO, SERBIN, SHAWN P., MEIR, PATRICK, UDDLING, JOHAN, TOGASHI, HENRIQUE F., TARVAINEN, LASSE, WEERASINGHE, LASANTHA K., EVANS, BRADLEY J., ISHIDA, F. YOKO, & DOMINGUES, TOMAS F. 2016. A test of the 'one-point method' for estimating maximum carboxylation capacity from field-measured, light-saturated photosynthesis. *New Phytologist*, **210**(3), 1130–1144.

DE SWAEF, TOM, PIETERS, OLIVIER, APPELTANS, SIMON, BORRA-SERRANO, IRENE, COUDRON, WILLEM, COUVREUR, VALENTIN, GARRÉ, SARAH, LOOTENS, PETER, NICOLAÏ, BART, POLS, LEROI, SAINT CAST, CLÉMENT, ŠALAGOVIČ, JAKUB, VAN HAEVERBEKE, MAXIME, STOCK, MICHIEL, & WYFFELS, FRANCIS. 2022. On the pivotal role of water potential to model plant physiological processes. *in silico Plants*, **4**(1), diab038.

DECHANT, BENJAMIN, RYU, YOUNGRYEL, BADGLEY, GRAYSON, ZENG, YELU, BERRY, JOSEPH A., ZHANG, YONGGUANG, GOULAS, YVES, LI, ZHAOHUI, ZHANG, QIAN, KANG, MINSEOK, LI, JI,

& MOYA, ISMAËL. 2020. Canopy structure explains the relationship between photosynthesis and sun-induced chlorophyll fluorescence in crops. *Remote Sensing of Environment*, **241**(May), 111733.

DECHANT, BENJAMIN, RYU, YOUNGRYEL, BADGLEY, GRAYSON, KÖHLER, PHILIPP, RASCHER, UWE, MIGLIAVACCA, MIRCO, ZHANG, YONGGUANG, TAGLIABUE, GIULIA, GUAN, KAIYU, ROSSINI, MICOL, GOULAS, YVES, ZENG, YELU, FRANKENBERG, CHRISTIAN, & BERRY, JOSEPH A. 2022. NIRVP: A robust structural proxy for sun-induced chlorophyll fluorescence and photosynthesis across scales. *Remote Sensing of Environment*, **268**(Jan.), 112763.

DELANDMETER, MATHIEU, LÉONARD, JOËL, FERCHAUD, FABIEN, HEINESCH, BERNARD, MANISE, TANGUY, FAURÈS, ARIANE, BINDELLE, JÉRÔME, & DUMONT, BENJAMIN. 2023. A comprehensive analysis of CO2 exchanges in agro-ecosystems based on a generic soil-crop model-derived methodology. *Agricultural and Forest Meteorology*, **340**, 109621.

DEMMIG-ADAMS, BARBARA, & ADAMS III, WILLIAM W. 2006. Photoprotection in an ecological context: the remarkable complexity of thermal energy dissipation. *New Phytologist*, **172**(1), 11–21. Publisher: John Wiley & Sons, Ltd.

DEMMIG-ADAMS, BARBARA, COHU, CHRISTOPHER M., MULLER, ONNO, & ADAMS, WILLIAM W. 2012. Modulation of photosynthetic energy conversion efficiency in nature: from seconds to seasons. *Photosynthesis Research*, **113**(1-3), 75–88.

DEMMIG-ADAMS, BARBARA, GARAB, GYOZO, ADAMS III, WILLIAM, & GOVINDJEE (eds). 2014. *Non-Photochemical Quenching and Energy Dissipation in Plants, Algae and Cyanobacteria*. Advances in Photosynthesis and Respiration, vol. 40. Dordrecht: Springer Netherlands.

DEVA, CHETAN R., URBAN, MILAN O., CHALLINOR, ANDREW J., FALLOON, PETE, & SVITÁKOVA, LENKA. 2020. Enhanced Leaf Cooling Is a Pathway to Heat Tolerance in Common Bean. *Frontiers in Plant Science*, **11**(Feb.), 19.

DEWAR, RODERICK, MAURANEN, ALEKSANTERI, MÄKELÄ, ANNIKKI, HÖLTTÄ, TEEMU, MEDLYN, BELINDA, & VESALA, TIMO. 2018. New insights into the covariation of stomatal, mesophyll and hydraulic conductances from optimization models incorporating nonstomatal limitations to photosynthesis. *New Phytologist*, **217**(2), 571–585.

DIAO, HAOYU, CERNUSAK, LUCAS A., SAURER, MATTHIAS, GESSLER, ARTHUR, SIEGWOLF, ROLF T. W., & LEHMANN, MARCO M. 2024. Uncoupling of stomatal conductance and photosynthesis at high temperatures: mechanistic insights from online stable isotope techniques. *New Phytologist*, **241**(6), 2366–2378.

DING, LEI, & CHAUMONT, FRANÇOIS. 2020. Are Aquaporins Expressed in Stomatal Complexes Promising Targets to Enhance Stomatal Dynamics? *Frontiers in Plant Science*, **11**(Apr.), 458.

DORIGO, W. A., WAGNER, W., HOHENSINN, R., HAHN, S., PAULIK, C., XAVER, A., GRUBER, A., DRUSCH, M., MECKLENBURG, S., VAN OEVELEN, P., ROBOCK, A., & JACKSON, T. 2011. The International Soil Moisture Network: a data hosting facility for global in situ soil moisture measurements. *Hydrology and Earth System Sciences*, **15**(5), 1675–1698.

DOTZLER, SANDRA, HILL, JOACHIM, BUDDENBAUM, HENNING, & STOFFELS, JOHANNES. 2015. The Potential of EnMAP and Sentinel-2 Data for Detecting Drought Stress Phenomena in Deciduous Forest Communities. *Remote Sensing*, **7**(10), 14227–14258.

DOUGHTY, RUSSELL, KUROSU, THOMAS P., PARAZOO, NICHOLAS, KÖHLER, PHILIPP, WANG, YUJIE, SUN, YING, & FRANKENBERG, CHRISTIAN. 2022. Global GOSAT, OCO-2, and OCO-3 solar-induced chlorophyll fluorescence datasets. *Earth System Science Data*, **14**(4), 1513–1529.

DRAKE, J.E., POWER, S.A., DUURSMA, R.A., MEDLYN, B.E., ASPINWALL, M.J., CHOAT, B., CREEK, D., EAMUS, D., MAIER, C., PFAUTSCH, S., SMITH, R.A., TJOELKER, M.G., & TISSUE, D.T. 2017. Stomatal and non-stomatal limitations of photosynthesis for four tree species under drought: A comparison of model formulations. *Agricultural and Forest Meteorology*, **247**(Dec.), 454–466.

DROUGHT 2018 TEAM, & ICOS ECOSYSTEM THEMATIC CENTRE. 2019. *Drought-2018 ecosystem eddy covariance flux product in FLUXNET-Archive format - release 2019-1*.

DRUSCH, MATTHIAS, MORENO, JOSE, DEL BELLO, UMBERTO, FRANCO, RAFFAELLA, GOULAS, YVES, HUTH, ANDREAS, KRAFT, STEFAN, MIDDLETON, ELIZABETH M., MIGLIETTA, FRANCO, MOHAMMED, GINA, NEDBAL, LADISLAV, RASCHER, UWE, SCHUTTEMEYER, DIRK, & VERHOEF, WOUT. 2017. The FLuorescence EXplorer Mission Concept—ESA's Earth Explorer 8. *IEEE Transactions on Geoscience and Remote Sensing*, **55**(3), 1273–1284.

DUDDEK, PATRICK, AHMED, MUTEZ ALI, JAVAUX, MATHIEU, VANDERBORGHT, JAN, LOVRIC, GORAN, KING, ANDREW, & CARMINATI, ANDREA. 2023. The effect of root hairs on root water uptake is determined by root–soil contact and root hair shrinkage. *New Phytologist*, **240**(6), 2484–2497.

DUMONT, BENJAMIN, HEINESCH, BERNARD, BODSON, BERNARD, BOGAERTS, GAËTAN, CHOPIN, HENRI, DE LIGNE, ANNE, DEMOULIN, LOÏC, DOUXFILS, BERNARD, ENGELMANN, THIBAUT, FAURÈS, ARIANE, LONGDOZ, BERNARD, MANISE, TANGUY, ORGUN, AYCHE, PIRET, ANDRÉ, & THYRION, THIBAUT. 2023a. *ETC L2 ARCHIVE, Lonzee, 2016-12-31–2023-09-30*.

DUMONT, BENJAMIN, HEINESCH, BERNARD, BODSON, BERNARD, BOGAERTS, GAËTAN, CHOPIN, HENRI, DE LIGNE, ANNE, DEMOULIN, LOÏC, DOUXFILS, BERNARD, ENGELMANN, THIBAUT, FAURÈS, ARIANE, LONGDOZ, BERNARD, MANISE, TANGUY, ORGUN, AYCHE, PIRET, ANDRÉ, & THYRION, THIBAUT. 2023b. *ETC L2 ARCHIVE, Lonzee, 2016-12-31–2023-09-30*.

DURNER, WOLFGANG, & OR, DANI. 2006. Soil water potential measurement. *Encyclopedia of hydrological sciences*.

DUURSMA, REMKO A. 2015. Plantecophys - An R Package for Analysing and Modelling Leaf Gas Exchange Data. *PLOS ONE*, **10**(11), e0143346.

DUURSMA, REMKO A., BLACKMAN, CHRISTOPHER J., LOPÉZ, ROSANA, MARTIN-STPAUL, NICOLAS K., COCHARD, HERVÉ, & MEDLYN, BELINDA E. 2019. On the minimum leaf conductance: its role in models of plant water use, and ecological and environmental controls. *New Phytologist*, **221**(2), 693–705.

ECKES-SHEPHARD, ANNEMARIE H., TIAVLOVSKY, EGOR, CHEN, YIZHAO, FONTI, PATRICK, & FRIEND, ANDREW D. 2021. Direct response of tree growth to soil water and its implications for terrestrial carbon cycle modelling. *Global Change Biology*, **27**(1), 121–135.

EGEA, GREGORIO, VERHOEF, ANNE, & VIDALE, PIER LUIGI. 2011. Towards an improved and more flexible representation of water stress in coupled photosynthesis–stomatal conductance models. *Agricultural and Forest Meteorology*, **151**(10), 1370–1384.

ELLER, CLEITON B., ROWLAND, LUCY, MENCUCCINI, MAURIZIO, ROSAS, TERESA, WILLIAMS, KARINA, HARPER, ANNA, MEDLYN, BELINDA E., WAGNER, YAEL, KLEIN, TAMIR, TEODORO, GRAZIELLE S., OLIVEIRA, RAFAEL S., MATOS, ILAINE S., ROSADO, BRUNO H. P., FUCHS, KATHRIN, WOHLFAHRT, GEORG, MONTAGNANI, LEONARDO, MEIR, PATRICK, SITCH, STEPHEN, & COX, PETER M. 2020. Stomatal optimization based on xylem hydraulics (SOX) improves land surface model simulation of vegetation responses to climate. *New Phytologist*, **226**(6), 1622–1637.

ENGINEER, CAWAS B., HASHIMOTO-SUGIMOTO, MIMI, NEGI, JUNTARO, ISRAELSSON-NORDSTRÖM, MARIA, AZOULAY-SHEMER, TAMAR, RAPPEL, WOUTER-JAN, IBA, KOH, & SCHROEDER, JULIAN I. 2016. CO2 Sensing and CO2 Regulation of Stomatal Conductance: Advances and Open Questions. *Trends in Plant Science*, **21**(1), 16–30.

ERENSTEIN, OLAF, JALETA, MOTI, MOTTALEB, KHONDOKER ABDUL, SONDER, KAI, DONOVAN, JASON, & BRAUN, HANS-JOACHIM. 2022. *Global Trends in Wheat Production, Consumption and Trade*. Cham: Springer International Publishing. Pages 47–66.

EVANS, JR, SHARKEY, TD, BERRY, JA, & FARQUHAR, GD. 1986. Carbon Isotope Discrimination measured Concurrently with Gas Exchange to Investigate CO2 Diffusion in Leaves of Higher Plants. *Functional Plant Biology*, **13**(2), 281–292.

EVETT, STEVEN R., STONE, KENNETH C., SCHWARTZ, ROBERT C., O'SHAUGHNESSY, SUSAN A., COLAIZZI, PAUL D., ANDERSON, SCOTT K., & ANDERSON, DAVID J. 2019. Resolving discrepancies between laboratory-determined field capacity values and field water content observations: implications for irrigation management. *Irrigation Science*, **37**(6), 751–759.

FAHAD, SHAH, BAJWA, ALI A., NAZIR, USMAN, ANJUM, SHAKEEL A., FAROOQ, AYESHA, ZOHAIB, ALI, SADIA, SEHRISH, NASIM, WAJID, ADKINS, STEVE, SAUD, SHAH, IHSAN, MUHAMMAD Z., ALHARBY, HESHAM, WU, CHAO, WANG, DEPENG, & HUANG, JIANLIANG. 2017. Crop Production under Drought and Heat Stress: Plant Responses and Management Options. *Frontiers in Plant Science*, **8**(June), 1147.

FALGE, EVA, BALDOCCHI, DENNIS, OLSON, RICHARD, ANTHONI, PETER, AUBINET, MARC, BERNHOFER, CHRISTIAN, BURBA, GEORGE, CEULEMANS, REINHART, CLEMENT, ROBERT, DOLMAN, HAN, GRANIER, ANDRÉ, GROSS, PATRICK, GRÜNWALD, THOMAS, HOLLINGER, DAVID, JENSEN, NIELS-OTTO, KATUL, GABRIEL, KERONEN, PETRI, KOWALSKI, ANDREW, LAI, CHUN TA, LAW, BEVERLEY E, MEYERS, TILDEN, MONCRIEFF, JOHN, MOORS, EDDY, MUNGER, J WILLIAM, PILEGAARD, KIM, RANNIK, ÜLLAR, REBMANN, CORINNA, SUYKER, ANDREW, TENHUNEN, JOHN, TU, KEVIN, VERMA, SHASHI, VESALA, TIMO, WILSON, KELL, & WOFSY, STEVE. 2001. Gap filling strategies for defensible annual sums of net ecosystem exchange. *Agricultural and Forest Meteorology*.

FAN, YING, MIGUEZ-MACHO, GONZALO, JOBBÁGY, ESTEBAN G., JACKSON, ROBERT B., & OTERO-CASAL, CARLOS. 2017. Hydrologic regulation of plant rooting depth. *Proceedings of the National Academy of Sciences*, **114**(40), 10572–10577.

FARQUHAR, G D, & SHARKEY, T D. 1982. Stomatal Conductance and Photosynthesis. *Annual Review of Plant Physiology*, **33**(1), 317–345. Publisher: Annual Reviews.

FARQUHAR, G. D., VON CAEMMERER, S., & BERRY, J. A. 1980. A biochemical model of photosynthetic CO2 assimilation in leaves of C3 species. *Planta*, **149**(1), 78–90.

FARQUHAR, GRAHAM D., & CERNUSAK, LUCAS A. 2012. Ternary effects on the gas exchange of isotopologues of carbon dioxide. *Plant, Cell & Environment*, **35**(7), 1221–1231.

FARQUHAR, GRAHAM D., VON CAEMMERER, SUSANNE, & BERRY, JOSEPH A. 2001. Models of Photosynthesis. *Plant Physiology*, **125**(1), 42–45.

FASSIOLI, FRANCESCA, DINSHAW, RAYOMOND, ARPIN, PAUL C., & SCHOLES, GREGORY D. 2014. Photosynthetic light harvesting: excitons and coherence. *Journal of The Royal Society Interface*, **11**(92), 20130901.

FENG, HUAIZE, XU, TONGREN, LIU, LIANGYUN, ZHOU, SHA, ZHAO, JINGXUE, LIU, SHAOMIN, XU, ZIWEI, MAO, KEBIAO, HE, XINLEI, ZHU, ZHONGLI, & CHAI, LINNA. 2021. Modeling Transpiration with Sun-Induced Chlorophyll Fluorescence Observations via Carbon-Water Coupling Methods. *Remote Sensing*, **13**(4), 804.

FICKLIN, DARREN L., & NOVICK, KIMBERLY A. 2017. Historic and projected changes in vapor pressure deficit suggest a continental-scale drying of the United States atmosphere. *Journal of Geophysical Research: Atmospheres*, **122**(4), 2061–2079.

FISCHER, E. M., SIPPEL, S., & KNUTTI, R. 2021. Increasing probability of record-shattering climate extremes. *Nature Climate Change*, **11**(8), 689–695.

FISHER, JOSHUA B., HUNTZINGER, DEBORAH N., SCHWALM, CHRISTOPHER R., & SITCH, STEPHEN. 2014. Modeling the Terrestrial Biosphere. *Annual Review of Environment and Resources*, **39**(1), 91–123.

FLEXAS, J. 2002. Drought-inhibition of Photosynthesis in C3 Plants: Stomatal and Non-stomatal Limitations Revisited. *Annals of Botany*, **89**(2), 183–189.

FLEXAS, J., BOTA, J., LORETO, F., CORNIC, G., & SHARKEY, T. D. 2004. Diffusive and Metabolic Limitations to Photosynthesis under Drought and Salinity in C_3 Plants. *Plant Biology*, **6**(3), 269–279.

FLEXAS, JAUME, & MEDRANO, HIPÓLITO. 2002. Energy dissipation in C3 plants under drought. *Functional Plant Biology*, **29**(10), 1209.

FLEXAS, JAUME, RIBAS-CARBÓ, MIQUEL, DIAZ-ESPEJO, ANTONIO, GALMÉS, JERONI, & MEDRANO, HIPÓLITO. 2008. Mesophyll conductance to CO_2 : current knowledge and future prospects. *Plant, Cell & Environment*, **31**(5), 602–621.

FLEXAS, JAUME, BARÓN, MATILDE, BOTA, JOSEFINA, DUCRUET, JEAN-MARC, GALLÉ, ALEXANDER, GALMÉS, JERONI, JIMÉNEZ, MIGUEL, POU, ALÍCIA, RIBAS-CARBÓ, MIQUEL, SAJNANI, CARLOTA, TOMÀS, MAGDALENA, & MEDRANO, HIPÓLITO. 2009. Photosynthesis limitations during water stress acclimation and recovery in the drought-adapted Vitis hybrid Richter-110 (V. berlandieri×V. rupestris). *Journal of Experimental Botany*, **60**(8), 2361–2377.

FLEXAS, JAUME, BARBOUR, MARGARET M., BRENDEL, OLIVER, CABRERA, HERNÁN M., CARRIQUÍ, MARC, DÍAZ-ESPEJO, ANTONIO, DOUTHE, CYRIL, DREYER, ERWIN, FERRIO, JUAN P., GAGO, JORGE, GALLÉ, ALEXANDER, GALMÉS, JERONI, KODAMA, NAOMI, MEDRANO, HIPÓLITO, NIINEMETS, ÜLO, PEGUERO-PINA, JOSÉ J., POU, ALICIA, RIBAS-CARBÓ, MIQUEL, TOMÁS, MAGDALENA, TOSENS, TIINA, & WARREN, CHARLES R. 2012. Mesophyll diffusion conductance to CO2: An unappreciated central player in photosynthesis. *Plant Science*, **193-194**(Sept.), 70–84.

FLEXAS, JAUME, CANO, FRANCISCO JAVIER, CARRIQUÍ, MARC, COOPMAN, RAFAEL E., MIZOKAMI, YUSUKE, THOLEN, DANNY, & XIONG, DONGLIANG. 2018a. *CO2 Diffusion Inside Photosynthetic Organs*. Cham: Springer International Publishing. Pages 163–208.

FLEXAS, JAUME, CARRIQUÍ, MARC, & NADAL, MIQUEL. 2018b. Gas exchange and hydraulics during drought in crops: who drives whom? *Journal of Experimental Botany*, **69**(16), 3791–3795.

FOKEN, THOMAS, AUBINET, MARC, & LEUNING, RAY. 2012. The Eddy Covariance Method. *Pages 1–19 of:* AUBINET, MARC, VESALA, TIMO, & PAPALE, DARIO (eds), *Eddy Covariance: A Practical Guide to Measurement and Data Analysis*. Dordrecht: Springer Netherlands.

FORD, TRENT W., & QUIRING, STEVEN M. 2019. Comparison of Contemporary In Situ, Model, and Satellite Remote Sensing Soil Moisture With a Focus on Drought Monitoring. *Water Resources Research*, **55**(2), 1565–1582.

FRANCK, FABRICE, JUNEAU, PHILIPPE, & POPOVIC, RADOVAN. 2002. Resolution of the Photosystem I and Photosystem II contributions to chlorophyll fluorescence of intact leaves at room temperature. *Biochimica et Biophysica Acta (BBA) - Bioenergetics*, **1556**(2-3), 239–246.

FRANKENBERG, CHRISTIAN, FISHER, JOSHUA B., WORDEN, JOHN, BADGLEY, GRAYSON, SAATCHI, SASSAN S., LEE, JUNG-EUN, TOON, GEOFFREY C., BUTZ, ANDRÉ, JUNG, MARTIN, KUZE, AKIHIKO, & YOKOTA, TATSUYA. 2011. New global observations of the terrestrial carbon cycle from GOSAT: Patterns of plant fluorescence with gross primary productivity: CHLOROPHYLL FLUORESCENCE FROM SPACE. *Geophysical Research Letters*, **38**(17), n/a–n/a.

FRANKS, PETER J. 2013. Passive and active stomatal control: either or both? *New Phytologist*, **198**(2), 325–327.

FRAPPART, FRÉDÉRIC, WIGNERON, JEAN-PIERRE, LI, XIAOJUN, LIU, XIANGZHUO, AL-YAARI, AMEN, FAN, LEI, WANG, MENGJIA, MOISY, CHRISTOPHE, LE MASSON, ERWAN, AOULAD LAFKIH, ZACHARIE, VALLÉ, CLÉMENT, YGORRA, BERTRAND, & BAGHDADI, NICOLAS. 2020. Global Monitoring of the Vegetation Dynamics from the Vegetation Optical Depth (VOD): A Review. *Remote Sensing*, **12**(18), 2915.

FRIEDLINGSTEIN, PIERRE, O'SULLIVAN, MICHAEL, JONES, MATTHEW W., ANDREW, ROBBIE M., GREGOR, LUKE, HAUCK, JUDITH, LE QUÉRÉ, CORINNE, LUIJKX, INGRID T., OLSEN, ARE, PETERS, GLEN P., PETERS, WOUTER, PONGRATZ, JULIA, SCHWINGSHACKL, CLEMENS, SITCH, STEPHEN, CANADELL, JOSEP G., CIAIS, PHILIPPE, JACKSON, ROBERT B., ALIN, SIMONE R., ALKAMA, RAMDANE, ARNETH, ALMUT, ARORA, VIVEK K., BATES, NICHOLAS R., BECKER, MEIKE, BELLOUIN, NICOLAS, BITTIG, HENRY C., BOPP, LAURENT, CHEVALLIER, FRÉDÉRIC, CHINI, LOUISE P., CRONIN, MARGOT, EVANS, WILEY, FALK, STEFANIE, FEELY, RICHARD A., GASSER, THOMAS, GEHLEN, MARION, GKRITZALIS, THANOS, GLOEGE, LUCAS, GRASSI, GIACOMO, GRUBER, NICOLAS, GÜRSES, ÖZGÜR, HARRIS, IAN, HEFNER, MATTHEW, HOUGHTON, RICHARD A., HURTT, GEORGE C., IIDA, YOSUKE, ILYINA, TATIANA, JAIN, ATUL K., JERSILD, ANNIKA, KADONO, KOJI, KATO, ETSUSHI, KENNEDY, DANIEL, KLEIN GOLDEWIJK, KEES, KNAUER, JÜRGEN, KORSBAKKEN, JAN IVAR, LANDSCHÜTZER, PETER, LEFÈVRE, NATHALIE, LINDSAY, KEITH, LIU, JUNJIE, LIU, ZHU, MARLAND, GREGG, MAYOT, NICOLAS, MCGRATH, MATTHEW J., METZL, NICOLAS, MONACCI, NATALIE M., MUNRO, DAVID R., NAKAOKA, SHIN-ICHIRO, NIWA, YOSUKE, O'BRIEN, KEVIN, ONO, TSUNEO, PALMER, PAUL I., PAN, NAIQING, PIERROT, DENIS, POCOCK, KATIE, POULTER, BENJAMIN, RESPLANDY, LAURE, ROBERTSON, EDDY, RÖDENBECK, CHRISTIAN, RODRIGUEZ, CARMEN, ROSAN, THAIS M., SCHWINGER, JÖRG, SÉFÉRIAN, ROLAND, SHUTLER, JAMIE D., SKJELVAN, INGUNN, STEINHOFF, TOBIAS, SUN, QING, SUTTON, ADRIENNE J., SWEENEY, COLM, TAKAO, SHINTARO, TANHUA, TOSTE, TANS, PIETER P., TIAN, XIANGJUN, TIAN, HANQIN, TILBROOK, BRONTE, TSUJINO, HIROYUKI, TUBIELLO, FRANCESCO, VAN DER WERF, GUIDO R., WALKER, ANTHONY P., WANNINKHOF,

RIK, WHITEHEAD, CHRIS, WILLSTRAND WRANNE, ANNA, WRIGHT, REBECCA, YUAN, WENPING, YUE, CHAO, YUE, XU, ZAEHLE, SÖNKE, ZENG, JIYE, & ZHENG, BO. 2022. Global Carbon Budget 2022. *Earth System Science Data*, **14**(11), 4811–4900.

FURBANK, ROBERT T., QUICK, W. PAUL, & SIRAULT, XAVIER R.R. 2015. Improving photosynthesis and yield potential in cereal crops by targeted genetic manipulation: Prospects, progress and challenges. *Field Crops Research*, **182**(Oct.), 19–29.

FÖRSTER, TH. 1948. Zwischenmolekulare Energiewanderung und Fluoreszenz. *Annalen der Physik*, **437**(1-2), 55–75.

GAGO, JORGE, DALOSO, DANILO M., CARRIQUÍ, MARC, NADAL, MIQUEL, MORALES, MELANIE, ARAÚJO, WAGNER L., NUNES-NESI, ADRIANO, & FLEXAS, JAUME. 2020. Mesophyll conductance: the leaf corridors for photosynthesis. *Biochemical Society Transactions*, **48**(2), 429–439.

GALMÉS, JERONI, MEDRANO, HIPÓLITO, & FLEXAS, JAUME. 2007. Photosynthetic limitations in response to water stress and recovery in Mediterranean plants with different growth forms. *New Phytologist*, **175**(1), 81–93.

GAMBETTA, GREGORY A., KNIPFER, THORSTEN, FRICKE, WIELAND, & MCELRONE, ANDREW J. 2017. *Aquaporins and Root Water Uptake*. Cham: Springer International Publishing. Pages 133–153.

GAMON, JOHN A., HUEMMRICH, K. FRED, WONG, CHRISTOPHER Y. S., ENSMINGER, INGO, GARRITY, STEVEN, HOLLINGER, DAVID Y., NOORMETS, ASKO, & PEÑUELAS, JOSEP. 2016. A remotely sensed pigment index reveals photosynthetic phenology in evergreen conifers. *Proceedings of the National Academy of Sciences*, **113**(46), 13087–13092.

GARBULSKY, MARTÍN F., PEÑUELAS, JOSEP, GAMON, JOHN, INOUE, YOSHIO, & FILELLA, IOLANDA. 2011. The photochemical reflectance index (PRI) and the remote sensing of leaf, canopy and ecosystem radiation use efficiencies: A review and meta-analysis. *Remote Sensing of Environment*, **115**(2), 281–297.

GARCÍA-PLAZAOLA, JOSÉ I., HERNÁNDEZ, ANTONIO, OLANO, JOSÉ M., & BECERRIL, JOSÉ M. 2003. The operation of the lutein epoxide cycle correlates with energy dissipation. *Functional Plant Biology*, **30**(3), 319.

GARCÍA-TEJERA, OMAR, ÁLVARO LÓPEZ-BERNAL, ORGAZ, FRANCISCO, TESTI, LUCA, & VILLALOBOS, FRANCISCO J. 2021. The pitfalls of water potential for irrigation scheduling. *Agricultural Water Management*, **243**, 106522.

GEBRECHORKOS, S. H., PENG, J., DYER, E., MIRALLES, D. G., VICENTE-SERRANO, S. M., FUNK, C., BECK, H. E., ASFAW, D. T., SINGER, M. B., & DADSON, S. J. 2023. Global high-resolution drought indices for 1981–2022. *Earth System Science Data*, **15**(12), 5449–5466.

GENTY, BERNARD, BRIANTAIS, JEAN-MARIE, & BAKER, NEIL R. 1989. The relationship between the quantum yield of photosynthetic electron transport and quenching of chlorophyll fluorescence. *Biochimica et Biophysica Acta (BBA) - General Subjects*, **990**(1), 87–92.

GENTY, BERNARD, WONDERS, JEANETTE, & BAKER, NEIL R. 1990. Non-photochemical quenching of Fo in leaves is emission wavelength dependent: consequences for quenching analysis and its interpretation. *Photosynthesis Research*, **26**(2), 133–139.

GERHARDS, MAX, ROCK, GILLES, SCHLERF, MARTIN, & UDELHOVEN, THOMAS. 2016. Water stress detection in potato plants using leaf temperature, emissivity, and reflectance. *International Journal of Applied Earth Observation and Geoinformation*, **53**(Dec.), 27–39.

GERVAIS, TAYLOR, CREELMAN, ALEXA, LI, XIU-QING, BIZIMUNGU, BENOIT, DE KOEYER, DAVID, & DAHAL, KESHAV. 2021. Potato Response to Drought Stress: Physiological and Growth Basis. *Frontiers in plant science*, **12**, 698060. Place: Switzerland.

GESSLER, ARTHUR, BÄCHLI, LUKAS, ROUHOLAHNEJAD FREUND, ELHAM, TREYDTE, KERSTIN, SCHAUB, MARCUS, HAENI, MATTHIAS, WEILER, MARKUS, SEEGER, STEFAN, MARSHALL, JOHN, HUG, CHRISTIAN, ZWEIFEL, ROMAN, HAGEDORN, FRANK, RIGLING, ANDREAS, SAURER, MATTHIAS, & MEUSBURGER, KATRIN. 2022. Drought reduces water uptake in beech from the drying topsoil, but no compensatory uptake occurs from deeper soil layers. *The New phytologist*, **233**(1), 194–206. Place: England.

GHOLIPOOR, M., SINCLAIR, T. R., RAZA, M. A. S., LÖFFLER, C., COOPER, M., & MESSINA, C. D. 2013. Maize Hybrid Variability for Transpiration Decrease with Progressive Soil Drying. *Journal of Agronomy and Crop Science*, **199**(1), 23–29.

GILMANOV, TAGIR G., WYLIE, BRUCE K., TIESZEN, LARRY L., MEYERS, TILDEN P., BARON, VERN S., BERNACCHI, CARL J., BILLESBACH, DAVID P., BURBA, GEORGE G., FISCHER, MARC L., GLENN, AARON J., HANAN, NIALL P., HATFIELD, JERRY L., HEUER, MARK W., HOLLINGER, STEVEN E., HOWARD, DANIEL M., MATAMALA, ROSER, PRUEGER, JOHN H., TENUTA, MARIO, & YOUNG, DAVID G. 2013. CO2 uptake and ecophysiological parameters of the grain crops of midcontinent North America: Estimates from flux tower measurements. *Agriculture, Ecosystems & Environment*, **164**(Jan.), 162–175.

GIMENO, TERESA E, SAAVEDRA, NOELIA, OGÉE, JÉRÔME, MEDLYN, BELINDA E, & WINGATE, LISA. 2019. A novel optimization approach incorporating non-stomatal limitations predicts stomatal behaviour in species from six plant functional types. *Journal of Experimental Botany*, **70**(5), 1639–1651.

GOFFART, JEAN-PIERRE, HAVERKORT, ANTON, STOREY, MICHAEL, HAASE, NORBERT, MARTIN, MICHEL, LEBRUN, PIERRE, RYCKMANS, DANIEL, FLORINS, DOMINIQUE, & DEMEULEMEESTER, KÜRT. 2022. Potato Production in Northwestern Europe (Germany, France, the Netherlands, United Kingdom, Belgium): Characteristics, Issues, Challenges and Opportunities. *Potato Research*, Jan.

GORDON, R. J., BROWN, D. M., & DIXON, M. A. 1997. Stomatal resistance of three potato cultivars as influenced by soil water status, humidity and irradiance. *Potato Research*, **40**(1), 47–57.

GOURLEZ DE LA MOTTE, LOUIS, BEAUCLAIRE, QUENTIN, HEINESCH, BERNARD, CUNTZ, MATHIAS, FOLTÝNOVÁ, LENKA, SIGUT, LADISLAV, KOWALSKA, NATALIA, MANCA, GIOVANNI, BALLARIN, IGNACIO, VINCKE, CAROLINE, ROLAND, MARILYN, IBROM, A., LOUSTEAU, DENIS, SIEBICKE, LUKAS, & BERNARD, LONGDOZ. 2020. Non-stomatal processes reduce gross primary productivity in temperate forest ecosystems during severe edaphic drought. *Philosophical Transactions of The Royal Society B Biological Sciences*, **In Press**(Mar.).

GOUTERMAN, MARTIN. 1961. Spectra of porphyrins. *Journal of Molecular Spectroscopy*, **6**, 138–163.

GRAF, ALEXANDER, KLOSTERHALFEN, ANNE, ARRIGA, NICOLA, BERNHOFER, CHRISTIAN, BOGENA, HEYE, BORNET, FRÉDÉRIC, BRÜGGEMANN, NICOLAS, BRÜMMER, CHRISTIAN, BUCHMANN, NINA, CHI, JINSHU, CHIPEAUX, CHRISTOPHE, CREMONESE, EDOARDO, CUNTZ,

MATTHIAS, DUŠEK, JIŘÍ, EL-MADANY, TAREK S., FARES, SILVANO, FISCHER, MILAN, FOLTÝNOVÁ, LENKA, GHARUN, MANA, GHIASI, SHIVA, GIELEN, BERT, GOTTSCHALK, PIA, GRÜNWALD, THOMAS, HEINEMANN, GÜNTHER, HEINESCH, BERNARD, HELIASZ, MICHAL, HOLST, JUTTA, HÖRTNAGL, LUKAS, IBROM, ANDREAS, INGWERSEN, JOACHIM, JURASINSKI, GERALD, KLATT, JANINA, KNOHL, ALEXANDER, KOEBSCH, FRANZISKA, KONOPKA, JAN, KORKIAKOSKI, MIKA, KOWALSKA, NATALIA, KREMER, PASCAL, KRUIJT, BART, LAFONT, SEBASTIEN, LÉONARD, JOËL, DE LIGNE, ANNE, LONGDOZ, BERNARD, LOUSTAU, DENIS, MAGLIULO, VINCENZO, MAMMARELLA, IVAN, MANCA, GIOVANNI, MAUDER, MATTHIAS, MIGLIAVACCA, MIRCO, MÖLDER, MEELIS, NEIRYNCK, JOHAN, NEY, PATRIZIA, NILSSON, MATS, PAUL-LIMOGES, EUGÉNIE, PEICHL, MATTHIAS, PITACCO, ANDREA, POYDA, ARNE, REBMANN, CORINNA, ROLAND, MARILYN, SACHS, TORSTEN, SCHMIDT, MARIUS, SCHRADER, FREDERIK, SIEBICKE, LUKAS, ŠIGUT, LADISLAV, TUITTILA, EEVA-STIINA, VARLAGIN, ANDREJ, VENDRAME, NADIA, VINCKE, CAROLINE, VÖLKSCH, INGO, WEBER, STEPHAN, WILLE, CHRISTIAN, WIZEMANN, HANS-DIETER, ZEEMAN, MATTHIAS, & VEREECKEN, HARRY. 2020. Altered energy partitioning across terrestrial ecosystems in the European drought year 2018. *Philosophical Transactions of the Royal Society B: Biological Sciences*, **375**(1810), 20190524.

GRANIER, A., BRÉDA, N., BIRON, P., & VILLETTE, S. 1999a. A lumped water balance model to evaluate duration and intensity of drought constraints in forest stands. *Ecological Modelling*, **116**(2-3), 269–283.

GRANIER, A., BRÉDA, N., BIRON, P., & VILLETTE, S. 1999b. A lumped water balance model to evaluate duration and intensity of drought constraints in forest stands. *Ecological Modelling*, **116**(2), 269–283.

GRANIER, A., REICHSTEIN, M., BRÉDA, N., JANSSENS, I.A., FALGE, E., CIAIS, P., GRÜNWALD, T., AUBINET, M., BERBIGIER, P., BERNHOFER, C., BUCHMANN, N., FACINI, O., GRASSI, G., HEINESCH, B., ILVESNIEMI, H., KERONEN, P., KNOHL, A., KÖSTNER, B., LAGERGREN, F., LINDROTH, A., LONGDOZ, B., LOUSTAU, D., MATEUS, J., MONTAGNANI, L., NYS, C., MOORS, E., PAPALE, D., PEIFFER, M., PILEGAARD, K., PITA, G., PUMPANEN, J., RAMBAL, S., REBMANN, C., RODRIGUES, A., SEUFERT, G., TENHUNEN, J., VESALA, T., & WANG, Q. 2007a. Evidence for soil water control on carbon and water dynamics in European forests during the extremely dry year: 2003. *Agricultural and Forest Meteorology*, **143**(1), 123–145.

GRANIER, A., REICHSTEIN, M., BRÉDA, N., JANSSENS, I.A., FALGE, E., CIAIS, P., GRÜNWALD, T., AUBINET, M., BERBIGIER, P., BERNHOFER, C., BUCHMANN, N., FACINI, O., GRASSI, G., HEINESCH, B., ILVESNIEMI, H., KERONEN, P., KNOHL, A., KÖSTNER, B., LAGERGREN, F., LINDROTH, A., LONGDOZ, B., LOUSTAU, D., MATEUS, J., MONTAGNANI, L., NYS, C., MOORS, E., PAPALE, D., PEIFFER, M., PILEGAARD, K., PITA, G., PUMPANEN, J., RAMBAL, S., REBMANN, C., RODRIGUES, A., SEUFERT, G., TENHUNEN, J., VESALA, T., & WANG, Q. 2007b. Evidence for soil water control on carbon and water dynamics in European forests during the extremely dry year: 2003. *Agricultural and Forest Meteorology*, **143**(1), 123–145.

GRASSI, GIACOMO, & MAGNANI, FEDERICO. 2005. Stomatal, mesophyll conductance and biochemical limitations to photosynthesis as affected by drought and leaf ontogeny in ash and oak trees. *Plant, Cell and Environment*, **28**(7), 834–849.

GRASSI, GIACOMO, RIPULLONE, FRANCESCO, BORGHETTI, MARCO, RADDI, SABRINA, & MAGNANI, FEDERICO. 2009. Contribution of diffusional and non-diffusional limitations to midday depression of photosynthesis in Arbutus unedo L. *Trees*, **23**(6), 1149–1161.

GRASSO, M., RENGA, A., FASANO, G., GRAZIANO, M.D., GRASSI, M., & MOCCIA, A. 2021. Design of an end-to-end demonstration mission of a Formation-Flying Synthetic Aperture Radar (FF-SAR) based on microsatellites. *Advances in Space Research*, **67**(11), 3909–3923. Satellite Constellations and Formation Flying.

GROSSIORD, CHARLOTTE, BUCKLEY, THOMAS N., CERNUSAK, LUCAS A., NOVICK, KIMBERLY A., POULTER, BENJAMIN, SIEGWOLF, ROLF T. W., SPERRY, JOHN S., & MCDOWELL, NATE G. 2020. Plant responses to rising vapor pressure deficit. *New Phytologist*, **226**(6), 1550–1566.

GROTJOHANN, I., & FROMME, P. 2013. Photosystem I. *Pages 503–507 of: Encyclopedia of Biological Chemistry*. Elsevier.

GU, LIANHONG, HAN, JIMEI, WOOD, JEFFREY D., CHANG, CHRISTINE Y-Y., & SUN, YING. 2019. Sun-induced Chl fluorescence and its importance for biophysical modeling of photosynthesis based on light reactions. *New Phytologist*, **223**(3), 1179–1191.

GU, ZHE, QI, ZHIMING, BURGHATE, RASIKA, YUAN, SHOUQI, JIAO, XIYUN, & XU, JUNZENG. 2020. Irrigation Scheduling Approaches and Applications: A Review. *Journal of Irrigation and Drainage Engineering*, **146**(6), 04020007.

GUANTER, L., ALONSO, L., GÓMEZ-CHOVA, L., AMORÓS-LÓPEZ, J., VILA, J., & MORENO, J. 2007. Estimation of solar-induced vegetation fluorescence from space measurements: ESTIMATION OF VEGETATION FLUORESCENCE. *Geophysical Research Letters*, **34**(8).

GUANTER, L., ABEN, I., TOL, P., KRIJGER, J. M., HOLLSTEIN, A., KÖHLER, P., DAMM, A., JOINER, J., FRANKENBERG, C., & LANDGRAF, J. 2015. Potential of the TROPOspheric Monitoring Instrument (TROPOMI) onboard the Sentinel-5 Precursor for the monitoring of terrestrial chlorophyll fluorescence. *Atmospheric Measurement Techniques*, **8**(3), 1337–1352.

GUANTER, LUIS, ZHANG, YONGGUANG, JUNG, MARTIN, JOINER, JOANNA, VOIGT, MAXIMILIAN, BERRY, JOSEPH A., FRANKENBERG, CHRISTIAN, HUETE, ALFREDO R., ZARCO-TEJADA, PABLO, LEE, JUNG-EUN, MORAN, M. SUSAN, PONCE-CAMPOS, GUILLERMO, BEER, CHRISTIAN, CAMPS-VALLS, GUSTAVO, BUCHMANN, NINA, GIANELLE, DAMIANO, KLUMPP, KATJA, CESCATTI, ALESSANDRO, BAKER, JOHN M., & GRIFFIS, TIMOTHY J. 2014. Global and time-resolved monitoring of crop photosynthesis with chlorophyll fluorescence. *Proceedings of the National Academy of Sciences*, **111**(14).

GUANTER, LUIS, BACOUR, CÉDRIC, SCHNEIDER, ANDREAS, ABEN, ILSE, VAN KEMPEN, TIM A., MAIGNAN, FABIENNE, RETSCHER, CHRISTIAN, KÖHLER, PHILIPP, FRANKENBERG, CHRISTIAN, JOINER, JOANNA, & ZHANG, YONGGUANG. 2021. The TROPOSIF global sun-induced fluorescence dataset from the Sentinel-5P TROPOMI mission. *Earth System Science Data*, **13**(11), 5423–5440.

HALEY, MELISSA B., & DUKES, MICHAEL D. 2012. Validation of Landscape Irrigation Reduction with Soil Moisture Sensor Irrigation Controllers. *Journal of Irrigation and Drainage Engineering*, **138**(2), 135–144.

HAN, JIMEI, CHANG, CHRISTINE Y-Y., GU, LIANHONG, ZHANG, YONGJIANG, MEEKER, ELIOT W., MAGNEY, TROY S., WALKER, ANTHONY P., WEN, JIAMING, KIRA, OZ, MCNAULL, SARAH, & SUN, YING. 2022a. The physiological basis for estimating photosynthesis from Chl *a* fluorescence. *New Phytologist*, **234**(4), 1206–1219.

HAN, JIMEI, GU, LIANHONG, WARREN, JEFFREY M, GUHA, ANIRBAN, MCLENNAN, DAVID A, ZHANG, WANGFENG, & ZHANG, YALI. 2022b. The roles of photochemical and non-photochemical

quenching in regulating photosynthesis depend on the phases of fluctuating light conditions. *Tree Physiology*, **42**(4), 848–861.

HARLEY, PETER C., LORETO, FRANCESCO, DI MARCO, GIORGIO, & SHARKEY, THOMAS D. 1992. Theoretical Considerations when Estimating the Mesophyll Conductance to CO $_2$ Flux by Analysis of the Response of Photosynthesis to CO $_2$. *Plant Physiology*, **98**(4), 1429–1436.

HARPER, ANNA B., WILLIAMS, KARINA E., MCGUIRE, PATRICK C., DURAN ROJAS, MARIA CAROLINA, HEMMING, DEBBIE, VERHOEF, ANNE, HUNTINGFORD, CHRIS, ROWLAND, LUCY, MARTHEWS, TOBY, BREDER ELLER, CLEITON, MATHISON, CAMILLA, NOBREGA, RODOLFO L. B., GEDNEY, NICOLA, VIDALE, PIER LUIGI, OTU-LARBI, FRED, PANDEY, DIVYA, GARRIGUES, SEBASTIEN, WRIGHT, AZIN, SLEVIN, DARREN, DE KAUWE, MARTIN G., BLYTH, ELEANOR, ARDÖ, JONAS, BLACK, ANDREW, BONAL, DAMIEN, BUCHMANN, NINA, BURBAN, BENOIT, FUCHS, KATHRIN, DE GRANDCOURT, AGNÈS, MAMMARELLA, IVAN, MERBOLD, LUTZ, MONTAGNANI, LEONARDO, NOUVELLON, YANN, RESTREPO-COUPE, NATALIA, & WOHLFAHRT, GEORG. 2021. Improvement of modeling plant responses to low soil moisture in JULESvn4.9 and evaluation against flux tower measurements. *Geoscientific Model Development*, **14**(6), 3269–3294.

HARRIS, JEANNE M. 2015. Abscisic Acid: Hidden Architect of Root System Structure. *Plants (Basel, Switzerland)*, **4**(3), 548–572. Place: Switzerland.

HARTICK, CARL, FURUSHO-PERCOT, CARINA, CLARK, MARTYN P., & KOLLET, STEFAN. 2022. An Interannual Drought Feedback Loop Affects the Surface Energy Balance and Cloud Properties. *Geophysical Research Letters*, **49**(22), e2022GL100924.

HATFIELD, JERRY L., & DOLD, CHRISTIAN. 2019. Water-Use Efficiency: Advances and Challenges in a Changing Climate. *Frontiers in Plant Science*, **10**(Feb.).

HAVERD, V., CUNTZ, M., NIERADZIK, L. P., & HARMAN, I. N. 2016. Improved representations of coupled soil–canopy processes in the CABLE land surface model (Subversion revision 3432). *Geoscientific Model Development*, **9**(9), 3111–3122.

HE, LIMING, CHEN, JING M., LIU, JANE, ZHENG, TING, WANG, RONG, JOINER, JOANNA, CHOU, SHUREN, CHEN, BIN, LIU, YANG, LIU, RONGGAO, & ROGERS, CHERYL. 2019. Diverse photosynthetic capacity of global ecosystems mapped by satellite chlorophyll fluorescence measurements. *Remote Sensing of Environment*, **232**(Oct.), 111344.

HEDGES, LARRY V., GUREVITCH, JESSICA, & CURTIS, PETER S. 1999. THE META-ANALYSIS OF RESPONSE RATIOS IN EXPERIMENTAL ECOLOGY. *Ecology*, **80**(4), 1150–1156. Publisher: John Wiley & Sons, Ltd.

HELM, LEVI T., SHI, HANYU, LERDAU, MANUEL T., & YANG, XI. 2020. Solar-induced chlorophyll fluorescence and short-term photosynthetic response to drought. *Ecological Applications*, **30**(5).

HENDRAWAN, VEMPI SATRIYA ADI, KIM, WONSIK, TOUGE, YOSHIYA, KE, SHI, & KOMORI, DAISUKE. 2022. A global-scale relationship between crop yield anomaly and multiscalar drought index based on multiple precipitation data. *Environmental Research Letters*, **17**(1), 014037.

HENTSCHEL, RAINER, HOMMEL, ROBERT, POSCHENRIEDER, WERNER, GROTE, RÜDIGER, HOLST, JUTTA, BIERNATH, CHRISTIAN, GESSLER, ARTHUR, & PRIESACK, ECKART. 2016. Stomatal conductance and intrinsic water use efficiency in the drought year 2003: a case study of European beech. *Trees*, **30**(1), 153–174.

HETHERINGTON, ALISTAIR M., & WOODWARD, F. IAN. 2003. The role of stomata in sensing and driving environmental change. *Nature*, **424**(6951), 901–908.

HOLLOWAY-PHILLIPS, MEISHA, CERNUSAK, LUCAS A., STUART-WILLIAMS, HILARY, UBIERNA, NEREA, & FARQUHAR, GRAHAM D. 2019. Two-Source 18O Method to Validate the CO18O-Photosynthetic Discrimination Model: Implications for Mesophyll Conductance1 [OPEN]. *Plant Physiology*, **181**(3), 1175–1190.

HORNERO, A., NORTH, P.R.J., ZARCO-TEJADA, P.J., RASCHER, U., MARTÍN, M.P., MIGLIAVACCA, M., & HERNANDEZ-CLEMENTE, R. 2021. Assessing the contribution of understory sun-induced chlorophyll fluorescence through 3-D radiative transfer modelling and field data. *Remote Sensing of Environment*, **253**, 112195.

HU, LU, ZHAO, TIANJIE, JU, WEIMIN, PENG, ZHIQING, SHI, JIANCHENG, RODRÍGUEZ-FERNÁNDEZ, NEMESIO J., WIGNERON, JEAN-PIERRE, COSH, MICHAEL H., YANG, KUN, LU, HUI, & YAO, PANPAN. 2023. A twenty-year dataset of soil moisture and vegetation optical depth from AMSR-E/2 measurements using the multi-channel collaborative algorithm. *Remote Sensing of Environment*, **292**(July), 113595.

HUANG, GUANJUN, YANG, YUHAN, ZHU, LELE, PENG, SHAOBING, & LI, YONG. 2021. Temperature responses of photosynthesis and stomatal conductance in rice and wheat plants. *Agricultural and Forest Meteorology*, **300**(Apr.), 108322.

HUANG, ZE. 2020. Soil water availability threshold indicator was determined by using plant physiological responses under drought conditions. *Ecological Indicators*, 10.

HULLEY, GLYNN C., GHENT, DARREN, GÖTTSCHE, FRANK M., GUILLEVIC, PIERRE C., MILDREXLER, DAVID J., & COLL, CÉSAR. 2019. 3 - Land Surface Temperature. *Pages 57–127 of:* HULLEY, GLYNN C., & GHENT, DARREN (eds), *Taking the Temperature of the Earth*. Elsevier.

HUMPHREY, V., & FRANKENBERG, C. 2023. Continuous ground monitoring of vegetation optical depth and water content with GPS signals. *Biogeosciences*, **20**(9), 1789–1811.

HUNT, E.RAYMOND, RUNNING, STEVEN W, & FEDERER, C.ANTHONY. 1991. Extrapolating plant water flow resistances and capacitances to regional scales. *Agricultural and Forest Meteorology*, **54**(2), 169–195.

HUO, RAN, LI, LU, CHEN, HUA, XU, CHONG-YU, CHEN, JIE, & GUO, SHENGLIAN. 2021. Extreme Precipitation Changes in Europe from the Last Millennium to the End of the Twenty-First Century. *Journal of Climate*, **34**(2), 567–588.

HÉROULT, ARNAUD, LIN, YAN-SHIH, BOURNE, AIMEE, MEDLYN, BELINDA E., & ELLSWORTH, DAVID S. 2013. Optimal stomatal conductance in relation to photosynthesis in climatically contrasting *Eucalyptus* species under drought: Stomatal responses of eucalyptus under drought. *Plant, Cell & Environment*, **36**(2), 262–274.

INTERGOVERNMENTAL PANEL ON CLIMATE CHANGE. 2023. *Climate Change 2021 – The Physical Science Basis: Working Group I Contribution to the Sixth Assessment Report of the Intergovernmental Panel on Climate Change*. 1 edn. Cambridge University Press.

IONITA, M., NAGAVCIUC, V., KUMAR, R., & RAKOVEC, O. 2020. On the curious case of the recent decade, mid-spring precipitation deficit in central Europe. *npj Climate and Atmospheric Science*, **3**(1), 49.

IONITA, MONICA, & NAGAVCIUC, VIORICA. 2021. Changes in drought features at the European level over the last 120 years. *Natural Hazards and Earth System Sciences*, **21**(5), 1685–1701.

J. D. JABRO, B. G. LEIB, & A. D. JABRO. 2005. ESTIMATING SOIL WATER CONTENT USING SITE-SPECIFIC CALIBRATION OF CAPACITANCE MEASUREMENTS FROM SENTEK ENVIROSCAN SYSTEMS. *Applied Engineering in Agriculture*, **21**(3), 393–399.

JACKSON, THOMAS J. 1993. III. Measuring surface soil moisture using passive microwave remote sensing. *Hydrological Processes*, **7**(2), 139–152.

JACKSON, THOMAS J., CHEN, DAOYI, COSH, MICHAEL, LI, FUQIN, ANDERSON, MARTHA, WALTHALL, CHARLES, DORIASWAMY, PAUL, & HUNT, E.RAY. 2004. Vegetation water content mapping using Landsat data derived normalized difference water index for corn and soybeans. *Remote Sensing of Environment*, **92**(4), 475–482. 2002 Soil Moisture Experiment (SMEX02).

JACKSON, T.J., & SCHMUGGE, T.J. 1991. Vegetation effects on the microwave emission of soils. *Remote Sensing of Environment*, **36**(3), 203–212.

JAGDHUBER, THOMAS, BAUR, MARTIN, AKBAR, RUZBEH, DAS, NARENDRA N., LINK, MORITZ, HE, LIAN, & ENTEKHABI, DARA. 2019. Estimation of active-passive microwave covariation using SMAP and Sentinel-1 data. *Remote Sensing of Environment*, **225**, 458–468.

JALAKAS, PIRKO, TAKAHASHI, YOHEI, WAADT, RAINER, SCHROEDER, JULIAN I., & MERILO, EBE. 2021. Molecular mechanisms of stomatal closure in response to rising vapour pressure deficit. *New Phytologist*, **232**(2), 468–475.

JARVIS, P. G., MONTEITH, JOHN LENNOX, & WEATHERLEY, PAUL EGERTON. 1976. The interpretation of the variations in leaf water potential and stomatal conductance found in canopies in the field. *Philosophical Transactions of the Royal Society of London. B, Biological Sciences*, **273**(927), 593–610.

JAVOT, HÉLÈNE, & MAUREL, CHRISTOPHE. 2002. The role of aquaporins in root water uptake. *Annals of botany*, **90**(3), 301–313. Place: England.

JIA, QIANLAN, LIU, ZHUNQIAO, GUO, CHENHUI, WANG, YAKAI, YANG, JINGJING, YU, QIANG, WANG, JING, ZHENG, FENLI, & LU, XIAOLIANG. 2023. Relationship between Photosynthetic CO2 Assimilation and Chlorophyll Fluorescence for Winter Wheat under Water Stress. *Plants*, **12**(19), 3365.

JIANG, SHOUZHENG, WU, JIE, WANG, ZHIHUI, HE, ZILING, WANG, MINGJUN, YAO, WEIWEI, & FENG, YU. 2023. Spatiotemporal variations of cropland carbon sequestration and water loss across China. *Agricultural Water Management*, **287**(Sept.), 108427.

JOHNSON, MATTHEW P. 2016. Photosynthesis. *Essays in Biochemistry*, **60**(3), 255–273.

JOINER, J., YOSHIDA, Y., VASILKOV, A. P., YOSHIDA, Y., CORP, L. A., & MIDDLETON, E. M. 2011. First observations of global and seasonal terrestrial chlorophyll fluorescence from space. *Biogeosciences*, **8**(3), 637–651.

JONARD, F., DE CANNIÈRE, S., BRÜGGEMANN, N., GENTINE, P., SHORT GIANOTTI, D.J., LOBET, G., MIRALLES, D.G., MONTZKA, C., PAGÁN, B.R., RASCHER, U., & VEREECKEN, H. 2020. Value of sun-induced chlorophyll fluorescence for quantifying hydrological states and fluxes: Current status and challenges. *Agricultural and Forest Meteorology*, **291**(Sept.), 108088.

JONARD, FRANÇOIS, FELDMAN, ANDREW F., SHORT GIANOTTI, DANIEL J., & ENTEKHABI, DARA. 2022. Observed water and light limitation across global ecosystems. *Biogeosciences*, **19**(23), 5575–5590.

JONES, H. G. 1985. Partitioning stomatal and non-stomatal limitations to photosynthesis. *Plant, Cell and Environment*, **8**(2), 95–104.

JOSHI, JAIDEEP, STOCKER, BENJAMIN D., HOFHANSL, FLORIAN, ZHOU, SHUANGXI, DIECKMANN, ULF, & PRENTICE, IAIN COLIN. 2022. Towards a unified theory of plant photosynthesis and hydraulics. *Nature Plants*, **8**(11), 1304–1316.

JUENGER, THOMAS E, & VERSLUES, PAUL E. 2022. Time for a drought experiment: Do you know your plants' water status? *The Plant Cell*, **35**(1), 10–23.

JUNG, M., NELSON, J., MIGLIAVACCA, M., EL-MADANY, T., PAPALE, D., REICHSTEIN, M., WALTHER, S., & WUTZLER, T. 2024. Technical note: Flagging inconsistencies in flux tower data. *Biogeosciences*, **21**(7), 1827–1846.

JUNG, MARTIN, SCHWALM, CHRISTOPHER, MIGLIAVACCA, MIRCO, WALTHER, SOPHIA, CAMPS-VALLS, GUSTAU, KOIRALA, SUJAN, ANTHONI, PETER, BESNARD, SIMON, BODESHEIM, PAUL, CARVALHAIS, NUNO, CHEVALLIER, FRÉDÉRIC, GANS, FABIAN, GOLL, DANIEL S., HAVERD, VANESSA, KÖHLER, PHILIPP, ICHII, KAZUHITO, JAIN, ATUL K., LIU, JUNZHI, LOMBARDOZZI, DANICA, NABEL, JULIA E. M. S., NELSON, JACOB A., O'SULLIVAN, MICHAEL, PALLANDT, MARTIJN, PAPALE, DARIO, PETERS, WOUTER, PONGRATZ, JULIA, RÖDENBECK, CHRISTIAN, SITCH, STEPHEN, TRAMONTANA, GIANLUCA, WALKER, ANTHONY, WEBER, ULRICH, & REICHSTEIN, MARKUS. 2020. Scaling carbon fluxes from eddy covariance sites to globe: synthesis and evaluation of the FLUXCOM approach. *Biogeosciences*, **17**(5), 1343–1365.

JUNTTILA, S., HÖLTTÄ, T., SAARINEN, N., KANKARE, V., YRTTIMAA, T., HYYPPÄ, J., & VASTARANTA, M. 2022. Close-range hyperspectral spectroscopy reveals leaf water content dynamics. *Remote Sensing of Environment*, **277**(Aug.), 113071.

KALA, J., DE KAUWE, M. G., PITMAN, A. J., LORENZ, R., MEDLYN, B. E., WANG, Y.-P, LIN, Y.-S, & ABRAMOWITZ, G. 2015a. Implementation of an optimal stomatal conductance scheme in the Australian Community Climate Earth Systems Simulator (ACCESS1.3b). *Geoscientific Model Development*, **8**(12), 3877–3889.

KALA, J., DE KAUWE, M. G., PITMAN, A. J., LORENZ, R., MEDLYN, B. E., WANG, Y.-P., LIN, Y.-S., & ABRAMOWITZ, G. 2015b. Implementation of an optimal stomatal conductance scheme in the Australian Community Climate Earth Systems Simulator (ACCESS1.3b). *Geoscientific Model Development*, **8**(12), 3877–3889.

KALMA, JETSE D., MCVICAR, TIM R., & MCCABE, MATTHEW F. 2008. Estimating Land Surface Evaporation: A Review of Methods Using Remotely Sensed Surface Temperature Data. *Surveys in Geophysics*, **29**(4-5), 421–469.

KANG, HYUNWOO, SRIDHAR, VENKATARAMANA, MAINUDDIN, MOHAMMED, & TRUNG, LE DUC. 2021. Future rice farming threatened by drought in the Lower Mekong Basin. *Scientific Reports*, **11**(1), 9383.

KAPILAN, RANGANATHAN, VAZIRI, MARYAM, & ZWIAZEK, JANUSZ J. 2018. Regulation of aquaporins in plants under stress. *Biological Research*, **51**(1), 4.

KATTENBORN, TEJA, RICHTER, RONNY, GUIMARÃES-STEINICKE, CLAUDIA, FEILHAUER, HANNES, & WIRTH, CHRISTIAN. 2022. AngleCam : Predicting the temporal variation of leaf angle distributions from image series with deep learning. *Methods in Ecology and Evolution*, **13**(11), 2531–2545.

KEELING, RALPH, & TANS, PIETER. 2023. *Trends in atmospheric carbon dioxide, National Oceanic and Atmospheric Administration, Global Monitoring Laboratory (NOAA/GML)*.

KEENAN, T, GARCIA, R, FRIEND, A D, ZAEHLE, S, GRACIA, C, & SABATE, S. 2009. Improved understanding of drought controls on seasonal variation in Mediterranean forest canopy CO2 and water fluxes through combined in situ measurements and ecosystem modelling. 22.

KEENAN, TREVOR, SABATE, SANTI, & GRACIA, CARLOS. 2010a. The importance of mesophyll conductance in regulating forest ecosystem productivity during drought periods. *Global Change Biology*, **16**(3), 1019–1034.

KEENAN, TREVOR, SABATE, SANTI, & GRACIA, CARLOS. 2010b. Soil water stress and coupled photosynthesis–conductance models: Bridging the gap between conflicting reports on the relative roles of stomatal, mesophyll conductance and biochemical limitations to photosynthesis. *Agricultural and Forest Meteorology*, **150**(3), 443–453.

KEENAN, TREVOR F., MIGLIAVACCA, MIRCO, PAPALE, DARIO, BALDOCCHI, DENNIS, REICHSTEIN, MARKUS, TORN, MARGARET, & WUTZLER, THOMAS. 2019. Widespread inhibition of daytime ecosystem respiration. *Nature Ecology & Evolution*, **3**(3), 407–415.

KELLER, BEAT, VASS, IMRE, MATSUBARA, SHIZUE, PAUL, KENNY, JEDMOWSKI, CHRISTOPH, PIERUSCHKA, ROLAND, NEDBAL, LADISLAV, RASCHER, UWE, & MULLER, ONNO. 2019. Maximum fluorescence and electron transport kinetics determined by light-induced fluorescence transients (LIFT) for photosynthesis phenotyping. *Photosynthesis Research*, **140**(2), 221–233.

KELLIHER, F.M., LEUNING, R., RAUPACH, M.R., & SCHULZE, E.-D. 1995. Maximum conductances for evaporation from global vegetation types. *Agricultural and Forest Meteorology*, **73**(1), 1–16.

KENNEDY, DANIEL, SWENSON, SEAN, OLESON, KEITH W., LAWRENCE, DAVID M., FISHER, ROSIE, LOLA DA COSTA, ANTONIO CARLOS, & GENTINE, PIERRE. 2019. Implementing Plant Hydraulics in the Community Land Model, Version 5. *Journal of Advances in Modeling Earth Systems*, **11**(2), 485–513.

KERR, YANN H., WALDTEUFEL, PHILIPPE, RICHAUME, PHILIPPE, WIGNERON, JEAN PIERRE, FERRAZZOLI, PAOLO, MAHMOODI, ALI, AL BITAR, AHMAD, CABOT, FRANÇOIS, GRUHIER, CLAIRE, JUGLEA, SILVIA ENACHE, LEROUX, DELPHINE, MIALON, ARNAUD, & DELWART, STEVEN. 2012. The SMOS Soil Moisture Retrieval Algorithm. *IEEE Transactions on Geoscience and Remote Sensing*, **50**(5), 1384–1403.

KHANAL, SAMI, FULTON, JOHN, & SHEARER, SCOTT. 2017. An overview of current and potential applications of thermal remote sensing in precision agriculture. *Computers and Electronics in Agriculture*, **139**, 22–32.

KIM, JONGMIN, RYU, YOUNGRYEL, DECHANT, BENJAMIN, LEE, HOJIN, KIM, HYUN SEOK, KORNFELD, ARI, & BERRY, JOSEPH A. 2021. Solar-induced chlorophyll fluorescence is non-linearly related to canopy photosynthesis in a temperate evergreen needleleaf forest during the fall transition. *Remote Sensing of Environment*, **258**(June), 112362.

KING, BRADLEY A., STARK, JEFFREY C., & NEIBLING, HOWARD. 2020. *Potato Irrigation Management*. Cham: Springer International Publishing. Pages 417–446.

KIRA, O., Y-Y. CHANG, C., GU, L., WEN, J., HONG, Z., & SUN, Y. 2021. Partitioning Net Ecosystem Exchange (NEE) of CO2 Using Solar-Induced Chlorophyll Fluorescence (SIF). *Geophysical Research Letters*, **48**(4), e2020GL091247. Publisher: John Wiley & Sons, Ltd.

KLEIN, TAMIR. 2014. The variability of stomatal sensitivity to leaf water potential across tree species indicates a continuum between isohydric and anisohydric behaviours. *Functional Ecology*, **28**(6), 1313–1320.

KNAUER, JÜRGEN, WERNER, CHRISTIANE, & ZAEHLE, SÖNKE. 2015. Evaluating stomatal models and their atmospheric drought response in a land surface scheme: A multibiome analysis. *Journal of Geophysical Research: Biogeosciences*, **120**(10), 1894–1911.

KNAUER, JÜRGEN, EL-MADANY, TAREK S., ZAEHLE, SÖNKE, & MIGLIAVACCA, MIRCO. 2018a. Bigleaf—An R package for the calculation of physical and physiological ecosystem properties from eddy covariance data. *PLOS ONE*, **13**(8), e0201114.

KNAUER, JÜRGEN, ZAEHLE, SÖNKE, MEDLYN, BELINDA E., REICHSTEIN, MARKUS, WILLIAMS, CHRISTOPHER A., MIGLIAVACCA, MIRCO, DE KAUWE, MARTIN G., WERNER, CHRISTIANE, KEITEL, CLAUDIA, KOLARI, PASI, LIMOUSIN, JEAN-MARC, & LINDERSON, MAJ-LENA. 2018b. Towards physiologically meaningful water-use efficiency estimates from eddy covariance data. *Global Change Biology*, **24**(2), 694–710.

KNAUER, JÜRGEN, ZAEHLE, SÖNKE, DE KAUWE, MARTIN G., BAHAR, NUR H. A., EVANS, JOHN R., MEDLYN, BELINDA E., REICHSTEIN, MARKUS, & WERNER, CHRISTIANE. 2019a. Effects of mesophyll conductance on vegetation responses to elevated CO $_2$ concentrations in a land surface model. *Global Change Biology*, **25**(5), 1820–1838.

KNAUER, JÜRGEN, ZAEHLE, SÖNKE, DE KAUWE, MARTIN G., HAVERD, VANESSA, REICHSTEIN, MARKUS, & SUN, YING. 2019b. Mesophyll conductance in land surface models: effects on photosynthesis and transpiration. *The Plant Journal*, Dec.

KNAUER, JÜRGEN, ZAEHLE, SÖNKE, DE KAUWE, MARTIN G., HAVERD, VANESSA, REICHSTEIN, MARKUS, & SUN, YING. 2020. Mesophyll conductance in land surface models: effects on photosynthesis and transpiration. *The Plant Journal*, **101**(4), 858–873.

KOFFI, E. N., RAYNER, P. J., NORTON, A. J., FRANKENBERG, C., & SCHOLZE, M. 2015. Investigating the usefulness of satellite-derived fluorescence data in inferring gross primary productivity within the carbon cycle data assimilation system. *Biogeosciences*, **12**(13), 4067–4084.

KOHONEN, K.-M., DEWAR, R., TRAMONTANA, G., MAURANEN, A., KOLARI, P., KOOIJMANS, L. M. J., PAPALE, D., VESALA, T., & MAMMARELLA, I. 2022. Intercomparison of methods to estimate gross primary production based on $CO_2 and COS flux measurements. Biogeosciences$, **19**$(17), 4067 - -4088$.

KOLBER, ZBIGNIEW, KLIMOV, DENIS, ANANYEV, GENNADY, RASCHER, UWE, BERRY, JOSEPH, & OSMOND, BARRY. 2005. Measuring photosynthetic parameters at a distance: laser induced fluorescence transient (LIFT) method for remote measurements of photosynthesis in terrestrial vegetation. *Photosynthesis Research*, **84**(1-3), 121–129.

KONG, JUWON, RYU, YOUNGRYEL, LIU, JIANGONG, DECHANT, BENJAMIN, REY-SANCHEZ, CAMILO, SHORTT, ROBERT, SZUTU, DAPHNE, VERFAILLIE, JOE, HOUBORG, RASMUS, & BALDOCCHI, DENNIS D. 2022. Matching high resolution satellite data and flux tower footprints improves their agreement in photosynthesis estimates. *Agricultural and Forest Meteorology*, **316**(Apr.), 108878.

KONINGS, ALEXANDRA G., & GENTINE, PIERRE. 2017. Global variations in ecosystem-scale isohydricity. *Global Change Biology*, **23**(2), 891–905.

KONINGS, ALEXANDRA G., RAO, KRISHNA, & STEELE-DUNNE, SUSAN C. 2019. Macro to micro: microwave remote sensing of plant water content for physiology and ecology. *New Phytologist*, **223**(3), 1166–1172.

KONINGS, ALEXANDRA G., SAATCHI, SASSAN S., FRANKENBERG, CHRISTIAN, KELLER, MICHAEL, LESHYK, VICTOR, ANDEREGG, WILLIAM R. L., HUMPHREY, VINCENT, MATHENY, ASHLEY M., TRUGMAN, ANNA, SACK, LAWREN, AGEE, ELIZABETH, BARNES, MALLORY L., BINKS, OLIVER, CAWSE-NICHOLSON, KERRY, CHRISTOFFERSEN, BRADLEY O., ENTEKHABI, DARA, GENTINE, PIERRE, HOLTZMAN, NATANIEL M., KATUL, GABRIEL G., LIU, YANLAN, LONGO, MARCOS, MARTINEZ-VILALTA, JORDI, MCDOWELL, NATE, MEIR, PATRICK, MENCUCCINI, MAURIZIO, MRAD, ASSAAD, NOVICK, KIMBERLY A., OLIVEIRA, RAFAEL S., SIQUEIRA, PAUL, STEELE-DUNNE, SUSAN C., THOMPSON, DAVID R., WANG, YUJIE, WEHR, RICHARD, WOOD, JEFFREY D., XU, XIANGTAO, & ZUIDEMA, PIETER A. 2021. Detecting forest response to droughts with global observations of vegetation water content. *Global Change Biology*, **27**(23), 6005–6024.

KOSUGI, YOSHIKO, TAKANASHI, SATORU, UEYAMA, MASAHITO, OHKUBO, SHINJIRO, TANAKA, HIROKI, MATSUMOTO, KAZUHO, YOSHIFUJI, NATSUKO, ATAKA, MIOKO, & SAKABE, AYAKA. 2013. Determination of the gas exchange phenology in an evergreen coniferous forest from 7 years of eddy covariance flux data using an extended big-leaf analysis. *Ecological Research*, **28**, 373–385.

KOU, XINYUE, HAN, WEIHUA, & KANG, JIAN. 2022. Responses of root system architecture to water stress at multiple levels: A meta-analysis of trials under controlled conditions. *Frontiers in Plant Science*, **13**.

KRAMER, DAVID M., JOHNSON, GILES, KIIRATS, OLAVI, & EDWARDS, GERALD E. 2004. New Fluorescence Parameters for the Determination of Q $_{A}$ Redox State and Excitation Energy Fluxes. *Photosynthesis Research*, **79**(2), 209–218.

KRICH, CHRISTOPHER, MAHECHA, MIGUEL D, MIGLIAVACCA, MIRCO, DE KAUWE, MARTIN G, GRIEBEL, ANNE, RUNGE, JAKOB, & MIRALLES, DIEGO G. 2022. Decoupling between ecosystem photosynthesis and transpiration: a last resort against overheating. *Environmental Research Letters*, **17**(4), 044013.

KRINNER, G., VIOVY, NICOLAS, DE NOBLET-DUCOUDRÉ, NATHALIE, OGÉE, JÉRÔME, POLCHER, JAN, FRIEDLINGSTEIN, PIERRE, CIAIS, PHILIPPE, SITCH, STEPHEN, & PRENTICE, I. COLIN. 2005. A dynamic global vegetation model for studies of the coupled atmosphere-biosphere system. *Global Biogeochemical Cycles*, **19**(1), 2003GB002199.

KROMDIJK, JOHANNES, GŁOWACKA, KATARZYNA, & LONG, STEPHEN P. 2019. Photosynthetic efficiency and mesophyll conductance are unaffected in Arabidopsis thaliana aquaporin knock-out lines. *Journal of Experimental Botany*, **71**(1), 318–329.

KRUSE, F., & LEFKOFF, A. 1999. Analysis of Spectral Data of Manmade Materials, Military Targets, and Background Using an Expert System Based Approach. Jan.

KUBISKE, MARK E., & PREGITZER, KURT S. 1996. Effects of elevated CO2 and light availability on the photosynthetic light response of trees of contrasting shade tolerance. *Tree Physiology*, **16**(3), 351–358.

KUKAL, MEETPAL S., & IRMAK, SUAT. 2023. Can limits of plant available water be inferred from soil moisture distributions? *Agricultural & Environmental Letters*, **8**(2), e20113.

KUMAR, ROHITASHW, SHANKAR, VIJAY, & JAT, MAHESH KUMAR. 2015. Evaluation of root water uptake models – a review. *ISH Journal of Hydraulic Engineering*, **21**(2), 115–124.

KUTSCH, W.L., AUBINET, M., BUCHMANN, N., SMITH, P., OSBORNE, B., EUGSTER, W., WATTENBACH, M., SCHRUMPF, M., SCHULZE, E.D., TOMELLERI, E., CESCHIA, E., BERNHOFER, C., BÉZIAT, P., CARRARA, A., DI TOMMASI, P., GRÜNWALD, T., JONES, M., MAGLIULO, V., MARLOIE, O., MOUREAUX, C., OLIOSO, A., SANZ, M.J., SAUNDERS, M., SØGAARD, H., & ZIEGLER, W. 2010. The net biome production of full crop rotations in Europe. *Agriculture, Ecosystems Environment*, **139**(3), 336–345. The carbon balance of European croplands.

KÖHLER, P., GUANTER, L., & JOINER, J. 2015. A linear method for the retrieval of sun-induced chlorophyll fluorescence from GOME-2 and SCIAMACHY data. *Atmospheric Measurement Techniques*, **8**(6), 2589–2608.

LAMOUR, JULIEN, DAVIDSON, KENNETH J., ELY, KIM S., LE MOGUÉDEC, GILLES, LEAKEY, ANDREW D. B., LI, QIANYU, SERBIN, SHAWN P., & ROGERS, ALISTAIR. 2022. An improved representation of the relationship between photosynthesis and stomatal conductance leads to more stable estimation of conductance parameters and improves the goodness-of-fit across diverse data sets. *Global Change Biology*, **28**(11), 3537–3556.

LASSLOP, G., MIGLIAVACCA, M., BOHRER, G., REICHSTEIN, M., BAHN, M., IBROM, A., JACOBS, C., KOLARI, P., PAPALE, D., VESALA, T., WOHLFAHRT, G., & CESCATTI, A. 2012. On the choice of the driving temperature for eddy-covariance carbon dioxide flux partitioning. *Biogeosciences*, **9**(12), 5243–5259.

LASSLOP, GITTA, REICHSTEIN, MARKUS, PAPALE, DARIO, RICHARDSON, ANDREW D., ARNETH, ALMUT, BARR, ALAN, STOY, PAUL, & WOHLFAHRT, GEORG. 2010. Separation of net ecosystem exchange into assimilation and respiration using a light response curve approach: critical issues and global evaluation: SEPARATION OF NEE INTO GPP AND RECO. *Global Change Biology*, **16**(1), 187–208.

LAWLOR, DAVID W., & TEZARA, WILMER. 2009. Causes of decreased photosynthetic rate and metabolic capacity in water-deficient leaf cells: a critical evaluation of mechanisms and integration of processes. *Annals of Botany*, **103**(4), 561–579.

LAWRENCE, DAVID M., FISHER, ROSIE A., KOVEN, CHARLES D., OLESON, KEITH W., SWENSON, SEAN C., BONAN, GORDON, COLLIER, NATHAN, GHIMIRE, BARDAN, VAN KAMPENHOUT, LEO, KENNEDY, DANIEL, KLUZEK, ERIK, LAWRENCE, PETER J., LI, FANG, LI, HONGYI, LOMBARDOZZI, DANICA, RILEY, WILLIAM J., SACKS, WILLIAM J., SHI, MINGJIE, VERTENSTEIN, MARIANA, WIEDER, WILLIAM R., XU, CHONGGANG, ALI, ASHEHAD A., BADGER, ANDREW M., BISHT, GAUTAM, VAN DEN BROEKE, MICHIEL, BRUNKE, MICHAEL A., BURNS, SEAN P., BUZAN, JONATHAN, CLARK, MARTYN, CRAIG, ANTHONY, DAHLIN, KYLA, DREWNIAK, BETH, FISHER, JOSHUA B., FLANNER, MARK, FOX, ANDREW M., GENTINE, PIERRE, HOFFMAN, FORREST, KEPPEL-ALEKS, GRETCHEN, KNOX, RYAN, KUMAR, SANJIV, LENAERTS, JAN, LEUNG, L. RUBY, LIPSCOMB, WILLIAM H., LU, YAQIONG, PANDEY, ASHUTOSH, PELLETIER, JON D., PERKET, JUSTIN, RANDERSON, JAMES T., RICCIUTO, DANIEL M., SANDERSON, BENJAMIN M.,

SLATER, ANDREW, SUBIN, ZACHARY M., TANG, JINYUN, THOMAS, R. QUINN, VAL MARTIN, MARIA, & ZENG, XUBIN. 2019. The Community Land Model Version 5: Description of New Features, Benchmarking, and Impact of Forcing Uncertainty. *Journal of Advances in Modeling Earth Systems*, **11**(12), 4245–4287.

LAWSON, TRACY, SIMKIN, ANDREW J., KELLY, GILOR, & GRANOT, DAVID. 2014. Mesophyll photosynthesis and guard cell metabolism impacts on stomatal behaviour. *New Phytologist*, **203**(4), 1064–1081.

LEAKEY, ANDREW D.B., FERGUSON, JOHN N., PIGNON, CHARLES P., WU, ALEX, JIN, ZHENONG, HAMMER, GRAEME L., & LOBELL, DAVID B. 2019. Water Use Efficiency as a Constraint and Target for Improving the Resilience and Productivity of C $_3$ and C $_4$ Crops. *Annual Review of Plant Biology*, **70**(1), 781–808.

LEE, JUNG-EUN, BERRY, JOSEPH A., VAN DER TOL, CHRISTIAAN, YANG, XI, GUANTER, LUIS, DAMM, ALEXANDER, BAKER, IAN, & FRANKENBERG, CHRISTIAN. 2015. Simulations of chlorophyll fluorescence incorporated into the Community Land Model version 4. *Global Change Biology*, **21**(9), 3469–3477.

LEE, SUNG-CHING, CHRISTEN, ANDREAS, BLACK, T. ANDREW, JASSAL, RACHHPAL S., KETLER, RICK, & NESIC, ZORAN. 2020. Partitioning of net ecosystem exchange into photosynthesis and respiration using continuous stable isotope measurements in a Pacific Northwest Douglas-fir forest ecosystem. *Agricultural and Forest Meteorology*, **292-293**, 108109.

LEMONNIER, P., & LAWSON, T. 2023. Calvin cycle and guard cell metabolism impact stomatal function. *Seminars in Cell & Developmental Biology*, Mar., S1084952123000502.

LEONOVA, ANASTASIA, HEGER, ADRIAN, VÁSCONEZ NAVAS, LIZETH K., JENSEN, KAI, & REISDORFF, CHRISTOPH. 2022. Fine root mortality under severe drought reflects different root distribution of Quercus robur and Ulmus laevis trees in hardwood floodplain forests. *Trees*, **36**(3), 1105–1115.

LEUNING, R. 1995. A critical appraisal of a combined stomatal-photosynthesis model for C3 plants. *Plant, Cell & Environment*, **18**(4), 339–355.

LI, BAORU, ZHANG, XIYING, MORITA, SHIGENORI, SEKIYA, NOBUHITO, ARAKI, HIDEKI, GU, HUIJIE, HAN, JIE, LU, YANG, & LIU, XIUWEI. 2022a. Are crop deep roots always beneficial for combating drought: A review of root structure and function, regulation and phenotyping. *Agricultural Water Management*, **271**, 107781.

LI, HELI, ZHAO, CHUNJIANG, YANG, GUIJUN, & FENG, HAIKUAN. 2015. Variations in crop variables within wheat canopies and responses of canopy spectral characteristics and derived vegetation indices to different vertical leaf layers and spikes. *Remote Sensing of Environment*, **169**(Nov.), 358–374.

LI, JIANHUI, CANG, ZHENMING, JIAO, FENG, BAI, XUEJING, ZHANG, DING, & ZHAI, RUICHANG. 2017. Influence of drought stress on photosynthetic characteristics and protective enzymes of potato at seedling stage. *Journal of the Saudi Society of Agricultural Sciences*, **16**(1), 82–88.

LI, QIAN, GAO, YANG, HAMANI, ABDOUL KADER MOUNKAILA, FU, YUANYUAN, LIU, JUNMING, WANG, HONGBO, & WANG, XINGPENG. 2023a. Effects of Warming and Drought Stress on the Coupling of Photosynthesis and Transpiration in Winter Wheat (Triticum aestivum L.). *Applied Sciences*, **13**(5), 2759.

LI, QIANYU, SERBIN, SHAWN P., LAMOUR, JULIEN, DAVIDSON, KENNETH J., ELY, KIM S., & ROGERS, ALISTAIR. 2022b (Jan.). *Implementation and evaluation of the unified stomatal optimization approach in the Functionally Assembled Terrestrial Ecosystem Simulator (FATES)*. preprint. Biogeosciences.

LI, RAN, LU, YAOJIE, PETERS, JENNIFER M. R., CHOAT, BRENDAN, & LEE, ANDREW J. 2020. Non-invasive measurement of leaf water content and pressure–volume curves using terahertz radiation. *Scientific Reports*, **10**(1), 21028.

LI, SHUANG, LIU, JUNMING, LIU, HAO, QIU, RANGJIAN, GAO, YANG, & DUAN, AIWANG. 2021a. Role of Hydraulic Signal and ABA in Decrease of Leaf Stomatal and Mesophyll Conductance in Soil Drought-Stressed Tomato. *Frontiers in Plant Science*, **12**(Apr.), 653186.

LI, XING, XIAO, JINGFENG, HE, BINBIN, ALTAF ARAIN, M., BERINGER, JASON, DESAI, ANKUR R., EMMEL, CARMEN, HOLLINGER, DAVID Y., KRASNOVA, ALISA, MAMMARELLA, IVAN, NOE, STEFFEN M., ORTIZ, PENÉLOPE SERRANO, REY-SANCHEZ, A. CAMILO, ROCHA, ADRIAN V., & VARLAGIN, ANDREJ. 2018a. Solar-induced chlorophyll fluorescence is strongly correlated with terrestrial photosynthesis for a wide variety of biomes: First global analysis based on OCO-2 and flux tower observations. *Global Change Biology*, **24**(9), 3990–4008.

LI, XING, XIAO, JINGFENG, HE, BINBIN, ALTAF ARAIN, M., BERINGER, JASON, DESAI, ANKUR R., EMMEL, CARMEN, HOLLINGER, DAVID Y., KRASNOVA, ALISA, MAMMARELLA, IVAN, NOE, STEFFEN M., ORTIZ, PENÉLOPE SERRANO, REY-SANCHEZ, A. CAMILO, ROCHA, ADRIAN V., & VARLAGIN, ANDREJ. 2018b. Solar-induced chlorophyll fluorescence is strongly correlated with terrestrial photosynthesis for a wide variety of biomes: First global analysis based on OCO-2 and flux tower observations. *Global Change Biology*, **24**(9), 3990–4008.

LI, XING, XIAO, JINGFENG, FISHER, JOSHUA B., & BALDOCCHI, DENNIS D. 2021b. ECOSTRESS estimates gross primary production with fine spatial resolution for different times of day from the International Space Station. *Remote Sensing of Environment*, **258**, 112360.

LI, XING, RYU, YOUNGRYEL, XIAO, JINGFENG, DECHANT, BENJAMIN, LIU, JIANGONG, LI, BOLUN, JEONG, SUNGCHAN, & GENTINE, PIERRE. 2023b. New-generation geostationary satellite reveals widespread midday depression in dryland photosynthesis during 2020 western U.S. heatwave. *Science Advances*, **9**(31), eadi0775.

LI, ZHAO-LIANG, TANG, BO-HUI, WU, HUA, REN, HUAZHONG, YAN, GUANGJIAN, WAN, ZHENGMING, TRIGO, ISABEL F., & SOBRINO, JOSÉ A. 2013. Satellite-derived land surface temperature: Current status and perspectives. *Remote Sensing of Environment*, **131**(Apr.), 14–37.

LI, ZHAO-LIANG, WU, HUA, DUAN, SI-BO, ZHAO, WEI, REN, HUAZHONG, LIU, XIANGYANG, LENG, PEI, TANG, RONGLIN, YE, XIN, ZHU, JINSHUN, SUN, YINGWEI, SI, MENGLIN, LIU, MENG, LI, JIAHAO, ZHANG, XIA, SHANG, GUOFEI, TANG, BO-HUI, YAN, GUANGJIAN, & ZHOU, CHENGHU. 2023c. Satellite Remote Sensing of Global Land Surface Temperature: Definition, Methods, Products, and Applications. *Reviews of Geophysics*, **61**(1), e2022RG000777. e2022RG000777 2022RG000777.

LIANG, SHUNLIN, & WANG, JINDI (eds). 2020. Chapter 7 - Land surface temperature and thermal infrared emissivity. *Pages 251–295 of:* LIANG, SHUNLIN, & WANG, JINDI (eds), *Advanced Remote Sensing (Second Edition)*, second edition edn. Academic Press.

LIANG, ZHIGUO, YU, YING, YANG, XIGUANG, & FAN, WENYI. 2023. Comparison of Canopy Clumping Index Measuring Methods and Analysis of Their Impact. *Remote Sensing*, **15**(2).

LIGUORI, NICOLETTA, PERIOLE, XAVIER, MARRINK, SIEWERT J., & CROCE, ROBERTA. 2015. From light-harvesting to photoprotection: structural basis of the dynamic switch of the major antenna complex of plants (LHCII). *Scientific Reports*, **5**(1), 15661.

LIMOUSIN, JEAN-MARC, MISSON, LAURENT, LAVOIR, ANNE-VIOLETTE, MARTIN, NICOLAS K., & RAMBAL, SERGE. 2010. Do photosynthetic limitations of evergreen *Quercus ilex* leaves change with long-term increased drought severity? *Plant, Cell & Environment*, Mar.

LIN, YAN-SHIH, MEDLYN, BELINDA E., DUURSMA, REMKO A., PRENTICE, I. COLIN, WANG, HAN, BAIG, SOFIA, EAMUS, DEREK, DE DIOS, VICTOR RESCO, MITCHELL, PATRICK, ELLSWORTH, DAVID S., DE BEECK, MAARTEN OP, WALLIN, GÖRAN, UDDLING, JOHAN, TARVAINEN, LASSE, LINDERSON, MAJ-LENA, CERNUSAK, LUCAS A., NIPPERT, JESSE B., OCHELTREE, TROY W., TISSUE, DAVID T., MARTIN-STPAUL, NICOLAS K., ROGERS, ALISTAIR, WARREN, JEFF M., DE ANGELIS, PAOLO, HIKOSAKA, KOUKI, HAN, QINGMIN, ONODA, YUSUKE, GIMENO, TERESA E., BARTON, CRAIG V. M., BENNIE, JONATHAN, BONAL, DAMIEN, BOSC, ALEXANDRE, LÖW, MARKUS, MACININS-NG, CATE, REY, ANA, ROWLAND, LUCY, SETTERFIELD, SAMANTHA A., TAUSZ-POSCH, SABINE, ZARAGOZA-CASTELLS, JOANA, BROADMEADOW, MARK S. J., DRAKE, JOHN E., FREEMAN, MICHAEL, GHANNOUM, OULA, HUTLEY, LINDSAY B., KELLY, JEFF W., KIKUZAWA, KIHACHIRO, KOLARI, PASI, KOYAMA, KOHEI, LIMOUSIN, JEAN-MARC, MEIR, PATRICK, LOLA DA COSTA, ANTONIO C., MIKKELSEN, TEIS N., SALINAS, NORMA, SUN, WEI, & WINGATE, LISA. 2015a. Optimal stomatal behaviour around the world. *Nature Climate Change*, **5**(5), 459–464.

LIN, YAN-SHIH, MEDLYN, BELINDA E, DUURSMA, REMKO A, PRENTICE, I COLIN, WANG, HAN, BAIG, SOFIA, EAMUS, DEREK, DE DIOS, VICTOR RESCO, MITCHELL, PATRICK, ELLSWORTH, DAVID S, *et al.* 2015b. Optimal stomatal behaviour around the world. *Nature Climate Change*, **5**(5), 459–464.

LIU, HUI, SONG, SONGBO, ZHANG, HUI, LI, YANHUA, NIU, LIANGJIE, ZHANG, JINGHUA, & WANG, WEI. 2022a. Signaling Transduction of ABA, ROS, and Ca2+ in Plant Stomatal Closure in Response to Drought. *International Journal of Molecular Sciences*, **23**(23).

LIU, WEIWEI, ATHERTON, JON, MÕTTUS, MATTI, GASTELLU-ETCHEGORRY, JEAN-PHILIPPE, MALENOVSKÝ, ZBYNĚK, RAUMONEN, PASI, ÅKERBLOM, MARKKU, MÄKIPÄÄ, RAISA, & PORCAR-CASTELL, ALBERT. 2019. Simulating solar-induced chlorophyll fluorescence in a boreal forest stand reconstructed from terrestrial laser scanning measurements. *Remote Sensing of Environment*, **232**, 111274.

LIU, XIANGZHUO, WIGNERON, JEAN-PIERRE, WAGNER, WOLFGANG, FRAPPART, FRÉDÉRIC, FAN, LEI, VREUGDENHIL, MARIETTE, BAGHDADI, NICOLAS, ZRIBI, MEHREZ, JAGDHUBER, THOMAS, TAO, SHENGLI, LI, XIAOJUN, WANG, HUAN, WANG, MENGJIA, BAI, XIAOJING, MOUSA, B.G., & CIAIS, PHILIPPE. 2023. A new global C-band vegetation optical depth product from ASCAT: Description, evaluation, and inter-comparison. *Remote Sensing of Environment*, **299**, 113850.

LIU, XINJIE, LIU, ZHUNQIAO, LIU, LIANGYUN, LU, XIAOLIANG, CHEN, JIDAI, DU, SHANSHAN, & ZOU, CHU. 2021. Modelling the influence of incident radiation on the SIF-based GPP estimation for maize. *Agricultural and Forest Meteorology*, **307**, 108522.

LIU, YIHONG, CHEN, JING M., HE, LIMING, ZHANG, ZHAOYING, WANG, RONG, ROGERS, CHERYL, FAN, WEILIANG, DE OLIVEIRA, GABRIEL, & XIE, XINYAO. 2022b. Non-linearity between gross primary productivity and far-red solar-induced chlorophyll fluorescence emitted from canopies of major biomes. *Remote Sensing of Environment*, **271**(Mar.), 112896.

LIU, ZHUNQIAO, ZHAO, FENG, LIU, XINJIE, YU, QIANG, WANG, YUNFEI, PENG, XIONGBIAO, CAI, HUANJIE, & LU, XIAOLIANG. 2022c. Direct estimation of photosynthetic CO2 assimilation from solar-induced chlorophyll fluorescence (SIF). *Remote Sensing of Environment*, **271**(Mar.), 112893.

LLOYD-HUGHES, BENJAMIN. 2014. The impracticality of a universal drought definition. *Theoretical and Applied Climatology*, **117**(3-4), 607–611.

LOGNOUL, M., DEBACQ, A., DE LIGNE, A., DUMONT, B., MANISE, T., BODSON, B., HEINESCH, B., & AUBINET, M. 2019. N2O flux short-term response to temperature and topsoil disturbance in a fertilized crop: An eddy covariance campaign. *Agricultural and Forest Meteorology*, **271**, 193–206.

LONG, S. P. 2003. Gas exchange measurements, what can they tell us about the underlying limitations to photosynthesis? Procedures and sources of error. *Journal of Experimental Botany*, **54**(392), 2393–2401.

LU, XIAOLIANG, LIU, ZHUNQIAO, ZHAO, FENG, & TANG, JIANWU. 2020. Comparison of total emitted solar-induced chlorophyll fluorescence (SIF) and top-of-canopy (TOC) SIF in estimating photosynthesis. *Remote Sensing of Environment*, **251**(Dec.), 112083.

LU, YAQIONG, WILLIAMS, IAN N., BAGLEY, JUSTIN E., TORN, MARGARET S., & KUEPPERS, LARA M. 2017. Representing winter wheat in the Community Land Model (version 4.5). *Geoscientific Model Development*, **10**(5), 1873–1888.

LUBITZ, WOLFGANG, CHRYSINA, MARIA, & COX, NICHOLAS. 2019. Water oxidation in photosystem II. *Photosynthesis Research*, **142**(1), 105–125.

LUNDGREN, MARJORIE R., & FLEMING, ANDREW J. 2020. Cellular perspectives for improving mesophyll conductance. *The Plant Journal*, **101**(4), 845–857.

LUO, SHENGMIN, LU, NING, ZHANG, CHAO, & LIKOS, WILLIAM. 2022. Soil water potential: A historical perspective and recent breakthroughs. *Vadose Zone Journal*, **21**(4), e20203.

LUO, XIANGZHONG, CHEN, JING M., LIU, JANE, BLACK, T. ANDREW, CROFT, HOLLY, STAEBLER, RALF, HE, LIMING, ARAIN, M. ALTAF, CHEN, BIN, MO, GANG, GONSAMO, ALEMU, & MCCAUGHEY, HARRY. 2018. Comparison of Big-Leaf, Two-Big-Leaf, and Two-Leaf Upscaling Schemes for Evapotranspiration Estimation Using Coupled Carbon-Water Modeling. *Journal of Geophysical Research: Biogeosciences*, **123**(1), 207–225.

LUPO, YANIV, & MOSHELION, MENACHEM. 2024. The balance of survival: Comparative drought response in wild and domesticated tomatoes. *Plant Science*, **339**(Feb.), 111928.

LUTALADIO, NEBAMBI, & CASTALDI, LUIGI. 2009. Potato: The hidden treasure. *Journal of Food Composition and Analysis*, **22**(6), 491–493.

LV, GUANGYI, JIN, JING, HE, MENGTING, & WANG, CHENGJIE. 2023. Soil Moisture Content Dominates the Photosynthesis of C3 and C4 Plants in a Desert Steppe after Long-Term Warming and Increasing Precipitation. *Plants*, **12**(16).

MA, LI, SUN, LEIGANG, WANG, SHAOQIANG, CHEN, JINGHUA, CHEN, BIN, ZHU, KAI, AMIR, MUHAMMAD, WANG, XIAOBO, LIU, YUANYUAN, WANG, PENGYUAN, WANG, JUNBANG, HUANG, MEI, & WANG, ZHAOSHENG. 2022. Analysis on the relationship between sun-induced chlorophyll fluorescence and gross primary productivity of winter wheat in northern China. *Ecological Indicators*, **139**, 108905.

MAES, WOUTER H., GENTINE, PIERRE, VERHOEST, NIKO E. C., & MIRALLES, DIEGO G. 2019. Potential evaporation at eddy-covariance sites across the globe. *Hydrology and Earth System Sciences*, **23**(2), 925–948.

MAGNEY, TROY S., VIERLING, LEE A., EITEL, JAN U.H., HUGGINS, DAVID R., & GARRITY, STEVEN R. 2016. Response of high frequency Photochemical Reflectance Index (PRI) measurements to environmental conditions in wheat. *Remote Sensing of Environment*, **173**, 84–97.

MAGNEY, TROY S., FRANKENBERG, CHRISTIAN, FISHER, JOSHUA B., SUN, YING, NORTH, GRETCHEN B., DAVIS, THOMAS S., KORNFELD, ARI, & SIEBKE, KATHARINA. 2017. Connecting active to passive fluorescence with photosynthesis: a method for evaluating remote sensing measurements of Chl fluorescence. *New Phytologist*, **215**(4), 1594–1608.

MAGNEY, TROY S., BARNES, MALLORY L., & YANG, XI. 2020. On the Covariation of Chlorophyll Fluorescence and Photosynthesis Across Scales. *Geophysical Research Letters*, **47**(23).

MAGUIRE, ANDREW J., EITEL, JAN U. H., GRIFFIN, KEVIN L., MAGNEY, TROY S., LONG, RYAN A., VIERLING, LEE A., SCHMIEGE, STEPHANIE C., JENNEWEIN, JYOTI S., WEYGINT, WILLIAM A., BOELMAN, NATALIE T., & BRUNER, SARAH G. 2020. On the Functional Relationship Between Fluorescence and Photochemical Yields in Complex Evergreen Needleleaf Canopies. *Geophysical Research Letters*, **47**(9).

MALEKI, MARAL, ARRIGA, NICOLA, ROLAND, MARILYN, WIENEKE, SEBASTIAN, BARRIOS, JOSÉ MIGUEL, VAN HOOLST, ROEL, PEÑUELAS, JOSEP, JANSSENS, IVAN A., & BALZAROLO, MANUELA. 2022. Soil water depletion induces discrepancies between in situ measured vegetation indices and photosynthesis in a temperate heathland. *Agricultural and Forest Meteorology*, **324**(Sept.), 109110.

MALONE, LORNA A., PROCTOR, MATTHEW S., HITCHCOCK, ANDREW, HUNTER, C. NEIL, & JOHNSON, MATTHEW P. 2021. Cytochrome b6f – Orchestrator of photosynthetic electron transfer. *Biochimica et Biophysica Acta (BBA) - Bioenergetics*, **1862**(5), 148380.

MANZONI, STEFANO, VICO, GIULIA, KATUL, GABRIEL, FAY, PHILIP A., POLLEY, WAYNE, PALMROTH, SARI, & PORPORATO, AMILCARE. 2011. Optimizing stomatal conductance for maximum carbon gain under water stress: a meta-analysis across plant functional types and climates: Optimal leaf gas exchange under water stress. *Functional Ecology*, **25**(3), 456–467.

MARCHIN, RENÉE M., BACKES, DIANA, OSSOLA, ALESSANDRO, LEISHMAN, MICHELLE R., TJOELKER, MARK G., & ELLSWORTH, DAVID S. 2022. Extreme heat increases stomatal conductance and drought-induced mortality risk in vulnerable plant species. *Global Change Biology*, **28**(3), 1133–1146. Publisher: John Wiley & Sons, Ltd.

MARCHIN, RENÉE M., MEDLYN, BELINDA E., TJOELKER, MARK G., & ELLSWORTH, DAVID S. 2023. Decoupling between stomatal conductance and photosynthesis occurs under extreme heat in broadleaf tree species regardless of water access. *Global Change Biology*, **29**(22), 6319–6335.

MARIN, MARIA, FEENEY, DS, BROWN, LK, NAVEED, MUHAMMAD, RUIZ, S, KOEBERNICK, NICOLAI, BENGOUGH, ANTHONY G, HALLETT, PD, ROOSE, TIINA, PUÉRTOLAS, J, *et al.* 2021. Significance of root hairs for plant performance under contrasting field conditions and water deficit. *Annals of Botany*, **128**(1), 1–16.

MARINO, GIOVANNI, HAWORTH, MATTHEW, SCARTAZZA, ANDREA, TOGNETTI, ROBERTO, & CENTRITTO, MAURO. 2020. A Comparison of the Variable J and Carbon-Isotopic Composition of

Sugars Methods to Assess Mesophyll Conductance from the Leaf to the Canopy Scale in Drought-Stressed Cherry. *International journal of molecular sciences*, **21**(4). Place: Switzerland.

MARRS, J. K., REBLIN, J. S., LOGAN, B. A., ALLEN, D. W., REINMANN, A. B., BOMBARD, D. M., TABACHNIK, D., & HUTYRA, L. R. 2020. Solar-Induced Fluorescence Does Not Track Photosynthetic Carbon Assimilation Following Induced Stomatal Closure. *Geophysical Research Letters*, **47**(15).

MARTIN, BJORN, & RUIZ-TORRES, NORMA A. 1992. Effects of Water-Deficit Stress on Photosynthesis, Its Components and Component Limitations, and on Water Use Efficiency in Wheat (*Triticum aestivum* L.). *Plant Physiology*, **100**(2), 733–739.

MARTINI, DAVID, SAKOWSKA, KAROLINA, WOHLFAHRT, GEORG, PACHECO-LABRADOR, JAVIER, VAN DER TOL, CHRISTIAAN, PORCAR-CASTELL, ALBERT, MAGNEY, TROY S., CARRARA, ARNAUD, COLOMBO, ROBERTO, EL-MADANY, TAREK S., GONZALEZ-CASCON, ROSARIO, MARTÍN, MARÍA PILAR, JULITTA, TOMMASO, MORENO, GERARDO, RASCHER, UWE, REICHSTEIN, MARKUS, ROSSINI, MICOL, & MIGLIAVACCA, MIRCO. 2022. Heatwave breaks down the linearity between sun-induced fluorescence and gross primary production. *New Phytologist*, **233**(6), 2415–2428.

MARTÍNEZ-VILALTA, JORDI, & GARCIA-FORNER, NÚRIA. 2017. Water potential regulation, stomatal behaviour and hydraulic transport under drought: deconstructing the iso/anisohydric concept. *Plant, cell & environment*, **40**(6), 962–976. Place: United States.

MARTÍNEZ-VILALTA, JORDI, POYATOS, RAFAEL, AGUADÉ, DAVID, RETANA, JAVIER, & MENCUCCINI, MAURIZIO. 2014. A new look at water transport regulation in plants. *New Phytologist*, **204**(1), 105–115.

MASSON-DELMOTTE, VP, ZHAI, PANMAO, PIRANI, SL, CONNORS, C, PÉAN, S, BERGER, N, CAUD, Y, CHEN, L, GOLDFARB, MI, & SCHEEL MONTEIRO, PEDRO M. 2021. Ipcc, 2021: Summary for policymakers. in: Climate change 2021: The physical science basis. contribution of working group i to the sixth assessment report of the intergovernmental panel on climate change.

MAVROVIC, ALEX, SONNENTAG, OLIVER, LEMMETYINEN, JUHA, BALTZER, JENNIFER L., KINNARD, CHRISTOPHE, & ROY, ALEXANDRE. 2023. Reviews and syntheses: Recent advances in microwave remote sensing in support of terrestrial carbon cycle science in Arctic–boreal regions. *Biogeosciences*, **20**(14), 2941–2970.

MAXWELL, KATE, & JOHNSON, GILES N. 2000. Chlorophyll fluorescence—a practical guide. *Journal of Experimental Botany*, **51**(345), 659–668.

MAYNARD, DANIEL S., BIALIC-MURPHY, LALASIA, ZOHNER, CONSTANTIN M., AVERILL, COLIN, VAN DEN HOOGEN, JOHAN, MA, HAOZHI, MO, LIDONG, SMITH, GABRIEL REUBEN, ACOSTA, ALICIA T. R., AUBIN, ISABELLE, BERENGUER, ERIKA, BOONMAN, COLINE C. F., CATFORD, JANE A., CERABOLINI, BRUNO E. L., DIAS, ARILDO S., GONZÁLEZ-MELO, ANDRÉS, HIETZ, PETER, LUSK, CHRISTOPHER H., MORI, AKIRA S., NIINEMETS, ÜLO, PILLAR, VALÉRIO D., PINHO, BRUNO X., ROSELL, JULIETA A., SCHURR, FRANK M., SHEREMETEV, SERGE N., DA SILVA, ANA CAROLINA, SOSINSKI, ÊNIO, VAN BODEGOM, PETER M., WEIHER, EVAN, BÖNISCH, GERHARD, KATTGE, JENS, & CROWTHER, THOMAS W. 2022. Global relationships in tree functional traits. *Nature Communications*, **13**(1), 3185.

MAZZARIELLO, A., ALBANO, R., LACAVA, T., MANFREDA, S., & SOLE, A. 2023. Intercomparison of recent microwave satellite soil moisture products on European ecoregions. *Journal of Hydrology*, **626**, 130311.

McAdam, Scott A. M., & Brodribb, Timothy J. 2016. Linking Turgor with ABA Biosynthesis: Implications for Stomatal Responses to Vapor Pressure Deficit across Land Plants. *Plant physiology*, **171**(3), 2008–2016. Place: United States.

Mcmaster, G. 1997. Growing degree-days: one equation, two interpretations. *Agricultural and Forest Meteorology*, **87**(4), 291–300.

Medlyn, B. E. 1998. Physiological basis of the light use efficiency model. *Tree Physiology*, **18**(3), 167–176.

Medlyn, B. E., Dreyer, E., Ellsworth, D., Forstreuter, M., Harley, P. C., Kirschbaum, M. U. F., Le Roux, X., Montpied, P., Strassemeyer, J., Walcroft, A., Wang, K., & Loustau, D. 2002. Temperature response of parameters of a biochemically based model of photosynthesis. II. A review of experimental data. *Plant, Cell and Environment*, **25**(9), 1167–1179.

Medlyn, Belinda E., Duursma, Remko A., Eamus, Derek, Ellsworth, David S., Prentice, I. Colin, Barton, Craig V. M., Crous, Kristine Y., De Angelis, Paolo, Freeman, Michael, & Wingate, Lisa. 2011a. Reconciling the optimal and empirical approaches to modelling stomatal conductance: RECONCILING OPTIMAL AND EMPIRICAL STOMATAL MODELS. *Global Change Biology*, **17**(6), 2134–2144.

Medlyn, Belinda E., Duursma, Remko A., Eamus, Derek, Ellsworth, David S., Prentice, I. Colin, Barton, Craig V. M., Crous, Kristine Y., De Angelis, Paolo, Freeman, Michael, & Wingate, Lisa. 2011b. Reconciling the optimal and empirical approaches to modelling stomatal conductance: RECONCILING OPTIMAL AND EMPIRICAL STOMATAL MODELS. *Global Change Biology*, **17**(6), 2134–2144.

Medlyn, Belinda E, De Kauwe, Martin G, Zaehle, Sönke, Walker, Anthony P, Duursma, Remko A, Luus, Kristina, Mishurov, Mikhail, Pak, Bernard, Smith, Benjamin, Wang, Ying-Ping, *et al.* 2016. Using models to guide field experiments: A priori predictions for the CO 2 response of a nutrient-and water-limited native Eucalypt woodland. *Global Change Biology*, **22**(8), 2834–2851.

Medlyn, Belinda E., De Kauwe, Martin G., Lin, Yan-Shih, Knauer, Jürgen, Duursma, Remko A., Williams, Christopher A., Arneth, Almut, Clement, Rob, Isaac, Peter, Limousin, Jean-Marc, Linderson, Maj-Lena, Meir, Patrick, Martin-StPaul, Nicolas, & Wingate, Lisa. 2017a. How do leaf and ecosystem measures of water-use efficiency compare? *New Phytologist*, **216**(3), 758–770.

Medlyn, Belinda E., De Kauwe, Martin G., Lin, Yan-Shih, Knauer, Jürgen, Duursma, Remko A., Williams, Christopher A., Arneth, Almut, Clement, Rob, Isaac, Peter, Limousin, Jean-Marc, Linderson, Maj-Lena, Meir, Patrick, Martin-StPaul, Nicolas, & Wingate, Lisa. 2017b. How do leaf and ecosystem measures of water-use efficiency compare? *New Phytologist*, **216**(3), 758–770.

Menne, David, Hübner, Christof, Trebbels, Dennis, & Willenbacher, Norbert. 2022. Robust Soil Water Potential Sensor to Optimize Irrigation in Agriculture. *Sensors (Basel, Switzerland)*, **22**(12). Place: Switzerland.

Merilo, Ebe, Yarmolinsky, Dmitry, Jalakas, Pirko, Parik, Helen, Tulva, Ingmar, Rasulov, Bakhtier, Kilk, Kalle, & Kollist, Hannes. 2018. Stomatal VPD Response: There Is More to the Story Than ABA. *Plant Physiology*, **176**(1), 851–864.

MERONI, M., ROSSINI, M., GUANTER, L., ALONSO, L., RASCHER, U., COLOMBO, R., & MORENO, J. 2009. Remote sensing of solar-induced chlorophyll fluorescence: Review of methods and applications. *Remote Sensing of Environment*, **113**(10), 2037–2051.

MIAO, ZEWEI, XU, MING, LATHROP, RICHARD G., & WANG, YUFEI. 2009. Comparison of the *A-C* $_c$ curve fitting methods in determining maximum ribulose 1·5-bisphosphate carboxylase/oxygenase carboxylation rate, potential light saturated electron transport rate and leaf dark respiration. *Plant, Cell & Environment*, **32**(2), 109–122.

MIGLIAVACCA, MIRCO, REICHSTEIN, MARKUS, RICHARDSON, ANDREW D., COLOMBO, ROBERTO, SUTTON, MARK A., LASSLOP, GITTA, TOMELLERI, ENRICO, WOHLFAHRT, GEORG, CARVALHAIS, NUNO, CESCATTI, ALESSANDRO, MAHECHA, MIGUEL D., MONTAGNANI, LEONARDO, PAPALE, DARIO, ZAEHLE, SÖNKE, ARAIN, ALTAF, ARNETH, ALMUT, BLACK, T. ANDREW, CARRARA, ARNAUD, DORE, SABINA, GIANELLE, DAMIANO, HELFTER, CAROLE, HOLLINGER, DAVID, KUTSCH, WERNER L., LAFLEUR, PETER M., NOUVELLON, YANN, REBMANN, CORINNA, DA ROCHA, HUMBERTO R., RODEGHIERO, MIRCO, ROUPSARD, OLIVIER, SEBASTIÀ, MARIA-TERESA, SEUFERT, GUENTHER, SOUSSANA, JEAN-FRANCOISE, & VAN DER MOLEN, MICHIEL K. 2011. Semiempirical modeling of abiotic and biotic factors controlling ecosystem respiration across eddy covariance sites. *Global Change Biology*, **17**(1), 390–409.

MIGUEZ, FERNANDO. 2023. *nlraa: Nonlinear Regression for Agricultural Applications*. R package version 1.9.7.

MINER, GRACE L., BAUERLE, WILLIAM L., & BALDOCCHI, DENNIS D. 2017. Estimating the sensitivity of stomatal conductance to photosynthesis: a review. *Plant, Cell & Environment*, **40**(7), 1214–1238.

MOESINGER, L., DORIGO, W., DE JEU, R., VAN DER SCHALIE, R., SCANLON, T., TEUBNER, I., & FORKEL, M. 2020. The global long-term microwave Vegetation Optical Depth Climate Archive (VODCA). *Earth Syst. Sci. Data*, **12**(1), 177–196. Publisher: Copernicus Publications.

MOHAMMED, GINA H., COLOMBO, ROBERTO, MIDDLETON, ELIZABETH M., RASCHER, UWE, VAN DER TOL, CHRISTIAAN, NEDBAL, LADISLAV, GOULAS, YVES, PÉREZ-PRIEGO, OSCAR, DAMM, ALEXANDER, MERONI, MICHELE, JOINER, JOANNA, COGLIATI, SERGIO, VERHOEF, WOUTER, MALENOVSKÝ, ZBYNĚK, GASTELLU-ETCHEGORRY, JEAN-PHILIPPE, MILLER, JOHN R., GUANTER, LUIS, MORENO, JOSE, MOYA, ISMAEL, BERRY, JOSEPH A., FRANKENBERG, CHRISTIAN, & ZARCO-TEJADA, PABLO J. 2019. Remote sensing of solar-induced chlorophyll fluorescence (SIF) in vegetation: 50 years of progress. *Remote Sensing of Environment*, **231**(Sept.), 111177.

MOMEN, MOSTAFA, WOOD, JEFFREY D., NOVICK, KIMBERLY A., PANGLE, ROBERT, POCKMAN, WILLIAM T., MCDOWELL, NATE G., & KONINGS, ALEXANDRA G. 2017. Interacting Effects of Leaf Water Potential and Biomass on Vegetation Optical Depth. *Journal of Geophysical Research: Biogeosciences*, **122**(11), 3031–3046.

MONTEITH, J. L. 1965. Evaporation and environment. *Symposia of the Society for Experimental Biology*, **19**, 205–234. Place: England.

MONTEITH, JOHN LENNOX, MOSS, C. J., COOKE, GEORGE WILLIAM, PIRIE, NORMAN WINGATE, & BELL, GEORGE DOUGLAS HUTTON. 1997. Climate and the efficiency of crop production in Britain. *Philosophical Transactions of the Royal Society of London. B, Biological Sciences*, **281**(980), 277–294. Publisher: Royal Society.

MONTGOMERY, R. B. 1948. VERTICAL EDDY FLUX OF HEAT IN THE ATMOSPHERE. *Journal of Atmospheric Sciences*, **5**(6), 265 – 274.

MONTOYA, F., CAMARGO, D., ORTEGA, J.F., CÓRCOLES, J.I., & DOMÍNGUEZ, A. 2016. Evaluation of Aquacrop model for a potato crop under different irrigation conditions. *Agricultural Water Management*, **164**(Jan.), 267–280.

MORIONDO, M., MASELLI, F., & BINDI, M. 2007. A simple model of regional wheat yield based on NDVI data. *European Journal of Agronomy*, **26**(3), 266–274.

MOROZUMI, TOMOKI, KATO, TOMOMICHI, KOBAYASHI, HIDEKI, SAKAI, YUMA, NAKASHIMA, NAOHISA, BUAREAL, KANOKRAT, NASAHARA, KENLO NISHIDA, AKITSU, TOMOKO KAWAGUCHI, MURAYAMA, SHOHEI, NODA, HIBIKI M., & MURAOKA, HIROYUKI. 2023a. Contributions of the understory and midstory to total canopy solar-induced chlorophyll fluorescence in a ground-based study in conjunction with seasonal gross primary productivity in a cool-temperate deciduous broadleaf forest. *Remote Sensing of Environment*, **284**, 113340.

MOROZUMI, TOMOKI, KATO, TOMOMICHI, KOBAYASHI, HIDEKI, SAKAI, YUMA, NAKASHIMA, NAOHISA, BUAREAL, KANOKRAT, NASAHARA, KENLO NISHIDA, AKITSU, TOMOKO KAWAGUCHI, MURAYAMA, SHOHEI, NODA, HIBIKI M., & MURAOKA, HIROYUKI. 2023b. Contributions of the understory and midstory to total canopy solar-induced chlorophyll fluorescence in a ground-based study in conjunction with seasonal gross primary productivity in a cool-temperate deciduous broadleaf forest. *Remote Sensing of Environment*, **284**(Jan.), 113340.

MOUREAUX, CHRISTINE, DEBACQ, ALAIN, BODSON, BERNARD, HEINESCH, BERNARD, & AUBINET, MARC. 2006. Annual net ecosystem carbon exchange by a sugar beet crop. *Agricultural and Forest Meteorology*, **139**(1), 25–39.

MOUREAUX, CHRISTINE, DEBACQ, ALAIN, HOYAUX, JULIEN, SULEAU, MARIE, TOURNEUR, DENIS, VANCUTSEM, FRANÇOISE, BODSON, BERNARD, & AUBINET, MARC. 2008. Carbon balance assessment of a Belgian winter wheat crop (Triticum aestivum L.). *Global Change Biology*, **14**(6), 1353–1366.

MOUREAUX, CHRISTINE, CESCHIA, ERIC, ARRIGA, NICOLA, BÉZIAT, PIERRE, EUGSTER, WERNER, KUTSCH, WERNER L., & PATTEY, ELIZABETH. 2012. *Eddy Covariance Measurements over Crops*. Dordrecht: Springer Netherlands. Pages 319–331.

MOYA, ISMAEL, LOAYZA, HILDO, LÓPEZ, MARIA LLANOS, QUIROZ, ROBERTO, OUNIS, ABDERRAHMANE, & GOULAS, YVES. 2019. Canopy chlorophyll fluorescence applied to stress detection using an easy-to-build micro-lidar. *Photosynthesis Research*, **142**(1), 1–15.

MRAD, ASSAAD, SEVANTO, SANNA, DOMEC, JEAN-CHRISTOPHE, LIU, YANLAN, NAKAD, MAZEN, & KATUL, GABRIEL. 2019. A Dynamic Optimality Principle for Water Use Strategies Explains Isohydric to Anisohydric Plant Responses to Drought. *Frontiers in Forests and Global Change*, **2**(Aug.), 49.

MULERO, GABRIEL, JIANG, DUO, BONFIL, DAVID J., & HELMAN, DAVID. 2023. Use of thermal imaging and the photochemical reflectance index (PRI) to detect wheat response to elevated CO2 and drought. *Plant, Cell & Environment*, **46**(1), 76–92.

MUÑOZ-SABATER, JOAQUÍN, DUTRA, EMANUEL, AGUSTÍ-PANAREDA, ANNA, ALBERGEL, CLÉMENT, ARDUINI, GABRIELE, BALSAMO, GIANPAOLO, BOUSSETTA, SOUHAIL, CHOULGA, MARGARITA, HARRIGAN, SHAUN, HERSBACH, HANS, *et al.* 2021. ERA5-Land: A state-of-the-art global reanalysis dataset for land applications. *Earth system science data*, **13**(9), 4349–4383.

MURCHIE, E.H., & LAWSON, T. 2013. Chlorophyll fluorescence analysis: a guide to good practice and understanding some new applications. *Journal of Experimental Botany*, **64**(13), 3983–3998.

MUSSE, M., HAJJAR, G., ALI, N., BILLIOT, B., JOLY, G., PÉPIN, J., QUELLEC, S., CHALLOIS, S., MARIETTE, F., CAMBERT, M., FONTAINE, C., NGO-DINH, C., JAMOIS, F., BARBARY, A., LECONTE, P., DELEU, C., & LEPORT, L. 2021. A global non-invasive methodology for the phenotyping of potato under water deficit conditions using imaging, physiological and molecular tools. *Plant Methods*, **17**(1), 81.

MWIYA, RICHWELL MUBITA, ZHANG, ZHANYU, ZHENG, CHENGXIN, & WANG, CE. 2020. Comparison of Approaches for Irrigation Scheduling Using AquaCrop and NSGA-III Models under Climate Uncertainty. *Sustainability*, **12**(18).

MYNENI, R.B., & WILLIAMS, D.L. 1994. On the relationship between FAPAR and NDVI. *Remote Sensing of Environment*, **49**(3), 200–211.

MÄKELÄ, A. 1996. Optimal Control of Gas Exchange during Drought: Theoretical Analysis. *Annals of Botany*, **77**(5), 461–468.

NADAL, MIQUEL, & FLEXAS, JAUME. 2018. M esophyll C onductance to CO 2 D iffusion : E ffects of D rought and O pportunities for I mprovement. *Pages 403–438 of: Water Scarcity and Sustainable Agriculture in Semiarid Environment*. Elsevier.

NARDINI, ANDREA, & SALLEO, SEBASTIANO. 2000. Limitation of stomatal conductance by hydraulic traits: sensing or preventing xylem cavitation? *Trees*, **15**, 14–24.

NELSON, JACOB A., CARVALHAIS, NUNO, MIGLIAVACCA, MIRCO, REICHSTEIN, MARKUS, & JUNG, MARTIN. 2018. Water-stress-induced breakdown of carbon–water relations: indicators from diurnal FLUXNET patterns. *Biogeosciences*, **15**(8), 2433–2447.

NELSON, JACOB A., PÉREZ-PRIEGO, OSCAR, ZHOU, SHA, POYATOS, RAFAEL, ZHANG, YAO, BLANKEN, PETER D., GIMENO, TERESA E., WOHLFAHRT, GEORG, DESAI, ANKUR R., GIOLI, BENIAMINO, LIMOUSIN, JEAN-MARC, BONAL, DAMIEN, PAUL-LIMOGES, EUGÉNIE, SCOTT, RUSSELL L., VARLAGIN, ANDREJ, FUCHS, KATHRIN, MONTAGNANI, LEONARDO, WOLF, SEBASTIAN, DELPIERRE, NICOLAS, BERVEILLER, DANIEL, GHARUN, MANA, BELELLI MARCHESINI, LUCA, GIANELLE, DAMIANO, ŠIGUT, LADISLAV, MAMMARELLA, IVAN, SIEBICKE, LUKAS, ANDREW BLACK, T., KNOHL, ALEXANDER, HÖRTNAGL, LUKAS, MAGLIULO, VINCENZO, BESNARD, SIMON, WEBER, ULRICH, CARVALHAIS, NUNO, MIGLIAVACCA, MIRCO, REICHSTEIN, MARKUS, & JUNG, MARTIN. 2020. Ecosystem transpiration and evaporation: Insights from three water flux partitioning methods across FLUXNET sites. *Global Change Biology*, **26**(12), 6916–6930.

NGUYEN, THU BINH-ANH, LEFOULON, CECILE, NGUYEN, THANH-HAO, BLATT, MICHAEL R., & CARROLL, WILLIAM. 2023. Engineering stomata for enhanced carbon capture and water-use efficiency. *Trends in Plant Science*, **28**(11), 1290–1309.

NIINEMETS, Ü., SONNINEN, E., & TOBIAS, M. 2004. Canopy gradients in leaf intercellular CO $_2$ mole fractions revisited: interactions between leaf irradiance and water stress need consideration. *Plant, Cell & Environment*, **27**(5), 569–583.

NIINEMETS, ÜLO, CESCATTI, ALESSANDRO, RODEGHIERO, MIRCO, & TOSENS, TIINA. 2006. Complex adjustments of photosynthetic potentials and internal diffusion conductance to current and previous light availabilities and leaf age in Mediterranean evergreen species *Quercus ilex*. *Plant, Cell & Environment*, **29**(6), 1159–1178.

NJOKU, ENI G., & ENTEKHABI, DARA. 1996. Passive microwave remote sensing of soil moisture. *Journal of Hydrology*, **184**(1), 101–129. Soil Moisture Theories and Observations.

NOLAN, RACHAEL H., BLACKMAN, CHRIS J., DE DIOS, VÍCTOR RESCO, CHOAT, BRENDAN, MEDLYN, BELINDA E., LI, XIMENG, BRADSTOCK, ROSS A., & BOER, MATTHIAS M. 2020. Linking Forest Flammability and Plant Vulnerability to Drought. *Forests*, **11**(7).

NOVICK, KIMBERLY A., FICKLIN, DARREN L., BALDOCCHI, DENNIS, DAVIS, KENNETH J., GHEZZEHEI, TEAMRAT A., KONINGS, ALEXANDRA G., MACBEAN, NATASHA, RAOULT, NINA, SCOTT, RUSSELL L., SHI, YUNING, SULMAN, BENJAMIN N., & WOOD, JEFFREY D. 2022. Confronting the water potential information gap. *Nature Geoscience*, **15**(3), 158–164.

NOVICK, KIMBERLY A., FICKLIN, DARREN L., GROSSIORD, CHARLOTTE, KONINGS, ALEXANDRA G., MARTÍNEZ-VILALTA, JORDI, SADOK, WALID, TRUGMAN, ANNA T., WILLIAMS, A. PARK, WRIGHT, ALEXANDRA J., ABATZOGLOU, JOHN T., DANNENBERG, MATTHEW P., GENTINE, PIERRE, GUAN, KAIYU, JOHNSTON, MIRIAM R., LOWMAN, LAUREN E.L., MOORE, DAVID J.P., & MCDOWELL, NATE G. 2024. The impacts of rising vapour pressure deficit in natural and managed ecosystems. *Plant Cell and Environment*. Publisher Copyright: © 2024 The Authors. Plant, Cell Environment published by John Wiley Sons Ltd.

NOZ CARPENA, RAFAEL MU LI, YUNCONG C., KLASSEN, WALDEMAR, & DUKES, MICHAEL D. 2005. Field Comparison of Tensiometer and Granular Matrix Sensor Automatic Drip Irrigation on Tomato. *HortTechnology horttech*, **15**(3), 584 – 590.

OBIDIEGWU, JUDE E. 2015. Coping with drought: stress and adaptive responses in potato and perspectives for improvement. *Frontiers in Plant Science*, **6**.

OBUKHOV, AM. 1951. Charakteristiki mikrostruktury vetra v prizemnom sloje atmosfery (Characteristics of the micro-structure of the wind in the surface layer of the atmosphere). *Izv AN SSSR, Ser Geofiz*, **3**, 49–68.

O'LEARY, MARION H. 1981. Carbon isotope fractionation in plants. *Phytochemistry*, **20**(4), 553–567.

OLIVER, REBECCA J., MERCADO, LINA M., CLARK, DOUG B., HUNTINGFORD, CHRIS, TAYLOR, CHRISTOPHER M., VIDALE, PIER LUIGI, MCGUIRE, PATRICK C., TODT, MARKUS, FOLWELL, SONJA, SHAMSUDHEEN SEMEENA, VALIYAVEETIL, & MEDLYN, BELINDA E. 2022. Improved representation of plant physiology in the JULES-vn5.6 land surface model: photosynthesis, stomatal conductance and thermal acclimation. *Geoscientific Model Development*, **15**(14), 5567–5592.

OOSTERBAAN, RJ, SHARMA, DP, SINGH, KN, & RAO, KVGK. 1990. Crop production and soil salinity: evaluation of field data from India by segmented linear regression with breakpoint. *Pages 373–383 of: Proceedings of the symposium on land drainage for salinity control in arid and semi-arid regions*, vol. 3. Citeseer.

OP DE BEECK, MAARTEN, LÖW, MARKUS, DECKMYN, GABY, & CEULEMANS, REINHART. 2010. A comparison of photosynthesis-dependent stomatal models using twig cuvette field data for adult beech (Fagus sylvatica L.). *Agricultural and Forest Meteorology*, **150**(4), 531–540.

OR, D., TULLER, M., & WRAITH, J.M. 2005. WATER POTENTIAL. *Pages 270–277 of:* HILLEL, DANIEL (ed), *Encyclopedia of Soils in the Environment*. Oxford: Elsevier.

OSMOND, BARRY, CHOW, WAH SOON, WYBER, RHYS, ZAVAFER, ALONSO, KELLER, BEAT, POGSON, BARRY J., & ROBINSON, SHARON A. 2017. Relative functional and optical absorption cross-sections of PSII and other photosynthetic parameters monitored in situ, at a distance with a time resolution of a few seconds, using a prototype light induced fluorescence transient (LIFT) device. *Functional Plant Biology*, **44**(10), 985.

OSMOND, C. B., BJÖRKMAN, O., & ANDERSON, D. J. 1980. Physiological Processes in Plant Ecology: the Structure for a Synthesis. *Pages 1–11 of:* OSMOND, C. B., BJÖRKMAN, O., & ANDERSON, D. J. (eds), *Physiological Processes in Plant Ecology: Toward a Synthesis with Atriplex*. Berlin, Heidelberg: Springer Berlin Heidelberg.

OUZOUNIS, THEOHARIS, RAZI PARJIKOLAEI, BEHNAZ, FRETTÃ©, XAVIER, ROSENQVIST, EVA, & OTTOSEN, CARL-OTTO. 2015. Predawn and high intensity application of supplemental blue light decreases the quantum yield of PSII and enhances the amount of phenolic acids, flavonoids, and pigments in Lactuca sativa. *Frontiers in Plant Science*, **6**(Feb.).

OWE, MANFRED, DE JEU, RICHARD, & HOLMES, THOMAS. 2008. Multisensor historical climatology of satellite-derived global land surface moisture. *Journal of Geophysical Research: Earth Surface*, **113**(F1). Publisher: John Wiley & Sons, Ltd.

PAGAY, VINAY. 2022. Evaluating a novel microtensiometer for continuous trunk water potential measurements in field-grown irrigated grapevines. *Irrigation Science*, **40**(1), 45–54.

PAN, TAO, HOU, SHUAI, LIU, YUJIE, & TAN, QINGHUA. 2019. Comparison of three models fitting the soil water retention curves in a degraded alpine meadow region. *Scientific Reports*, **9**(1), 18407.

PAPALE, DARIO, REICHSTEIN, MARKUS, AUBINET, MARC, CANFORA, E, BERNHOFER, C, KUTSCH, W, LONGDOZ, BERNARD, RAMBAL, SERGE, VALENTINI, R, VESALA, T, *et al.* 2006. Towards a standardized processing of Net Ecosystem Exchange measured with eddy covariance technique: algorithms and uncertainty estimation. *Biogeosciences*, **3**(4), 571–583.

PARKER, N., & PATRIGNANI, A. 2021. Evaluating Traditional and Modern Laboratory Techniques for Determining Permanent Wilting Point. *Kansas Agricultural Experiment Station Research Reports*, **7**(5).

PARRY, M. A. J. 2002. Rubisco Activity: Effects of Drought Stress. *Annals of Botany*, **89**(7), 833–839.

PASCHALIS, ATHANASIOS, FATICHI, SIMONE, ZSCHEISCHLER, JAKOB, CIAIS, PHILIPPE, BAHN, MICHAEL, BOYSEN, LENA, CHANG, JINFENG, DE KAUWE, MARTIN, ESTIARTE, MARC, GOLL, DANIEL, HANSON, PAUL J., HARPER, ANNA B., HOU, ENQING, KIGEL, JAIME, KNAPP, ALAN K., LARSEN, KLAUS S., LI, WEI, LIENERT, SEBASTIAN, LUO, YIQI, MEIR, PATRICK, NABEL, JULIA E. M. S., OGAYA, ROMÀ, PAROLARI, ANTHONY J., PENG, CHANGHUI, PEÑUELAS, JOSEP, PONGRATZ, JULIA, RAMBAL, SERGE, SCHMIDT, INGER K., SHI, HAO, STERNBERG, MARCELO, TIAN, HANQIN, TSCHUMI, ELISABETH, UKKOLA, ANNA, VICCA, SARA, VIOVY, NICOLAS, WANG, YING-PING, WANG, ZHUONAN, WILLIAMS, KARINA, WU, DONGHAI, & ZHU, QIUAN. 2020. Rainfall manipulation experiments as simulated by terrestrial biosphere models: Where do we stand? *Global Change Biology*, **26**(6), 3336–3355.

PASTORELLO, GILBERTO, TROTTA, CARLO, CANFORA, ELEONORA, CHU, HOUSEN, CHRISTIANSON, DANIELLE, CHEAH, YOU-WEI, POINDEXTER, CRISTINA, CHEN, JIQUAN, ELBASHANDY, ABDELRAHMAN, HUMPHREY, MARTY, ISAAC, PETER, POLIDORI, DIEGO, RIBECA, ALESSIO, INGEN, CATHARINE, ZHANG, LEIMING, AMIRO, BRIAN, AMMANN, CHRISTOF, ARAIN, M., ARDÖ, JONAS, & PAPALE, DARIO. 2020. The FLUXNET2015 dataset and the ONEFlux processing pipeline for eddy covariance data. *Scientific Data*, **7**(July).

PATERNOSTER, RAYMOND, BRAME, ROBERT, MAZEROLLE, PAUL, & PIQUERO, ALEX. 1998. USING THE CORRECT STATISTICAL TEST FOR THE EQUALITY OF REGRESSION COEFFICIENTS. *Criminology*, **36**(4), 859–866.

PEEK, MICHAEL S., LEFFLER, A. JOSHUA, HIPPS, LARRY, IVANS, SASHA, RYEL, RONALD J., & CALDWELL, MARTYN M. 2006. Root turnover and relocation in the soil profile in response to seasonal soil water variation in a natural stand of Utah juniper (Juniperus osteosperma). *Tree physiology*, **26**(11), 1469–1476. Place: Canada.

PEI, YANYAN, DONG, JINWEI, ZHANG, YAO, YUAN, WENPING, DOUGHTY, RUSSELL, YANG, JILIN, ZHOU, DECHENG, ZHANG, LIANGXIA, & XIAO, XIANGMING. 2022. Evolution of light use efficiency models: Improvement, uncertainties, and implications. *Agricultural and Forest Meteorology*, **317**(Apr.), 108905.

PENUELAS, JOSEP, FILELLA, IOLANDA, & GAMON, JOHN A. 1995. Assessment of photosynthetic radiation-use efficiency with spectral reflectance. *New Phytologist*, **131**(3), 291–296.

PEREZ-MARTIN, ALFONSO, MICHELAZZO, CHIARA, TORRES-RUIZ, JOSE M., FLEXAS, JAUME, FERNÁNDEZ, JOSÉ E., SEBASTIANI, LUCA, & DIAZ-ESPEJO, ANTONIO. 2014. Regulation of photosynthesis and stomatal and mesophyll conductance under water stress and recovery in olive trees: correlation with gene expression of carbonic anhydrase and aquaporins. *Journal of Experimental Botany*, **65**(12), 3143–3156.

PEREZ-PRIEGO, OSCAR. 2021. Plant Chamber Measurements. *Pages 1585–1601 of:* FOKEN, THOMAS (ed), *Springer Handbook of Atmospheric Measurements*. Cham: Springer International Publishing. Series Title: Springer Handbooks.

PERONA, PAOLO, FLURY, RETO, BARRY, D. ANDREW, & SCHWARZ, MASSIMILIANO. 2022. Tree root distribution modelling in different environmental conditions. *Ecological Engineering*, **185**, 106811.

PETERS, WOUTER, VAN DER VELDE, IVAR R., VAN SCHAIK, ERIK, MILLER, JOHN B., CIAIS, PHILIPPE, DUARTE, HENRIQUE F., VAN DER LAAN-LUIJKX, INGRID T., VAN DER MOLEN, MICHIEL K., SCHOLZE, MARKO, SCHAEFER, KEVIN, VIDALE, PIER LUIGI, VERHOEF, ANNE, WÅRLIND, DAVID, ZHU, DAN, TANS, PIETER P., VAUGHN, BRUCE, & WHITE, JAMES W. C. 2018. Increased water-use efficiency and reduced CO2 uptake by plants during droughts at a continental scale. *Nature Geoscience*, **11**(10), 744–748.

PETRÍK, PETER, PETEK-PETRIK, ANJA, MUKARRAM, MOHAMMAD, SCHULDT, BERNHARD, & LAMARQUE, LAURENT J. 2023. Leaf physiological and morphological constraints of water-use efficiency in C3 plants. *AoB PLANTS*, **15**(4), plad047.

PFÜNDEL, ERHARD E. 2021. Simultaneously measuring pulse-amplitude-modulated (PAM) chlorophyll fluorescence of leaves at wavelengths shorter and longer than 700 nm. *Photosynthesis Research*, **147**(3), 345–358.

PFÜNDEL, ERHARD E., KLUGHAMMER, CHRISTOF, MEISTER, ARMIN, & CEROVIC, ZORAN G. 2013. Deriving fluorometer-specific values of relative PSI fluorescence intensity from quenching of F(0) fluorescence in leaves of Arabidopsis thaliana and Zea mays. *Photosynthesis research*, **114**(3), 189–206. Place: Netherlands.

PHAM, KHANH, KIM, DONGKU, YOON, YUEMYUNG, & CHOI, HANGSEOK. 2019. Analysis of neural network based pedotransfer function for predicting soil water characteristic curve. *Geoderma*, **351**, 92–102.

PICKERING, MARK, CESCATTI, ALESSANDRO, & DUVEILLER, GREGORY. 2022. Sun-induced fluorescence as a proxy for primary productivity across vegetation types and climates. *Biogeosciences*, **19**(20), 4833–4864.

PIERRAT, Z., MAGNEY, T., YANG, X., KHAN, A., & ALBERT, L. 2023. *Ecosystem observations from every angle, Eos, 104*. Accessed on 04 04,2024.

PIERUSCHKA, R., ALBRECHT, H., MULLER, O., BERRY, J. A., KLIMOV, D., KOLBER, Z. S., MALENOVSKY, Z., & RASCHER, U. 2014. Daily and seasonal dynamics of remotely sensed photosynthetic efficiency in tree canopies. *Tree Physiology*, **34**(7), 674–685.

PINHEIRO, C., & CHAVES, M. M. 2011. Photosynthesis and drought: can we make metabolic connections from available data? *Journal of Experimental Botany*, **62**(3), 869–882.

PIRASTEH-ANOSHEH, HADI, SAED-MOUCHESHI, ARMIN, PAKNIYAT, HASSAN, & PESSARAKLI, MOHAMMAD. 2016. Stomatal responses to drought stress. *Pages 24–40 of:* AHMAD, PARVAIZ (ed), *Water Stress and Crop Plants*. Chichester, UK: John Wiley & Sons, Ltd.

PLASCYK, JAMES A., & GABRIEL, FRED C. 1975. The Fraunhofer Line Discriminator MKII-An Airborne Instrument for Precise and Standardized Ecological Luminescence Measurement. *IEEE Transactions on Instrumentation and Measurement*, **24**(4), 306–313.

PONS, THIJS L., FLEXAS, JAUME, VON CAEMMERER, SUSANNE, EVANS, JOHN R., GENTY, BERNARD, RIBAS-CARBO, MIQUEL, & BRUGNOLI, ENRICO. 2009. Estimating mesophyll conductance to CO2: methodology, potential errors, and recommendations. *Journal of Experimental Botany*, **60**(8), 2217–2234.

PORCAR-CASTELL, ALBERT, TYYSTJÄRVI, ESA, ATHERTON, JON, VAN DER TOL, CHRISTIAAN, FLEXAS, JAUME, PFÜNDEL, ERHARD E., MORENO, JOSE, FRANKENBERG, CHRISTIAN, & BERRY, JOSEPH A. 2014. Linking chlorophyll a fluorescence to photosynthesis for remote sensing applications: mechanisms and challenges. *Journal of Experimental Botany*, **65**(15), 4065–4095.

PORCAR-CASTELL, ALBERT, MALENOVSKÝ, ZBYNĚK, MAGNEY, TROY, VAN WITTENBERGHE, SHARI, FERNÁNDEZ-MARÍN, BEATRIZ, MAIGNAN, FABIENNE, ZHANG, YONGGUANG, MASEYK, KADMIEL, ATHERTON, JON, ALBERT, LOREN P., ROBSON, THOMAS MATTHEW, ZHAO, FENG, GARCIA-PLAZAOLA, JOSE-IGNACIO, ENSMINGER, INGO, RAJEWICZ, PAULINA A., GREBE, STEFFEN, TIKKANEN, MIKKO, KELLNER, JAMES R., IHALAINEN, JANNE A., RASCHER, UWE, & LOGAN, BARRY. 2021. Chlorophyll a fluorescence illuminates a path connecting plant molecular biology to Earth-system science. *Nature Plants*, **7**(8), 998–1009.

POWELL, THOMAS L., GALBRAITH, DAVID R., CHRISTOFFERSEN, BRADLEY O., HARPER, ANNA, IMBUZEIRO, HEWLLEY M. A., ROWLAND, LUCY, ALMEIDA, SAMUEL, BRANDO, PAULO M., DA COSTA, ANTONIO CARLOS LOLA, COSTA, MARCOS HEIL, LEVINE, NAOMI M., MALHI, YADVINDER, SALESKA, SCOTT R., SOTTA, ELENEIDE, WILLIAMS, MATHEW, MEIR, PATRICK, & MOORCROFT, PAUL R. 2013. Confronting model predictions of carbon fluxes with measurements of Amazon forests subjected to experimental drought. *New Phytologist*, **200**(2), 350–365.

PRADHAN, ALIZA, AHER, LALITKUMAR, HEGDE, VINAY, JANGID, KRISHNA KUMAR, & RANE, JAGADISH. 2022. Cooler canopy leverages sorghum adaptation to drought and heat stress. *Scientific Reports*, **12**(1), 4603.

PRENTICE, I. C., LIANG, X., MEDLYN, B. E., & WANG, Y.-P. 2015. Reliable, robust and realistic: the three R's of next-generation land-surface modelling. *Atmospheric Chemistry and Physics*, **15**(10), 5987–6005.

PRENTICE, I. COLIN, DONG, NING, GLEASON, SEAN M., MAIRE, VINCENT, & WRIGHT, IAN J. 2014. Balancing the costs of carbon gain and water transport: testing a new theoretical framework for plant functional ecology. *Ecology Letters*, **17**(1), 82–91.

PUCHI, PAULINA F., DALMONECH, DANIELA, VANGI, ELIA, BATTIPAGLIA, GIOVANNA, TOGNETTI, ROBERTO, & COLLALTI, ALESSIO. 2024. Contrasting patterns of water use efficiency and annual radial growth among European beech forests along the Italian peninsula. *Scientific reports*, **14**(1), 6526. Place: England.

PÉREZ-BUENO, MARÍA LUISA, PINEDA, MÓNICA, & BARÓN, MATILDE. 2019. Phenotyping Plant Responses to Biotic Stress by Chlorophyll Fluorescence Imaging. *Frontiers in Plant Science*, **10**(Sept.), 1135.

QUESADA-RUIZ, S., ATTIÉ, J.-L., LAHOZ, W. A., ABIDA, R., RICAUD, P., EL AMRAOUI, L., ZBINDEN, R., PIACENTINI, A., JOLY, M., ESKES, H., SEGERS, A., CURIER, L., DE HAAN, J., KUJANPÄÄ, J., OUDE NIJHUIS, A. C. P., TAMMINEN, J., TIMMERMANS, R., & VEEFKIND, P. 2020. Benefit of ozone observations from Sentinel-5P and future Sentinel-4 missions on tropospheric composition. *Atmospheric Measurement Techniques*, **13**(1), 131–152.

QUETIN, G. R., ANDEREGG, L. D. L., BOVING, I., ANDEREGG, W. R. L., & TRUGMAN, A. T. 2023. Observed forest trait velocities have not kept pace with hydraulic stress from climate change. *Global Change Biology*, **29**(18), 5415–5428.

R CORE TEAM. 2020. *R: A Language and Environment for Statistical Computing*. R Foundation for Statistical Computing, Vienna, Austria.

RAES, DIRK, STEDUTO, PASQUALE, HSIAO, THEODORE C., & FERERES, ELIAS. 2009. AquaCropThe FAO Crop Model to Simulate Yield Response to Water: II. Main Algorithms and Software Description. *Agronomy Journal*, **101**(3), 438.

RAESCH, ANNA, MULLER, ONNO, PIERUSCHKA, ROLAND, & RASCHER, UWE. 2014. Field Observations with Laser-Induced Fluorescence Transient (LIFT) Method in Barley and Sugar Beet. *Agriculture*, **4**(2), 159–169.

RAINES, CHRISTINE A. 2022. Improving plant productivity by re-tuning the regeneration of RuBP in the Calvin–Benson–Bassham cycle. *New Phytologist*, **236**(2), 350–356. _eprint: https://nph.onlinelibrary.wiley.com/doi/pdf/10.1111/nph.18394.

RAMBAL, SERGE, OURCIVAL, JEAN-MARC, JOFFRE, RICHARD, MOUILLOT, FLORENT, NOUVELLON, YANN, REICHSTEIN, MARKUS, & ROCHETEAU, ALAIN. 2003. Drought controls over conductance and assimilation of a Mediterranean evergreen ecosystem: scaling from leaf to canopy. *Global Change Biology*, **9**(12), 1813–1824.

RAMÍREZ, DAVID A., YACTAYO, WENDY, RENS, LIBBY R., ROLANDO, JOSÉ L., PALACIOS, SUSAN, DE MENDIBURU, FELIPE, MARES, VÍCTOR, BARREDA, CAROLINA, LOAYZA, HILDO, MONNEVEUX, PHILIPPE, ZOTARELLI, LINCOLN, KHAN, AWAIS, & QUIROZ, ROBERTO. 2016. Defining biological thresholds associated to plant water status for monitoring water restriction effects: Stomatal conductance and photosynthesis recovery as key indicators in potato. *Agricultural Water Management*, **177**(Nov.), 369–378.

RASCHER, U., ALONSO, L., BURKART, A., CILIA, C., COGLIATI, S., COLOMBO, R., DAMM, A., DRUSCH, M., GUANTER, L., HANUS, J., HYVÄRINEN, T., JULITTA, T., JUSSILA, J., KATAJA, K., KOKKALIS, P., KRAFT, S., KRASKA, T., MATVEEVA, M., MORENO, J., MULLER, O., PANIGADA,

C., PIKL, M., PINTO, F., PREY, L., PUDE, R., ROSSINI, M., SCHICKLING, A., SCHURR, U., SCHÜTTEMEYER, D., VERRELST, J., & ZEMEK, F. 2015. Sun-induced fluorescence - a new probe of photosynthesis: First maps from the imaging spectrometer *HyPlant*. *Global Change Biology*, **21**(12), 4673–4684.

RATZMANN, GREGOR, ZAKHAROVA, LIUBOV, & TIETJEN, BRITTA. 2019. Optimal leaf water status regulation of plants in drylands. *Scientific Reports*, **9**(1), 3768.

REBMANN, CORINNA, AUBINET, MARC, SCHMID, HAPE, ARRIGA, NICOLA, AURELA, MIKA, BURBA, GEORGE, CLEMENT, ROBERT, DE LIGNE, ANNE, FRATINI, GERARDO, GIELEN, BERT, GRACE, JOHN, GRAF, ALEXANDER, GROSS, PATRICK, HAAPANALA, SAMI, HERBST, MATHIAS, HÖRTNAGL, LUKAS, IBROM, ANDREAS, JOLY, LILIAN, KLJUN, NATASCHA, KOLLE, OLAF, KOWALSKI, ANDREW, LINDROTH, ANDERS, LOUSTAU, DENIS, MAMMARELLA, IVAN, MAUDER, MATTHIAS, MERBOLD, LUTZ, METZGER, STEFAN, MÖLDER, MEELIS, MONTAGNANI, LEONARDO, PAPALE, DARIO, PAVELKA, MARIAN, PEICHL, MATTHIAS, ROLAND, MARILYN, SERRANO-ORTIZ, PENÉLOPE, SIEBICKE, LUKAS, STEINBRECHER, RAINER, TUOVINEN, JUHA-PEKKA, VESALA, TIMO, WOHLFAHRT, GEORG, & FRANZ, DANIELA. 2018. ICOS eddy covariance flux-station site setup: a review. *International Agrophysics*, **32**(4), 471–494.

REICHSTEIN, M., TENHUNEN, J. D., ROUPSARD, O., OURCIVAL, J.-M., RAMBAL, S., DORE, S., & VALENTINI, R. 2002. Ecosystem respiration in two Mediterranean evergreen Holm Oak forests: drought effects and decomposition dynamics. *Functional Ecology*, **16**(1), 27–39.

REICHSTEIN, M., CIAIS, P., PAPALE, D., VALENTINI, R., RUNNING, S., VIOVY, N., CRAMER, W., GRANIER, A., OGÉE, J., ALLARD, V., AUBINET, M., BERNHOFER, CHR., BUCHMANN, N., CARRARA, A., GRÜNWALD, T., HEIMANN, M., HEINESCH, B., KNOHL, A., KUTSCH, W., LOUSTAU, D., MANCA, G., MATTEUCCI, G., MIGLIETTA, F., OURCIVAL, J.M., PILEGAARD, K., PUMPANEN, J., RAMBAL, S., SCHAPHOFF, S., SEUFERT, G., SOUSSANA, J.-F., SANZ, M.-J., VESALA, T., & ZHAO, M. 2007. Reduction of ecosystem productivity and respiration during the European summer 2003 climate anomaly: a joint flux tower, remote sensing and modelling analysis. *Global Change Biology*, **13**(3), 634–651.

REICHSTEIN, MARKUS. 2003. Inverse modeling of seasonal drought effects on canopy CO_2 /H_2O exchange in three Mediterranean ecosystems. *Journal of Geophysical Research*, **108**(D23).

REICHSTEIN, MARKUS, TENHUNEN, JOHN D., ROUPSARD, OLIVIER, OURCIVAL, JEAN-MARC, RAMBAL, SERGE, MIGLIETTA, FRANCO, PERESSOTTI, ALESSANDRO, PECCHIARI, MARCO, TIRONE, GIAMPIERO, & VALENTINI, RICCARDO. 2002. Severe drought effects on ecosystem CO2 and H2O fluxes at three Mediterranean evergreen sites: revision of current hypotheses? *Global Change Biology*, **8**(10), 999–1017.

REICHSTEIN, MARKUS, TENHUNEN, JOHN, ROUPSARD, OLIVIER, OURCIVAL, JEAN-MARC, RAMBAL, SERGE, MIGLIETTA, FRANCO, PERESSOTTI, ALESSANDRO, PECCHIARI, MARCO, TIRONE, GIAMPIERO, & VALENTINI, RICCARDO. 2003. Inverse modeling of seasonal drought effects on canopy CO2/H2O exchange in three Mediterranean ecosystems. *Journal of Geophysical Research: Atmospheres*, **108**(D23).

REICHSTEIN, MARKUS, FALGE, EVA, BALDOCCHI, DENNIS, PAPALE, DARIO, AUBINET, MARC, BERBIGIER, PAUL, BERNHOFER, CHRISTIAN, BUCHMANN, NINA, GILMANOV, TAGIR, GRANIER, ANDRE, GRUNWALD, THOMAS, HAVRANKOVA, KATKA, ILVESNIEMI, HANNU, JANOUS, DALIBOR, KNOHL, ALEXANDER, LAURILA, TUOMAS, LOHILA, ANNALEA, LOUSTAU,

DENIS, MATTEUCCI, GIORGIO, MEYERS, TILDEN, MIGLIETTA, FRANCO, OURCIVAL, JEAN-MARC, PUMPANEN, JUKKA, RAMBAL, SERGE, ROTENBERG, EYAL, SANZ, MARIA, TENHUNEN, JOHN, SEUFERT, GUNTHER, VACCARI, FRANCESCO, VESALA, TIMO, YAKIR, DAN, & VALENTINI, RICCARDO. 2005. On the separation of net ecosystem exchange into assimilation and ecosystem respiration: review and improved algorithm. *Global Change Biology*, **11**(9), 1424–1439.

REICHSTEIN, MARKUS, BAHN, MICHAEL, CIAIS, PHILIPPE, FRANK, DOROTHEA, MAHECHA, MIGUEL D., SENEVIRATNE, SONIA I., ZSCHEISCHLER, JAKOB, BEER, CHRISTIAN, BUCHMANN, NINA, FRANK, DAVID C., PAPALE, DARIO, RAMMIG, ANJA, SMITH, PETE, THONICKE, KIRSTEN, VAN DER VELDE, MARIJN, VICCA, SARA, WALZ, ARIANE, & WATTENBACH, MARTIN. 2013. Climate extremes and the carbon cycle. *Nature*, **500**(7462), 287–295.

REINHARDT, KEITH, & SMITH, WILLIAM K. 2008. Impacts of cloud immersion on microclimate, photosynthesis and water relations of Abies fraseri (Pursh.) Poiret in a temperate mountain cloud forest. *Oecologia*, **158**(2), 229–238.

REITZ, O., BOGENA, H., NEUWIRTH, B., SANCHEZ-AZOFEIFA, A., GRAF, A., BATES, J., & LEUCHNER, M. 2023. Environmental Drivers of Gross Primary Productivity and Light Use Efficiency of a Temperate Spruce Forest. *Journal of Geophysical Research: Biogeosciences*, **128**(2), e2022JG007197.

REYNOLDS-HENNE, CHRISTINA E., LANGENEGGER, ANITA, MANI, JAN, SCHENK, NICOLE, ZUMSTEG, ANITA, & FELLER, URS. 2010. Interactions between temperature, drought and stomatal opening in legumes. *Environmental and Experimental Botany*, **68**(1), 37–43.

RICHARDS, LA. 1948. Porous plate apparatus for measuring moisture retention and transmission by soil. *Soil Science*, **66**(2), 105–110.

RICHARDS, LISA A, & WEAVER, L. R. 1943. FIFTEEN-ATMOSPHERE PERCENTAGE AS RELATED TO THE PERMANENT WILTING PERCENTAGE. *Soil Science*, **56**, 331–340.

RICHARDSON, KATHERINE, STEFFEN, WILL, LUCHT, WOLFGANG, BENDTSEN, JØRGEN, CORNELL, SARAH E., DONGES, JONATHAN F., DRÜKE, MARKUS, FETZER, INGO, BALA, GOVINDASAMY, VON BLOH, WERNER, FEULNER, GEORG, FIEDLER, STEPHANIE, GERTEN, DIETER, GLEESON, TOM, HOFMANN, MATTHIAS, HUISKAMP, WILLEM, KUMMU, MATTI, MOHAN, CHINCHU, NOGUÉS-BRAVO, DAVID, PETRI, STEFAN, PORKKA, MIINA, RAHMSTORF, STEFAN, SCHAPHOFF, SIBYLL, THONICKE, KIRSTEN, TOBIAN, ARNE, VIRKKI, VILI, WANG-ERLANDSSON, LAN, WEBER, LISA, & ROCKSTRÖM, JOHAN. 2023. Earth beyond six of nine planetary boundaries. *Science Advances*, **9**(37), eadh2458.

RIEDESEL, LUDWIG, MÖLLER, MARKUS, HORNEY, PETER, GOLLA, BURKHARD, PIEPHO, HANS-PETER, KAUTZ, TIMO, & FEIKE, TIL. 2023. Timing and intensity of heat and drought stress determine wheat yield losses in Germany. *PLOS ONE*, **18**(7), e0288202.

ROBINSON, DAVID A., HOPMANS, JAN W., FILIPOVIC, VILIM, VAN DER PLOEG, MARTINE, LEBRON, INMA, JONES, SCOTT B., REINSCH, SABINE, JARVIS, NICK, & TULLER, MARKUS. 2019. Global environmental changes impact soil hydraulic functions through biophysical feedbacks. *Global Change Biology*, **25**(6), 1895–1904.

ROGERS, ALISTAIR, MEDLYN, BELINDA E., DUKES, JEFFREY S., BONAN, GORDON, VON CAEMMERER, SUSANNE, DIETZE, MICHAEL C., KATTGE, JENS, LEAKEY, ANDREW D. B., MERCADO, LINA M., NIINEMETS, ÜLO, PRENTICE, I. COLIN, SERBIN, SHAWN P., SITCH, STEPHEN, WAY, DANIELLE A., & ZAEHLE, SÖNKE. 2017. A roadmap for improving the representation of photosynthesis in Earth system models. *New Phytologist*, **213**(1), 22–42.

ROGGER, JULIAN, MILLS, BENJAMIN J. W., GERYA, TARAS V., & PELLISSIER, LOÏC. 2024. Speed of thermal adaptation of terrestrial vegetation alters Earth's long-term climate. *Science Advances*, **10**(9), eadj4408.

ROMERO, ANGELA P., ALARCÓN, ANDRÉS, VALBUENA, RAÚL I., & GALEANO, CARLOS H. 2017. Physiological Assessment of Water Stress in Potato Using Spectral Information. *Frontiers in Plant Science*, **8**(Sept.).

ROTIMI OJO, E., BULLOCK, PAUL R., & FITZMAURICE, JOHN. 2015. Field Performance of Five Soil Moisture Instruments in Heavy Clay Soils. *Soil Science Society of America Journal*, **79**(1), 20–29.

ROUHI, V., SAMSON, R., LEMEUR, R., & DAMME, P. VAN. 2007. Photosynthetic gas exchange characteristics in three different almond species during drought stress and subsequent recovery. *Environmental and Experimental Botany*, **59**(2), 117–129.

ROUSI, EFI, KORNHUBER, KAI, BEOBIDE-ARSUAGA, GORATZ, LUO, FEI, & COUMOU, DIM. 2022. Accelerated western European heatwave trends linked to more-persistent double jets over Eurasia. *Nature Communications*, **13**(1), 3851.

RYU, YOUNGRYEL, BERRY, JOSEPH A., & BALDOCCHI, DENNIS D. 2019. What is global photosynthesis? History, uncertainties and opportunities. *Remote Sensing of Environment*, **223**(Mar.), 95–114.

SABOT, MANON E. B., DE KAUWE, MARTIN G., PITMAN, ANDY J., MEDLYN, BELINDA E., VERHOEF, ANNE, UKKOLA, ANNA M., & ABRAMOWITZ, GAB. 2020. Plant profit maximization improves predictions of European forest responses to drought. *New Phytologist*, **226**(6), 1638–1655.

SABOT, MANON E. B., DE KAUWE, MARTIN G., PITMAN, ANDY J., MEDLYN, BELINDA E., ELLSWORTH, DAVID S., MARTIN-STPAUL, NICOLAS K., WU, JIN, CHOAT, BRENDAN, LIMOUSIN, JEAN-MARC, MITCHELL, PATRICK J., ROGERS, ALISTAIR, & SERBIN, SHAWN P. 2022. One Stomatal Model to Rule Them All? Toward Improved Representation of Carbon and Water Exchange in Global Models. *Journal of Advances in Modeling Earth Systems*, **14**(4).

SAMANIEGO, L., THOBER, S., KUMAR, R., WANDERS, N., RAKOVEC, O., PAN, M., ZINK, M., SHEFFIELD, J., WOOD, E. F., & MARX, A. 2018. Anthropogenic warming exacerbates European soil moisture droughts. *Nature Climate Change*, **8**(5), 421–426.

SANDS, P.J, HACKETT, C, & NIX, H.A. 1979. A model of the development and bulking of potatoes (Solanum Tuberosum L.) I. Derivation from well-managed field crops. *Field Crops Research*, **2**(Jan.), 309–331.

SAVVIDES, ANDREAS M., & FOTOPOULOS, VASILEIOS. 2018. Two Inexpensive and Non-destructive Techniques to Correct for Smaller-Than-Gasket Leaf Area in Gas Exchange Measurements. *Frontiers in Plant Science*, **9**(Apr.), 548.

SCHAAP, MARCEL G., LEIJ, FEIKE J., & VAN GENUCHTEN, MARTINUS TH. 2001. rosetta: a computer program for estimating soil hydraulic parameters with hierarchical pedotransfer functions. *Journal of Hydrology*, **251**(3), 163–176.

SCHICKLING, ANKE, MATVEEVA, MARIA, DAMM, ALEXANDER, SCHWEEN, JAN H., WAHNER, ANDREAS, GRAF, ALEXANDER, CREWELL, SUSANNE, & RASCHER, UWE. 2016. Combining Sun-Induced Chlorophyll Fluorescence and Photochemical Reflectance Index Improves Diurnal Modeling of Gross Primary Productivity. *Remote Sensing*, **8**(7).

SCHMID, HANS PETER. 2002. Footprint modeling for vegetation atmosphere exchange studies: a review and perspective. *Agricultural and Forest Meteorology*, **113**(1-4), 159–183.

SCHMIEGE, STEPHANIE C, HESKEL, MARY, FAN, YUZHEN, & WAY, DANIELLE A. 2023. It's only natural: Plant respiration in unmanaged systems. *Plant Physiology*, **192**(2), 710–727.

SCHREIBER, ULRICH. 2004. Pulse-Amplitude-Modulation (PAM) Fluorometry and Saturation Pulse Method: An Overview. *Pages 279–319 of:* PAPAGEORGIOU, GEORGE CHRISTOS, & GOVINDJEE (eds), *Chlorophyll a Fluorescence*, vol. 19. Dordrecht: Springer Netherlands. Series Title: Advances in Photosynthesis and Respiration.

SCHUTTEMEYER, D., BURBA, M., DRUSCH, M., ELFVING, A., & MECKLENBURG, S. 2018. ESA's Campaign Activities in Support of the FLEX Mission. *Pages 3924–3926 of: IGARSS 2018 - 2018 IEEE International Geoscience and Remote Sensing Symposium*. Valencia: IEEE.

SCHÜTT, ALEXANDER, BECKER, JOSCHA N., GRÖNGRÖFT, ALEXANDER, SCHAAF-TITEL, SELINA, & ESCHENBACH, ANNETTE. 2022. Soil water stress at young urban street-tree sites in response to meteorology and site parameters. *Urban Forestry Urban Greening*, **75**, 127692.

SCOFFONI, CHRISTINE, MCKOWN, ATHENA D., RAWLS, MICHAEL, & SACK, LAWREN. 2012. Dynamics of leaf hydraulic conductance with water status: quantification and analysis of species differences under steady state. *Journal of Experimental Botany*, **63**(2), 643–658.

SELLIN, ARNE, EENSALU, EVE, & NIGLAS, AIGAR. 2010. Is distribution of hydraulic constraints within tree crowns reflected in photosynthetic water-use efficiency? An example of Betula pendula. *Ecological Research*, **25**(1), 173–183.

SERRANO-FINETTI, ERNESTO, CASTILLO, EDUARDO, ALEJOS, SMITH, & LEÓN HILARIO, L.M. 2023. Toward noninvasive monitoring of plant leaf water content by electrical impedance spectroscopy. *Computers and Electronics in Agriculture*, **210**(July), 107907.

SHA, ZONGYAO, BAI, YONGFEI, LI, RUREN, LAN, HAI, ZHANG, XUELIANG, LI, JONATHON, LIU, XUEFENG, CHANG, SHUJUAN, & XIE, YICHUN. 2022. The global carbon sink potential of terrestrial vegetation can be increased substantially by optimal land management. *Communications Earth & Environment*, **3**(1), 8.

SHARKEY, THOMAS D. 2016. What gas exchange data can tell us about photosynthesis: Gas exchange data and photosynthesis. *Plant, Cell & Environment*, **39**(6), 1161–1163.

SHARKEY, THOMAS D., BERNACCHI, CARL J., FARQUHAR, GRAHAM D., & SINGSAAS, ERIC L. 2007. Fitting photosynthetic carbon dioxide response curves for C $_3$ leaves. *Plant, Cell & Environment*, **30**(9), 1035–1040.

SHEN, QIU, LIN, JINGYU, YANG, JIANHUA, ZHAO, WENHUI, & WU, JIANJUN. 2022. Exploring the Potential of Spatially Downscaled Solar-Induced Chlorophyll Fluorescence to Monitor Drought Effects on Gross Primary Production in Winter Wheat. *IEEE Journal of Selected Topics in Applied Earth Observations and Remote Sensing*, **15**, 2012–2022.

SHI, SHAOMIN, CONG, WEIWEI, LU, SEN, ZHAO, TIANHONG, WANG, FENG, & LU, QI. 2022. Can SIF and NPQ be used in the photosynthesis rate simulation of plants subjected to drought? *Environmental and Experimental Botany*, **203**(Nov.), 105067.

SHI, XIAOXIAO, & BLOOM, ARNOLD. 2021. Photorespiration: The Futile Cycle? *Plants*, **10**(5), 908.

SHIMAZAKI, KEN-ICHIRO, DOI, MICHIO, ASSMANN, SARAH M., & KINOSHITA, TOSHINORI. 2007. Light Regulation of Stomatal Movement. *Annual Review of Plant Biology*, **58**(1), 219–247. _eprint: https://doi.org/10.1146/annurev.arplant.57.032905.105434.

SHIN, YU KYEONG, BHANDARI, SHIVA RAM, JO, JUNG SU, SONG, JAE WOO, & LEE, JUN GU. 2021. Effect of Drought Stress on Chlorophyll Fluorescence Parameters, Phytochemical Contents, and Antioxidant Activities in Lettuce Seedlings. *Horticulturae*, **7**(8), 238.

SIBRET, THOMAS, BAUTERS, MARIJN, BULONZA, EMMANUEL, LEFEVRE, LODEWIJK, CERUTTI, PAOLO OMAR, LOKONDA, MICHEL, MBIFO, JOSÉ, MICHEL, BAUDOUIN, VERBEECK, HANS, & BOECKX, PASCAL. 2022. CongoFlux – The First Eddy Covariance Flux Tower in the Congo Basin. *Frontiers in Soil Science*, **2**.

SIEBERS, MATTHEW H., GOMEZ-CASANOVAS, NURIA, FU, PENG, MEACHAM-HENSOLD, KATHERINE, MOORE, CAITLIN E., & BERNACCHI, CARL J. 2021. Emerging approaches to measure photosynthesis from the leaf to the ecosystem. *Emerging Topics in Life Sciences*, **5**(2), 261–274.

SILVA-DÍAZ, CECILIA, RAMÍREZ, DAVID A., RODRÍGUEZ-DELFÍN, ALFREDO, DE MENDIBURU, FELIPE, RINZA, JAVIER, NINANYA, JOHAN, LOAYZA, HILDO, & QUIROZ, ROBERTO. 2020. Unraveling Ecophysiological Mechanisms in Potatoes under Different Irrigation Methods: A Preliminary Field Evaluation. *Agronomy*, **10**(6), 827.

SINCLAIR, T. R., MURPHY, C. E., & KNOERR, K. R. 1976. Development and Evaluation of Simplified Models for Simulating Canopy Photosynthesis and Transpiration. *The Journal of Applied Ecology*, **13**(3), 813.

SINGH, GURBACHAN. 1969. A review of the soil-moisture relationship in potatoes. *American Potato Journal*, **46**(10), 398–403.

SIPPEL, SEBASTIAN, REICHSTEIN, MARKUS, MA, XUANLONG, MAHECHA, MIGUEL D., LANGE, HOLGER, FLACH, MILAN, & FRANK, DOROTHEA. 2018. Drought, Heat, and the Carbon Cycle: a Review. *Current Climate Change Reports*, **4**(3), 266–286.

SOLOMON, SUSAN, PLATTNER, GIAN-KASPER, KNUTTI, RETO, & FRIEDLINGSTEIN, PIERRE. 2009. Irreversible climate change due to carbon dioxide emissions. *Proceedings of the National Academy of Sciences*, **106**(6), 1704–1709.

SONAWANE, BALASAHEB V., & COUSINS, ASAPH B. 2019. Uncertainties and limitations of using carbon-13 and oxygen-18 leaf isotope exchange to estimate the temperature response of mesophyll CO2 conductance in C3 plants. *New Phytologist*, **222**(1), 122–131.

SORRENTINO, GIUSEPPE, HAWORTH, MATTHEW, WAHBI, SAID, MAHMOOD, TARIQ, ZUOMIN, SHI, & CENTRITTO, MAURO. 2016. Abscisic Acid Induces Rapid Reductions in Mesophyll Conductance to Carbon Dioxide. *PLOS ONE*, **11**(2), e0148554.

SOUDANI, K., HMIMINA, G., DELPIERRE, N., PONTAILLER, J.-Y., AUBINET, M., BONAL, D., CAQUET, B., DE GRANDCOURT, A., BURBAN, B., FLECHARD, C., GUYON, D., GRANIER, A., GROSS, P., HEINESH, B., LONGDOZ, B., LOUSTAU, D., MOUREAUX, C., OURCIVAL, J.-M., RAMBAL, S., SAINT ANDRÉ, L., & DUFRÊNE, E. 2012. Ground-based Network of NDVI measurements for tracking temporal dynamics of canopy structure and vegetation phenology in different biomes. *Remote Sensing of Environment*, **123**(Aug.), 234–245.

SPEARMAN, C. 1904. The Proof and Measurement of Association between Two Things. *The American Journal of Psychology*, **15**(1), 72.

SPERRY, JOHN S., & LOVE, DAVID M. 2015. What plant hydraulics can tell us about responses to climate-change droughts. *New Phytologist*, **207**(1), 14–27.

SPERRY, JOHN S., WANG, YUJIE, WOLFE, BRETT T., MACKAY, D. SCOTT, ANDEREGG, WILLIAM R. L., MCDOWELL, NATE G., & POCKMAN, WILLIAM T. 2016. Pragmatic hydraulic theory predicts stomatal responses to climatic water deficits. *New Phytologist*, **212**(3), 577–589.

SPERRY, JOHN S., VENTURAS, MARTIN D., ANDEREGG, WILLIAM R. L., MENCUCCINI, MAURIZIO, MACKAY, D. SCOTT, WANG, YUJIE, & LOVE, DAVID M. 2017. Predicting stomatal responses to the environment from the optimization of photosynthetic gain and hydraulic cost: A stomatal optimization model. *Plant, Cell & Environment*, **40**(6), 816–830.

SPINONI, JONATHAN, VOGT, JÜRGEN V., NAUMANN, GUSTAVO, BARBOSA, PAULO, & DOSIO, ALESSANDRO. 2018. Will drought events become more frequent and severe in Europe? *International Journal of Climatology*, **38**(4), 1718–1736.

SPRENGER, HEIKE, KUROWSKY, CHRISTINA, HORN, RENATE, ERBAN, ALEXANDER, SEDDIG, SYLVIA, RUDACK, KATHARINA, FISCHER, AXEL, WALTHER, DIRK, ZUTHER, ELLEN, KÖHL, KARIN, HINCHA, DIRK K., & KOPKA, JOACHIM. 2016. The drought response of potato reference cultivars with contrasting tolerance. *Plant, Cell & Environment*, **39**(11), 2370–2389.

STALHAM, M. A., & ALLEN, E. J. 2001. Effect of variety, irrigation regime and planting date on depth, rate, duration and density of root growth in the potato (*Solanum tuberosum*) crop. *The Journal of Agricultural Science*, **137**(3), 251–270.

STALHAM, M. A., & ALLEN, E. J. 2004. Water uptake in the potato (Solanum tuberosum) crop. *The Journal of Agricultural Science*, **142**(4), 373–393.

STEELE-DUNNE, SUSAN C., MCNAIRN, HEATHER, MONSIVAIS-HUERTERO, ALEJANDRO, JUDGE, JASMEET, LIU, PANG-WEI, & PAPATHANASSIOU, KOSTAS. 2017. Radar Remote Sensing of Agricultural Canopies: A Review. *IEEE Journal of Selected Topics in Applied Earth Observations and Remote Sensing*, **10**(5), 2249–2273.

STIRBET, ALEXANDRINA, LAZÁR, DUŠAN, GUO, YA, & GOVINDJEE, GOVINDJEE. 2020. Photosynthesis: basics, history and modelling. *Annals of Botany*, **126**(4), 511–537.

STOCKER, BENJAMIN D., ZSCHEISCHLER, JAKOB, KEENAN, TREVOR F., PRENTICE, I. COLIN, PEÑUELAS, JOSEP, & SENEVIRATNE, SONIA I. 2018. Quantifying soil moisture impacts on light use efficiency across biomes. *New Phytologist*, **218**(4), 1430–1449.

SULEAU, MARIE, MOUREAUX, CHRISTINE, DUFRANNE, DELPHINE, BUYSSE, PAULINE, BODSON, BERNARD, DESTAIN, JEAN-PIERRE, HEINESCH, BERNARD, DEBACQ, ALAIN, & AUBINET, MARC. 2011. Respiration of three Belgian crops: Partitioning of total ecosystem respiration in its heterotrophic, above- and below-ground autotrophic components. *Agricultural and Forest Meteorology*, **151**(5), 633–643.

SULIS, MAURO, COUVREUR, VALENTIN, KEUNE, JESSICA, CAI, GAOCHAO, TREBS, IVONNE, JUNK, JUERGEN, SHRESTHA, PRABHAKAR, SIMMER, CLEMENS, KOLLET, STEFAN J., VEREECKEN, HARRY, & VANDERBORGHT, JAN. 2019. Incorporating a root water uptake model based on the hydraulic architecture approach in terrestrial systems simulations. *Agricultural and Forest Meteorology*, **269-270**, 28–45.

SUN, JINDONG, FENG, ZHAOZHONG, LEAKEY, ANDREW D.B., ZHU, XINGUANG, BERNACCHI, CARL J., & ORT, DONALD R. 2014. Inconsistency of mesophyll conductance estimate causes the inconsistency for the estimates of maximum rate of Rubisco carboxylation among the linear, rectangular and non-rectangular hyperbola biochemical models of leaf photosynthesis—A case study of CO2 enrichment and leaf aging effects in soybean. *Plant Science*, **226**, 49–60. Photosynthesis in a climate change scenario.

SUN, LI RONG, WANG, YI BIN, HE, SHI BIN, & HAO, FU SHUN. 2018. Mechanisms for Abscisic Acid Inhibition of Primary Root Growth. *Plant signaling & behavior*, **13**(9), e1500069. Place: United States.

SUTTON, ROWAN T., DONG, BUWEN, & GREGORY, JONATHAN M. 2007. Land/sea warming ratio in response to climate change: IPCC AR4 model results and comparison with observations. *Geophysical Research Letters*, **34**(2), 2006GL028164.

SWINBANK, W. C. 1951. THE MEASUREMENT OF VERTICAL TRANSFER OF HEAT AND WATER VAPOR BY EDDIES IN THE LOWER ATMOSPHERE. *Journal of Atmospheric Sciences*, **8**(3), 135 – 145.

TABARI, HOSSEIN. 2020. Climate change impact on flood and extreme precipitation increases with water availability. *Scientific Reports*, **10**(1), 13768.

TAN, ZHENG-HONG, WU, ZHI-XIANG, HUGHES, ALICE C., SCHAEFER, DOUGLAS, ZENG, JIYE, LAN, GUO-YU, YANG, CHUANG, TAO, ZHONG-LIANG, CHEN, BANG-QIAN, TIAN, YAO-HUA, SONG, LIANG, JATOI, MUHAMMAD TAHIR, ZHAO, JUN-FU, & YANG, LIAN-YAN. 2017. On the ratio of intercellular to ambient CO2 (c i/c a) derived from ecosystem flux. *International Journal of Biometeorology*, **61**(12), 2059–2071.

TARIN, TONANTZIN, NOLAN, RACHAEL H., MEDLYN, BELINDA E., CLEVERLY, JAMES, & EAMUS, DEREK. 2020a. Water-use efficiency in a semi-arid woodland with high rainfall variability. *Global Change Biology*, **26**(2), 496–508.

TARIN, TONANTZIN, NOLAN, RACHAEL H., MEDLYN, BELINDA E., CLEVERLY, JAMES, & EAMUS, DEREK. 2020b. Water-use efficiency in a semi-arid woodland with high rainfall variability. *Global Change Biology*, **26**(2), 496–508.

TARVAINEN, LASSE, WALLIN, GÖRAN, RÄNTFORS, MATS, & UDDLING, JOHAN. 2013. Weak vertical canopy gradients of photosynthetic capacities and stomatal responses in a fertile Norway spruce stand. *Oecologia*, **173**(4), 1179–1189.

TAYLOR, THOMAS E., ELDERING, ANNMARIE, MERRELLI, ARONNE, KIEL, MATTHÄUS, SOMKUTI, PETER, CHENG, CECILIA, ROSENBERG, ROBERT, FISHER, BRENDAN, CRISP, DAVID, BASILIO, RALPH, BENNETT, MATTHEW, CERVANTES, DANIEL, CHANG, ALBERT, DANG, LAN, FRANKENBERG, CHRISTIAN, HAEMMERLE, VANCE R., KELLER, GRAZIELA R., KUROSU, THOMAS, LAUGHNER, JOSHUA L., LEE, RICHARD, MARCHETTI, YULIYA, NELSON, ROBERT R., O'DELL, CHRISTOPHER W., OSTERMAN, GREGORY, PAVLICK, RYAN, ROEHL, COLEEN, SCHNEIDER, ROBERT, SPIERS, GARY, TO, CATHY, WELLS, CHRISTOPHER, WENNBERG, PAUL O., YELAMANCHILI, AMRUTA, & YU, SHANSHAN. 2020. OCO-3 early mission operations and initial (vEarly) XCO2 and SIF retrievals. *Remote Sensing of Environment*, **251**, 112032.

TAZOE, YOUSHI, VON CAEMMERER, SUSANNE, ESTAVILLO, GONZALO M., & EVANS, JOHN R. 2011. Using tunable diode laser spectroscopy to measure carbon isotope discrimination and mesophyll conductance to CO2 diffusion dynamically at different CO2 concentrations. *Plant, Cell & Environment*, **34**(4), 580–591.

TEULING, ADRIAAN J., UIJLENHOET, REMKO, HUPET, FRANÇOIS, & TROCH, PETER A. 2006. Impact of plant water uptake strategy on soil moisture and evapotranspiration dynamics during drydown. *Geophysical Research Letters*, **33**(3).

THOM, A. S. 1972. Momentum, mass and heat exchange of vegetation. *Quarterly Journal of the Royal Meteorological Society*, **98**(415), 124–134.

THOMPSON, ANDREW J., MULHOLLAND, BARRY J., JACKSON, ALISON C., MCKEE, JOHN M. T., HILTON, HOWARD W., SYMONDS, RACHAEL C., SONNEVELD, TINEKE, BURBIDGE, ALAN, STEVENSON, PATRICK, & TAYLOR, IAN B. 2007. Regulation and manipulation of ABA biosynthesis in roots. *Plant, cell & environment*, **30**(1), 67–78. Place: United States.

TIAN, FENG, BRANDT, MARTIN, LIU, YI Y., RASMUSSEN, KJELD, & FENSHOLT, RASMUS. 2017. Mapping gains and losses in woody vegetation across global tropical drylands. *Global Change Biology*, **23**(4), 1748–1760.

TORETI, ANDREA, BELWARD, ALAN, PEREZ-DOMINGUEZ, IGNACIO, NAUMANN, GUSTAVO, LUTERBACHER, JÜRG, CRONIE, OTTMAR, SEGUINI, LORENZO, MANFRON, GIACINTO, LOPEZ-LOZANO, RAUL, BARUTH, BETTINA, VAN DEN BERG, MAURITS, DENTENER, FRANK, CEGLAR, ANDREJ, CHATZOPOULOS, THOMAS, & ZAMPIERI, MATTEO. 2019. The Exceptional 2018 European Water Seesaw Calls for Action on Adaptation. *Earth's Future*, **7**(6), 652–663.

TRAMONTANA, GIANLUCA, MIGLIAVACCA, MIRCO, JUNG, MARTIN, REICHSTEIN, MARKUS, KEENAN, TREVOR F., CAMPS-VALLS, GUSTAU, OGEE, JEROME, VERRELST, JOCHEM, & PAPALE, DARIO. 2020. Partitioning net carbon dioxide fluxes into photosynthesis and respiration using neural networks. *Global Change Biology*, **26**(9), 5235–5253.

TRENBERTH, KEVIN E., DAI, AIGUO, VAN DER SCHRIER, GERARD, JONES, PHILIP D., BARICHIVICH, JONATHAN, BRIFFA, KEITH R., & SHEFFIELD, JUSTIN. 2014. Global warming and changes in drought. *Nature Climate Change*, **4**(1), 17–22.

TRIFUNOV, VIOLETA TEODORA, SHADAYDEH, MAHA, RUNGE, JAKOB, REICHSTEIN, MARKUS, & DENZLER, JOACHIM. 2021. A Data-Driven Approach to Partitioning Net Ecosystem Exchange Using a Deep State Space Model. *IEEE Access*, **9**, 107873–107883.

TRIPATHY, BAISHNAB CHARAN, & OELMÜLLER, RALF. 2012. Reactive oxygen species generation and signaling in plants. *Plant signaling & behavior*, **7**(12), 1621–1633. Place: United States.

TRUGMAN, A. T., MEDVIGY, D., MANKIN, J. S., & ANDEREGG, W. R. L. 2018. Soil Moisture Stress as a Major Driver of Carbon Cycle Uncertainty. *Geophysical Research Letters*, **45**(13), 6495–6503.

TULLER, M., & OR, D. 2005. WATER RETENTION AND CHARACTERISTIC CURVE. *Pages 278–289 of: Encyclopedia of Soils in the Environment*. Elsevier.

TULLER, MARKUS, OR, DANI, & DUDLEY, LYNN M. 1999. Adsorption and capillary condensation in porous media: Liquid retention and interfacial configurations in angular pores. *Water Resources Research*, **35**(7), 1949–1964.

TUZET, A., PERRIER, A., & LEUNING, R. 2003. A coupled model of stomatal conductance, photosynthesis and transpiration. *Plant, Cell & Environment*, **26**(7), 1097–1116.

TUZET, ANDRÉE, GRANIER, ANDRÉ, BETSCH, PAULINE, PEIFFER, MARIANNE, & PERRIER, ALAIN. 2017. Modelling hydraulic functioning of an adult beech stand under non-limiting soil water and severe drought condition. *Ecological Modelling*, **348**, 56–77.

ULLAH, ARIF, & DRAL, PAVLO O. 2022. Predicting the future of excitation energy transfer in light-harvesting complex with artificial intelligence-based quantum dynamics. *Nature Communications*, **13**(1), 1930.

URBAN, JOSEF, INGWERS, MILES, MCGUIRE, MARY ANNE, & TESKEY, ROBERT O. 2017a. Stomatal conductance increases with rising temperature. *Plant Signaling & Behavior*, **12**(8), e1356534.

URBAN, LAURENT, AARROUF, JAWAD, & BIDEL, LUC P. R. 2017b. Assessing the Effects of Water Deficit on Photosynthesis Using Parameters Derived from Measurements of Leaf Gas Exchange and of Chlorophyll a Fluorescence. *Frontiers in Plant Science*, **8**(Dec.).

URBAN, O., HLAVÁČOVÁ, M., KLEM, K., NOVOTNÁ, K., RAPANTOVÁ, B., SMUTNÁ, P., HORÁKOVÁ, V., HLAVINKA, P., ŠKARPA, P., & TRNKA, M. 2018. Combined effects of drought and high temperature on photosynthetic characteristics in four winter wheat genotypes. *Field Crops Research*, **223**(June), 137–149.

VALENTINI, R., EPRON, D., ANGELIS, P., MATTEUCCI, G., & DREYER, E. 1995. In situ estimation of net CO2 assimilation, photosynthetic electron flow and photorespiration in Turkey oak (Q. cerris L.) leaves: diurnal cycles under different levels of water supply. *Plant, Cell and Environment*, **18**(6), 631–640.

VAN DER TOL, C., VERHOEF, W., & ROSEMA, A. 2009. A model for chlorophyll fluorescence and photosynthesis at leaf scale. *Agricultural and Forest Meteorology*, **149**(1), 96–105.

VAN DER TOL, C., BERRY, J. A., CAMPBELL, P. K. E., & RASCHER, U. 2014. Models of fluorescence and photosynthesis for interpreting measurements of solar-induced chlorophyll fluorescence. *Journal of Geophysical Research: Biogeosciences*, **119**(12), 2312–2327. Publisher: John Wiley & Sons, Ltd.

VAN DER WOUDE, AUKE M., PETERS, WOUTER, JOETZJER, EMILIE, LAFONT, SÉBASTIEN, KOREN, GERBRAND, CIAIS, PHILIPPE, RAMONET, MICHEL, XU, YIDI, BASTOS, ANA, BOTÍA, SANTIAGO, SITCH, STEPHEN, DE KOK, REMCO, KNEUER, TOBIAS, KUBISTIN, DAGMAR, JACOTOT, ADRIEN, LOUBET, BENJAMIN, HERIG-COIMBRA, PEDRO-HENRIQUE, LOUSTAU, DENIS, & LUIJKX, INGRID T. 2023. Temperature extremes of 2022 reduced carbon uptake by forests in Europe. *Nature Communications*, **14**(1), 6218.

VAN EMMERIK, TIM, STEELE-DUNNE, SUSAN C., JUDGE, JASMEET, & VAN DE GIESEN, NICK. 2015. Impact of Diurnal Variation in Vegetation Water Content on Radar Backscatter From Maize During Water Stress. *IEEE Transactions on Geoscience and Remote Sensing*, **53**(7), 3855–3869.

VAN EMMERIK, TIM, STEELE-DUNNE, SUSAN, PAGET, AARON, OLIVEIRA, RAFAEL S., BITTENCOURT, PAULO R. L., BARROS, FERNANDA DE V., & VAN DE GIESEN, NICK. 2017. Water stress detection in the Amazon using radar. *Geophysical Research Letters*, **44**(13), 6841–6849.

VAN GENUCHTEN, M. TH. 1980. A Closed-form Equation for Predicting the Hydraulic Conductivity of Unsaturated Soils. *Soil Science Society of America Journal*, **44**(5), 892–898.

VAN SUNDERT, KEVIN, BRUNE, VERONIKA, BAHN, MICHAEL, DEUTSCHMANN, MARIO, HASIBEDER, ROLAND, NIJS, IVAN, & VICCA, SARA. 2020. Post-drought rewetting triggers substantial K release and shifts in leaf stoichiometry in managed and abandoned mountain grasslands. *Plant and Soil*, **448**(1), 353–368.

VAN WILDER, LISA, DEVLEESSCHAUWER, BRECHT, CLAYS, ELS, DE BUYSER, STEFANIE, VAN DER HEYDEN, JOHAN, CHARAFEDDINE, RANA, BOECKXSTAENS, PAULINE, DE BACQUER,

DIRK, VANDEPITTE, SOPHIE, & DE SMEDT, DELPHINE. 2022. The impact of multimorbidity patterns on health-related quality of life in the general population: results of the Belgian Health Interview Survey. *Quality of Life Research*, **31**(2), 551–565.

VANIKIOTIS, THEOFILOS, STAGAKIS, STAVROS, & KYPARISSIS, ARIS. 2021. MODIS PRI performance to track Light Use Efficiency of a Mediterranean coniferous forest: Determinants, restrictions and the role of LUE range. *Agricultural and Forest Meteorology*, **307**, 108518.

VERHOEF, ANNE, & EGEA, GREGORIO. 2014. Modeling plant transpiration under limited soil water: Comparison of different plant and soil hydraulic parameterizations and preliminary implications for their use in land surface models. *Agricultural and Forest Meteorology*, **191**(June), 22–32.

VERMA, MANISH, SCHIMEL, DAVID, EVANS, BRADLEY, FRANKENBERG, CHRISTIAN, BERINGER, JASON, DREWRY, DARREN T., MAGNEY, TROY, MARANG, IAN, HUTLEY, LINDSAY, MOORE, CAITLIN, & ELDERING, ANNMARIE. 2017. Effect of environmental conditions on the relationship between solar-induced fluorescence and gross primary productivity at an OzFlux grassland site. *Journal of Geophysical Research: Biogeosciences*, **122**(3), 716–733. Publisher: John Wiley & Sons, Ltd.

VEROMANN-JÜRGENSON, LINDA-LIISA, TOSENS, TIINA, LAANISTO, LAURI, & NIINEMETS, ÜLO. 2017. Extremely thick cell walls and low mesophyll conductance: welcome to the world of ancient living! *Journal of Experimental Botany*, **68**(7), 1639–1653.

VICCA, S., GILGEN, A. K., CAMINO SERRANO, M., DREESEN, F. E., DUKES, J. S., ESTIARTE, M., GRAY, S. B., GUIDOLOTTI, G., HOEPPNER, S. S., LEAKEY, A. D. B., OGAYA, R., ORT, D. R., OSTROGOVIC, M. Z., RAMBAL, S., SARDANS, J., SCHMITT, M., SIEBERS, M., VAN DER LINDEN, L., VAN STRAATEN, O., & GRANIER, A. 2012. Urgent need for a common metric to make precipitation manipulation experiments comparable. *New Phytologist*, **195**(3), 518–522.

VIDALE, P. L., EGEA, G., MCGUIRE, P. C., TODT, M., PETERS, W., MÜLLER, O., BALAN-SAROJINI, B., & VERHOEF, A. 2021. On the Treatment of Soil Water Stress in GCM Simulations of Vegetation Physiology. *Frontiers in Environmental Science*, **9**(Aug.), 689301.

VOGEL, M. M., ZSCHEISCHLER, J., WARTENBURGER, R., DEE, D., & SENEVIRATNE, S. I. 2019. Concurrent 2018 Hot Extremes Across Northern Hemisphere Due to Human-Induced Climate Change. *Earth's Future*, **7**(7), 692–703.

VON CAEMMERER, SUSANNE. 2013. Steady-state models of photosynthesis: Steady-state models of photosynthesis. *Plant, Cell & Environment*, **36**(9), 1617–1630.

VOS, J., & OYARZ N, P. J. 1987. Photosynthesis and stomatal conductance of potato leaves?effects of leaf age, irradiance, and leaf water potential. *Photosynthesis Research*, **11**(3), 253–264.

WALKER, ANTHONY P., JOHNSON, ABBEY L., ROGERS, ALISTAIR, ANDERSON, JEREMIAH, BRIDGES, ROBERT A., FISHER, ROSIE A., LU, DAN, RICCIUTO, DANIEL M., SERBIN, SHAWN P., & YE, MING. 2021. Multi-hypothesis comparison of Farquhar and Collatz photosynthesis models reveals the unexpected influence of empirical assumptions at leaf and global scales. *Global Change Biology*, **27**(4), 804–822. Publisher: John Wiley & Sons, Ltd.

WALKER, BERKLEY J., & ORT, DONALD R. 2015. Improved method for measuring the apparent CO2 photocompensation point resolves the impact of multiple internal conductances to CO2 to net gas exchange. *Plant, Cell & Environment*, **38**(11), 2462–2474.

WALKER, BERKLEY J., ORR, DOUGLAS J., CARMO-SILVA, ELIZABETE, PARRY, MARTIN A. J., BERNACCHI, CARL J., & ORT, DONALD R. 2017. Uncertainty in measurements of the photorespiratory CO2 compensation point and its impact on models of leaf photosynthesis. *Photosynthesis Research*, **132**(3), 245–255.

WALTHERT, LORENZ, GANTHALER, ANDREA, MAYR, STEFAN, SAURER, MATTHIAS, WALDNER, PETER, WALSER, MARCO, ZWEIFEL, ROMAN, & VON ARX, GEORG. 2021. From the comfort zone to crown dieback: sequence of physiological stress thresholds in mature European beech trees across progressive drought. *Science of the Total Environment*, **753**, 141792.

WANG, FENG-XIN, KANG, YAOHU, LIU, SHI-PING, & HOU, XIAO-YAN. 2007. Effects of soil matric potential on potato growth under drip irrigation in the North China Plain. *Agricultural Water Management*, **88**(1), 34–42.

WANG, HAIBO, & XIAO, JINGFENG. 2021. Improving the Capability of the SCOPE Model for Simulating Solar-Induced Fluorescence and Gross Primary Production Using Data from OCO-2 and Flux Towers. *Remote Sensing*, **13**(4), 794.

WANG, JUN, HUANG, GUANHUA, LI, JIUSHENG, ZHENG, JIANHUA, HUANG, QUANZHONG, & LIU, HAIJUN. 2017. Effect of soil moisture-based furrow irrigation scheduling on melon (Cucumis melo L.) yield and quality in an arid region of Northwest China. *Agricultural Water Management*, **179**, 167–176. Special Issue on Improving Agricultural Water Productivity to Ensure Food Security under Changing Environments Overseen by: Brent Clothier.

WANG, NA, CLEVERS, JAN G.P.W., WIENEKE, SEBASTIAN, BARTHOLOMEUS, HARM, & KOOISTRA, LAMMERT. 2022. Potential of UAV-based sun-induced chlorophyll fluorescence to detect water stress in sugar beet. *Agricultural and Forest Meteorology*, **323**(Aug.), 109033.

WANG, SHUSEN, YANG, YAN, & TRISHCHENKO, ALEXANDER P. 2009. Assessment of canopy stomatal conductance models using flux measurements. *Ecological Modelling*, **220**(17), 2115–2118.

WANG, XIAOPING, CHEN, JING M., & JU, WEIMIN. 2020a. Photochemical reflectance index (PRI) can be used to improve the relationship between gross primary productivity (GPP) and sun-induced chlorophyll fluorescence (SIF). *Remote Sensing of Environment*, **246**, 111888.

WANG, XIAOXIAO, WANG, WENCHENG, HUANG, JIANLIANG, PENG, SHAOBING, & XIONG, DONGLIANG. 2018a. Diffusional conductance to CO $_2$ is the key limitation to photosynthesis in salt-stressed leaves of rice (*Oryza sativa*). *Physiologia Plantarum*, **163**(1), 45–58.

WANG, XIAOXIAO, DU, TINGTING, HUANG, JIANLIANG, PENG, SHAOBING, & XIONG, DONGLIANG. 2018b. Leaf hydraulic vulnerability triggers the decline in stomatal and mesophyll conductance during drought in rice. *Journal of Experimental Botany*, **69**(16), 4033–4045.

WANG, YING PING, KOWALCZYK, EVA, LEUNING, RAY, ABRAMOWITZ, GAB, RAUPACH, MICHAEL R., PAK, BERNARD, VAN GORSEL, EVA, & LUHAR, ASHOK. 2011. Diagnosing errors in a land surface model (CABLE) in the time and frequency domains. *Journal of Geophysical Research*, **116**(G1), G01034.

WANG, YUJIE, SPERRY, JOHN S., ANDEREGG, WILLIAM R. L., VENTURAS, MARTIN D., & TRUGMAN, ANNA T. 2020b. A theoretical and empirical assessment of stomatal optimization modeling. *New Phytologist*, **227**(2), 311–325.

WARREN, C. 2006a. Temperature response of photosynthesis and internal conductance to CO2: results from two independent approaches. *Journal of Experimental Botany*, **57**(12), 3057–3067.

WARREN, CHARLES. 2006b. Estimating the internal conductance to CO(2) movement. *Functional plant biology : FPB*, **33**(5), 431–442. Place: Australia.

WILLIAMS, I N, TORN, M S, RILEY, W J, & WEHNER, M F. 2014. Impacts of climate extremes on gross primary production under global warming. *Environmental Research Letters*, **9**(9), 094011.

WILSON, K. B., BALDOCCHI, D. D., & HANSON, P. J. 2000. Quantifying stomatal and non-stomatal limitations to carbon assimilation resulting from leaf aging and drought in mature deciduous tree species. *Tree Physiology*, **20**(12), 787–797.

WILSON, KELL, GOLDSTEIN, ALLEN, FALGE, EVA, AUBINET, MARC, BALDOCCHI, DENNIS, BERBIGIER, PAUL, BERNHOFER, CHRISTIAN, CEULEMANS, REINHART, DOLMAN, HAN, FIELD, CHRIS, GRELLE, ACHIM, IBROM, ANDREAS, LAW, B.E, KOWALSKI, ANDY, MEYERS, TILDEN, MONCRIEFF, JOHN, MONSON, RUSS, OECHEL, WALTER, TENHUNEN, JOHN, VALENTINI, RICCARDO, & VERMA, SHASHI. 2002. Energy balance closure at FLUXNET sites. *Agricultural and Forest Meteorology*, **113**(1-4), 223–243.

WOHLFAHRT, G., GERDEL, K., MIGLIAVACCA, M., ROTENBERG, E., TATARINOV, F., MÜLLER, J., HAMMERLE, A., JULITTA, T., SPIELMANN, F. M., & YAKIR, D. 2018. Sun-induced fluorescence and gross primary productivity during a heat wave. *Scientific Reports*, **8**(1), 14169.

WOHLFAHRT, GEORG, & GALVAGNO, MARTA. 2017. Revisiting the choice of the driving temperature for eddy covariance CO2 flux partitioning. *Agricultural and Forest Meteorology*, **237-238**(May), 135–142.

WOLF, ADAM, ANDEREGG, WILLIAM R. L., & PACALA, STEPHEN W. 2016. Optimal stomatal behavior with competition for water and risk of hydraulic impairment. *Proceedings of the National Academy of Sciences*, **113**(46), E7222–E7230.

WOLFE, BRETT T., DETTO, MATTEO, ZHANG, YONG-JIANG, ANDERSON-TEIXEIRA, KRISTINA J., BRODRIBB, TIM, COLLINS, ADAM D., CRAWFORD, CHLOE, DICKMAN, L. TURIN, ELY, KIM S., FRANCISCO, JESSICA, GURRY, PRESTON D., HANCOCK, HAIGAN, KING, CHRISTOPHER T., MAJEKOBAJE, ADELODUN R., MALLETT, CHRISTIAN J., MCDOWELL, NATE G., MENDHEIM, ZACHARY, MICHALETZ, SEAN T., MYERS, DANIEL B., PRICE, TY J., ROGERS, ALISTAIR, SACK, LAWREN, SERBIN, SHAWN P., SIDDIQ, ZAFAR, WILLIS, DAVID, WU, JIN, ZAILAA, JOSEPH, & WRIGHT, S. JOSEPH. 2023. Leaves as bottlenecks: The contribution of tree leaves to hydraulic resistance within the soil plant atmosphere continuum. *Plant, Cell & Environment*, **46**(3), 736–746.

WONG, S. C., COWAN, I. R., & FARQUHAR, G. D. 1979. Stomatal conductance correlates with photosynthetic capacity. *Nature*, **282**(5737), 424–426.

WUTZLER, THOMAS, LUCAS-MOFFAT, ANTJE, MIGLIAVACCA, MIRCO, KNAUER, JÜRGEN, SICKEL, KERSTIN, ŠIGUT, LADISLAV, MENZER, OLAF, & REICHSTEIN, MARKUS. 2018. Basic and extensible post-processing of eddy covariance flux data with REddyProc. *Biogeosciences*, **15**(16), 5015–5030.

XIA, YE, FU, CONGSHENG, WU, HAOHAO, WU, HUAWU, ZHANG, HAIXIA, CAO, YANG, & ZHU, ZICHUN. 2021. Influences of Extreme Events on Water and Carbon Cycles of Cropland Ecosystems: A Comprehensive Exploration Combining Site and Global Modeling. *Water Resources Research*, **57**(11), e2021WR029884.

XIAO, JINGFENG, CHEVALLIER, FREDERIC, GOMEZ, CECILE, GUANTER, LUIS, HICKE, JEFFREY A., HUETE, ALFREDO R., ICHII, KAZUHITO, NI, WENJIAN, PANG, YONG, RAHMAN,

ABDULLAH F., SUN, GUOQING, YUAN, WENPING, ZHANG, LI, & ZHANG, XIAOYANG. 2019. Remote sensing of the terrestrial carbon cycle: A review of advances over 50 years. *Remote Sensing of Environment*, **233**(Nov.), 111383.

XIAO, JINGFENG, FISHER, JOSHUA B., HASHIMOTO, HIROFUMI, ICHII, KAZUHITO, & PARAZOO, NICHOLAS C. 2021. Emerging satellite observations for diurnal cycling of ecosystem processes. *Nature Plants*, **7**(7), 877–887.

XIAO, YI, & ZHU, XIN-GUANG. 2017. Components of mesophyll resistance and their environmental responses: A theoretical modelling analysis. *Plant, Cell & Environment*, **40**(11), 2729–2742.

XIONG, DONGLIANG, DOUTHE, CYRIL, & FLEXAS, JAUME. 2018. Differential coordination of stomatal conductance, mesophyll conductance, and leaf hydraulic conductance in response to changing light across species: Coordination of CO $_2$ diffusion and H $_2$ O transport inside leaves. *Plant, Cell & Environment*, **41**(2), 436–450.

XU, HANG, ZHANG, ZHIQIANG, CHEN, JIQUAN, ZHU, MENGXUN, & KANG, MANCHUN. 2017. Cloudiness regulates gross primary productivity of a poplar plantation under different environmental conditions. *Canadian Journal of Forest Research*, **47**(5), 648–658.

XU, L., & BALDOCCHI, D. D. 2003. Seasonal trends in photosynthetic parameters and stomatal conductance of blue oak (Quercus douglasii) under prolonged summer drought and high temperature. *Tree Physiology*, **23**(13), 865–877.

XU, SHAN, ATHERTON, JON, RIIKONEN, ANU, ZHANG, CHAO, OIVUKKAMÄKI, JAAKKO, MACARTHUR, ALASDAIR, HONKAVAARA, EIJA, HAKALA, TEEMU, KOIVUMÄKI, NIKO, LIU, ZHIGANG, & PORCAR-CASTELL, ALBERT. 2021a. Structural and photosynthetic dynamics mediate the response of SIF to water stress in a potato crop. *Remote Sensing of Environment*, **263**(Sept.), 112555.

XU, XIANGTAO, KONINGS, ALEXANDRA G., LONGO, MARCOS, FELDMAN, ANDREW, XU, LIANG, SAATCHI, SASSAN, WU, DONGHAI, WU, JIN, & MOORCROFT, PAUL. 2021b. Leaf surface water, not plant water stress, drives diurnal variation in tropical forest canopy water content. *New Phytologist*, **231**(1), 122–136.

YANG, JULIA C., MAGNEY, TROY S., YAN, DONG, KNOWLES, JOHN F., SMITH, WILLIAM K., SCOTT, RUSSELL L., & BARRON-GAFFORD, GREG A. 2020a. The Photochemical Reflectance Index (PRI) Captures the Ecohydrologic Sensitivity of a Semiarid Mixed Conifer Forest. *Journal of Geophysical Research: Biogeosciences*, **125**(11), e2019JG005624. e2019JG005624 2019JG005624.

YANG, MENGXIANG, HE, JIAWEI, SUN, ZHUANGZHUANG, LI, QING, CAI, JIAN, ZHOU, QIN, WOLLENWEBER, BERND, JIANG, DONG, & WANG, XIAO. 2023. Drought priming mechanisms in wheat elucidated by in-situ determination of dynamic stomatal behavior. *Frontiers in Plant Science*, **14**(Feb.), 1138494.

YANG, PEIQI, VAN DER TOL, CHRISTIAAN, VERHOEF, WOUT, DAMM, ALEXANDER, SCHICKLING, ANKE, KRASKA, THORSTEN, MULLER, ONNO, & RASCHER, UWE. 2019. Using reflectance to explain vegetation biochemical and structural effects on sun-induced chlorophyll fluorescence. *Remote Sensing of Environment*, **231**(Sept.), 110996.

YANG, PEIQI, VAN DER TOL, CHRISTIAAN, CAMPBELL, PETYA K. E., & MIDDLETON, ELIZABETH M. 2021. Unraveling the physical and physiological basis for the solar- induced chlorophyll fluorescence and photosynthesis relationship using continuous leaf and canopy measurements of a corn crop. *Biogeosciences*, **18**(2), 441–465.

YANG, XI, TANG, JIANWU, MUSTARD, JOHN F., LEE, JUNG-EUN, ROSSINI, MICOL, JOINER, JOANNA, MUNGER, J. WILLIAM, KORNFELD, ARI, & RICHARDSON, ANDREW D. 2015. Solar-induced chlorophyll fluorescence that correlates with canopy photosynthesis on diurnal and seasonal scales in a temperate deciduous forest. *Geophysical Research Letters*, **42**(8), 2977–2987. Publisher: John Wiley & Sons, Ltd.

YANG, XIAOLONG, LIU, LIHUA, YIN, ZHIKAI, WANG, XINGYU, WANG, SHOUBING, & YE, ZIPIAO. 2020b. Quantifying photosynthetic performance of phytoplankton based on photosynthesis–irradiance response models. *Environmental Sciences Europe*, **32**, 1–13.

YAO, LU, LIU, YI, YANG, DONGXU, CAI, ZHAONAN, WANG, JING, LIN, CHAO, LU, NAIMENG, LYU, DAREN, TIAN, LONGFEI, WANG, MAOHUA, YIN, ZENGSHAN, ZHENG, YUQUAN, & WANG, SISI. 2022. Retrieval of solar-induced chlorophyll fluorescence (SIF) from satellite measurements: comparison of SIF between TanSat and OCO-2. *Atmospheric Measurement Techniques*, **15**(7), 2125–2137.

YAO, YITONG, HUMPHREY, VINCENT, KONINGS, ALEXANDRA G., WANG, YUJIE, YIN, YI, HOLTZMAN, NATANIEL, WOOD, JEFFREY D., BAR-ON, YINON, & FRANKENBERG, CHRISTIAN. 2024. Investigating Diurnal and Seasonal Cycles of Vegetation Optical Depth Retrieved From GNSS Signals in a Broadleaf Forest. *Geophysical Research Letters*, **51**(6), e2023GL107121. e2023GL107121 2023GL107121.

YIN, JIABO, GENTINE, PIERRE, SLATER, LOUISE, GU, LEI, POKHREL, YADU, HANASAKI, NAOTA, GUO, SHENGLIAN, XIONG, LIHUA, & SCHLENKER, WOLFRAM. 2023. Future socio-ecosystem productivity threatened by compound drought–heatwave events. *Nature Sustainability*, **6**(3), 259–272.

YIN, XINYOU, & AMTHOR, JEFFREY S. 2024. Estimating leaf day respiration from conventional gas exchange measurements. *New Phytologist*, **241**(1), 52–58.

YU, LIUYANG, GAO, XIAODONG, & ZHAO, XINING. 2020a. Global synthesis of the impact of droughts on crops' water-use efficiency (WUE): Towards both high WUE and productivity. *Agricultural Systems*, **177**(Jan.), 102723.

YU, YING, PIAO, JINXIN, FAN, WENYI, & YANG, XIGUANG. 2020b. Modified photochemical reflectance index to estimate leaf maximum rate of carboxylation based on spectral analysis. *Environmental Monitoring and Assessment*, **192**, 1–11.

YU, ZHEN, WANG, JINGXIN, LIU, SHIRONG, RENTCH, JAMES S, SUN, PENGSEN, & LU, CHAOQUN. 2017. Global gross primary productivity and water use efficiency changes under drought stress. *Environmental Research Letters*, **12**(1), 014016.

YUAN, WENPING, CAI, WENWEN, NGUY-ROBERTSON, ANTHONY, FANG, HUAJUN, SUYKER, ANDREW, CHEN, YANG, DONG, WENJIE, LIU, SHUGUANG, & ZHANG, HAICHENG. 2015. Uncertainty in simulating gross primary production of cropland ecosystem from satellite-based models. *Agricultural and Forest Meteorology*, **207**(July).

ZAIT, YOTAM, & SCHWARTZ, AMNON. 2018. Climate-Related Limitations on Photosynthesis and Drought-Resistance Strategies of Ziziphus spina-christi. *Frontiers in Forests and Global Change*, **1**(Sept.).

ZENES, NICOLE, KERR, KELLY L., TRUGMAN, ANNA T., & ANDEREGG, WILLIAM R. L. 2020. Competition and Drought Alter Optimal Stomatal Strategy in Tree Seedlings. *Frontiers in Plant Science*, **11**(May), 478.

ZENG, JINGYU, ZHOU, TAO, QU, YANPING, BENTO, VIRGÍLIO A., QI, JUNYU, XU, YIXIN, LI, YING, & WANG, QIANFENG. 2023. An improved global vegetation health index dataset in detecting vegetation drought. *Scientific Data*, **10**(1), 338.

ZENG, YELU, BADGLEY, GRAYSON, DECHANT, BENJAMIN, RYU, YOUNGRYEL, CHEN, MIN, & BERRY, J.A. 2019. A practical approach for estimating the escape ratio of near-infrared solar-induced chlorophyll fluorescence. *Remote Sensing of Environment*, **232**(Oct.), 111209.

ZHAN, WEIWEI, YANG, XI, RYU, YOUNGRYEL, DECHANT, BENJAMIN, HUANG, YU, GOULAS, YVES, KANG, MINSEOK, & GENTINE, PIERRE. 2022. Two for one: Partitioning CO2 fluxes and understanding the relationship between solar-induced chlorophyll fluorescence and gross primary productivity using machine learning. *Agricultural and Forest Meteorology*, **321**, 108980.

ZHANG, CHAO, FILELLA, IOLANDA, LIU, DAIJUN, OGAYA, ROMÀ, LLUSIÀ, JOAN, ASENSIO, DOLORES, & PEÑUELAS, JOSEP. 2017. Photochemical Reflectance Index (PRI) for Detecting Responses of Diurnal and Seasonal Photosynthetic Activity to Experimental Drought and Warming in a Mediterranean Shrubland. *Remote Sensing*, **9**(11).

ZHANG, KE, JUN CHAO, LI, QING WANG, QING, CHUN HUANG, YING, HUA LIU, RONG, HONG, YANG, TU, YONG, QU, WEI, & YIN YE, JIN. 2019a. Using multi-satellite microwave remote sensing observations for retrieval of daily surface soil moisture across China. *Water Science and Engineering*, **12**(2), 85–97.

ZHANG, PEIPEI, LIU, HAIQIU, LI, HANGZHOU, YAO, JIANEN, CHEN, XIU, & FENG, JINYING. 2023a. Using enhanced vegetation index and land surface temperature to reconstruct the solar-induced chlorophyll fluorescence of forests and grasslands across latitude and phenology. *Frontiers in Forests and Global Change*, **6**.

ZHANG, PENG, YANG, XIN, MANEVSKI, KIRIL, LI, SHENGLAN, WEI, ZHENHUA, ANDERSEN, MATHIAS NEUMANN, & LIU, FULAI. 2022a. Physiological and Growth Responses of Potato (Solanum Tuberosum L.) to Air Temperature and Relative Humidity under Soil Water Deficits. *Plants*, **11**(9), 1126.

ZHANG, YAO, ZHOU, SHA, GENTINE, PIERRE, & XIAO, XIANGMING. 2019b. Can vegetation optical depth reflect changes in leaf water potential during soil moisture dry-down events? *Remote Sensing of Environment*, **234**, 111451.

ZHANG, YONGGEN, & SCHAAP, MARCEL G. 2017. Weighted recalibration of the Rosetta pedotransfer model with improved estimates of hydraulic parameter distributions and summary statistics (Rosetta3). *Journal of Hydrology*, **547**, 39–53.

ZHANG, YONGGUANG, GUANTER, LUIS, BERRY, JOSEPH A., JOINER, JOANNA, VAN DER TOL, CHRISTIAAN, HUETE, ALFREDO, GITELSON, ANATOLY, VOIGT, MAXIMILIAN, & KÖHLER, PHILIPP. 2014. Estimation of vegetation photosynthetic capacity from space-based measurements of chlorophyll fluorescence for terrestrial biosphere models. *Global Change Biology*, **20**(12), 3727–3742.

ZHANG, YONGGUANG, GUANTER, LUIS, BERRY, JOSEPH A., VAN DER TOL, CHRISTIAAN, YANG, XI, TANG, JIANWU, & ZHANG, FANGMIN. 2016. Model-based analysis of the relationship between sun-induced chlorophyll fluorescence and gross primary production for remote sensing applications. *Remote Sensing of Environment*, **187**(Dec.), 145–155.

ZHANG, YONGGUANG, GUANTER, LUIS, JOINER, JOANNA, SONG, LIAN, & GUAN, KAIYU. 2018. Spatially-explicit monitoring of crop photosynthetic capacity through the use of space-based chlorophyll fluorescence data. *Remote Sensing of Environment*, **210**(June), 362–374.

ZHANG, YONGGUANG, ZHANG, QIAN, LIU, LIANGYUN, ZHANG, YANGJIAN, WANG, SHAOQIANG, JU, WEIMIN, ZHOU, GUANGSHENG, ZHOU, LI, TANG, JIANWU, ZHU, XUDONG, WANG, FENG, HUANG, YING, ZHANG, ZHAOYING, QIU, BO, ZHANG, XIAOKANG, WANG, SONGHAN, HUANG, CHANGPING, TANG, XUGUANG, & ZHANG, JINSONG. 2021. ChinaSpec: A Network for Long-Term Ground-Based Measurements of Solar-Induced Fluorescence in China. *Journal of Geophysical Research: Biogeosciences*, **126**(3), e2020JG006042. e2020JG006042 2020JG006042.

ZHANG, YUAN, NARAYANAPPA, DEVARAJU, CIAIS, PHILIPPE, LI, WEI, GOLL, DANIEL, VUICHARD, NICOLAS, DE KAUWE, MARTIN G., LI, LAURENT, & MAIGNAN, FABIENNE. 2022b (June). *Evaluating the vegetation-atmosphere coupling strength of ORCHIDEE land surface model (v7266)*. preprint. Biogeosciences.

ZHANG, ZHAOYING, CHEN, JING M., ZHANG, YONGGUANG, & LI, MANCHUN. 2023b. Improving the ability of solar-induced chlorophyll fluorescence to track gross primary production through differentiating sunlit and shaded leaves. *Agricultural and Forest Meteorology*, **341**, 109658.

ZHAO, FENG, GUO, YIQING, VERHOEF, WOUT, GU, XINGFA, LIU, LIANGYUN, & YANG, GUIJUN. 2014. A Method to Reconstruct the Solar-Induced Canopy Fluorescence Spectrum from Hyperspectral Measurements. *Remote Sensing*, **6**(10), 10171–10192.

ZHAO, WENHUI, RONG, YUPING, ZHOU, YANGZHEN, ZHANG, YANRONG, LI, SHENG, & LIU, LEIZHEN. 2024. The Relationship of Gross Primary Productivity with NDVI Rather than Solar-Induced Chlorophyll Fluorescence Is Weakened under the Stress of Drought. *Remote Sensing*, **16**(3).

ZHOU, HUAILIN, ZHOU, GUANGSHENG, HE, QIJIN, ZHOU, LI, JI, YUHE, & LV, XIAOMIN. 2021. Capability of leaf water content and its threshold values in reflection of soil–plant water status in maize during prolonged drought. *Ecological Indicators*, **124**(May), 107395.

ZHOU, RONG, KONG, LINGPENG, WU, ZHEN, ROSENQVIST, EVA, WANG, YINLEI, ZHAO, LIPING, ZHAO, TONGMIN, & OTTOSEN, CARL-OTTO. 2019a. Physiological response of tomatoes at drought, heat and their combination followed by recovery. *Physiologia Plantarum*, **165**(2), 144–154.

ZHOU, SHUANG-XI, PRENTICE, I. COLIN, & MEDLYN, BELINDA E. 2019b. Bridging Drought Experiment and Modeling: Representing the Differential Sensitivities of Leaf Gas Exchange to Drought. *Frontiers in Plant Science*, **9**(Jan.).

ZHOU, SHUANGXI, DUURSMA, REMKO A., MEDLYN, BELINDA E., KELLY, JEFF W.G., & PRENTICE, I. COLIN. 2013. How should we model plant responses to drought? An analysis of stomatal and non-stomatal responses to water stress. *Agricultural and Forest Meteorology*, **182-183**(Dec.), 204–214.

ZHOU, SHUANGXI, MEDLYN, BELINDA, SABATÉ, SANTIAGO, SPERLICH, DOMINIK, PRENTICE, I. COLIN, & WHITEHEAD, DAVID. 2014. Short-term water stress impacts on stomatal, mesophyll and biochemical limitations to photosynthesis differ consistently among tree species from contrasting climates. *Tree Physiology*, **34**(10), 1035–1046.

ZHU, K., YUAN, F.H., WANG, A.Z., WU, J.B., GUAN, D.X., JIN, C.J., FLEXAS, J., GONG, C.J., ZHANG, H.X., & ZHANG, Y.S. 2021. Stomatal, mesophyll and biochemical limitations to soil drought and rewatering in relation to intrinsic water-use efficiency in Manchurian ash and Mongolian oak. *Photosynthetica*, Jan.

ZI-PIAO, YE. 2010. A review on modeling of responses of photosynthesis to light and CO₂. *Chinese Journal of Plant Ecology*, **34**(6), 727.

ZIVCAK, MAREK, BRESTIC, MARIAN, KALAJI, HAZEM M., & GOVINDJEE. 2014. Photosynthetic responses of sun- and shade-grown barley leaves to high light: is the lower PSII connectivity in shade leaves associated with protection against excess of light? *Photosynthesis Research*, **119**(3), 339–354.

ZOOGMAN, P., LIU, X., SULEIMAN, R. M., PENNINGTON, W. F., FLITTNER, D. E., AL-SAADI, J. A., HILTON, B. B., NICKS, D. K., NEWCHURCH, M. J., CARR, J. L., JANZ, S. J., ANDRASCHKO, M. R., AROLA, A., BAKER, B. D., CANOVA, B. P., CHAN MILLER, C., COHEN, R. C., DAVIS, J. E., DUSSAULT, M. E., EDWARDS, D. P., FISHMAN, J., GHULAM, A., GONZÁLEZ ABAD, G., GRUTTER, M., HERMAN, J. R., HOUCK, J., JACOB, D. J., JOINER, J., KERRIDGE, B. J., KIM, J., KROTKOV, N. A., LAMSAL, L., LI, C., LINDFORS, A., MARTIN, R. V., MCELROY, C. T., MCLINDEN, C., NATRAJ, V., NEIL, D. O., NOWLAN, C. R., O'SULLIVAN, E. J., PALMER, P. I., PIERCE, R. B., PIPPIN, M. R., SAIZ-LOPEZ, A., SPURR, R. J. D., SZYKMAN, J. J., TORRES, O., VEEFKIND, J. P., VEIHELMANN, B., WANG, H., WANG, J., & CHANCE, K. 2017. Tropospheric Emissions: Monitoring of Pollution (TEMPO). *Journal of quantitative spectroscopy & radiative transfer*, **186**(Jan.), 17–39. Place: England.

ZOU, XIAOCHEN, MÕTTUS, MATTI, TAMMEORG, PRIIT, TORRES, CLARA LIZARAZO, TAKALA, TURE, PISEK, JAN, MÄKELÄ, PIRJO, STODDARD, F.L., & PELLIKKA, PETRI. 2014. Photographic measurement of leaf angles in field crops. *Agricultural and Forest Meteorology*, **184**(Jan.), 137–146.

ZWETSLOOT, MARIE J., & BAUERLE, TARYN L. 2021. Repetitive seasonal drought causes substantial species-specific shifts in fine-root longevity and spatio-temporal production patterns in mature temperate forest trees. *New Phytologist*, **231**(3), 974–986.